

Entanglement and control of quantum states

Thomas Wellens

Entanglement and control of quantum states

Dissertation der Fakultät für Physik
der Ludwig-Maximilians-Universität München



vorgelegt von Thomas Wellens
aus Solothurn

München, den 1. März 2002

1. Gutachter: Priv. Doz. Dr. A. Buchleitner
 2. Gutachter: Prof. Dr. B.-G. Englert
- Tag der mündlichen Prüfung: 3. Mai 2002

Zusammenfassung

Im ersten Teil der vorliegenden Arbeit untersuchen wir die Präparation einer einzelnen Mode des quantisierten Strahlungsfeldes in einen beliebigen Quantenzustand durch resonante Wechselwirkung mit einer Reihe von Zwei-Niveau-Atomen. Die Präparation erfolgt durch Wahl eines geeigneten (im allgemeinen verschränkten) Anfangszustands der Atome, und benötigt weder eine Messung des atomaren Endzustands, noch eine Kontrolle der Atom-Feld-Wechselwirkung. Dieses Verfahren ist auch bei gemischten Anfangszuständen des Feldes anwendbar. Wir erläutern, wie man den optimalen atomaren Anfangszustand auffinden kann, welcher den gewünschten Feldzustand mit maximaler Güte erzeugt, und zeigen durch numerische Berechnungen die Umsetzbarkeit unseres Präparationsverfahrens.

Im zweiten Teil demonstrieren wir die rauschinduzierte Kontrolle von Quantensprüngen in einem fundamentalen offenen Quantensystem. Neben der Wechselwirkung mit einem Fluss aufeinanderfolgender Zwei-Niveau-Atome ist das Feld hierbei auch an eine thermische Umgebung gekoppelt. Bei bestimmter Wahl der experimentellen Parameter wird das Photonenfeld bistabil und vollzieht Quantensprünge zwischen zwei metastabilen Zuständen. In der Gegenwart eines schwachen, periodischen Signals (d.h. einer Modulation des Anfangszustandes der den Resonator durchquerenden Zwei-Niveau-Atome) wird die beste Synchronisierung der Quantensprünge mit diesem Signal bei einer optimalen, *nichtverschwindenden* Temperatur der Umgebung erzielt. Dieser Effekt der stochastischen Resonanz ist in verschiedenen Komponenten des Blochvektors nach Austritt der Atome aus dem Resonator beobachtbar.

Der dritte Teil behandelt ein spezielles Problem in der Charakterisierung von Verschränkung zwischen zwei quantenmechanischen Zwei-Niveau-Systemen. Wir betrachten die optimale Zerlegung eines Zustands zweier Qubits in einen verschränkten und einen separablen Anteil, wobei das Gewicht von letzterem maximiert wird, und leiten notwendige und hinreichende Bedingungen für die Optimalität der Zerlegung her.

Abstract

In the first part of this thesis, we examine the preparation of a single-mode radiation field in arbitrary pure quantum states via resonant interaction with a sequence of two-level atoms. The preparation is achieved by choosing an appropriate (in general entangled) initial state of the atomic sequence, and does neither require a final state measurement of the atoms, nor a control of the atom-field interaction. Furthermore, the method is applicable also when starting from mixed initial field states. We show how to determine the optimal initial atomic state which prepares the desired field state with the maximum fidelity, and prove the feasibility of our state preparation method by numerical calculations.

In the second part, we demonstrate the noise-induced control of quantum jumps in a fundamental open quantum system. Here, in addition to the subsequent interaction with a flux of two-level atoms, the quantized field is also coupled to a thermal environment. Under certain experimental conditions, the photon field exhibits a bistable behavior, with quantum jumps between two metastable states. In the presence of a small periodic signal (i.e., a modulation of the initial state of the two-level atoms crossing the single-mode resonator), the best synchronization of these quantum jumps with the signal is achieved at an optimal, *nonvanishing* temperature of the environment. This stochastic resonance effect can be observed in different components of the atomic Bloch vector on exit from the cavity.

The third part treats a specific problem concerning the characterization of entanglement between two quantum mechanical two-level systems. We consider the optimal decomposition of a two-qubit state into an entangled and a separable part, with maximal weight of the latter, and derive necessary and sufficient conditions for the optimality of the decomposition.

This thesis emerged under the guidance of Andreas Buchleitner. I am very grateful to Andreas, who encouraged and supported me in the past few years. Gladly, I commemorate the collaboration with him, which was instructive and stimulating, not only from a physical point of view.

The work was carried out at the Max-Planck-Institute for Physics of Complex Systems in Dresden, and partly also at the Center for Theoretical Physics of the Polish Academy of Sciences in Warsaw. I want to thank Marek Kuś and Karol Życzkowski for many fruitful discussions, and their hospitality during my stay in Poland. I gratefully acknowledge generous support by the DAAD.

I am also grateful to Burkhard Kümmerner, with whom I shared illuminating discussions about some mathematical aspects of this thesis.

Last, but not least, I thank my colleagues Klaus Hornberger, Andreas Krug, Sandro Wimberger, Florian Mintert, Javier Madroñero, Peter Schlagheck, Cord Müller, Vyacheslav Shatokhin, Dima Dmitriev, Juyeon Yi, Nilüfer Baba, Ivo Håring, Christian Siedschlag, Tobias Schneider, Anatole Kenfack, Jim Hague, Nils Hasselmann, and others, for creating a truly international and friendly atmosphere in the institute, which was fun to work in.

Contents

1	Introduction	1
1.1	Background and formulation of the problem	1
1.2	Structure of the thesis	5
I	Quantum State Preparation via Asymptotic Completeness	7
2	Atom-field interaction	9
2.1	Single atom	9
2.2	Sequence of N atoms	13
2.2.1	Entanglement between field and atoms	14
2.2.2	Entanglement between the atoms	15
3	Asymptotic completeness	17
3.1	Scattering theory and quantum Markov chains	18
3.2	Definition of asymptotic completeness	20
3.3	Sufficient conditions for asymptotic completeness	21
3.3.1	Invariant states of the Jaynes-Cummings model	22
3.3.2	Time-reversal symmetry of the Jaynes-Cummings model	23
3.3.3	A preparation scheme based on the sufficient conditions	23
4	State preparation with a finite number of atoms	25
4.1	Maximum fidelity and optimal atomic state	25
4.2	Initial field state: vacuum	28
4.2.1	Conjecture	29
4.2.2	Optimal choice of the vacuum Rabi angle	32
4.2.3	How many atoms are needed?	34
4.3	Arbitrary initial field state	35
5	Numerical results	37
5.1	Test of the conjecture	38
5.1.1	Number states	38
5.1.2	Phase states	40
5.1.3	Coherent states	43
5.1.4	Randomly chosen target states	45
5.2	Properties of the optimal atomic states	50

5.2.1	Number states	51
5.2.2	Phase states	51
5.2.3	Coherent states	54
5.3	Mixed initial field states	57
5.4	Reaching the limit of asymptotic completeness	61
5.4.1	Convergence of the fidelity	61
5.4.2	Convergence of the optimal initial atomic state	66
5.4.3	Other initial atomic states than the optimal one	69
5.4.4	Independence from the initial field state	74
6	The influence of noise	77
6.1	Cavity dissipation	77
6.1.1	Decay of the fidelity of a field state	78
6.1.2	Influence of the decay upon the state preparation	80
6.2	Imperfect initial atomic state	85
6.3	Fluctuations of the vacuum Rabi angle	86
II	Noise-Assisted Control of Quantum Jumps	91
7	The coherently pumped micromaser	93
7.1	Experimental setup	94
7.2	Preparation and detection of the atoms	95
7.2.1	Coherent and incoherent pumping	95
7.2.2	Final state detection	95
7.3	Dynamics of the photon field	97
7.3.1	Master equation	98
7.3.2	Stationary state	99
8	Bistability of the maser dynamics	103
8.1	Quantum jumps of the maser field	103
8.2	Transition rates	105
8.2.1	Incoherent pumping	106
8.2.2	Coherent pumping	106
9	Stochastic resonance	113
9.1	Modulation of the initial atomic state	114
9.2	Optimal synchronization of the quantum jumps	115
9.3	Quantitative analysis of the synchronization effect	117
9.3.1	First harmonic - the stochastic resonance peak	118
9.3.2	Suppression of higher harmonics	120
III	Entanglement of mixed two-qubit states	123
10.1	Entanglement measures	125
10.2	Optimal Lewenstein-Sanpera decomposition	128
10.3	Does the optimal LSD yield a measure of entanglement?	131
10.4	Proof of Theorem 1	133

10.5 Proof of Theorem 2	138
11 Conclusion	141
A Some properties of $M^{(\rho_0)}$	145
B A small combinatorial lemma	151
C Quantum trajectories	153
D Two-qubit lemmata	157

Chapter 1

Introduction

1.1 Background and formulation of the problem

In the last few years, much progress has been achieved in controlling individual quantum systems. Since the beginning of the eighties, it is possible to perform experiments with single trapped atoms [1, 2, 3, 4, 5, 6], and recently the ability to transport single atoms over macroscopic distances has been demonstrated [7, 8]. Also the control of the internal quantum state of atoms or molecules is - to some extent - within the realm of current experimental techniques. In principle, this can be done by applying external *classical* fields, for example appropriately tailored sequences of laser pulses, such that the unitary evolution induced by the corresponding time-dependent Hamilton operator transfers the system from a well defined initial state to the desired target state [9, 10, 11, 12, 13]. Although, under very general conditions, mathematics ensures the existence of a suitable control field [14, 15], there are still enormous practical difficulties, especially for systems with many degrees of freedom (e.g., molecules consisting of more than two atoms): already the numerical computation of the solution may be intractable, let alone the experimental realization of the required control field, which usually needs a a very complicated spectral and temporal structure. Nevertheless, some success has been achieved: for example, coherent population transfer between different rotational levels of simple molecules [16], or between magnetic atomic sublevels [17] was demonstrated, coherent superpositions of atomic Rydberg states of a single electron can be produced in the laboratory [18, 19, 20], and the branching ratio of different products of chemical reactions can be controlled by an appropriate laser pulse [21].

However, a complete quantum state control, i.e., the ability to perform arbitrary unitary operations (as would be required, e.g., for quantum computing [22, 23]), is only possible for relatively simple systems. The most fundamental example is a two-level atom, where arbitrary rotations of the Bloch vector can be achieved by a classical electromagnetic field in resonance with the energy difference between the two atomic levels (e.g., chapter 15.3 in [24]). Another fundamental quantum system is the quantized harmonic oscillator, which is realized experimentally as the radiation field in a single-mode cavity. In analogy to the above mentioned examples of controlling atoms or molecules, we could try

to manipulate the quantum state of the photon field by coupling to a classical dipole. However, using the results of [14, 15], one easily verifies that in this case the specific commutation relations between the photon annihilation and creation operators a and a^\dagger prevent the preparation of arbitrary field states.*

The situation might improve if we let the photon field interact with another *quantum* system, for example with atoms, instead of a classical control system. Here, a fundamental difficulty arises, since the target and control system may (and in general will) become entangled with each other during their interaction. In the presence of entanglement, no well defined pure quantum states can be attributed to any of the two subsystems, what obviously prevents our purpose to prepare the photon field in an arbitrary pure quantum state. A possible way to circumvent this dilemma is to perform a measurement on the atoms, thereby projecting also the photon field onto a pure state [25, 26, 27]. Naturally, since the result of the measurement is not certain, the state preparation can then only succeed with a finite probability. Hence, if we want to achieve a deterministic state preparation, we have to look for a way to avoid the final atom-field entanglement. One possibility is to design an appropriate time-dependent cavity QED interaction which leads finally to an unentangled state of field and the control system, with the field in the desired target state [28, 29, 30, 31]. In spirit, the latter idea is similar to the method of semiclassical control mentioned above: the evolution of the atom-field system is controlled by the application of classical external fields which influence either directly the internal state of the atom, or the atom-field coupling strength.

An alternative idea is to use a *simple, time-independent* atom-field interaction, and to perform the control by choosing an appropriate initial state of the control system. This method requires the ability to prepare the control system in the appropriate initial state, which finally leads to the desired field state. A priori, it is not certain whether a suitable initial state of the control system exists. Indeed, if the Hilbert space of the control system is of finite dimension M_2 , the following simple argument suggests a negative answer: let us assume that we want to prepare an arbitrary field state $|\chi\rangle$ in a photon field subspace of finite dimension M_1 , starting from a well defined initial state $|\chi_0\rangle$ (e.g., the cavity vacuum). Then, the Hilbert space of all possible initial states $|\chi_0\rangle \otimes |\psi_0\rangle$ of the atoms-field system is of dimension M_2 , and likewise the space of the corresponding final states $|\Psi\rangle = U|\chi_0\rangle \otimes |\psi_0\rangle$, after the unitary interaction U . On the other hand, the space of the *desired* final states $|\chi\rangle \otimes |\psi\rangle$ (with arbitrary final atomic state $|\psi\rangle$) is also of dimension M_2 . Since, typically, two M_2 dimensional subspaces of a $M_1 \times M_2$ dimensional space do not intersect (if $M_1 > 2$), we do not expect that we can prepare arbitrary field states by using a finite dimensional control system. We may ask, however, if we can come close to the desired field state if we choose M_2 large enough.

This idea will be followed in the first part of this thesis. Here, we choose an

*The set of all unitary evolutions induced by a Hamiltonian of the form $H = \omega a^\dagger a + d(t)(a + a^\dagger)$ [where the scalar function $d(t)$ represents an arbitrarily time-dependent classical dipole] is the (four-dimensional) Lie group generated by the observables $a^\dagger a$, $a + a^\dagger$, $i(a - a^\dagger)$, and $\mathbb{1}$, which is but a subset of *all* unitary evolutions in the infinite-dimensional Hilbert space of the harmonic oscillator.

atoms-field interaction as simple as possible: the control system consists of a sequence of N two-level atoms that resonantly interact with the quantized field mode one after the other (each atom with the same time-of-flight through the cavity). We assume that we are able to prepare our control system in arbitrary states, possibly also including entanglement between the N atoms. Now, the question is: for an arbitrary desired target field state $|\chi\rangle$, does there exist an initial state of the N atoms, such that after the atoms have crossed the cavity, the field is in the state $|\chi\rangle$? As discussed above, we can expect a positive answer only in the limit $N \rightarrow \infty$ of infinitely many atoms interacting with the cavity field. Indeed, we will show that, in this limit, the *asymptotic completeness* [32] of the atoms-field interaction ensures the existence of such a state. Thereby, we are able to control the quantum state of the field, provided that we can control the state of the atoms, even without accessing the interaction Hamiltonian. In a similar vein, it was shown recently [33] that, given a fixed Hamiltonian acting on the joint Hilbert space of a quantum system and its controller, under certain conditions quantum operations such as state preparations, measurements and unitary implementations on the system can be performed by quantum operations on the controller only.

Furthermore, the asymptotic completeness also predicts that, again in the limit $N \rightarrow \infty$, the required initial atomic state is independent of the initial field state, i.e., the field can be prepared in the desired final state without knowing its initial state. In this case, the information about the initial field state is completely transferred to the exiting atoms. Note that the independence from the initial field state can only be achieved when using a quantum control system: a Hamiltonian evolution of the target system alone, as induced by a classical controller (in the absence of dissipation), will always retain the dependence on the initial state (i.e., initially orthogonal states will be mapped on orthogonal final states).

In the realistic case of a finite number N of atoms, however, the asymptotic completeness is not precisely realized. Then, the state preparation is not possible with perfect fidelity, and the optimal initial atomic state, which achieves the maximum fidelity, not only depends on the desired target state, but also on the initial field state. Nevertheless, as we will show, quite good results can be achieved with a not too large number of atoms: starting from the vacuum as initial field state, a fidelity of more than 99% can be achieved for the preparation of arbitrary field states including at most n photons by using $N = 2n$ atoms. Moreover, when increasing N , the fidelity reaches the ideal value 1 exponentially fast. In general, the number of atoms required for a given level of fidelity depends linearly on the maximum photon number of the target state. Hence, since the atomic Hilbert space is 2^N -dimensional, the dimension of the control system scales exponentially with the dimension of the target system. This is the price we have to pay in order to avoid the entanglement between atoms and field without controlling the interaction Hamiltonian.

Note that the preparation of the photon field in arbitrary *pure* quantum states requires the absence of any source of noise acting on the cavity field, which would reduce the purity of the field state. Hence, the influence of the dissipation induced by the coupling of the field to the cavity walls, or of other sources of

noise, such as fluctuations of the time-of-flight of the individual atoms through the cavity, should be kept as low as possible. For the same reason, we have to avoid any entanglement between the field and the exiting atoms: otherwise, a measurement on the exiting atoms and the associated state reduction of the atoms-field system would also constitute an unpredictable, random influence on the photon field (commonly termed ‘measurement noise’).

If we do not aim at a *perfect* quantum state control, however, some noise can also be helpful. The second part of this thesis is devoted to such a case. Here, we consider a modification of the above setup for the state preparation, which is experimentally more practical, but holds some inherent sources of noise: instead of a fixed finite number N of atoms, which must be entangled before the atoms-field interaction, in order to avoid finally the entanglement with the field, we have a steady flux of atoms, all entering the cavity in the same initial single-atom state. On exit from the cavity, the final state of each atom is measured, with the resulting measurement noise for the photon field, as discussed above. The other sources of noise are the dissipation due to the coupling of the field to the cavity walls (which can be neglected only for a small number of atoms interacting with the cavity field), and the random arrival times of the atoms.

The interplay between the interaction of the cavity field with the atoms on one hand (resulting in a positive energy transfer to the photon field, since the atoms enter the cavity mainly in the upper state), and with the heat bath on the other hand (resulting in a negative energy transfer), leads to a stationary state of the photon field far from thermal equilibrium. Under certain conditions, the stationary state may consist of two metastable states. Then, the photon field exhibits a *bistable* behavior, with transitions between those two states at random times. Since the time interval needed for one such transition is very short compared to the average residence times in the two states, and the transitions are - at least partly - triggered by the quantum mechanical measurement process on the exiting atoms, they have been termed ‘quantum jumps’ [34], although they do not occur instantaneously (as the quantum jumps between atomic energy eigenstates postulated by Bohr [35], and experimentally observed, e.g., in [3, 4, 5]), but rather involve several subsequent atomic detection events. The *average* residence times in the two metastable states may be controlled by experimentally accessible parameters, for example by changing the temperature of the heat bath or the initial state in which the two-level atoms enter the cavity. Nevertheless, each *individual* quantum jump occurs at a random, unpredictable time. The regularity of the quantum jumps may be enhanced, however, by a small external signal, for example a periodic modulation of the complex amplitudes $a(t)$ and $b(t)$ which define the initial state of an atom entering the cavity at time t . If we now vary the strength of the noise by increasing the temperature of the heat bath, we observe the optimal synchronization of the quantum jumps with the small periodic signal (which in itself is not strong enough to drive the system deterministically from one metastable state to the other) at a *finite, nonvanishing* temperature. Thereby, an improved control over the quantum jumps of the photon field can be achieved by adding some noise to the system.

This cooperative effect between noise and a small periodic signal is known as

stochastic resonance [36, 37], and has been extensively studied in many physical, biological, and chemical systems [38-50]. Also the quantum regime has been addressed [51-56], which provides additional transitions mechanisms between the two metastable states, such as quantum tunneling, or - as in our example - the noise associated with the quantum mechanical measurement process. Furthermore, quantum mechanics allows us to prepare the atoms in coherent superpositions of the upper and lower state before they enter the cavity, and also to measure them in different final states after exit from the cavity. We are therefore especially interested to investigate the influence of an injected or measured atomic coherence on the stochastic resonance effect.

The third part of the thesis, finally, is devoted to the description of entanglement in bipartite mixed quantum systems. Apart from the fact that entanglement plays an important role in the two above quantum control schemes, as discussed above, this third part has no direct connection to the first two parts. Specifically, we consider the optimal decomposition of an entangled two-qubit state of full rank into a sum of an entangled and a mixed state, with maximal weight of the latter, and prove sufficient and necessary conditions for the optimality of the decomposition.

1.2 Structure of the thesis

The thesis is divided into three parts. In **part I**, we study the preparation of quantum states of the photon field using a sequence of two-level atoms.

To start with, **chapter 2** introduces the atoms-field interaction (according to the Jaynes-Cummings model) which will be used throughout the whole thesis, and discusses its relevant properties for the state preparation.

In **chapter 3**, we show that the interaction fulfills the property of asymptotic completeness, and how this property enables us - in the limit of infinitely many atoms - to prepare the photon field in arbitrary quantum states, irrespective of the initial field state.

With a finite number of atoms, however, only a finite fidelity of the state preparation can be achieved. **Chapter 4** shows how to calculate the optimal initial atomic state which reaches the maximum fidelity. The time-reversal symmetry of the atoms-field interaction supplies us with an estimation of the optimal atomic state and the number of atoms needed to reach a given level of fidelity.

In **chapter 5**, the feasibility of our state preparation method is demonstrated by numerical calculations. Considering both the vacuum and mixed states as initial field states and various different final field states, we test the validity of the above estimation, and examine some properties of the required initial atomic states. Furthermore, we also study the convergence of our state preparation scheme towards the limit of asymptotic completeness.

Chapter 6 examines the stability of our state preparation method against various sources of noise. In particular, it is shown that the effect of cavity dissipation cannot be diminished by choosing a different initial atomic state.

Part II is devoted to the control of quantum jumps in an open quantum

system. In contrast to the first part, here noise plays an essential role and actually may help us to control the state of the photon field.

In **chapter 7**, we introduce the coherently pumped micromaser, which is a modification of the setup used in part I for the state preparation. We derive the master equation describing the dynamics of the photon field. Under certain conditions, the stationary state of the photon field is a mixture of two well-separated metastable states.

As demonstrated in **chapter 8**, this leads to a bistable behavior of the photon field in a single realization of the maser dynamics, if the final state of the exiting atoms is measured. We show how to determine the rates of the quantum jumps of the photon field between the two metastable states, and discuss the influence of an injected atomic coherence, and of different measurement schemes.

In **chapter 9**, we feed a small periodic signal into the maser by modulation of the initial atomic state. According to the mechanism of stochastic resonance, we demonstrate the best synchronization of the quantum jumps with this signal at an optimal nonvanishing temperature of the environment. This effect can be observed in different components of the atomic Bloch vector of the exiting atoms.

Finally, **part III** is devoted to the characterization of entangled states. After giving a brief introduction to the quantitative description of entanglement, we present and prove new results on the best separable approximation of an arbitrary entangled two-qubit state of full rank.

Chapter 11 concludes the thesis, and briefly addresses some open questions.

Part I

Quantum State Preparation via Asymptotic Completeness

Chapter 2

Atom-field interaction

The first part of this thesis treats the preparation of arbitrary quantum states of a single mode electromagnetic field via interaction with a sequence of two-level atoms. As described in the introduction, we want to achieve the preparation only by the right choice of the (possibly entangled) initial state of the atoms, without performing any final state measurement on the atoms, nor controlling the interaction Hamiltonian between atoms and field.

Consequently, we choose the atoms-field interaction as simple as possible: the atoms cross the cavity, which confines the photon field, one after the other, and the interaction of each single atom with the photon field is given by the same unitary operator. As for the latter, we consider a resonant interaction according to the Jaynes-Cummings model [57, 58], which can be regarded as the simplest model of the interaction a single atom and the quantized radiation field.

The thereby defined atoms-field interaction describes the physical system which will be studied throughout the first two parts of this thesis. Its most important properties are summarized in this chapter, with emphasis put on the aspects relevant for the state preparation.

2.1 Single atom

As the basic element of our atoms-field interaction, let us first examine the interaction of the field with a *single* atom. We assume that the atom interacts with the field resonantly: the energy difference between the two atomic energy eigenstates equals the energy of a single photon of the cavity mode, or, in other terms, a single quantum in the excitation of the harmonic oscillator represented by the quantized field mode. Then, each atom can exchange at most one photon with the field, and, according to the Jaynes-Cummings model [57, 58], the interaction is described by the following unitary operator (in the rotating wave

approximation, see, e.g., chapter 14.1 in [59]):*

$$U = e^{-i\phi(a^\dagger\sigma + a\sigma^\dagger)}. \quad (2.1)$$

Here, a , a^\dagger are the photon annihilation/creation operators, and $\sigma = |d\rangle\langle u|$, $\sigma^\dagger = |u\rangle\langle d|$ the ladder operators for the two-level atom, with upper and lower level $|u\rangle$ and $|d\rangle$, respectively. The parameter $\phi = gt_{\text{int}}$ is the vacuum Rabi angle, where t_{int} denotes the time-of-flight of the atom through the cavity, and g quantifies the strength of the atom-field coupling.

If the cavity is initially in a number state $|n\rangle$, and the atom enters the cavity in either $|u\rangle$ or $|d\rangle$, then the interaction has the following effect:

$$U|n\rangle \otimes |u\rangle = \cos(\phi\sqrt{n+1}) |n\rangle \otimes |u\rangle - i \sin(\phi\sqrt{n+1}) |n+1\rangle \otimes |d\rangle, \quad (2.2)$$

$$U|n\rangle \otimes |d\rangle = \cos(\phi\sqrt{n}) |n\rangle \otimes |d\rangle - i \sin(\phi\sqrt{n}) |n-1\rangle \otimes |u\rangle. \quad (2.3)$$

Since the states $|n\rangle \otimes |u\rangle$ and $|n\rangle \otimes |d\rangle$, $n = 0, 1, 2, \dots$, form a complete basis of the Hilbert space of field and atom, Eqs. (2.2,2.3) give the complete solution of the Jaynes-Cummings interaction. Its properties have been thoroughly investigated, among them the so-called ‘Cummings collapse’ [58, 60, 61] and ‘revivals’ [62]. As being relevant for the state preparation, let us mention here the following particular features of the Jaynes-Cummings dynamics:

- *Rabi oscillations:* during the interaction, atom and field oscillate between the states $|n\rangle \otimes |u\rangle$ and $|n+1\rangle \otimes |d\rangle$, with the Rabi frequency $\Omega_n = g\sqrt{n+1}$. (An example is shown in Fig. 2.1a, see below.) Consequently, the probability that an atom entering the cavity (with n photons inside) in the state $|u\rangle$ (or $|d\rangle$) emits (or absorbs) a photon in the cavity, is given by $|B_{n+1}|^2 = \sin^2(\phi\sqrt{n+1})$ (or by $|B_n|^2$).
- *Trapping states:* if ϕ fulfills a $|n_t\rangle$ -trapping state condition [63, 64], i.e., $\phi = k\pi/\sqrt{n_t+1}$, with $k \in \mathbb{Z}$, then $|B_{n_t+1}|^2 = 0$, that is, there is no way of transferring any photon number population from n_t to n_t+1 , or vice versa. Hence, if we want to prepare field states including photon numbers higher than n , we must avoid $|n_t\rangle$ -trapping states with $n_t \leq n$ through a proper choice of the vacuum Rabi angle ϕ .
- *Conservation of H_0 :* the Jaynes-Cummings interaction Hamiltonian $H_{\text{int}} \propto a\sigma^\dagger + a^\dagger\sigma$ commutes with the free Hamiltonian $H_0 \propto a^\dagger a + \sigma^\dagger\sigma$ of atom and field (see also footnote *). Consequently, an eigenstate of H_0 will remain an eigenstate of H_0 during the interaction (2.1). As we will see later (chapter 4 and 5), this property simplifies the theoretical treatment of the preparation of photon number states (i.e., eigenstates of the photon number $a^\dagger a$).

*For simplicity, we do not explicitly take into account the free evolution of atom and field. In the case of resonance between atom and field, the free Hamiltonian $H_0 = \hbar\omega(a^\dagger a + \sigma^\dagger\sigma)$ commutes with the interaction Hamiltonian $H_{\text{int}} = \hbar g(a^\dagger\sigma + a\sigma^\dagger)$. Consequently, the free evolution causes only additional phase factors (of the same frequency ω for both atom and field) which are independent of the interaction.

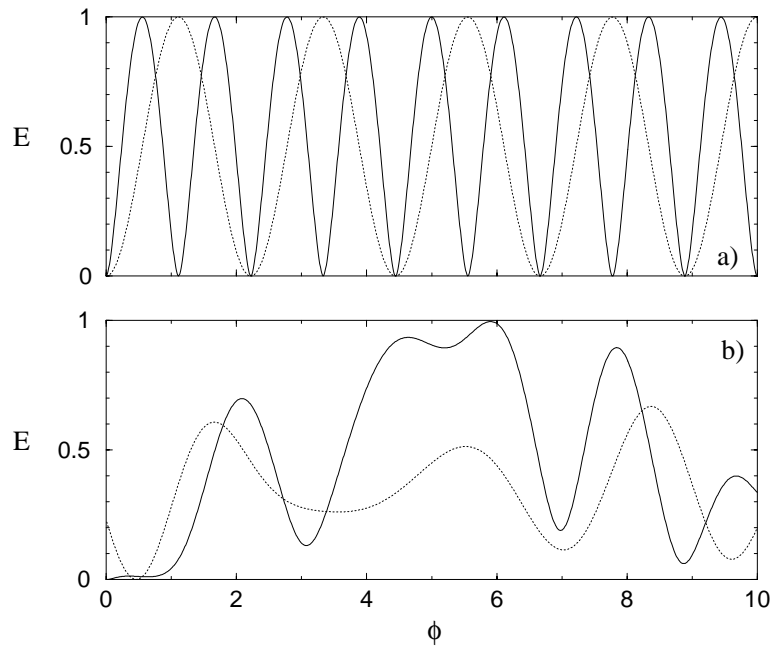


Figure 2.1: Entropy of entanglement E [see Eq. (2.8)] between the field and a single atom (solid line) and upper state population of the atom (dotted line) during the Jaynes-Cummings interaction (2.1). The initial states of field and atom are: (a) the 2-photon state, $|\chi_0\rangle = |2\rangle$, and the atom in the lower state, $|\psi_0\rangle = |d\rangle$, and (b) the coherent state $|\chi_0\rangle = |\alpha\rangle$, $\alpha = 1$, and $|\psi_0\rangle = i 0.480 |u\rangle + 0.877 |d\rangle$. Fig. 2.1(a) demonstrates the Rabi oscillations between the states $|2\rangle \otimes |d\rangle$ and $|1\rangle \otimes |u\rangle$ of field and atom, whereas the dynamics is more complicated in (b). Notice that atom and field hardly entangle in (b), for $\phi < 1$.

- Obviously, atom and field are in general *entangled* after the interaction. As pointed out in the introduction, this is a major problem for the preparation of pure field states. Although, in exceptional cases, atom and field can finally be again in a product state (e.g., if the field starts in a number state $|n\rangle$, the atom in state $|u\rangle$, and $\phi = (k + 1/2)\pi/\sqrt{n + 1}$, $k \in \mathbb{Z}$, corresponding to a full Rabi cycle; see also [65] for other, nontrivial examples), this is certainly not the case for arbitrary field states and a fixed vacuum Rabi angle ϕ . However, as we will see later, the situation changes if we consider the interaction with several atoms.

Two examples

In order to illustrate the points listed above, we present two examples in Fig. 2.1. We plotted the entanglement between atom and field and the upper state population of the atom during the Jaynes-Cummings interaction (2.1), as a function of the vacuum Rabi angle $\phi = g t_{\text{int}}$. As a quantitative measure of the atom-field entanglement, we use the entropy of entanglement [66], see Eq. (2.8) below. The first case (a), where the initial states of field and atom are the 2-photon Fock

state, $|\chi_0\rangle = |2\rangle$, and the atom's lower state, $|\psi_0\rangle = |d\rangle$, respectively, demonstrates the Rabi oscillation between the states $|2, d\rangle$ and $|1, u\rangle$, i.e., between vanishing and maximal upper state population of the atom. The values of ϕ (parameterized by the coupling constant g and/or the interaction time t_{int}) with vanishing upper state population fulfill the $|2\rangle$ -trapping state condition. Since the atom is then described by the pure state $|d\rangle$, also the entanglement between atom and field vanishes at those points, and likewise if the upper state population equals 1. In contrast, field and atom are maximally entangled whenever upper and lower state are equally populated.

In Fig. 2.1(b), the field is initially in a coherent state $|\chi_0\rangle = |\alpha\rangle$ [67] with mean photon number $|\alpha|^2 = 1$, and the atom in the state $|\psi_0\rangle = i 0.480 |u\rangle + 0.877 |d\rangle$. (The reason for this special choice of the atomic initial state will be clarified further down in this section.) Since the field state $|\alpha\rangle$ is a coherent superposition of different photon number states, and since the frequency of the Rabi oscillations depends on the photon number, the dynamics is now described by the corresponding superposition of Rabi cycles with different frequencies, what leads to a more complicated behavior than in Fig. 2.1(a). Remarkably, atom and field *hardly entangle* for not too large vacuum Rabi angles $\phi < 1$. Furthermore, we have found that, in this regime, the consequently almost pure field state (remember that we assume the absence of noise or environment coupling in this chapter) is in fact, like the initial field state, also *almost a coherent state* $|\alpha'\rangle$ (i.e., its expectation value with respect to $|\alpha'\rangle$ is almost 1). Due to energy conservation, its mean photon number $|\alpha'|^2$ can be deduced from the atom's upper state population. As we have confirmed by some numerical tests, this seems to be a general property of the Jaynes-Cummings interaction: if the field is initially in a coherent state, one always finds an initial atomic state (like the state $|\psi_0\rangle$ in Fig. 2.1b), such that the field will stay very close to a coherent state $|\alpha(t)\rangle$ during the atom-field interaction, if ϕ is not too large. The *smaller* the amplitude $|\alpha|^2$ of the initial state, the longer is the time during which a large overlap of the field state with a coherent state can be maintained. In chapter 5.2 we will see that this property of the Jaynes-Cummings interaction allows an efficient preparation of coherent states.

In order to avoid confusion, let us mention here also the following semiclassical limit of the Jaynes-Cummings interaction. Also there, for initial coherent field states $|\alpha\rangle$ with *large* $|\alpha|^2$, and the initial atomic states $(|u\rangle \pm |d\rangle)/\sqrt{2}$ (if α is real), atom and field also *hardly entangle* during the interaction [68]. In contrast to the situation illustrated in Fig. 2.1(b), for a classical field the disentanglement is preserved also at long interaction times, and the field does not stay in a coherent state, but rather becomes squeezed in a way which leaves the mean photon number constant. Consequently, also the atom's upper state population remains constant. (Only the phase of the atomic state rotates with frequency $g/2|\alpha|$ [68]).

2.2 Sequence of N atoms

Since a single atom can at most exchange one photon with the photon field, we need obviously more than one atom in order to prepare the field in an arbitrary state. We assume that the atoms cross the cavity one after the other, so that at most one atom is present in the cavity at any time. For simplicity, the time of flight t_{int} through the cavity is taken to be constant for each individual atom. Under these circumstances, the total interaction U_N of the field with a sequence of N atoms is a product of identical single-atom interactions:[†]

$$U_N = U^{(N)}U^{(N-1)} \dots U^{(1)}, \quad (2.4)$$

where $U^{(i)}$ denotes the interaction of the field with the i -th atom as given by Eq. (2.1). The above interaction is very similar to the one of the micromaser [69]. However, only the case where the incoming atoms enter the cavity in a product of single-atom states has so far been experimentally realized, whereas we will consider entangled initial atomic states in the following. Furthermore, the standard theoretical description of the micromaser [70] deals with a steady flux of atoms through the cavity. Then, the dissipation of the cavity field cannot be neglected - in contrast to the above case of a finite number N of atoms, where the total interaction time is very much shorter than the cavity decay time (if N is not too large), see chapter 6.1. In the presence of dissipation, the maser dynamics is described by a master equation rather than a unitary interaction like Eq. (2.4). The standard treatment of the micromaser will become relevant in the second part of the thesis, see chapter 7.

The above unitary operator U_N maps the initial state of field and atoms (i.e., the state just before the first atom enters the cavity) onto their final state (i.e., just after the last atom has left the cavity). We assume that the cavity field is initially not entangled with the atoms, the latter being prepared in a pure state $|\psi_0\rangle$, which - as already mentioned above - may exhibit entanglement between different atoms. For simplicity, let us first assume that also the field starts in some pure initial state $|\chi_0\rangle$, e.g., the cavity vacuum. (Later, the requirement of a pure field state will be dropped: the state preparation is possible also for mixed initial field states.) Then, application of the interaction operator U_N ,

$$U_N|\chi_0\rangle \otimes |\psi_0\rangle = |\Psi\rangle, \quad (2.5)$$

yields the final state $|\Psi\rangle$, which - typically - will be an entangled state. We come back to this point below.

Due to the structure of U_N as a product of single-atom operators, the properties of the Jaynes-Cummings interaction with a single atom, discussed in the previous section, remain valid in the case of N atoms. In particular, if ϕ fulfills a trapping state condition, we cannot circumvent the barrier at the corresponding photon number n_t by choosing a suitably entangled state of the N atoms:

[†]The free evolution of atoms and field between subsequent atoms need not explicitly be taken into account, compare the footnote on page 10. Since dissipation is neglected, the arrival times of the individual atoms are therefore irrelevant (as long as there is at most one atom present in the cavity at the same time).

the transition from n_t to $n_t + 1$ photons is equally forbidden for each individual atom (since ϕ is constant), and, due to the linearity of quantum mechanics, entangling the atoms cannot help us to cross the barrier (since, obviously, any entangled state can be written as a superposition of product states).

Also the conservation of the free Hamiltonian $H_0 = a^\dagger a + \sum_i \sigma_i^\dagger \sigma_i$ (in units of ω) still applies, i.e., an eigenstate of H_0 will remain an eigenstate of H_0 after the atoms-field interaction. The atomic part $\sum_i \sigma_i^\dagger \sigma_i$ of H_0 counts the number of atoms in the upper state $|u\rangle$ and will therefore be called ‘atomic excitation number’. From the conservation of H_0 , it follows that, if the field is initially in a number state $|n\rangle$ and the atoms in a state $|\psi\rangle$ with excitation number k , the final atomic state obtained by projecting the field onto the number state $|n'\rangle$ after the interaction U_N also has a well defined excitation number, namely $k' = k + n - n'$, i.e.:

$$\text{if } \sum_{i=1}^N \sigma_i^\dagger \sigma_i |\psi\rangle = k |\psi\rangle, \text{ and } |\psi'\rangle = \langle n' | U_N | n, \psi \rangle,$$

$$\text{then } \sum_{i=1}^N \sigma_i^\dagger \sigma_i |\psi'\rangle = (k + n - n') |\psi'\rangle. \quad (2.6)$$

In the following, we will refer to Eq. (2.6) as ‘excitation number conservation’, or simply ‘energy conservation’.

However, for $N > 1$, all considerations about the final atom-field entanglement are complicated by the fact that the atoms may initially be entangled between themselves. As soon as the first atom interacts with the cavity field, the field will then be entangled also with the other atoms, already before they have entered the cavity. Hence, by choosing an appropriately entangled initial atomic state, we are able to influence the final entanglement of $|\Psi\rangle$ between field and atoms, and maybe even achieve an unentangled final state. The question is: given any desired field state $|\chi\rangle$ (which may be an arbitrary quantum state of the harmonic oscillator), is it possible, by choosing an appropriate initial atomic state $|\psi_0\rangle$, to generate an unentangled final state

$$|\Psi\rangle = |\chi\rangle \otimes |\psi\rangle ? \quad (2.7)$$

As we will see below, this is indeed possible, if we admit an infinite number N of atoms interacting with the cavity field. Moreover, in this limit, the required initial atomic state $|\psi_0\rangle$ is independent of the initial field state $|\chi_0\rangle$. The mathematical reason behind the ability to prepare arbitrary field states, independently of $|\chi_0\rangle$, is the property of asymptotic completeness, which we will explain in the next chapter.

Before that, however, we want to close this chapter with some technical remarks about the quantitative description of entanglement.

2.2.1 Entanglement between field and atoms

At first, we will define the measure of the entanglement between field and atoms which we have used in Fig. 2.1 (for a single atom, $N = 1$). Here, we are dealing

with a bipartite quantum system, consisting of the photon field on the one hand and of the atoms on the other hand. To simplify matters, we will consider only pure states of the atoms-field system. (The entanglement properties of *mixed* states will be discussed in part III, for the simplest case of a system composed of two two-level systems.) This is the case if field and atoms are *initially* in a pure state, since we assume a unitary evolution (2.4) of atoms and field (without coupling to an environment). For pure states of bipartite quantum systems, however, there exists a unique measure of entanglement [71, 72], namely the entropy of entanglement [66]. It is given in terms of the atoms' reduced state ρ , i.e., the state which is obtained if we look at the atoms alone and average over the field by taking the partial trace. [Equivalently, we could also consider the reduced *field* state by tracing over the atoms, without modifying the following Eq. (2.8).] Then, the entropy of entanglement is defined as the von-Neumann entropy S of the reduced state:

$$E = S(\rho) = -\text{Tr}\{\rho \log_{2^N}(\rho)\}. \quad (2.8)$$

The basis 2^N of the logarithm is required to normalize the maximum value $S_{\max} = 1$ of the entropy, which is assumed if ρ is proportional to the identity in the 2^N -dimensional atomic space (the so-called 'maximally mixed' state). In the general case of a $M_1 \times M_2$ -dimensional quantum system, the logarithm has to be taken with respect to the basis M_1 if $M_1 \leq M_2$, or M_2 otherwise. (In our present case, the field is infinite-dimensional, i.e., $M_1 = \infty$, whereas $M_2 = 2^N$.)

The interpretation of the measure (2.8) is as follows: since the state of the total system is completely known (as a pure state), any loss of knowledge about the states of the subsystems (as quantified, e.g., by the von-Neumann entropy) must be due to quantum correlations, or entanglement, between the two subsystems.

2.2.2 Entanglement between the atoms

Remember that, since we want to prepare the field in a pure state, the entanglement between field and atoms should finally vanish. As discussed above, we need (in general) an entangled initial atomic state for this purpose. In chapter 5.2, we will examine some entanglement properties of the required atomic states. The quantitative description of the entanglement between the atoms, however, is complicated by the fact that we are dealing with a many-particle system. Even for pure states, a unique way of quantifying entanglement by a single number between many particles does not exist [73, 74, 75, 76, 77]. For example, we can look at the degree of entanglement between the first and second atom, or between the third and fourth atom, which may be very different. Hence, one scalar quantity is not sufficient for a complete characterization of many-particle entanglement. At present, it is still unclear (to our knowledge) how many independent quantities (i.e., invariants under local[‡] unitary transformations [78]) would be needed. However, we do not intend to go into further details of this complicated issue, but rather look for a simple way to

[‡]Here, 'local' means: acting only on one single particle.

find out whether some entanglement between the N atoms injected into the cavity is present. For this purpose, we consider the reduced density matrix of each individual atom

$$\rho_i = \text{tr}_{j \neq i}(|\psi_0\rangle\langle\psi_0|), \quad i = 1, \dots, N. \quad (2.9)$$

Here, the partial trace is taken over all the other atoms, $j \neq i$. According to Eq. (2.8), the entropy of ρ_i quantifies how much the i -th atom is entangled with the other ones. Instead of the entropy, however, we prefer to use the largest eigenvalue $p_i \geq \frac{1}{2}$ of ρ_i , which is a monotonously decreasing function of the von-Neumann entropy [i.e., $S(\rho_i) = -p_i \log(p_i) - (1-p_i) \log(1-p_i)$][§], and therefore also provides a good measure of entanglement. The reason for this choice is the following additional property of p_i : it gives an upper bound for the overlap of $|\psi_0\rangle$ with any product state of the N atoms, as can be easily seen as follows:

$$\begin{aligned} |\langle\psi_0|\psi^{(1)}, \dots, \psi^{(N)}\rangle|^2 &\leq \sum_{\substack{k_j=u,d \\ j \neq i}} |\langle\psi_0|k_1, \dots, k_{i-1}, \psi^{(i)}, k_{i+1}, \dots, k_N\rangle|^2 = \\ &= \langle\psi^{(i)}|\rho_i|\psi^{(i)}\rangle \leq p_i. \end{aligned} \quad (2.10)$$

Here, the sum is over a complete basis of the remaining atoms, $j \neq i$, which is nothing else than the partial trace in Eq. (2.9). Since Eq. (2.10) is valid for each i , the smallest one of the p_i 's gives us the tightest upper bound (among the different p_i 's) for the overlap with a product state. Conversely, if all the p_i 's are close to 1, then the state $|\psi_0\rangle$ is close to a product state.[¶] Let us note, however, that the N quantities p_i do not *completely* describe the entanglement properties of $|\psi_0\rangle$. For example, the two states

$$\left(\underbrace{|u\rangle \otimes |u\rangle \otimes \dots \otimes |u\rangle}_N + \underbrace{|d\rangle \otimes |d\rangle \otimes \dots \otimes |d\rangle}_N \right) / \sqrt{2} \quad (2.11)$$

(sometimes called a ‘N-particle cat state’) and

$$\frac{1}{\sqrt{2}} \left(|u\rangle \otimes |u\rangle + |d\rangle \otimes |d\rangle \right) \otimes \dots \otimes \frac{1}{\sqrt{2}} \left(|u\rangle \otimes |u\rangle + |d\rangle \otimes |d\rangle \right) \quad (2.12)$$

are not distinguished by the p_i 's. Although in both cases $p_i = 1/2$ for each i , i.e., each atom is maximally entangled with the other ones, in the second state (2.12), which is a product of two-particle states, the atom is entangled only with one neighboring atom, whereas the first case (2.11) exhibits true N -particle entanglement.

[§]Proof: $dS/dp_i = -\log(p_i) + \log(1-p_i) < 0$ for $p_i > \frac{1}{2}$ (which is always the case in a two-level system).

[¶]We believe that also a *lower* bound for the maximum overlap of $|\psi_0\rangle$ with a product state in terms of the p_i 's can be derived, e.g., something like $|\langle\psi_0|\psi^{(1)}, \dots, \psi^{(N)}\rangle|^2 \geq p_1 \dots p_N$, or $\geq \sum_i p_i - (N-1)$, but so far could not demonstrate it explicitly.

Chapter 3

Asymptotic completeness

In this chapter, we define the concept of asymptotic completeness [32, 79], and show that the atoms-field interaction introduced in the previous chapter, Eqs. (2.1, 2.4), fulfills this property. As we will see, this allows - in the limit $N \rightarrow \infty$ of infinitely many atoms interacting with the field - to prepare the field in an arbitrary desired quantum state $|\chi\rangle$, i.e., the field-atoms system in a factoring state $|\chi\rangle \otimes |\psi\rangle$. Moreover, in this limit, the required initial atomic state $|\psi_0\rangle$ does not depend on the initial state of the field.

Originally, asymptotic completeness is an important concept in scattering theory, where it is required for defining the central object of interest, the scattering transformation. As we will try to explain in the following chapter 3.1, also our atoms-field interaction, Eqs. (2.1,2.4), can be, in some sense, viewed as a scattering process. This will serve as a motivation for the definition of asymptotic completeness of quantum Markov chains in chapter 3.2, where also its consequences for the state preparation will be examined.

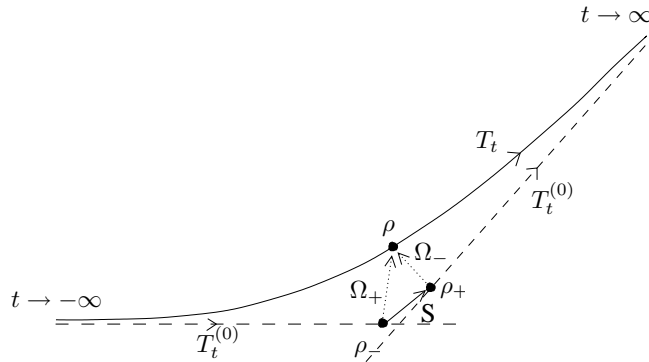


Figure 3.1: A scattering process is called *asymptotically complete*, if every state which is asymptotically free in the distant past ($t \rightarrow -\infty$), will again be asymptotically free in the distant future ($t \rightarrow \infty$) [79].

3.1 Scattering theory and quantum Markov chains

We start by giving a very brief summary of the basic concepts in scattering theory, following the introductory chapter of [79]. Generally, the purpose of scattering theory is to establish a relation between certain states of interacting systems, namely those which are asymptotically free in the distant past or future. An essential prerequisite is the existence and uniqueness of scattering states, which allow the definition of the Møller operators Ω_{\pm} as follows: if T_t denotes the time evolution in the presence of the interaction, and $T_t^{(0)}$ the free evolution, then $\Omega_{\pm} = \lim_{t \rightarrow \mp\infty} T_{-t} T_t^{(0)}$. Those operators map the incoming (or outgoing) free states ρ_- (or ρ_+) onto the corresponding interacting scattering states $\rho = \Omega_+ \rho_-$ (or $\rho = \Omega_- \rho_+$, respectively). The next step would be to obtain the scattering transformation $S = (\Omega_-)^{-1} \Omega_+$, which maps the incoming onto the outgoing free states, see Fig. 3.1. Obviously, this is only possible (as a bijective transformation) if the range of Ω_+ equals the range of Ω_- . This property is called ‘weak *asymptotic completeness*’.* In other words, asymptotic completeness requires that every state which is asymptotically free in the distant past, will again be asymptotically free in the distant future.

The above construction of the scattering transformation is quite general and applies both for classical and quantum systems. In [32], the authors make a further step, and introduce concepts known from scattering theory into the theory of quantum Markov chains. In general, a quantum Markov chain can roughly be described as follows (see, e.g., [80] for more details): a quantum system \mathcal{A} interacts subsequently with an infinite sequence of identical other quantum systems \mathcal{C} , as visualized by the following picture:

$$\begin{array}{c} \dots \otimes \mathcal{C} \otimes \mathcal{C} \otimes \dots \\ \left. \begin{array}{c} \mathcal{A} \\ \otimes \\ \mathcal{C} \end{array} \right\} U \\ \xrightarrow{S} \dots \otimes \mathcal{C} \otimes \dots \end{array}$$

The shift operator S moves the sequence one step to the right so that the next \mathcal{C} may interact with \mathcal{A} via the unitary interaction operator U . Obviously, the atoms-field interaction (2.4) described in the previous chapter is very similar to the above picture of a quantum Markov chain: here, \mathcal{A} represents the quantized field mode, whereas the \mathcal{C} ’s are the two-level atoms. In order to complete the agreement, we have to clarify the role of the shift operator in Eq. (2.4): if U denotes the interaction (2.1) with a fixed single atom (formally the ‘zero-th’ atom), then the interaction with the i -th atom reads $U^{(i)} = S^{-i} U S^i$. Consequently, the interaction operator $U_N = U^{(N)} \dots U^{(1)}$, Eq. (2.4), can also be written as

$$U_N = S^{-N} (U S)^N. \quad (3.1)$$

Hence, the definition of U_N implies that after the interaction $(U S)^N$ with N atoms, the whole atomic sequence is shifted back again via S^{-N} to its original

*The property ‘asymptotic completeness’ additionally requires that the range of Ω_+ (or Ω_-) covers all states of the interacting system which do not remain bound.

position. This may remind us of the definition of the Møller operators, as will be further discussed below.

The name ‘Markov chain’ can be justified as follows: for any chain of the above described form, the time evolution of the field fulfills the Markov property, i.e., its state at all future times can be calculated if we only know its present state at time t . Reversely, every Markovian evolution of the field can be represented by a quantum Markov chain. (A stationary Markov process, which is invariant under arbitrary time shifts, is obtained if all atoms enter the cavity in the same initial state.)

We are now ready to apply the concepts of scattering theory outlined above to our quantum Markov chain. Here, the number N of atoms having crossed the cavity takes the role of the time t , whereas the free evolution corresponds to the shift S . Hence, the evolution of the interacting system reads $T_N = (US)^N$, and the free evolution $T_N^{(0)} = S^N$. Now, one might think of defining the Møller operators in the same way as above: $\Omega_+ = \lim_{N \rightarrow -\infty} T_{-N} T_N^{(0)} = \lim_{N \rightarrow -\infty} (U_N)^{-1}$, according to Eq. (3.1), and likewise $\Omega_- = \lim_{N \rightarrow \infty} (U_N)^{-1}$. However, these expressions are mathematically not well defined.[†] The situation changes if we switch into the Heisenberg picture, where the operators acting on atoms and field evolve in time. Then, the evolution $U_N^\dagger O U_N$ of an arbitrary operator O can be properly defined also in the limit $N \rightarrow \infty$ [81]. In analogy to the above notion of asymptotic completeness, saying that every scattering state will be asymptotically free for $t \rightarrow \infty$, the authors of [32] introduced the following definition: the atoms-field interaction is asymptotically complete if - in the limit $N \rightarrow \infty$ of infinitely many atoms interacting with the photon field - every operator evolves ‘freely’, i.e., such as if there was no interaction between atoms and field. This is the case if the operator $U_N^\dagger O U_N$ restricted onto the field and the incoming atoms (i.e., those which have not yet interacted with the field)[‡] approaches the identity operator if $N \rightarrow \infty$ (since then, due to $U^\dagger \mathbb{1} U = \mathbb{1}$, the interaction of all the following incoming atoms with the field will have no effect). Due to the property of any operator O acting on an infinite tensor product, namely that O may differ from the identity only on finitely many atoms[†], this is again the case if only any *field* operator $O = A \otimes \mathbb{1}$ turns into an operator acting only on the outgoing atoms. Thereby, we have arrived at the following

[†]Operators on an infinite tensor product $\mathcal{C} \otimes \mathcal{C} \otimes \dots$ can only be properly defined if we require that every operator can be arbitrarily well approximated by an operator which differs from the identity only on finitely many \mathcal{C} 's [81]. Since $U \neq \mathbb{1}$ acting on \mathcal{C} , this is obviously not fulfilled by objects like $\lim_{N \rightarrow \pm\infty} U_N$ or $\lim_{N \rightarrow \pm\infty} (U_N)^{-1}$.

[‡]Note that, when changing from the Schrödinger to the Heisenberg picture, the role of incoming and outgoing atoms is exchanged: when evaluating the operator $U_N^\dagger O U_N = U^{(1)\dagger} \dots U^{(N)\dagger} O U^{(N)} \dots U^{(1)}$ after interaction with N atoms, see Eq. (2.4), we first have to apply the interaction $U^{(N)}$ with the *last* atom onto the operator O . In this sense, time is reversed in the Heisenberg picture.

3.2 Definition of asymptotic completeness

Asymptotic completeness is a property of the asymptotic behavior of the atoms-field interaction in the limit of infinitely many atoms. It is defined as follows:[§]

Every observable A of the photon field develops (in the Heisenberg picture) into an observable M_A of the atoms:

$$\lim_{N \rightarrow \infty} U_N^\dagger (A \otimes \mathbb{1}) U_N = \mathbb{1} \otimes M_A. \quad (3.2)$$

Here, U_N denotes the unitary interaction of the field with N subsequent atoms, see Eq. (2.4). In particular, asymptotic completeness is fulfilled by the Jaynes-Cummings interaction (2.2,2.3) - at least if the vacuum Rabi angle ϕ (which, remember!, is assumed to be constant for each single atom) does not fulfill a trapping state condition. (Otherwise, asymptotic completeness is still valid if the Hilbert space of the photon field is restricted to a subspace without trapping states.) Before demonstrating this, however, let us give a physical interpretation of the above equation, and discuss some of its general implications.

We have to keep in mind that, in the Heisenberg picture, the state vectors are constant, i.e., all expectation values are taken with respect to the initial state of atoms and field. Now, according to Eq. (3.2), the expectation value of any photon field observable A , after interaction with $N \rightarrow \infty$ atoms, is given by the expectation value of the atomic operator M_A with respect to the initial atomic state, irrespective of the initial field state. Hence, we may reformulate the property of asymptotic completeness equivalently to Eq. (3.2) as follows:

(a) *The field loses the memory about its initial state after the interaction with infinitely many atoms.*

Furthermore, if we take into account that the evolution of atoms and field is unitary, we can draw the following conclusion from Eq. (3.2):

(b) *Any field state $|\chi\rangle$ can be prepared by choosing an appropriate initial atomic state $|\psi_0\rangle$.*

In order to derive property (b), we consider $A = |\chi\rangle\langle\chi|$, the projector on the desired field state $|\chi\rangle$. Then, after a unitary evolution, which does not change

[§]In order to specify the operator norm in which (3.2) holds, a more precise definition is as follows [32]: there exist strictly positive states ρ_f and ρ_a for the field and a *single* atom, respectively, (e.g., thermal equilibrium corresponding to nonzero temperature) such that for every field observable A there exists an atomic observable M_A such that the expectation value of $(U_N^\dagger (A \otimes \mathbb{1}) U_N - \mathbb{1} \otimes M_A)^2$ (where the square is needed to make the operator positive) with respect to the state $\rho = \rho_f \otimes \rho_a \otimes \rho_a \otimes \dots$ (with infinitely many atoms, all in the same state ρ_a) vanishes in the limit $N \rightarrow \infty$. (Here, N only defines the number of atoms interacting with the cavity field, whereas M_A and ρ are independent of N , i.e., they refer to the total infinite sequence of atoms, including also the atoms which have not yet interacted with the field for a given N .) As a consequence, the expectation values of the two operators on the left and right hand side of Eq. (3.2) with respect to any state which differs from ρ only on the field and on *finitely* many atoms, are equal in the limit $N \rightarrow \infty$ [81]. Thereby, e.g., the case that infinitely many atoms enter the cavity in the upper state, which may lead to a divergent field state, is excluded.

the spectrum of an operator, also $M_{|\chi\rangle\langle\chi|}$ is a projector, in the infinite dimensional atomic Hilbert space. If we now choose any state $|\psi_0\rangle$ from the range of $M_{|\chi\rangle\langle\chi|}$ as initial atomic state, the expectation value of $|\chi\rangle\langle\chi|$ after the atoms-field interaction (evaluated with respect to $|\chi_0\rangle \otimes |\psi_0\rangle$), i.e., the probability of finding the field finally in the desired state $|\chi\rangle$, is 1. In the Schrödinger picture, this reads:

$$\lim_{N \rightarrow \infty} U_N |\chi_0\rangle \otimes |\psi_0\rangle = |\chi\rangle \otimes |\psi_{\chi_0}\rangle, \quad \forall |\chi_0\rangle. \quad (3.3)$$

Obviously, the final state exhibits *no entanglement* of the field with the atoms. Furthermore, as a consequence of the above property (a), the desired field state $|\chi\rangle$ is created *irrespective of the initial field state* $|\chi_0\rangle$. Consequently, asymptotic completeness enables us to prepare an arbitrary field state *without knowing its initial state*. In the following, we will call this property, which combines the two above properties (a) and (b), ‘*universal preparability*’.

Equivalence of asymptotic completeness and universal preparability

Above, we have argued that asymptotic completeness, Eq. (3.2), implies universal preparability. Although it is not immediately obvious, it can be shown [82] that also the reverse is true: the fact that any field state can be prepared by choosing an appropriate initial atomic state, independently of the initial field state (= universal preparability), implies that also for (almost) all other atomic initial states the field finally does not depend on its initial state (= asymptotic completeness). Hence, asymptotic completeness and universal preparability are in fact equivalent.

This equivalence is also useful if we want to check whether a given atoms-field interaction fulfills the property of asymptotic completeness. Following this idea, we will give in the next section sufficient conditions for asymptotic completeness which have a simple physical meaning. Apart from enabling us to verify immediately this property in the case of the Jaynes-Cummings interaction, this will also illustrate that asymptotic completeness is not only a specific property of the Jaynes-Cummings interaction, but is actually valid for more general realizations of quantum Markov chains. For example, within our general setting of atoms interacting with a quantized field, we can certainly relax the condition of resonance between atoms and field (as long as transfer of energy between atoms and field is possible), or the two-level structure of the atoms, etc.

3.3 Sufficient conditions for asymptotic completeness

The following two conditions are sufficient for asymptotic completeness:

- (i) existence of a unique pure *invariant state*: there exists a single-atom state $|\tilde{\psi}\rangle$ such that the cavity field, while interacting with an infinite sequence $|\tilde{\psi}\rangle \otimes |\tilde{\psi}\rangle \otimes \dots$ of such identically prepared atoms, converges

into a uniquely determined *pure* invariant state $|\tilde{\chi}\rangle$, independently of the initial field state. (Then, the field state $|\tilde{\chi}\rangle$ obviously has to be invariant under the interaction with a single atom in the initial state $|\tilde{\psi}\rangle$.)

- (ii) *time reversal symmetry*: if the field state $|\chi_2\rangle$ can be prepared from the initial state $|\chi_1\rangle$, then also vice versa $|\chi_1\rangle$ from $|\chi_2\rangle$.

Before demonstrating how these two conditions enable us to prepare an arbitrary field state $|\chi\rangle$, starting from an unknown initial state (what, as mentioned above, is equivalent to asymptotic completeness), let us at first verify that the Jaynes-Cummings interaction fulfills both conditions.

3.3.1 Invariant states of the Jaynes-Cummings model

As for condition (i), an infinite sequence $|d\rangle \otimes |d\rangle \otimes \dots$ of atoms in the ground state $|d\rangle$ absorbs all photons from the cavity field, which consequently ends up in the vacuum state $|0\rangle$. Strictly speaking, this is only true in the absence of trapping states, i.e., if the transition probability $|B_n|^2 = \sin^2(\phi\sqrt{n})$ from n to $n-1$ photons (see chapter 2.1) is larger than zero for all photon numbers n . Otherwise, the vacuum as unique invariant state can be restored by restricting the Hilbert space of the photon field to a subspace without trapping states (i.e., considering only field states with maximum photon number below the first trapping state).

Although the existence of one unique pure invariant state is already sufficient in order to fulfill property (i), we want to note here that the vacuum is not the only one: in fact, for each atomic state $|\tilde{\psi}\rangle = a|u\rangle + b|d\rangle$ with $|a|^2 < |b|^2$, the infinite sequence $|\tilde{\psi}\rangle \otimes |\tilde{\psi}\rangle \otimes \dots$ will finally force the field to converge into the pure state $|\tilde{\chi}\rangle$ whose photon number amplitudes $d_n = \langle n|\tilde{\chi}\rangle$ are defined by the following recursion relation (in the absence of trapping states):

$$d_n = i \frac{a}{b} \cot(\phi\sqrt{n}/2) d_{n-1}, \quad n \geq 1, \quad (3.4)$$

where d_0 is determined by normalization. These states are known in the literature as ‘cotangent states’ [83, 84]. The condition $|a|^2 < |b|^2$ is required to guarantee the normalizability of the thereby defined state [81]. (In other words: if the atoms enter the cavity mainly in the upper state, the field state diverges for $N \rightarrow \infty$, unless stopped by a trapping state.) This condition can be dropped in the presence of an odd trapping state, i.e., $\phi = k\pi/\sqrt{n_t + 1}$ with odd k (and corresponding restriction of the photon field Hilbert space to photon numbers not larger than n_t). Then, for an arbitrary atomic state (i.e., also $|a|^2 \geq |b|^2$), the field converges into the above cotangent state, whereas in the case of an even trapping state (i.e., with even k) a *mixed* stationary field state will be reached [83] (apart from the trivial cases $|\tilde{\psi}\rangle = |d\rangle$ or $|\tilde{\psi}\rangle = |u\rangle$, where the stationary states are $|0\rangle$ and $|n_t\rangle$, respectively). Note that, in the limit $\phi \rightarrow 0$, we can replace the cotangent in Eq. (3.4) by the inverse $2/(\phi\sqrt{n})$ of its argument. Then, the cotangent state reduces to a coherent state $|\alpha\rangle = \sum_n \alpha^n |n\rangle / \sqrt{n!}$ (modulo normalization), with $\alpha = 2ia/b\phi$.

3.3.2 Time-reversal symmetry of the Jaynes-Cummings model

As for condition (ii) above, the interaction (2.4) fulfills the following time reversal symmetry:

$$U_N^{-1} = (\mathbb{1} \otimes T_N)^{-1} U_N (\mathbb{1} \otimes T_N), \quad (3.5)$$

where the atomic time reversal operator T_N is defined as follows: after reversing the order of the N atoms, it performs a phase shift $|d\rangle \rightarrow -|d\rangle$ on each single atom [the latter amounts to a multiplication of the atomic ladder operators σ, σ^\dagger by a factor of -1 , which yields the inverse of the single-atom interaction (2.1)]:

$$T_N |i_N \dots i_1\rangle = -1^{i_1 + \dots + i_N} |i_1 \dots i_N\rangle. \quad (3.6)$$

Here, each i_j , $j = 1, \dots, N$, is either 0 or 1, corresponding to the j -th atom in the upper or lower state $|u\rangle$ or $|d\rangle$, respectively.

Eq. (3.5) implies the desired time reversal property (ii): if

$$U_N |\chi_1\rangle \otimes |\psi_1\rangle = |\chi_2\rangle \otimes |\psi_2\rangle, \quad (3.7)$$

i.e., $|\chi_2\rangle$ can be prepared from $|\chi_1\rangle$, it follows by application of Eq. (3.5) that

$$U_N |\chi_2\rangle \otimes T_N |\psi_2\rangle = |\chi_1\rangle \otimes T_N |\psi_1\rangle, \quad (3.8)$$

i.e., $|\chi_1\rangle$ can be prepared from $|\chi_2\rangle$.

3.3.3 A preparation scheme based on the sufficient conditions

It is easy to see how the above two conditions enable us to prepare an arbitrary field state $|\chi\rangle$, starting from an unknown initial state (and, as mentioned above, the ability to do this is equivalent to asymptotic completeness): first, we prepare the field in the invariant state $|\tilde{\chi}\rangle$, making use of condition (i). Then, we exploit the time-reversal condition (ii), which enables us to generate the desired field state $|\chi\rangle$ from $|\tilde{\chi}\rangle$ (since the reverse process is possible according to condition (i)). Thereby, we have found one possible preparation scheme. Evidently, it consists of two steps: the first step is needed to purify the field (i.e., to remove the dependence on the initial field state), while the actual preparation of $|\chi\rangle$ takes place in the second step.

Note, however, that the above scheme requires an infinite number of atoms for an exact state preparation. In the more realistic case of finite N , the preparation is only possible with limited accuracy, as quantified by the fidelity of the state preparation, see Eq. (4.1) in the following chapter. Hence, we should ask whether the procedure described above is also the most efficient one, which maximizes the fidelity for a given number of atoms. In fact, using the above scheme with a given number N of atoms, we would have to divide the N atoms into two subsequences $|\psi_0^{(1,2)}\rangle$ of length N_1 and $N_2 = N - N_1$ for the first and second step of the preparation, respectively. In particular, the initial atomic state would be a product state of the form $|\psi_0\rangle = |\psi_0^{(2)}\rangle \otimes |\psi_0^{(1)}\rangle$. Since, in principle, arbitrarily entangled atomic states are allowed, we should not expect that such a product state will give the optimal result. For example, the optimal

initial state could be a superposition of states with different lengths $N_{1,2}$ of the purification and preparation steps. Moreover, we cannot a priori exclude the existence of other preparation strategies which do not distinguish at all between purification and preparation (even not in the limit $N \rightarrow \infty$). Finally, for a finite number N of atoms, also the independence of the final field state from its initial state will not be precisely realized. Therefore, the optimal preparation strategy for finite N could also depend on the initial field state.

As the above discussion reveals, the state preparation with a finite number N of atoms - the natural scenario for any physical implementation of asymptotic completeness in the laboratory - bears some additional complications compared to the idealized case $N \rightarrow \infty$. In particular, the following questions arise:

- What is the highest possible fidelity of the state preparation, and how fast do we reach the ideal value 1 predicted by asymptotic completeness, when increasing the number N of atoms?
- Which initial atomic state do we have to choose in order to reach the maximum fidelity?
- How do maximum fidelity and optimal initial atomic state depend on the initial field state?

We will turn to these questions in the following two chapters, where we examine the state preparation through a finite number N of atoms.

Chapter 4

State preparation with a finite number of atoms

As demonstrated in the previous chapter, in the limit of infinitely many atoms, the asymptotic completeness of the atoms-field interaction ensures the existence of an appropriate initial atomic state which prepares the field in an arbitrary desired state. In a real laboratory experiment, however, we only have finitely many atoms at our disposal. The main limitation on the number N of atoms is imposed by the necessity to generate the required entangled initial atomic state in the 2^N -dimensional atomic Hilbert space. Hence, the crucial question is whether the state preparation is - at least approximately - also possible by using a not too large finite number of atoms. In other words: how fast is the limit of asymptotic completeness reached if we increase the number N of atoms?

As a first step to answer this question, we will show in this chapter how to determine the optimal initial atomic state which prepares the desired field state with the highest possible accuracy, given a finite number N of atoms. Whereas the optimal atomic state $|\psi_0^{(\text{opt})}\rangle$ can always be found by a numerical diagonalization of a $2^N \times 2^N$ matrix, we will also derive a general analytical estimation of $|\psi_0^{(\text{opt})}\rangle$, based on the time-reversal symmetry of the Jaynes-Cummings interaction, which we expect to achieve almost the optimum result of the state preparation. (The validity of this conjecture will be tested numerically in chapter 5.1.) Furthermore, for the case of the vacuum as the initial field state, this estimation allows us to draw some conclusions about the convergence to the limit of asymptotic completeness, and the number N of atoms needed to reach a given level of fidelity.

4.1 Maximum fidelity and optimal atomic state

To start with, we need a quantitative measure for the quality of the state preparation. For this purpose, the simplest choice is the *fidelity* F with respect to $|\chi\rangle$, defined as the expectation value of the projector $|\chi\rangle\langle\chi| \otimes \mathbb{1}$ onto the desired field state $|\chi\rangle$, that is, the probability to find the field in the desired

state when performing a measurement.*

Given the initial field state ρ_0 (which may be a mixed state), and the atomic initial state $|\psi_0\rangle$, the fidelity after the atoms-field interaction reads:

$$F = \text{Tr} \left\{ (\rho_0 \otimes |\psi_0\rangle\langle\psi_0|) U_N^\dagger (|\chi\rangle\langle\chi| \otimes \mathbb{1}) U_N \right\}. \quad (4.1)$$

In order to find the optimal $|\psi_0\rangle$, which prepares the desired target state $|\chi\rangle$ with the maximum fidelity, starting from a given initial field state ρ_0 , we split the trace in Eq. (4.1) into the partial traces tr_a and tr_f over the atoms and the field, respectively. Doing so, the trace over the atomic subspace yields the expectation value

$$F = \langle\psi_0| M^{(\rho_0)} |\psi_0\rangle \quad (4.2)$$

of the following (hermitian) atomic operator

$$M^{(\rho_0)} = \text{tr}_f \left\{ (\rho_0 \otimes \mathbb{1}) U_N^\dagger (|\chi\rangle\langle\chi| \otimes \mathbb{1}) U_N \right\}. \quad (4.3)$$

Hence, $M^{(\rho_0)}$ contains the complete information on the fidelity of the state preparation for an arbitrary atomic initial state $|\psi_0\rangle$. An efficient method to calculate the operator $M^{(\rho_0)}$, making use of the product structure of the interaction U_N , see Eq. (2.4), is described in appendix A.

From the asymptotic completeness, Eq. (3.2), we know that, in the limit $N \rightarrow \infty$, the operator $M^{(\rho_0)}$ loses the dependence on the initial field state ρ_0 and, according to Eq. (3.2), converges to a projection $M_{|\chi\rangle\langle\chi|}$ onto the atomic space. The corresponding range of atomic states is infinitely dimensional, since also the projection onto the desired field state $|\chi\rangle\langle\chi| \otimes \mathbb{1}$ on the left hand side of Eq. (3.2) has this property (due to the identity on the atomic space), and the spectrum is unchanged by the unitary atoms-field interaction. Consequently, we can expect that - also in the case of finite N - there will be more than one atomic initial state preparing the desired field state $|\chi\rangle$ with high fidelity.

At first, however, we will concentrate on the *optimal* initial atomic state which yields the maximum fidelity. (Other initial atomic states will be examined in chapter 5.4.3.) From Eq. (4.2), it follows that:

*Throughout this thesis, we will consider only *pure* target field states $|\chi\rangle$. The preparation of mixed field states is fundamentally different, since atoms and field need not finally be in a product state. (The desired mixed field state could also be obtained as a pure *entangled* state of field and atoms.) Note, however, that if we can prepare pure states, mixed field states ρ can be prepared by decomposing them into pure states, i.e., $\rho = \sum_i p_i |\chi_i\rangle\langle\chi_i|$, and choosing as initial atomic state the corresponding mixture of atomic states for the preparation of the $|\chi_i\rangle$'s. However, the problem of the *optimal* preparation of ρ (with respect to some measure of fidelity for mixed states, see below) remains unsolved: firstly, a given state ρ can be decomposed in many different ways, and, secondly, the optimal initial atomic state need not necessarily be a mixture of the above described form. (Instead, the desired mixed final field state could also be obtained from a *pure* initial atomic state, if atoms and field are finally in an entangled state). Finally, it is unclear how to define the fidelity with respect to a mixed state: there exist several ways of quantifying the deviation of the final field state ρ' from the desired state ρ . Common examples are: the Hilbert-Schmidt metric $D_{\text{HS}}(\rho, \rho') = \sqrt{\text{tr}[(\rho - \rho')^2]}$ [85], the Bures metric $D_{\text{B}}(\rho, \rho') = \sqrt{2(1 - \text{tr}[(\rho^{1/2}\rho'\rho^{1/2})^{1/2})]}$ [86], and the quantum relative entropies $S(\rho||\rho') = \text{tr}(\rho \ln \rho - \rho \ln \rho')$ or $S(\rho' || \rho)$ [87].

The maximum fidelity F_{\max} is the largest eigenvalue of $M^{(\rho_0)}$, and the optimal initial atomic state $|\psi_0^{(\text{opt})}\rangle$ is the corresponding eigenvector.

This allows to calculate numerically the optimal initial atomic state and the corresponding maximum fidelity for any initial and final field states and a given number N of atoms - at least if N is not too large.[†] Before turning to numerical calculations in chapter 5, however, we will try to derive some general properties of our preparation scheme. In particular, for the case of the vacuum as initial field state, we will derive an analytical lower bound for the maximum fidelity, which can be evaluated also for very large numbers N of atoms, and will give us some insight into the asymptotic behavior $N \rightarrow \infty$. For this purpose, we will make use of the time-reversal symmetry of the atoms-field interaction, Eq. (3.5).

Time-reversal property of the maximum fidelity

In order to find out how the time-reversal symmetry is reflected by the maximum fidelity, in the case that the field is initially in a pure state, $\rho_0 = |\chi_0\rangle\langle\chi_0|$, we rewrite the fidelity with respect to $|\chi\rangle$ in a way where the initial and final states appear more symmetrically:

$$F = \max_{|\psi\rangle} |\langle\chi, \psi|U_N|\chi_0, \psi_0\rangle|^2. \quad (4.4)$$

In the following, we will refer to the state $|\psi\rangle$ where the maximum in Eq. (4.4) is assumed as the ‘final atomic state’. It is uniquely determined by the projection of the (entangled) total final state $|\Psi\rangle = U_N|\chi_0, \psi_0\rangle$ onto the target field state, which leaves the atoms in the pure state

$$|\psi\rangle = \langle\chi|U_N|\chi_0, \psi_0\rangle/\sqrt{F}. \quad (4.5)$$

The factor \sqrt{F} , which is needed to normalize the state, equals the success probability of the projection onto the desired field state $|\chi\rangle$, that is, the fidelity of the state preparation. Obviously, the overlap of $|\Psi\rangle$ with any other final state $|\chi, \psi'\rangle$, $\psi \neq \psi'$ is then strictly smaller than F (unless, of course, $F = 0$, where no final atomic state is defined). Now, the maximum fidelity is obtained by maximizing also over the initial atomic states:

$$F_{\max} = \max_{|\psi\rangle, |\psi_0\rangle} |\langle\chi, \psi|U_N|\chi_0, \psi_0\rangle|^2. \quad (4.6)$$

Taking into account the time-reversal symmetry of U_N , see Eq. (3.5), it is obvious from Eq. (4.6) that:[‡]

[†]Note that the dimension 2^N of the atomic Hilbert space increases exponentially fast with N , finally exceeding the available computational resources. E.g., for $N = 15$, the storage of the hermitian matrix $M^{(\rho_0)}$ takes about 10 GB RAM. Even with the currently largest parallel machines, it would not be possible to get much higher than $N \simeq 20$.

[‡]More generally, not only F_{\max} , but the whole spectra of the two operators $M^{|\chi_0\rangle\langle\chi_0|}$ (for the preparation of $|\chi\rangle$ out of $|\chi_0\rangle$) and $M_0^{|\chi\rangle\langle\chi|}$ (vice versa) are identical at any given N . This time-reversal property of $M^{|\chi_0\rangle\langle\chi_0|}$ is proven in appendix A.

The maximum fidelity for the preparation of $|\chi\rangle$ out of the initial state $|\chi_0\rangle$ equals the maximum fidelity for the reverse process of preparing $|\chi_0\rangle$ out of $|\chi\rangle$.

We have already come across the corresponding statement for $F_{\max} = 1$, in chapter 3.3: the time-reversal symmetry expressed thereby was the second sufficient condition (ii) for asymptotic completeness.

4.2 Initial field state: vacuum

Furthermore, the reader may remember from chapter 3.3 that the time-reversal property provided us with an explicit scheme for the preparation of $|\chi\rangle$, which relied on the fact that the vacuum state can always be generated by sufficiently many ground state atoms. Let us therefore first examine the case $\rho_0 = |0\rangle\langle 0|$, i.e., the field is initially in the vacuum state. Following the scheme of chapter 3.3 (the purification step is obviously not needed), we obtain the required initial atomic state from the time-reversed process of generating the vacuum from $|\chi\rangle$ by injecting all atoms in the ground state. Consequently, we proceed as follows: starting from the initial state $|\chi\rangle \otimes |d\dots d\rangle$, we apply the inverse interaction and project the resulting (entangled) final state onto the field vacuum:

$$|\psi'_0\rangle = \langle 0|U_N^\dagger|\chi, d\dots d\rangle/\sqrt{F'} \quad (4.7)$$

$$= T_N \langle 0|U_N|\chi, d\dots d\rangle/\sqrt{F'}. \quad (4.8)$$

Here, we have used the time-reversal symmetry (3.5), and the fact that the atomic time reversal operator T_N leaves the state $|d\dots d\rangle$ unchanged (apart from a possible minus sign, which is irrelevant, since any state vector can be multiplied by an arbitrary phase factor). The normalization factor is given by

$$F' = \langle \chi, d\dots d|U_N(|0\rangle\langle 0| \otimes \mathbb{1})U_N^\dagger|\chi, d\dots d\rangle \quad (4.9)$$

$$= |\langle 0, \psi'_0|U_N^\dagger|\chi, d\dots d\rangle|^2 \quad (4.10)$$

Here, Eq. (4.10) follows from Eq. (4.9) by definition of $|\psi'_0\rangle$, Eq. (4.7). The physical interpretation of F' is as follows: it equals the probability of finding the cavity in the vacuum state, after the field - initially in state $|\chi\rangle$ - has interacted with N ground state atoms. The state $|\psi'_0\rangle$ then is the time-reversed atomic final state, as obvious from Eq. (4.8).

Since F' equals the overlap of the final state $|\Psi\rangle = U_N|0, \psi'_0\rangle$ with $|\chi, d\dots d\rangle$, see Eq. (4.10), it gives a lower bound for the fidelity F of the state preparation with $|\psi'_0\rangle$ as initial atomic state, see Eq. (4.4). One might think that, due to the time reversal symmetry, F should be in fact equal to F' . This is true if and only if the final atomic state $|\psi\rangle = \langle \chi|U_N|0, \psi'_0\rangle/\sqrt{F}$ is again equal to $|d\dots d\rangle$. Hence, the condition for $F = F'$ reads

$$|d\dots d\rangle \stackrel{!}{=} |\psi\rangle = \langle \chi|U_N|0, \psi'_0\rangle/\sqrt{F} \quad (4.11)$$

$$= \langle \chi|U_N(|0\rangle\langle 0| \otimes \mathbb{1})U_N^\dagger|\chi, d\dots d\rangle/\sqrt{FF'} \quad (4.12)$$

$$= \frac{1}{\sqrt{FF'}} M_0^{|\chi\rangle\langle \chi|}|d\dots d\rangle. \quad (4.13)$$

Here, we have used the definition of $|\psi'_0\rangle$, Eq. (4.7), in the second line, and the definition of $M_0^{|\chi\rangle\langle\chi|}$ [like Eq. (4.3), but for the preparation of the vacuum starting from the initial state $|\chi\rangle$], together with the time reversal symmetry, Eq. (3.5), in the third line. Hence, $F = F'$ if and only if $|d\dots d\rangle$ is an eigenstate of $M_0^{|\chi\rangle\langle\chi|}$.[§] Due to the time-reversal property of $M^{|\chi_0\rangle\langle\chi_0|}$, see appendix A, this is again the case if and only if $|\psi'_0\rangle$ is an eigenstate of $M^{|\chi_0\rangle\langle\chi_0|}$ with eigenvalue F' .[¶]

Note that if $|\chi\rangle = |n\rangle$ is a number state, $|\psi'_0\rangle$ must be an eigenvector of $M^{|0\rangle\langle 0|}$ with $F = F'$, since $|\psi\rangle = |d\dots d\rangle$ follows from the excitation number conservation, see Eq. (2.6). However, even if $|\psi'_0\rangle$ is an eigenvector of $M^{|0\rangle\langle 0|}$, the eigenvalue F need not necessarily be the largest eigenvalue F_{\max} . In any case, the fidelity F is a lower bound to the *maximum* fidelity:

$$F' \leq F \leq F_{\max}. \quad (4.14)$$

4.2.1 Conjecture

According to Eqs. (4.10) and (4.6), equality in (4.14), i.e., $F' = F_{\max}$, is equivalent to the following statement:

The optimal way of generating the field state $|\chi\rangle$, starting from the vacuum, is such that the final atomic state is the ground state $|d\dots d\rangle$.

By virtue of the time reversal property of the maximum fidelity (see end of chapter 4.1), this is again equivalent to:

The optimal way of generating the vacuum, starting from the initial field state $|\chi\rangle$, is to inject all atoms in the ground state.

Intuitively, this statement seems to be very convincing: if all atoms are injected in their ground state they can absorb the maximum amount of energy from the field. Nevertheless, the reader should be warned that, as our numerical results in chapter 5.1 will show, the above conjecture is in general *not* fulfilled, although it gives a good approximation in most cases.

Since F' refers to a definite final atomic state $|d\dots d\rangle$, it is easier to calculate than the fidelity F , where no assumption is made about the final atomic state. (Even harder is the calculation of the maximum fidelity F_{\max} , where both initial and final atomic state are unknown.) In fact, we will now derive a simple formula for F' .

A simple formula for the lower bound F'

First, let us consider the case $|\chi\rangle = |n\rangle$, where $|n\rangle$ is the number state with n photons. As already stated above, F' equals the probability of finding the

[§]The eigenvalue then has to be F' .

[¶]Here, we have to include explicitly the condition that the eigenvalue is F' , since the mere fact that $|\psi'_0\rangle$ is an eigenstate of $M^{|\chi_0\rangle\langle\chi_0|}$, with arbitrary eigenvalue $F \geq F'$, does not guarantee the corresponding final atomic state to be $|d\dots d\rangle$.

cavity in the vacuum state, after the field - initially in state $|n\rangle$ - has interacted with N ground state atoms. Hence, if we assume that we measure the final state $|u\rangle$ or $|d\rangle$ of each single atom after the interaction, then F' equals the probability of detecting n out of the N atoms in the upper state $|u\rangle$ (thereby absorbing all n photons from the cavity). However, according to the Jaynes-Cummings model, see chapter 2.1, the probability of detecting a single atom in $|u\rangle$ after interaction with initially m photons in the cavity is given by $P_u(m) = \sin^2(\phi\sqrt{m})$, and similarly $P_d(m) = \cos^2(\phi\sqrt{m})$. Consequently, summing over all the $\binom{N}{n}$ different possibilities to detect n out of the N atoms in the upper state (and the remaining $N - n$ ones in the lower state), we obtain

$$F'(n) = \prod_{j=1}^n P_u(j) \sum_{\substack{k_0, \dots, k_n \geq 0 \\ k_0 + \dots + k_n = N - n}} \prod_{i=0}^n [P_d(i)]^{k_i}. \quad (4.15)$$

In the sum, k_i denotes the number of $|d\rangle$ -detections between the i -th and $(i+1)$ -th $|u\rangle$ -detection, i.e., the index i counts the number of absorbed photons. Using the lemma from Appendix B, we can transform the sum over the $n+1$ variables k_i into a sum over only one variable k . Inserting the above expressions for P_u and P_d yields

$$F'(n) = 1 - \sum_{k=1}^n \cos^{2N}(\phi\sqrt{k}) \prod_{\substack{i=1 \\ i \neq k}}^n \frac{\sin^2(\phi\sqrt{i})}{\sin^2(\phi\sqrt{i}) - \sin^2(\phi\sqrt{k})}. \quad (4.16)$$

It is evident that $F'(n) \rightarrow 1$ when $N \rightarrow \infty$, if all the factors $\cos^2(\phi\sqrt{k})$, $k = 1, \dots, n$, are smaller than 1, or - in other words - if there are no trapping states. Furthermore, the appearance of N in the exponent points at an exponentially fast convergence in the limit $N \rightarrow \infty$, i.e., $1 - F \propto 10^{-\lambda|N}$, where the rate λ of the convergence is given by the logarithm of the largest one of these cosine factors.^{||}

Next, we consider an arbitrary target field state $|\chi\rangle = \sum_n c_n |n\rangle$. Note that, in general, if we can prepare various field states (e.g., number states) with high fidelity, this does not mean that we can also prepare any superposition of those states with equal accuracy, since the corresponding final atomic states may be different. However, such a conclusion is allowed for the lower bound F' , which always refers to the same atomic final state $|d\dots d\rangle$. Indeed, if we insert $|\chi\rangle = \sum_n c_n |n\rangle$ and $\langle\chi| = \sum_m c_m^* \langle m|$ into Eq. (4.9), we make the following observation: all cross terms with $n \neq m$ vanish, since projecting the state $U^\dagger |m, d\dots d\rangle$ onto the field vacuum yields (due to the excitation number conservation, see chapter 2.2) an atomic state with excitation number m (i.e., m atoms in the upper state), which is orthogonal to any state with excitation number n . Hence, we have

$$F' = \sum_n |c_n|^2 F'(n). \quad (4.17)$$

^{||}In the following, we will always use the logarithm with respect to the basis 10.

Again, it is obvious that $F' \rightarrow 1$ for $N \rightarrow \infty$, since this is true for each $F'(n)$. In contrast to the behavior of each single $F'(n)$, however, the overall convergence need not necessarily be exponentially fast if the sum contains infinitely many terms, as it is the case, e.g., for coherent states. On the other hand, in the case of a finite sum $n \leq M$, again the largest one of the factors $\cos^2(\phi\sqrt{k})$, $k = 1, \dots, M$, will determine the rate of convergence in the asymptotic limit.

In chapter 5.1, we present numerical results which compare F_{\max} with the lower bound F' . We will see that if the desired field state is a number state, $F' = F_{\max}$ is valid exactly (at least in the optimal regime of the vacuum Rabi angle), whereas it still gives a good approximation for a general target field state. Furthermore, as we will show in chapter 5.4.1, the convergence of $F_{\max} \rightarrow 1$ follows the behavior of F' described above.

Estimation of the fidelity F achieved with $|\psi'_0\rangle$

Having at hand a simple formula for the lower bound F' , Eqs. (4.16,4.17), the next step would be to derive a similar formula for the fidelity F , Eq. (4.2), which is achieved with the initial atomic state $|\psi'_0\rangle$, Eq. (4.7). This would be useful for testing the validity of the conjecture $F_{\max} = F'$, which necessarily implies $F' = F$, see Eq. (4.14). As already mentioned above, F is more difficult to calculate than F' , since the final atomic state is unknown. However, we know that for the preparation of number states $|n\rangle$ out of the vacuum through the initial atomic state $|\psi'_0\rangle$, Eq. (4.7), with $N \geq n$, the final atomic state is always $|\psi\rangle = |d\dots d\rangle$ [due to the atomic excitation number conservation, Eq. (2.6)], and consequently $F = F'$. Using this fact, we may try to calculate F for an arbitrary target state.

If we denote the initial atomic state $|\psi'_0\rangle$ for the preparation of the number state $|n\rangle$ according to Eq. (4.7) by $|\psi_0^{(n)}\rangle$, we have:

$$U_N|0, \psi_0^{(n)}\rangle = \sqrt{F'(n)} |n, d\dots d\rangle + \sqrt{1 - F'(n)} \sum_{\substack{m \\ m < n}} d_m^{(n)} |m, \psi_m^{(n)}\rangle. \quad (4.18)$$

This defines the final atomic states $|\psi_m^{(n)}\rangle$ belonging to the undesired final photon numbers $m \neq n$. The corresponding coefficients fulfill the normalization condition $\sum_m |d_m^{(n)}|^2 = 1$. Note that photon numbers larger than n do not occur in the final state, since the state $|\psi_0^{(n)}\rangle$ has excitation number n . For the same reason, each state $|\psi_m^{(n)}\rangle$ has excitation number $n - m$.

Let us now consider an arbitrary target state $|\chi\rangle = \sum_n c_n |n\rangle$. According to Eq. (4.7), the state $\sqrt{F'}|\psi'_0\rangle$ is linear in $|\chi\rangle$; hence we may write

$$|\psi'_0\rangle = \sum_n c_n \frac{\sqrt{F'(n)}}{\sqrt{F'}} |\psi_0^{(n)}\rangle. \quad (4.19)$$

According to Eq. (4.18), this leads to the following final atomic state (obtained by projecting the total final state $U_N|0, \psi'_0\rangle$ onto the target field state):

$$|\psi\rangle = \sum_n |c_n|^2 \frac{F'(n)}{\sqrt{F'}} |d\dots d\rangle +$$

$$+ \sum_{m < n} \frac{\sqrt{F'(n)} \sqrt{1 - F'(n)}}{\sqrt{F'}} c_m^* c_n d_m^{(n)} |\psi_m^{(n)}\rangle. \quad (4.20)$$

Here, we have not yet normalized $|\psi\rangle$. In fact, the norm of the state (4.20) is just the probability that the projection onto the desired field state succeeds, or - in other words - the fidelity F which we want to calculate. Obviously, the calculation of the norm would be very much simplified if the states $|d \dots d\rangle$ and $|\psi_m^{(n)}\rangle$ were all orthogonal to each other. Note that, as mentioned above, each state $|\psi_m^{(n)}\rangle$ has a well defined excitation number $n - m$ and is therefore orthogonal to $|d \dots d\rangle$ and to each $|\psi_{m'}^{(n')}\rangle$ with $n' - m' \neq n - m$. However, states having the same excitation number may in principle interfere with each other. Depending on the phases of the photon number amplitudes c_n , the interference may be for each excitation number destructive or constructive.

In order to obtain an estimation, we have to make some simplifying assumptions: firstly, we assume that the phases of c_n are randomly chosen, such that the interference is expected to vanish. This approximation applies at least for the average of F over all states with the same photon number distribution $|c_n|^2$. Secondly, we assume that the coefficients $d_m^{(n)}$ are approximately equally distributed in m , i.e., $d_m^{(n)} = 1/\sqrt{n}$. As evident from the sum over m in Eq. (4.20), the exact distribution of the $d_m^{(n)}$'s only plays an important role if the photon number distribution $|c_m|^2$ of the target field state strongly fluctuates. (For such target field states, the following estimation has to be handled with care.) With these assumptions, we arrive at:

$$F \simeq F' + \sum_{m < n} \frac{F'(n)(1 - F'(n))}{n F'} |c_n|^2 |c_m|^2 \quad (4.21)$$

$$\simeq F' + \sum_n |c_n|^2 \frac{1 - F'(n)}{n} \sum_{m < n} |c_m|^2. \quad (4.22)$$

The second line is valid if the terms $F'(n)$ are very close to 1. We will come back to this estimation later in chapter 5.1, where we will compare the deviation of F from F' for different target field states.

4.2.2 Optimal choice of the vacuum Rabi angle

At first, however, let us return to the expressions (4.16) and (4.17) for the lower bound F' , which we have already used to infer on the convergence behavior of F' in the limit $N \rightarrow \infty$. As we have seen, for the preparation of a target state including a finite number n of photons, the convergence will be exponentially fast, with the convergence rate λ given by the logarithm of the largest one of the factors $\cos^2(\phi\sqrt{m})$, $m = 1, \dots, n$.

The rate of convergence obviously depends on the vacuum Rabi angle ϕ , which is the only experimental parameter of our atoms-field interaction (2.1,2.4). In order to achieve a convergence as fast as possible, we will now try to find the optimal value of ϕ . For this purpose, we have to maximize the smallest one of the transition probabilities $|B_m|^2 = 1 - \cos^2(\phi\sqrt{m})$. As an example, the case

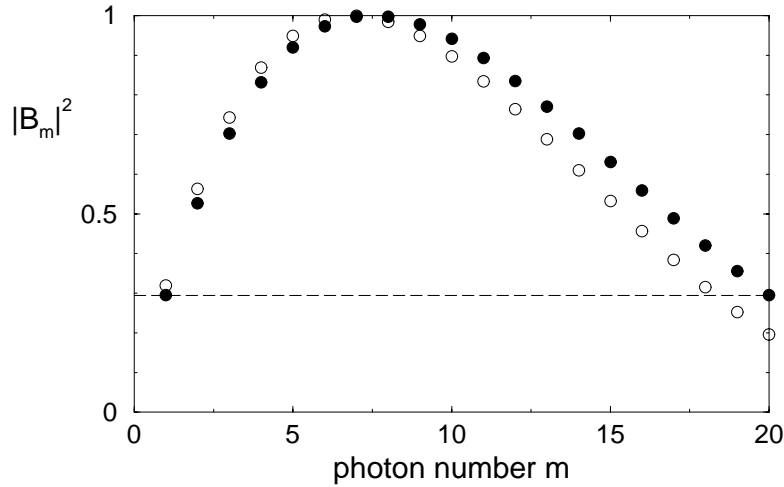


Figure 4.1: Transition probabilities $|B_m|^2 = \sin^2(\phi\sqrt{m})$ between m and $m - 1$ photons for $m = 1, \dots, 20$. Obviously, the optimal value $\phi_{\text{opt}}^{(20)} = 0.574$ (filled circles), which maximizes the minimum of the transition probabilities, fulfills the condition $|B_1|^2 = |B_{20}|^2$ (marked by the horizontal dashed line). Then, increasing ϕ would decrease $|B_{20}|^2$, whereas a smaller ϕ would lead to a smaller value of $|B_1|^2$. As an example, the open circles represent a too large value of the vacuum Rabi angle ($\phi = 0.6$), where the minimum of the transition probabilities is smaller than in the optimal case.

$n = 20$ is shown in Fig. 4.1. From this figure, it is evident that the optimal value $\phi_{\text{opt}}^{(n)}$ can in general be found as follows: it is the smallest positive ϕ which fulfills the condition $\sin^2(\phi) = \sin^2(\phi\sqrt{n})$. ** The solution is given by

$$\phi_{\text{opt}}^{(n)} = \frac{\pi}{1 + \sqrt{n}}. \quad (4.23)$$

As we will verify by numerical calculations in chapter 5.1 (Figs. 5.1 and 5.2), the above expression (4.23) gives a quite good approximation to the optimal value of ϕ - especially in the asymptotic regime of very high fidelities.

The case is more complicated if the target field state contains arbitrarily large photon numbers, such as, e.g., the coherent states. If we want to apply the above scheme, we have to introduce a cut-off at some photon number n , and then choose ϕ according to Eq. (4.23). The cut-off would depend on our desired level of fidelity (or the level of fidelity which can be reached with the given number N of atoms): for a very precise state preparation, we have to take into account also very high photon numbers, and, according to Eq. (4.23),

***This is the optimal solution if we restrict ourselves to not too large values of ϕ . Mathematically, it is possible to choose ϕ such that all transition probabilities are arbitrarily close to 1. We will not consider such cases, since such values of ϕ would be unreasonably large, corresponding to an extremely long time-of-flight $t_{\text{int}} = \phi/g$ of the atoms through the cavity. This would lead to larger fluctuations of ϕ as a result of a finite velocity spread of the atoms (compare chapter 6.2), and the cavity dissipation could no longer be neglected (compare chapter 6.1), neither the finite radiative lifetime of the atoms.

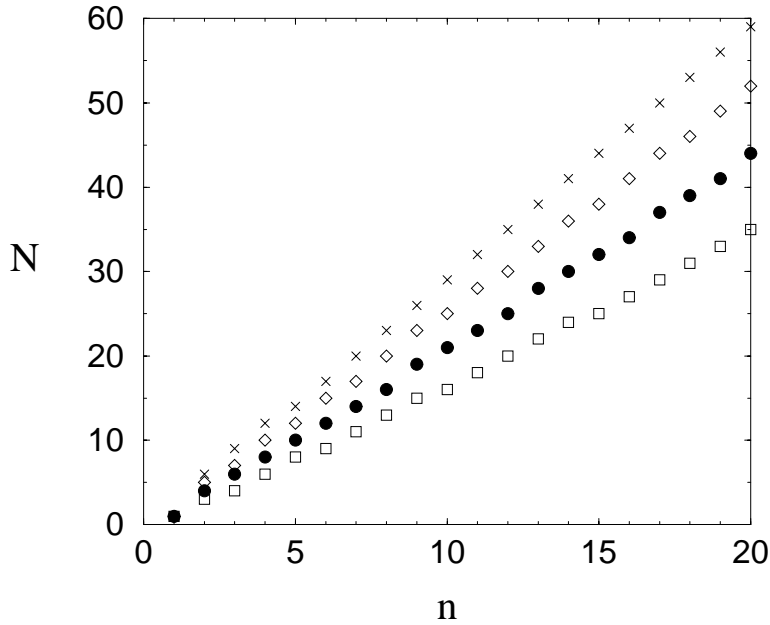


Figure 4.2: Minimum number of atoms N needed to prepare the number state $|n\rangle$ out of the cavity field vacuum $|0\rangle$ with fidelity $F'(n) \geq 1 - \epsilon$, $\epsilon = 10^{-1}, 10^{-2}, 10^{-3}, 10^{-4}$ (from bottom to top). For each n , the optimal value of the vacuum Rabi angle ϕ was chosen [approximately given by the estimation (4.23)]. To prepare $|n\rangle$ with uncertainty $\epsilon < 10^{-2}$ ($\epsilon < 10^{-4}$), $N \simeq 2n$ ($N \simeq 3n$) atoms suffice.

choose a lower value of ϕ . Hence, the optimal value of ϕ depends more strongly on the number N of atoms than in the above case of finite photon numbers.

4.2.3 How many atoms are needed?

As we have now an idea how to choose the vacuum Rabi angle ϕ , Eq. (4.23), and the initial atomic state, Eq. (4.7), the question remains: how many atoms do we need in order to reach a given level of fidelity? Fig. 4.2 shows the answer. Here, we plotted the minimum number N of atoms needed to achieve $F'(n) \geq 1 - \epsilon$, with $\epsilon = 10^{-1}, 10^{-2}, 10^{-3}, 10^{-4}$, as a function of the target photon number n . Note that, since $F'(i) < F'(j)$ for $i > j$, $F'(n)$ is a lower bound for the fidelity of preparing any field state including photon numbers not higher than n , see Eq. (4.17). From Fig. 4.2, we see that the required number of atoms grows approximately linearly with the photon number n : about $2n$ (or $3n$) atoms are sufficient for $F \geq 99\%$ (or $F \geq 99.99\%$), if the vacuum Rabi angle ϕ is chosen properly (see chapter 4.2.2). The linear behavior of N reveals a scale invariance of the fidelity $F'(n)$: if we multiply the target photon number n and the number N of atoms by the same factor, and scale the vacuum Rabi angle according to Eq. (4.23), then $F'(n)$ remains unchanged.

We have to keep in mind, however, that F' , Eq. (4.9), is only a lower bound for the maximum fidelity F_{\max} , and therefore Fig. 4.2 might considerably over-

estimate the number of atoms which would be needed if we used the optimal initial atomic state instead of $|\psi'_0\rangle$. In chapter 5.1, however, we will give numerical evidence that this is not the case. In particular, for the preparation of number states (in the optimal regime of ϕ), the conjecture $F_{\max} = F'$ will be found to be valid exactly.

4.3 Arbitrary initial field state

Let us now consider the case of an arbitrary initial field state ρ_0 . We know already that in the limit of asymptotic completeness, the final field state is independent of the initial field state. As already mentioned in chapter 3, this allows - in the limit $N \rightarrow \infty$ - the preparation of $|\chi\rangle$ for an arbitrary initial state ρ_0 , which may also be a mixed field state.

For a finite number N of atoms, however, the limit of asymptotic completeness is not precisely realized, and the optimal initial atomic state for the preparation of $|\chi\rangle$ depends also on the initial field state ρ_0 . Note that we can in general not exploit the time-reversal symmetry of the atoms-field interaction in order to obtain an estimation of the optimal initial atomic state, as we could for the vacuum $|0\rangle$ as initial field state, see chapter 4.2. Nevertheless, we may try - as a first guess - to use the same initial atomic state $|\psi'_0\rangle$, Eq. (4.7), which we found in chapter 4.2 for the vacuum as initial field state, also when starting from other initial field states. (From the asymptotic completeness property, we know that the state $|\psi'_0\rangle$ will do at least in the limit $N \rightarrow \infty$.)

Based on the sufficient conditions for asymptotic completeness, we have proposed another recipe in chapter 3.3.3: first, inject a sufficient number N_1 of ground state atoms into the cavity in order to prepare the vacuum ('purification'). With the remaining $N_2 = N - N_1$ atoms, continue as described above, choosing the state $|\psi'_0\rangle$ by inserting N_2 instead of N in Eq. (4.7).

However, these two strategies do not contradict each other. We have already mentioned in chapter 3.3.3 the problem how to choose N_1 and N_2 . We will now argue that, in fact, we may expect good results with the preparation step alone, i.e., $N_1 = 0$. The reason is as follows: the state $|\psi'_0\rangle$ is obtained by injecting N_2 ground state atoms into the cavity with initial state $|\chi\rangle$, see Eq. (4.8). However, if $F'(\chi)$ is very close to 1 (otherwise, we cannot hope to achieve a good fidelity, and we have to increase N), the field will almost have reached the vacuum, already before the last atom has arrived. Hence, the last few atoms leave the cavity in the ground state. After time reversal T_N , this means that the first atoms of $|\psi'_0\rangle$ enter the cavity in the ground state, which is just what we need for an efficient purification.

At present, we are not able to prove rigorously that the state $|\psi'_0\rangle$, Eq. (4.7), in general yields a higher fidelity than injecting the first few atoms in the ground state, and then choosing the state $|\psi'_0\rangle$ only for the remaining atoms. However, our numerical calculations in chapter 5.3 indicate that this is indeed the case.

Chapter 5

Numerical results

Using the methods described in the previous chapter, we are now able to investigate numerically the feasibility of our state preparation technique for various target field states $|\chi\rangle$.

At first, we will assume, as already in chapter 4, that the cavity is initially in the vacuum state. In this case, the time reversal argument gave us an explicit expression for the initial atomic state $|\psi'_0\rangle$, Eq. (4.7), and an analytical lower bound F' for the maximum fidelity F_{\max} , see Eqs. (4.16,4.17). From the latter, we could derive an estimation for the optimal choice of the vacuum Rabi angle, Eq. (4.23), and for the number N of atoms needed in order to achieve a given level of fidelity. However, it remains to be shown that the maximum fidelity does not considerably exceed the lower bound F' . This will be done in chapter 5.1, where we test our conjecture $F_{\max} \simeq F'$ for various kinds of target states.

Experimentally, the most difficult task is to generate the initial atomic states needed for the state preparation. In chapter 5.2, we will examine some properties of those states. Whereas, in general, the optimal initial states exhibit entanglement between different atoms, we will see that the states required for the preparation of coherent field states can well be approximated by product states of the N atoms.

From the property of asymptotic completeness (see chapter 3), we know that the state preparation is also possible when starting from mixed initial field states. Although the optimal initial atomic state in general differs from the case resulting with the field initially in the vacuum, we may expect, as argued in chapter 3.3 and 4.3, that the state $|\psi'_0\rangle$, Eq. (4.7), achieves almost the maximum fidelity. The validity of this conjecture will be tested in chapter 5.3.

Furthermore, we also have to examine the convergence to the limit of asymptotic completeness when increasing the number of atoms (chapter 5.4). Here, the central question with respect to the state preparation is the convergence behavior of the maximum fidelity. Remember that expressions (4.16) and (4.17) for the lower bound F' (when starting from the vacuum as initial field state) predict an *exponentially fast* convergence towards the ideal value 1, if the target field state has a finite maximum photon number. In chapter 5.4.1, we will test whether also the maximum fidelity follows this behavior, and how the initial field state influences the convergence rate. The convergence behavior of the

optimal initial atomic state will be studied in chapter 5.4.2.

Apart from the ability to prepare arbitrary field states $|\chi\rangle$ by using the *optimal* initial atomic state, however, asymptotic completeness, Eq. (3.2), also implies that there exist other initial atomic states which prepare $|\chi\rangle$ with high fidelity. Furthermore, in the limit $N \rightarrow \infty$, the final field state should be independent of its initial state for any arbitrary initial atomic state (i.e., not necessarily one which prepares $|\chi\rangle$ with high fidelity). We will examine these consequences of Eq. (3.2) in chapters 5.4.3 and 5.4.4.

5.1 Test of the conjecture

At first, let us test our conjecture that, if the field initially starts in the vacuum state, the maximum fidelity is equal to the lower bound F' , Eqs. (4.16,4.17). If so, the state $|\psi'_0\rangle$, Eq. (4.7), gives the optimal initial atomic state for the preparation of $|\chi\rangle$, or - equivalently - $|d\dots d\rangle$ the optimal *final* atomic state (or - again equivalently, due to the time reversal symmetry - $|d\dots d\rangle$ the optimal initial state for the preparation of the vacuum starting from $|\chi\rangle$).

5.1.1 Number states

We begin with number states, $|\chi\rangle = |n\rangle$ (also called ‘Fock states’), and the field initially in the vacuum state. The number states have a property which simplifies the theoretical treatment of their preparation compared to other field states: as already alluded to in chapter 2.2, and elaborated in appendix A, the optimal initial atomic state for the preparation of number states always has a well defined excitation number k (i.e., k atoms in the upper state), compare Eq. (2.6). Obviously, k must be at least as large as n , and the difference $k - n$ is the excitation number of the final atomic state. Furthermore, as already mentioned in chapter 4.2, the state $|\psi'_0\rangle$, see Eq. (4.7), is an eigenstate of $M^{(\rho_0)}$, Eq. (4.3), with eigenvalue F' , Eq. (4.16) (which would be the maximum eigenvalue according to the conjecture), and therefore the fidelity F achieved by the initial atomic state $|\psi'_0\rangle$ equals F' , compare Eq. (4.2). Now, the solid line in Fig. 5.1 shows the maximum fidelity F_{\max} for the preparation of the first five number states $|n\rangle$, $n = 1, \dots, 5$, with $N = 10$ atoms, compared to the lower bound $F' = F$ (dotted line), as a function of the vacuum Rabi angle ϕ . The fidelity is plotted on a logarithmic scale, i.e., $f = -\log(1 - F)$. In the following we will always use this logarithmic scale, since we are especially interested in the regime of very high fidelities.

At some values of the vacuum Rabi angle, we observe zeros of the fidelity in Fig. 5.1. These can be easily explained: as discussed in chapter 2, if ϕ fulfills an $|m\rangle$ -trapping state condition with $m < n$, i.e., at $\phi = \pi/\sqrt{m+1}$ and integer multiples thereof, the photon number can never exceed m , and the fidelity with respect to $|n\rangle$ has to vanish. These values of ϕ are marked by the vertical dashed lines in Fig. 5.1. For higher target photon numbers n , the net of zeros becomes denser, and, consequently, the optimal value of ϕ , which maximizes the fidelity of the state preparation, should be found below the first relevant trapping state. Remember that we have already derived a more precise

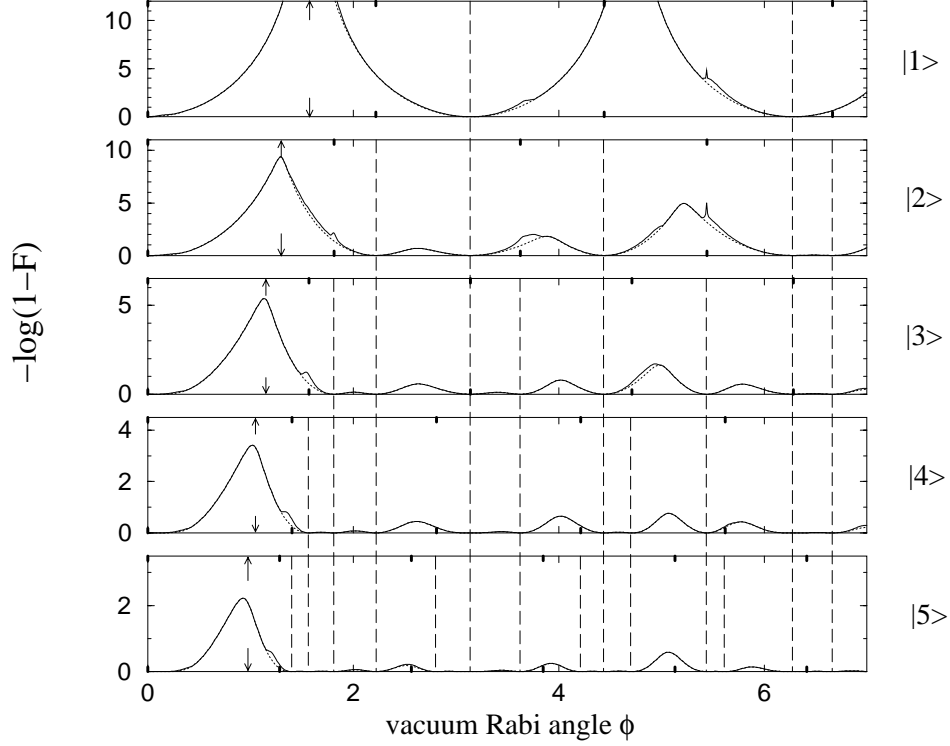


Figure 5.1: Maximum fidelity F_{\max} (solid line) and lower bound F' , Eq. (4.16), (dotted line), for the preparation of the cavity field states $|\chi\rangle = |n\rangle$, $n = 1 \dots, 5$, with a sequence of $N = 10$ atoms injected into the resonator, as a function of the vacuum Rabi angle ϕ . The initial field state is the vacuum $|0\rangle$. The vertical dashed lines denote the zeros of the fidelity due to $|m\rangle$ -trapping states with $m < n$, i.e., at $\phi = \pi/\sqrt{m+1}$ and integer multiples thereof. The fairly good agreement of F_{\max} with F' (note the logarithmic scale!) shows that our conjecture ‘the optimal final atomic state is $|d \dots d\rangle$ ’ is valid for most values of ϕ - in particular also for the optimum regime below the first trapping state of the field. Deviations of F_{\max} from F' are observed (in most cases) at $|n\rangle$ -trapping states (small tick marks). The arrows denote the estimation (4.23) of the optimal vacuum Rabi angle, see chapter 4.2.2.

estimation of the optimal ϕ in chapter 4.2.2. The values predicted by Eq. (4.23) are marked by the little arrows in Fig. 5.1, and, indeed, they give a quite good approximation to the real optimal ϕ . For larger photon numbers, the agreement is not as good as for smaller ones. This is not surprising: the estimation (4.23) was based on the asymptotic behavior of F' , and hence should be better if the fidelity is very close to 1.

Let us now compare the maximum fidelity F_{\max} (solid line) and the lower bound F' (dotted line). Indeed, for most values of the vacuum Rabi angle, F' is equal to F_{\max} , in particular also in the above mentioned optimal regime of ϕ . Hence, for Fock state preparation, our conjecture ‘the optimal final atomic state is $|d \dots d\rangle$ ’ is valid in most cases. However, some deviations can be observed in the vicinity of trapping states. In fact, if ϕ is chosen such that the desired target field state $|n\rangle$ is a trapping state, we immediately find an alternative procedure of preparing $|n\rangle$, namely injecting all atoms in the upper state $|u \dots u\rangle$. Since the atoms can then only *emit* photons into the field, the trapping state condition ensures that - in the limit $N \rightarrow \infty$ - the field converges into the state $|n\rangle$. The thereby achieved fidelity can be calculated in a very similar way as F' in chapter 4.2. Indeed, we find the very same expression (4.15) as for the fidelity F' according to the scheme given by the conjecture. However, the observed deviations of F_{\max} from F' show that in the vicinity of such trapping states neither of those two strategies is the optimal one.

An exception is the case $n = 1$: we have found (see appendix A) that at odd 1-photon trapping states [i.e., $\phi = (2k + 1)\pi/\sqrt{2}$, $k \in \mathbb{Z}$], the atoms-field interaction fulfills a particular symmetry, which leads to a highly degenerate $M^{(0)\langle 0|}$, with only two eigenvalues F_{\max} and F_{\min} , both 2^{N-1} -fold degenerate. Furthermore, for $|\chi_0\rangle = |0\rangle$ and $|\chi\rangle = |1\rangle$, the smaller eigenvalue F_{\min} obviously has to be zero. (If we inject all atoms in the ground state, the field will remain in the vacuum state.) Since we know that - for the preparation of number states - F' is an eigenvalue of $M^{(0)\langle 0|}$, and $F' = 1 - \cos^{2N}(\phi) > 0$ according to Eq. (4.16), it follows that $F_{\max} = F'$. Consequently, we do not observe any deviation of F_{\max} from F' at the odd 1-photon trapping states (at $\phi = \pi/\sqrt{2} = 2.22$ and $\phi = 3\pi/\sqrt{2} = 6.66$) in Fig. 5.1. However, at other values of ϕ , deviations of F_{\max} from F' can be found also in the case $n = 1$, namely near the $|2\rangle$ -trapping states.* This indicates that, in these cases, also the 2-photon state is populated during the optimal preparation process. In contrast, for those values of ϕ where the conjecture $F_{\max} = F'$ is fulfilled, the photon field never populates higher photon numbers than the target photon number n (since, as mentioned above, the initial atomic state $|\psi'_0\rangle$ has excitation number n).

5.1.2 Phase states

The situation changes if the desired field state is a superposition of number states. Then, the state $|\psi'_0\rangle$, Eq. (4.7), is in general not an eigenstate of $M^{(\rho_0)}$ (unlike the situation for the number states, see above), which implies that the

*Also at the even $|1\rangle$ trapping state, i.e., $\phi = \sqrt{2}\pi$, the maximum fidelity F_{\max} differs from F' . However, since already F' is extremely large in this case ($f' = -\log(1 - F') \simeq 12$), the deviation is not visible on the scale of Fig. 5.1.

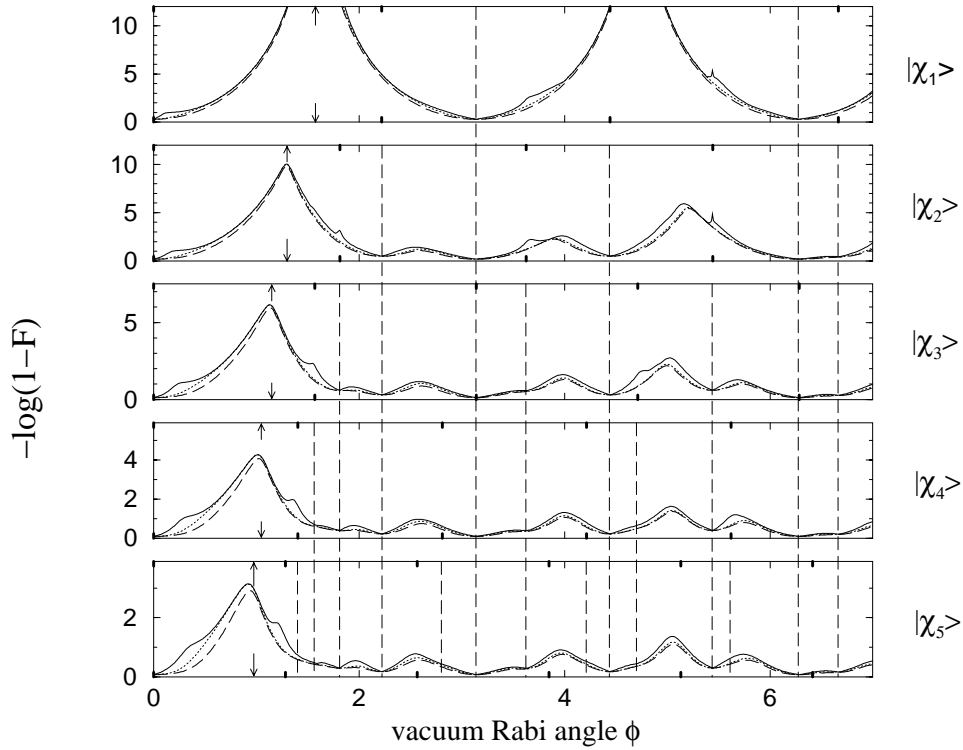


Figure 5.2: Maximum fidelity F_{\max} (solid line), fidelity F achieved with $|\psi'_0\rangle$, Eq. (4.7) (dotted), and F' , Eq. (4.17), (dashed), for the preparation of the phase states $|\chi_n\rangle = \sum_{i=0}^n |i\rangle / \sqrt{n+1}$ of the cavity field, truncated at $n = 1, \dots, 5$, with $N = 10$ atoms injected into the resonator. The initial field state is the vacuum $|0\rangle$. The agreement of F_{\max} with F' is fairly good, on the logarithmic scale. The $|m\rangle$ -trapping states with $m < n$ are denoted by the vertical dashed lines.

fidelity F achieved with $|\psi'_0\rangle$ as initial atomic state is strictly smaller than the maximum fidelity, and strictly larger than the lower bound F' , i.e., $F' < F < F_{\max}$. As an example, we consider the truncated phase states $|\chi_n\rangle = \sum_{i=0}^n |i\rangle / \sqrt{n+1}$. In some sense, those states are the complement of the number states examined above: whereas the latter possess a well defined field intensity (given by the photon number), but with completely undetermined phase, the truncated phase state $|\chi_n\rangle$ has a uniform photon number distribution (in the finite dimensional space of at most n photons), and is as close as possible to a state with a well defined phase [88].

The numerical results (F_{\max} , F and F' as a function of ϕ) for the phase states as target states are shown in Fig. 5.2. Comparing with Fig. 5.1, we see that the maximum fidelity (solid line) is higher for the phase states than for the corresponding number states, especially for the higher photon numbers. The reason is obvious: the phase states are easier to prepare since not the whole field population has to be transferred to the maximum photon number. Furthermore, the fidelity for the preparation of the phase states does not exhibit any zeros since the target state has a nonvanishing overlap with the vacuum (in

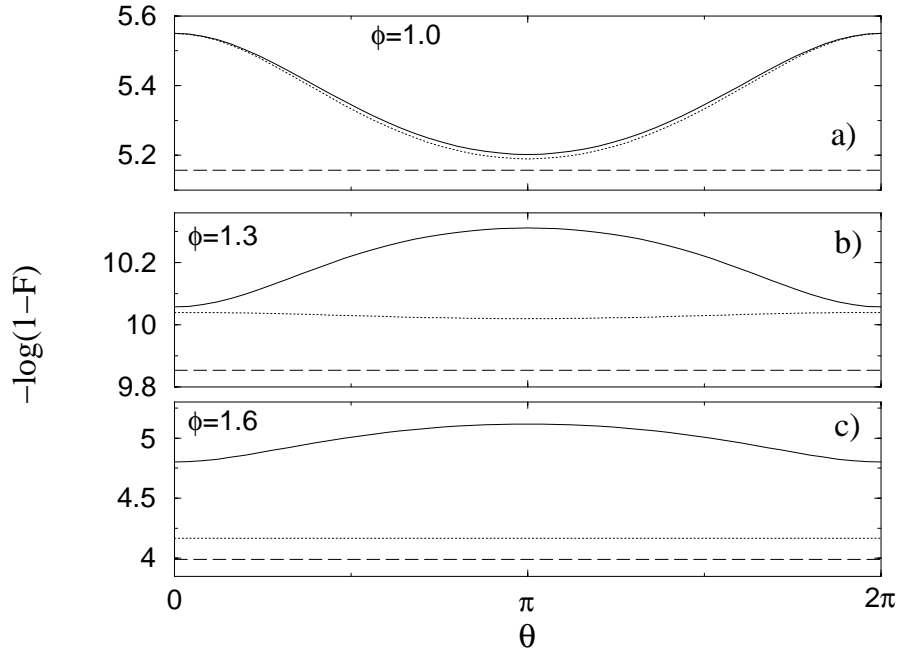


Figure 5.3: Maximum fidelity F_{\max} (solid line), fidelity F achieved with $|\psi'_0\rangle$ (dotted), Eq. (4.7), and F' (dashed), Eq. (4.17), for the preparation of the state $|\chi\rangle = (|0\rangle + |1\rangle + e^{i\theta}|2\rangle)/\sqrt{3}$, with $N = 10$, as a function of the phase θ . We chose three different vacuum Rabi angles: (b) the optimal value $\phi_{\text{opt}}^{(2)} = 1.3$ (compare Fig. 5.2 and chapter 4.2.2), (a) $\phi = 1.0$, and (c) $\phi = 1.6$. The initial field state is the vacuum $|0\rangle$. Whereas in (b) and (c) the maximum fidelity for the preparation of $(|0\rangle + |1\rangle - |2\rangle)/\sqrt{3}$ (i.e., $\theta = \pi$) is slightly higher than the one of $(|0\rangle + |1\rangle + |2\rangle)/\sqrt{3}$ (i.e., $\theta = 0$), the opposite is true for the lowest value $\phi = 1.0$ of the vacuum Rabi angle in (a).

contrast to the number states, where zeros are observed at trapping states, see the vertical dashed lines in Fig. 5.1). Apart from that, however, the behavior of F_{\max} is in both cases quite similar, which indicates that the fidelity is predominantly determined by the maximum photon number of the target field state. In particular, the optimal values of ϕ , estimated by the small arrows according to Eq. (4.23), are almost the same as in Fig. 5.1.

In contrast to Fig. 5.1, however, Fig. 5.2 shows small deviations (on a logarithmic scale) of the lower bound F' from the maximum fidelity F_{\max} (dashed vs. solid line), even in those regions where no deviations are present for the number states. Nevertheless, we find that - in the optimal regime of ϕ below the first trapping state - the initial atomic state $|\psi'_0\rangle$ from Eq. (4.7) gives nearly the optimum result, i.e., $F \simeq F_{\max}$ (dotted vs. solid line). In contrast, for higher values of the vacuum Rabi angle, F is closer to F' than to F_{\max} .

Varying the phases of the coherent superposition

Since, in general, $F_{\max} > F'$, whereas $F_{\max} = F'$ in the case of number states (at least if ϕ is not close to a trapping state), the fidelity for the preparation of a coherent superposition of number states is higher than the correspondingly weighted sum of fidelities for the preparation of the various number states, see Eq. (4.17). Hence, we may expect that the maximum fidelity not only depends on the photon number populations $|\langle n|\chi\rangle|^2$ of the target field state, but also on the phases of the photon number amplitudes. An example is shown in Fig. (5.3). Here, we varied the phase of the 2-photon amplitude of the truncated phase state $|\chi_2\rangle$, i.e., we considered target states of the form $|\chi_\theta\rangle = (|0\rangle + |1\rangle + e^{i\theta}|2\rangle)/\sqrt{3}$. [Note that any state $e^{i\theta_0}|0\rangle + e^{i\theta_1}|1\rangle + e^{i\theta_2}|2\rangle$ can be written in this form by (i) multiplication with a global phase, and (ii) multiplication of the n -photon amplitude, $n = 0, 1, 2$, with a relative phase $e^{in\tilde{\theta}}$. This leaves the Jaynes-Cummings interaction (2.1) invariant, if, simultaneously, the atomic states are transformed according to $|d\rangle \rightarrow e^{-i\tilde{\theta}}|d\rangle$.] As can be seen in Fig. 5.3, the influence of the phase θ depends on the vacuum Rabi angle: whereas for the two higher values $\phi = 1.3$ (b) and 1.6 (c), the maximum fidelity F_{\max} of the preparation of $(|0\rangle + |1\rangle - |2\rangle)/\sqrt{3}$ is higher than the one of $(|0\rangle + |1\rangle + |2\rangle)/\sqrt{3}$, the opposite is true for $\phi = 1.0$ (a). In the latter case, the fidelity F achieved by $|\psi'_0\rangle$ is very close to F_{\max} , while it is closer to F' for the highest value of ϕ . We have checked that the mean value of F (averaged over a uniform distribution of the phase θ) agrees exactly with the estimation (4.21). This is not surprising if we look at the two assumptions made in the derivation of Eq. (4.21): (i) the interference between the different final atomic states in Eq. (4.20) is cancelled by the phase average, and (ii) the distribution of the coefficients $d_m^{(n)}$, $m < n$ is irrelevant if the photon number distribution $|c_m|^2$ of the target state is constant. As for point (i), the fact that F is almost independent of θ in (c) shows that the different final atomic states are (almost) orthogonal to each other in this case.

Note, however, the small scale of the fidelity axis in Fig. 5.3: the variation of F_{\max} is not larger than about 10% on the logarithmic scale. This underlines the approximate validity of the conjecture $F_{\max} \simeq F'$ for states with arbitrarily chosen phases. Below, we will give evidence that this is not only true in the example of Fig. 5.3, but also for states with an arbitrarily chosen photon number distribution (in a finite dimensional photon subspace).

5.1.3 Coherent states

Next, let us consider coherent states $|\alpha\rangle = \exp(-|\alpha|^2/2) \sum_n \alpha^n |n\rangle / \sqrt{n!}$ [67], see Fig. 5.4. These states are as close as possible to classical field states, which have both a definite intensity and phase. Since they exhibit a nonvanishing population also of high photon numbers, they are more difficult to prepare than number states with the same mean photon number. Furthermore, the discrepancies between F_{\max} , F and F' are larger than for the phase states. The larger difference between F and F' is also predicted by the estimation of F , Eq. (4.22): according to this equation, a large population $|c_n|^2$ of high

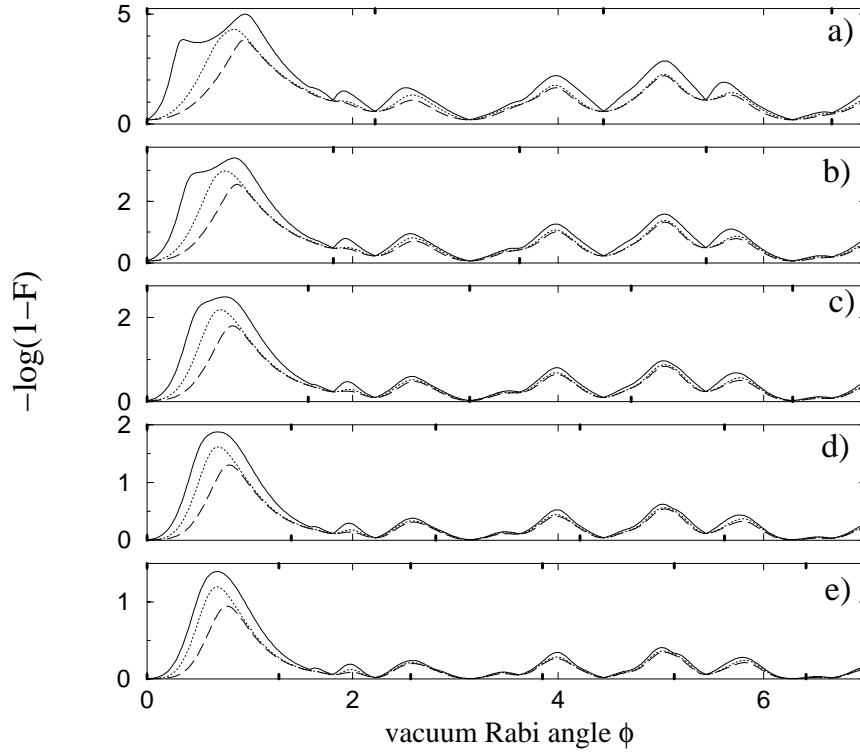


Figure 5.4: Maximum fidelity F_{\max} (solid line), fidelity F achieved with $|\psi'_0\rangle$ (dotted), Eq. (4.7), and F' (dashed), Eq. (4.17), for the preparation of the coherent field states $|\chi\rangle = |\alpha\rangle$ with mean photon numbers $|\alpha|^2 = 1, 2, \dots, 5$ (a-e), upon injection of a sequence of $N = 10$ atoms into the resonator, as a function of the vacuum Rabi angle ϕ . The initial field state is the vacuum $|0\rangle$. Although the difference of F_{\max} and F' is larger than for the number and phase states (Figs. 5.1 and 5.2), the state $|\psi'_0\rangle$ (dotted line), Eq. (4.7), achieves the maximum fidelity (solid line) with quite good approximation.

photon numbers n , where the term $(1 - F'(n))/n$ is larger than for low photon numbers (since the fidelity $F'(n)$ decreases with increasing photon number n), is necessary to obtain a large difference $F - F'$. On the other hand, on the logarithmic scale of Fig. 5.4, the difference between F and F' is not given by $F - F'$ but rather by $f - f' = -\log(1 - F) + \log(1 - F')$. On the logarithmic scale, however, even a small linear difference $F - F'$ will appear very large if the fidelity F' is close to 1, which requires a large population of *low* photon numbers, see Eq. (4.17). As a compromise, a huge difference between F and F' on the logarithmic scale is obtained for small but nonvanishing populations of high photon numbers, as it is the case for the coherent states. Note that the largest deviations between F and F' are observed for low vacuum Rabi angles (i.e., short interaction times). This is also predicted by Eq. (4.21): for larger ϕ , the fidelity $F'(n)$ for higher photon numbers n will be extremely low, due to the presence of trapping states (see the vertical dashed lines in Fig. 5.1). Then, the approximation which leads from Eq. (4.21) to (4.22), namely that all the

terms $F'(n)$ are close to 1, is not valid, and the presence of those terms $F'(n)$ in Eq. (4.21) reduces the difference between $F - F'$.

In the regime of small vacuum Rabi angles, also the difference of the maximum fidelity F_{\max} as compared to F and F' is quite large, especially for the states with small α . For example, for $\alpha = 1$ and $\phi = 0.35$, the maximum fidelity F_{\max} is more than three orders of magnitude larger than the lower bound F' . Using the time reversal argument, we conclude that in those cases there exist much more efficient ways of creating the vacuum starting from a coherent state $|\alpha\rangle$ than injecting all atoms in the ground state (which would yield fidelity F'). This case will be examined in more detail in chapter 5.2, see Fig. 5.10. In the optimum regime of the vacuum Rabi angle, however (where F_{\max} assumes its maximum), the fidelity F (dotted line) achieved with the atomic state $|\psi'_0\rangle$, Eq. (4.7), is not very far from the maximum fidelity [on the logarithmic scale, the relative difference $(f_{\max} - f)/f_{\max}$ varies from about 10% to 20%].

5.1.4 Randomly chosen target states

Above, we have tested the validity of our conjecture $F_{\max} \simeq F'$ for three different kinds of target states: photon number states, truncated phase states, and coherent states. We want to stress, however, that our state preparation scheme not only works for specific target states familiar from standard texts on quantum optics, but for arbitrary ones. To demonstrate this, we will now consider randomly chosen field states. In order to define a proper measure used for the random choice of a target state, we will restrict ourselves to a finite dimensional subspace of target states, namely those with maximum photon number not higher than M . Now, for pure states in a finite dimensional Hilbert space, the natural uniform measure is given by the Haar measure (which is the only measure invariant under arbitrary unitary operations). For the generation of a random state $|\chi\rangle$ according to this measure, we use the Hurwitz parameterization [89, 90]:

$$|\chi\rangle = \sum_{n=0}^M e^{i\phi_n} \cos(\theta_n) \prod_{m=n+1}^M \sin(\theta_m) |n\rangle. \quad (5.1)$$

(For $n = M$, the product $\prod_{m=n+1}^M$ in the above equation is defined as 1.) Here, $\phi_0 = \theta_0 = 0$, whereas for $n > 0$, the ϕ_n 's are chosen according to a uniform distribution in $[0, 2\pi]$, and $\theta_n = \arcsin(\xi_n^{1/2n})$, with the ξ_n 's uniformly distributed in $[0, 1]$.[†]

Fig. 5.5 shows the result of our numerical calculations, for field states with up to $M = 4$ photons. According to Eq. (5.1), we drew 10 000 random states. For each state, we calculated the maximum fidelity F_{\max} and the lower bound F' , using $N = 8$ atoms, and the vacuum Rabi angle $\phi_{\text{opt}}^{(4)} = 1.05$ [according to the estimation (4.23) of the optimal ϕ , see chapter 4.2.2]. In order to test the validity of the conjecture, we determined the relative difference Δf_{rel} of $f_{\max} = -\log(1 - F_{\max})$ and $f' = -\log(1 - F')$ on the logarithmic scale, i.e.,

[†]In general, $2M$ real parameters are needed to specify a state: $2M+2$ for the $M+1$ complex amplitudes, minus 1 due to normalization, minus 1 due to the irrelevant global phase.

$\Delta f_{\text{rel}} = (f_{\text{max}} - f')/f_{\text{max}}$, and plotted it as a function of the maximum fidelity in Fig. 5.5(b). For comparison, also the photon number states $|n\rangle$, the truncated phase states $|\chi_n\rangle$, the truncated coherent states (see caption of Fig. 5.5), and the state $|\tilde{\chi}_4\rangle = (|0\rangle + |1\rangle - |2\rangle + |3\rangle + |4\rangle)/\sqrt{5}$ are shown. As already mentioned above, for the preparation of number states, the conjecture $F_{\text{max}} = F'$ is exactly valid (if ϕ is not close to a trapping state), which implies $\Delta f_{\text{rel}} = 0$. Furthermore, the number states seem to be the only states with this property: only for very few of the 10 000 random states shown in Fig. 5.5(b), the deviation Δf_{rel} is close to zero, and we have checked that all these states are close to number states (i.e., the population of one photon number strongly prevails). On the other hand, for the whole random ensemble, the difference Δf_{rel} almost never exceeds 15%, whereas the mean value of Δf_{rel} is about 7%. This confirms the approximate validity of the conjecture $F_{\text{max}} \simeq F'$ in the general case.

In order to interpret the structure in the distribution observed in Fig. 5.5(b), we first want to note the following: of all states in the subspace with up to 4 photons, the 4-photon number state is most difficult to prepare, i.e., its maximum fidelity is the smallest one. [However, note that with $N = 8$ atoms, we can still achieve a fidelity of more than 99%, i.e. $f_{\text{max}} = f'(4) = 2.25$ on the logarithmic scale.] The fidelities for the other photon number states, $n < 4$, are more than one order of magnitude higher. Hence, in the expression (4.17) of the lower bound F' , mainly the 4-photon term contributes to the sum, and we obtain the following estimation

$$\begin{aligned} f' &= -\log \left(\sum_{i=0}^4 |c_i|^2 (1 - F'(i)) \right) \\ &\simeq f'(4) + \log(|c_4|^2), \end{aligned} \quad (5.2)$$

which is valid if the population $|c_4|^2$ of the 4-photon state is not too small (i.e., larger than $10^{-f'(4)+f'(3)} = 0.06$, such that the term $i = 4$ prevails in the above sum over i), or - equivalently - if $f' > f'(3)$. According to Eq. (5.2), the fidelity f' (and, hence, approximately also f_{max}) is basically determined by the 4-photon population of the target state. In particular, for all states with $f_{\text{max}} \gtrsim f'(3) = 3.5$, the 4-photon population $|c_4|^2$ is very small, while $|c_4|^2$ approaches the value 1 if f_{max} decreases from $f'(3)$ to $f'(4)$. In the latter regime, we observe in Fig. 5.5(b) a relatively narrow distribution of Δf_{rel} , which is confined between a quite well defined lower and upper bound, respectively. Since Δf_{rel} quantifies the difference between the maximum fidelity f_{max} and the lower bound f' , this means that not only the lower bound f' is almost completely determined by $|c_4|^2$, as we know from (5.2), but also f_{max} does not strongly vary for different target states with constant $|c_4|^2$. In particular, the phases of the target state's photon number amplitudes do not have a very large influence (which is also consistent with our previous results from Fig. 5.3.) As an example, we plotted in Fig. 5.5(b) the truncated phase state $|\chi_4\rangle$ and the corresponding manifold of states with uniform photon number distribution. Here, the deviations Δf_{rel} form an almost straight line between the truncated phase state $|\chi_4\rangle$ and the state $|\tilde{\chi}_4\rangle$, which has a negative 2-photon amplitude. It is easy to see why the manifold corresponds to a one dimensional and almost

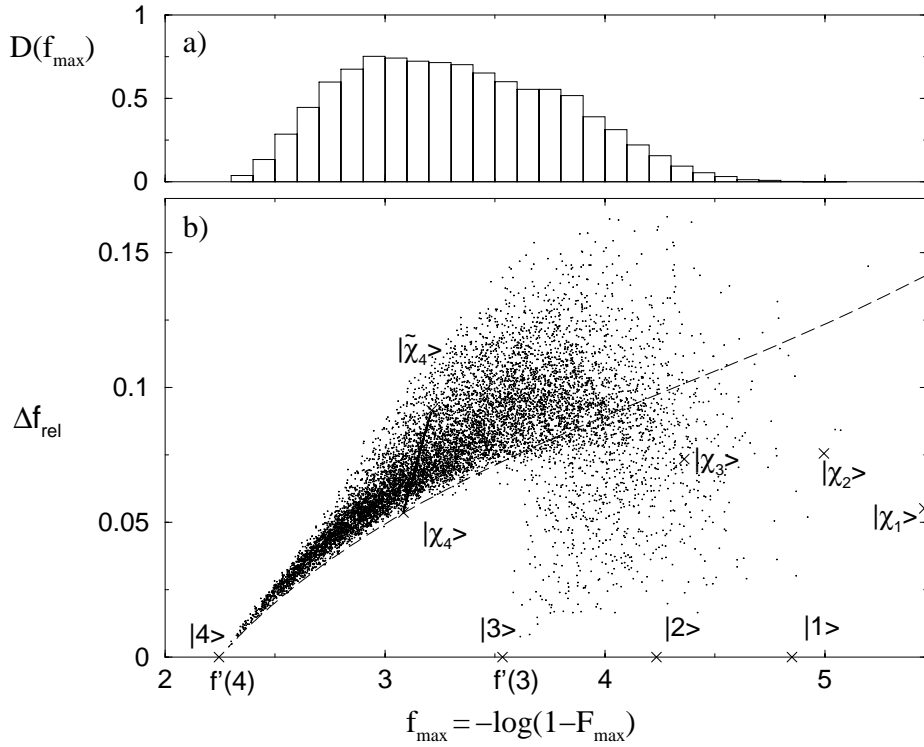


Figure 5.5: (a) Distribution $D(f_{\max})$ of the maximum fidelity (on a logarithmic scale), for the preparation of 10 000 randomly chosen target field states, according to Eq. (5.1), with up to $M = 4$ photons. The number of atoms is $N = 8$, and the vacuum Rabi angle $\phi_{\text{opt}}^{(4)} = 1.05$, according to the estimation (4.23). (b) Relative difference $\Delta f_{\text{rel}} = (f_{\max} - f')/f_{\max}$ of the maximum fidelity F_{\max} and F' (on the logarithmic scale), for the same 10 000 random target states as in (a), plotted as a function of the maximum fidelity. Each dot corresponds to one state. For comparison, also the photon number states $|n\rangle$, the truncated phase states $|\chi_n\rangle$, and the state $|\tilde{\chi}_4\rangle = (|0\rangle + |1\rangle - |2\rangle + |3\rangle + |4\rangle)/\sqrt{5}$ are shown. Furthermore, the dashed line displays the manifold of the truncated coherent states (i.e., the states obtained by projection of the coherent states $|\alpha\rangle$ onto the photon subspace with up to 4 photons), whereas the line connecting the two states $|\chi_4\rangle$ and $|\tilde{\chi}_4\rangle$ represents the manifold of all states with uniform photon number distribution. In the regime $f_{\max} < f'(3)$, we observe a relatively narrow distribution of the difference Δf_{rel} , confined between an upper and lower bound (the latter being quite well reproduced by the truncated coherent states).

straight line: since for all states with uniform photon number distribution, the lower bound f' is the same, the difference Δf_{rel} only depends on f_{max} , i.e., $\Delta f_{\text{rel}} = 1 - f'/f_{\text{max}}$, which is close to a straight line if f_{max} varies only within a small range. What we cannot explain, however, is why the states $|\chi_4\rangle$ and $|\tilde{\chi}_4\rangle$ are the end points of this line. [Compare also the case $M = 2$ in Fig. 5.3(b), where - at the optimal value of ϕ - the maximum fidelity is smallest for the state $|\chi_2\rangle$.] Remarkably, the state $|\chi_4\rangle$ is very close to the lower bound of the distribution, which is also quite well reproduced by the manifold of the truncated coherent states (see caption of Fig. 5.5). However, this does not remain true if we consider other values of the maximum photon number M , see Fig. 5.6, where the case $M = 5$ is shown.

The situation changes, however, if the 4-photon amplitude is so small that Eq. (5.2) is not a good approximation. This happens for states with fidelity larger than the fidelity $f'(3)$ of the 3-photon state. [From the distribution of f_{max} in Fig. 5.5(a), we see that about one third of all states fulfills this condition.] Then, f_{max} and f' are no longer mainly determined by $|c_4|^2$, and the deviation Δf_{rel} may take a larger range of values, in particular also very small values close to the photon number states, $n < 4$. Nevertheless, as evident from Fig. 5.5(b), such exceptions are very rare, and most states follow the above typical behavior observed in the regime $f_{\text{max}} < f'(3)$.

Finally, let us stress that the above interpretations of Fig. 5.5 do not only hold in the case of $M = 4$, but seem to be of general validity. We have checked that for $M = 2, 3$, and 5 (choosing in each case the optimal vacuum Rabi angle, see chapter 4.2.2) the whole picture is very similar (higher photon numbers are presently not accessible to numerical calculations of a large ensemble of states, since the required number of atoms in order to achieve high fidelities would be too large), see Fig. 5.6. This reminds us of the scale invariance of the fidelity $F'(n)$ observed in Fig. 4.2.

Note, however, that the situation is different for the preparation of the coherent states $|\alpha\rangle$. These are not contained in a subspace with a finite number of photons, but have nonvanishing population also at very high photon numbers. Since, as we have seen above, in the finite-dimensional case the fidelity predominantly depends on the population of the highest photon number, we expect that also the coherent state's small population of high photon numbers is important for the state preparation (as already discusses in chapter 5.1.3, too). This agrees with the fact that the maximum fidelity (on the logarithmic scale) for the coherent states is quite different from the fidelity for the truncated coherent states shown in Fig. 5.5. From Fig. 5.4, we know that the deviations from the conjecture $F_{\text{max}} \simeq F'$ are considerably larger than in the finite dimensional case. (In the optimal regime of ϕ , the difference Δf_{rel} varies from about 20%, for $|\alpha|^2 = 1$, to about 40%, for $|\alpha|^2 = 5$, and is approximately constant when changing the number of atoms, compare also Fig. 5.13b.)

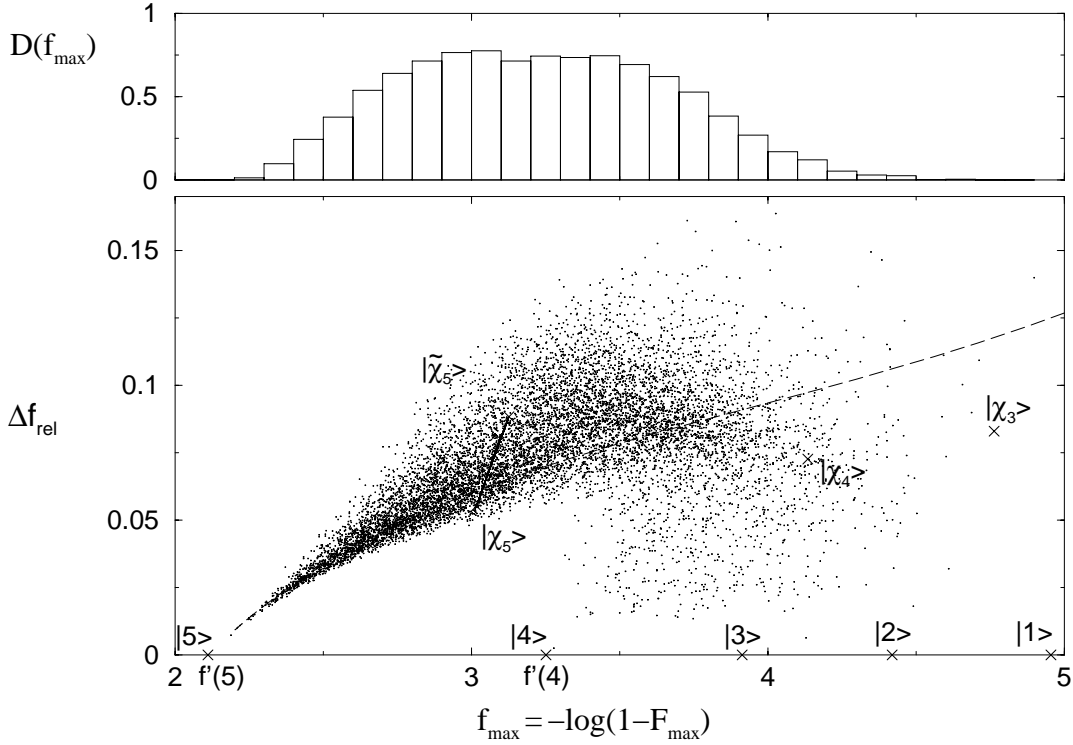


Figure 5.6: Same as Fig. 5.5, for the preparation of 10 000 randomly chosen target states with maximum photon number $M = 5$, using $N = 10$ atoms, and the optimal vacuum Rabi angle $\phi_{\text{opt}}^{(5)} = 0.97$. The distributions of the maximum fidelity f_{max} , and of its deviation Δf_{rel} from the lower bound f' , are very similar to the case $M = 4$ and $N = 8$ depicted in Fig. 5.5. This demonstrates the scale invariance of the maximum fidelity (see also Fig. 4.2), which remains approximately constant, if the number of atoms is scaled linearly with the maximum photon number of the target state, and the optimum value of the vacuum Rabi angle is chosen, see Eq. (4.23). In contrast to the case $M = 4$, Fig. 5.5, the truncated coherent states (dashed line) do not reproduce the lower bound of the distribution, and the phase state $|\chi_5\rangle$ does not exactly define the lower edge of the manifold of the states with uniform photon number distribution. Its upper edge is given by the state $|\tilde{\chi}_5\rangle = (|0\rangle + |1\rangle + |2\rangle - |3\rangle + |4\rangle + |5\rangle)/\sqrt{6}$.

In summary, the conjecture $F_{\max} = F'$ is valid exactly only for number states, if the vacuum Rabi angle is not close to a trapping state condition, whereas for other states it still gives a good approximation in most cases. Hence, we get a quite good approximation to the optimal strategy (which yields the maximum fidelity) for preparing an arbitrary field state $|\chi\rangle$ from the vacuum $|0\rangle$, simply by using the time reversal symmetry (3.5), and the fact that the vacuum can always be prepared by a sequence of ground state atoms. In particular, the conclusions in chapter 4.2 about the convergence of the fidelity, the optimal choice of the vacuum Rabi angle, see Eq. (4.2.2), and the number of atoms needed for the preparation of $|n\rangle$, see Fig. 4.2, which were based on the analytical expressions for the lower bound F' , Eqs. (4.16,4.17), can be expected to remain valid also for the maximum fidelity. Note, however, that we considered only a fixed number of atoms, namely $N = 10$. Therefore, it remains to be shown that the conjecture $F_{\max} \simeq F'$ is also valid for other values of N . This will be done in chapter 5.4.1, where we will examine the convergence of the maximum fidelity in the limit $N \rightarrow \infty$.

However, we observe larger deviations from the conjecture $F_{\max} \simeq F'$ for coherent states and small values of the vacuum Rabi angle. This case will be examined in more detail in the following chapter 5.2.

5.2 Properties of the optimal atomic states

As the above results, in particular Fig. 4.2, show, we can achieve quite high fidelities of the state preparation by using a relatively small number of atoms. The required initial atomic state can either be chosen according to the conjecture, Eq. (4.7), which gives in many cases a very good approximation, or - for not too large numbers N of atoms - be calculated numerically, as described in Appendix A.

Nevertheless, the experimental preparation of this (in general entangled) atomic state is a formidable task. Recently, experimental entanglement between four trapped ions has been reported in [91], and a procedure which successfully entangled two atoms and a single-photon cavity mode, but - in principle - can also operate on larger numbers of particles, is described in [92]. However, e.g., for $N = 10$ atoms, the atomic Hilbert space has a dimension of 2^{10} , which means that about 2000 real parameters have to be controlled. The same fact would also make a complete description of the atomic states very lengthy.

However, to get at least a rough idea, we investigate a few properties of the optimal initial atomic states in the following. For simplicity, we will concentrate on the single-particle properties, which are described by the reduced density matrices ρ_i of the individual atoms, see Eq. (2.9). From ρ_i , we can extract the ground state population of the i -th atom:

$$p_i^{(d)} = \langle d | \rho_i | d \rangle. \quad (5.3)$$

Furthermore, as discussed at the end of chapter 2, the largest eigenvalue p_i of ρ_i tells us how much the i -th atom is entangled with the other ones (remember: $p_i = 1/2$ indicates maximal, and $p_i = 1$ no entanglement).

5.2.1 Number states

Fig. 5.7 shows the above properties of the optimal initial atomic state, for the preparation of the number states $|n\rangle$ with $N = 10$ atoms, starting from the vacuum as initial field state. On the left, the eigenvalues p_i are plotted, whereas the right hand side shows the population of the lower state $p_i^{(d)}$ for each single atom. In fact, the left and right hand side are here very closely related: remember that the optimal initial atomic state for the preparation of number states always has a well defined excitation number (see chapter 2.2 and appendix A). As a consequence [which can be easily deduced from Eq. (2.9)], the reduced state ρ_i is diagonal in the $\{|u\rangle, |d\rangle\}$ basis, and the largest eigenvalue p_i is given by $p_i = \max\{p_i^{(d)}, 1 - p_i^{(d)}\}$ (i.e., the left hand side of Fig. 5.7 is obtained from the right one by reflecting all $p_i^{(d)}$'s smaller than $1/2$ at the axis $p_i^{(d)} = 1/2$). In other words: each atom is as much entangled with the other ones as it can be, given the value of its ground state population. (Obviously, the largest eigenvalue p of a 2×2 density matrix ρ cannot be smaller than its ground or upper state population, $p^{(d)}$ or $1 - p^{(d)}$.)

For each field state $|n\rangle$, the optimal value of the vacuum Rabi angle ϕ was chosen (see chapter 4.2.2). As shown above, in this case the optimal initial atomic state is given by $|\psi'_0\rangle$, Eq. (4.7), where the first few atoms enter the cavity mainly in the ground state $|d\rangle$. The one-photon state $|1\rangle$ is a special case, since for $\phi = \pi/2$ (i.e., half a vacuum Rabi cycle), the preparation succeeds with perfect fidelity if the first $N - 1$ atoms enter the cavity in the ground and the last one in the excited state. For higher number states $|n\rangle$, $n > 1$, the initial atomic state exhibits entanglement between different atoms. As can be seen in Fig. 5.7, the $(N - n)$ -th atom is most strongly entangled with the other ones. Consequently, the ground state population of this atom is closest to $1/2$. For the subsequent atoms, the ground state population further decreases, until it almost reaches zero about halfway between the $(N - n)$ -th and the last atom. We have checked that, at this point, most of the photon field population is concentrated at intermediate photon numbers m , where the transition probability $|B_m|^2$ is close to 1 (compare Fig. 4.1). Consequently, the injection of an atom close to the upper state (i.e., with almost vanishing ground state population) can provide a very efficient transport of the photon number distribution towards higher values. However, at the end of the sequence, the initial atomic ground state population increases again.

5.2.2 Phase states

The case of truncated phase states (see chapter 5.1) as target states is illustrated in Fig. 5.8. Here, the optimal initial atomic state is not exactly equal, but very close to the state $|\psi'_0\rangle$, Eq. (4.7), which agrees with the observation in Fig. 5.2 that the fidelity achieved with $|\psi'_0\rangle$ almost reaches the maximum fidelity. In fact, on the scale of Fig. 5.8, the difference between both results would be indistinguishable. Consequently, since the state $\sqrt{F^N}|\psi'_0\rangle$ is linear in $|\chi\rangle = \sum_i |i\rangle/\sqrt{n+1}$, see Eq. (4.7), the initial atomic state $|\psi'_0\rangle$ is given by the corresponding superposition of initial states $|\psi_0^{(i)}\rangle$ for the preparation of

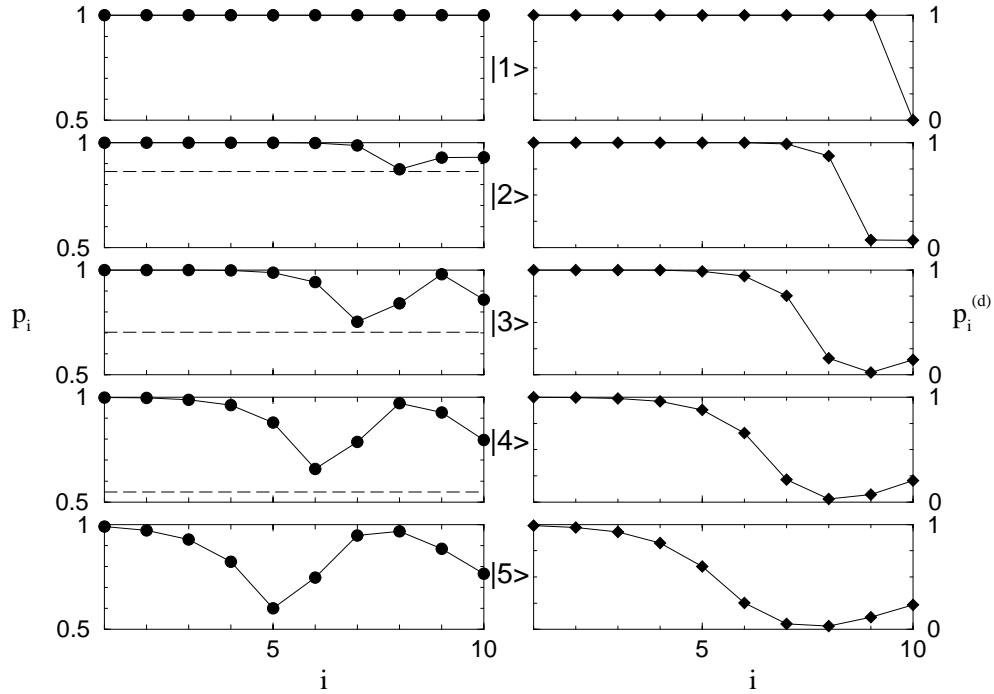


Figure 5.7: Optimal initial atomic state for the preparation of the number states $|n\rangle$, $n = 1, \dots, 5$ (top to bottom), starting from the vacuum as initial field state with $N = 10$ atoms. The left column shows the amount of entanglement of the i -th atom with the other ones [i.e., the largest eigenvalue p_i of the reduced density matrix ρ_i , see Eq. (2.9), where $p_i = 1/2$ indicates maximal and $p_i = 1$ no entanglement]. Moreover, the horizontal dashed lines indicate the maximum overlap of the atomic states with a product state of the N atoms, which is bounded from above by the smallest p_i , compare Eq. (2.10). (In the case $n = 5$, the maximum overlap is 42%.) The right column shows the population $p_i^{(d)}$ of the ground state. For each value of n , the optimal vacuum Rabi angle was chosen [approximately given by the estimation (4.1)]: $\phi = 1.57, 1.30, 1.13, 1.02$, and 0.93 (from $n = 1$ to $n = 5$). For $n > 1$, the $(N - n)$ -th atom is most strongly entangled with the other ones.

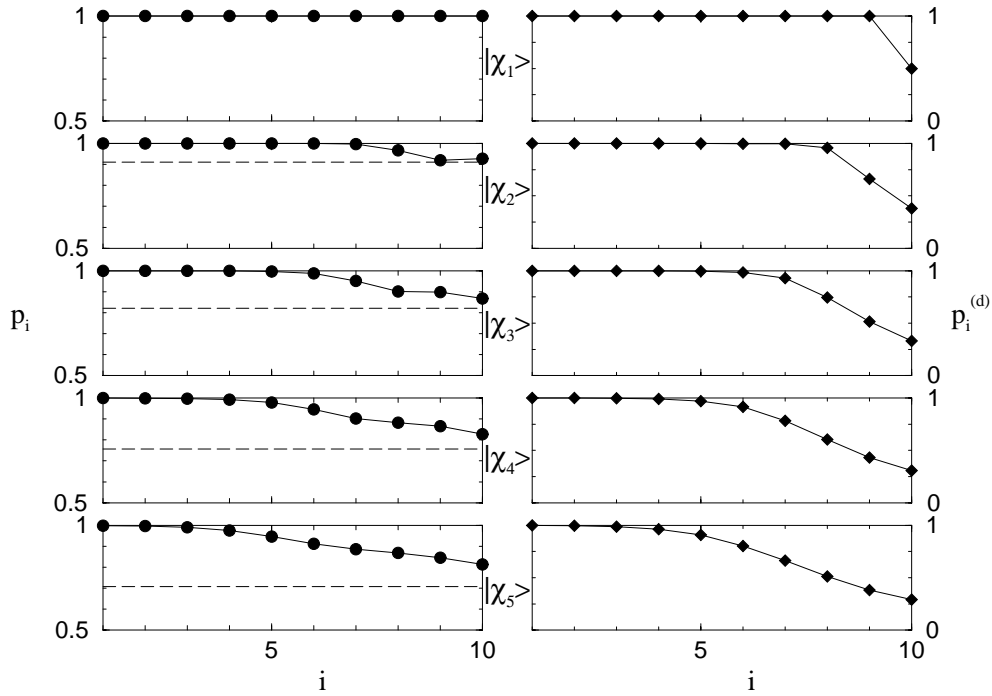


Figure 5.8: Optimal initial atomic state for the preparation of the phase states $|\chi_n\rangle$, truncated at $n = 1, \dots, 5$ (from top to bottom), starting from the vacuum as initial field state with $N = 10$ atoms. As in Fig. 5.7, the ground state population of the i -th atom (right hand side) and its entanglement with the other ones (left hand side) are shown. For each value of n , the optimal vacuum Rabi angle was chosen (the same as in Fig. 5.7). The ground state population $p_i^{(d)}$ monotonically decreases from the first to the last atom. The horizontal dashed lines indicate the maximum overlap of the atomic states with a product state of the N atoms, which is higher than in the corresponding case of a number state, compare Fig. 5.7.

the number states $|i\rangle = |0\rangle, |1\rangle, \dots, |n\rangle$. (Note, however, that the $|\psi_0'^{(i)}\rangle$'s are not identical to the states depicted in Fig. 5.7 for $i < n$, since for the latter the value of the vacuum Rabi angle has been optimized for each individual i .) In particular, the ground state population of each atom in $|\psi_0'\rangle$ is determined by the sum of the ground state populations of the $|\psi_0'^{(i)}\rangle$'s (as can be easily deduced from the fact that the $|\psi_0'^{(i)}\rangle$'s have different excitation numbers i , see chapter 2.2 and appendix A). Consequently, as in the case of number states, the first few atoms enter the cavity mainly in the ground state. For the subsequently injected atoms, the ground state population monotonically decreases, as evident from Fig. 5.8.

The entanglement properties, however, cannot be so easily inferred from the number state case. Since the initial atomic state $|\psi_0'\rangle$ does not have a well defined excitation number, unlike the case of number states, the largest eigenvalue p_i of the reduced density matrix is not given in terms of the ground

state population. As can be seen from the left hand side of Fig. 5.8, also p_i monotonically decreases, so that the last atom is most strongly entangled with the other ones. Remember that the smallest p_i gives an upper bound for the overlap of the atomic state with a product state, see Eq. (2.10). In order to test how tight this upper bound is, we have calculated the maximum overlap with a product state numerically, by optimization over the set of all product states, and plotted the results as horizontal dashed lines. As can be seen (also in Figs. 5.7 and 5.9), the approximation is quite good especially for large values of the maximum overlap. If we compare Figs. 5.8 and 5.7, we see that the initial atomic state for the preparation of phase states has a larger overlap with a product state than in the corresponding case of preparing a number state.

5.2.3 Coherent states

Fig. 5.9 shows the same characteristic quantities of the initial atomic state for the preparation of coherent states $|\alpha\rangle$. Note that, since a classical field is always in a coherent state, these can be easily prepared by coupling the cavity to a classical field source, and turning the intensity low enough. Therefore, we may ask whether this property is somehow reflected also in our preparation scheme, and, as we will see below, this indeed is the case.

In Fig. 5.9, the optimal state $|\psi\rangle$ is compared with the state $|\psi'_0\rangle$, Eq. (4.7). The ground state population of each atom monotonically decreases, in the optimal case almost linearly. Remarkably, both states exhibit much less entanglement than above for the preparation of number states and also the phase states (note the different scales!), especially the optimal state. Hence, coherent states are easier to prepare in the sense that a rather high fidelity can be achieved by using a product state of the N injected atoms. In fact, the product state $|\psi^{(1)}, \dots, \psi^{(N)}\rangle$, where each $|\psi^{(i)}\rangle$ is the eigenvector of the reduced state ρ_i corresponding to the largest eigenvalue p_i , has a large overlap with the optimal atomic state: it almost reaches the numerically evaluated *maximum* overlap with a product state, which is marked by the horizontal dashed lines. Consequently, the fidelity achieved with this product state is approximately as high as the maximum fidelity multiplied by the value of the horizontal dashed line [compare Eq. (6.14), which gives a lower bound for the fidelity achieved by atomic states deviating from the optimal one], i.e., it varies from about 99% for $|\alpha|^2 = 1$, to 87% for $|\alpha|^2 = 5$.

Preparation of coherent states using atomic product states

We have checked that, if the optimal initial atomic state is close to a product state, also the final atomic state (or, equivalently, the optimal initial state for the reverse process of preparing the vacuum, starting from a coherent state $|\alpha\rangle$) has this property. As an example, we show in Fig. 5.10 the initial and final atomic states for the preparation of the coherent state $\alpha = 1$, starting from the vacuum as initial field state, and again with $N = 10$ atoms. Here, we chose a smaller vacuum Rabi angle than before in Fig. 5.9, namely $\phi = 0.35$, in order to examine the large deviation of $F_{\max} = 99.986\%$ from $F' = 74.2\%$ observed in Fig. 5.4(a)

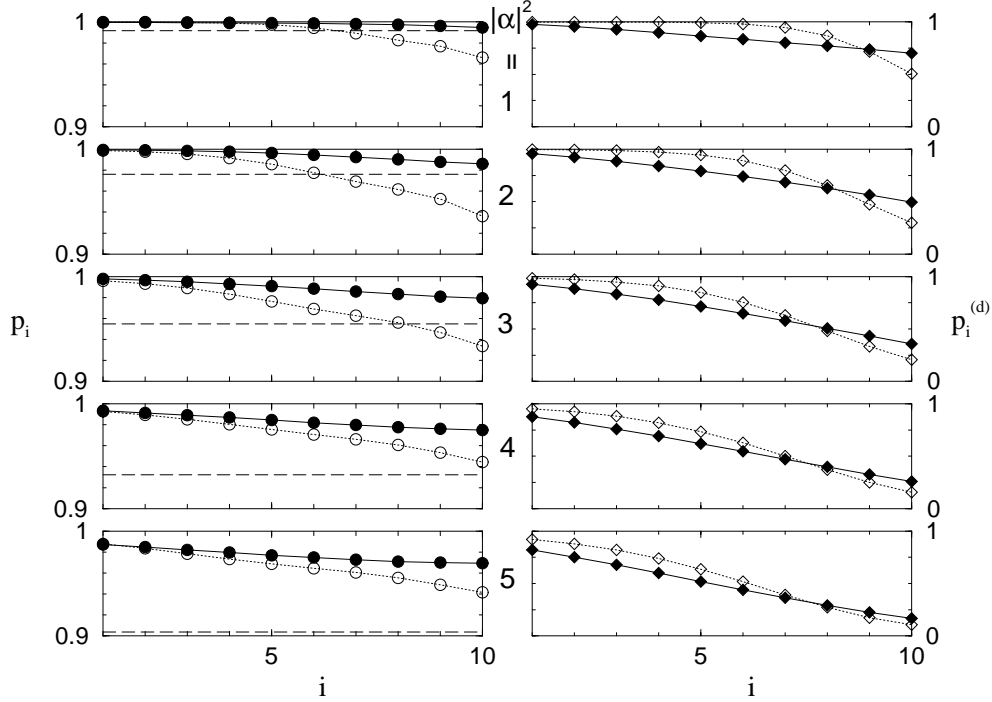


Figure 5.9: Optimal initial atomic state for the preparation of the coherent states $|\alpha\rangle$ with mean photon numbers $|\alpha|^2 = 1, \dots, 5$ (from top to bottom). The state preparation through injection of $N = 10$ atoms starts with the field initially in the vacuum state. As in Figs. 5.7 and 5.8, the ground state population of the i -th atom (right hand side) and its entanglement with the other ones (left hand side) are shown. The solid symbols represent the optimal initial atomic state which is compared to the state $|\psi'_0\rangle$ (open symbols), Eq. (4.7). The optimal values of the vacuum Rabi angles (compare Fig. 5.4) are chosen, i.e., $\phi = 0.95, 0.85, 0.76, 0.69,$ and 0.68 (from $|\alpha|^2 = 1$ to $|\alpha|^2 = 5$). The horizontal dashed lines indicate the maximum overlap of the optimal atomic states with a product state of the N atoms. Note the small scale on the p_i -axis (left hand side): the initial atomic state for the preparation of coherent states is almost a product state.

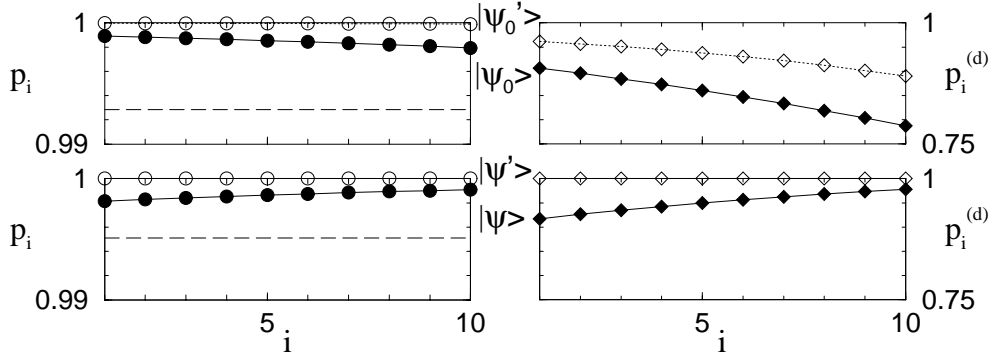


Figure 5.10: Optimal initial atomic state $|\psi_0\rangle$ (top) for the preparation of the coherent state $|\alpha\rangle$ with mean photon number $|\alpha|^2 = 1$, starting from the vacuum as initial field state, with $N = 10$ atoms. Also the corresponding final atomic state $|\psi\rangle$, Eq. (4.5) is shown (bottom). As in Figs. 5.7-5.9, we plotted the ground state population of the i -th atom (right hand side) and its entanglement with the other ones (left hand side). The solid symbols represent the optimal initial atomic state (whose maximum overlap with a product state is again indicated by the horizontal dashed line), whereas the open symbols characterize the state $|\psi'_0\rangle$, for comparison. By definition of $|\psi'_0\rangle$, Eq. (4.7), the corresponding final atomic state is $|\psi'\rangle = |d \dots d\rangle$. All states are very well approximated by product states (note the fine scale on the p_i axis!). The vacuum Rabi angle is $\phi = 0.35$ - the point where a large deviation of $F_{\max} = 99.986\%$ from the lower bound $F' = 74.2\%$ is observed in Fig. 5.4(a). Using the time-reversal argument, we conclude that, when starting from the coherent state $\alpha = 1$, the cavity vacuum can be much more efficiently prepared than by injecting all atoms in the ground state (which would yield fidelity F'), namely by using as initial atomic state the time-reversed final state $T_N|\psi\rangle$ [where T_N essentially reverses the order of the atoms, compare Eq. (3.5)], thereby obtaining the maximum fidelity F_{\max} .

at $\phi = 0.35$. As can be seen, both the initial and final atomic state can be very well approximated by a product state of the N atoms. Hence, when preparing coherent field states, each single atom enters and leaves the cavity almost in a pure state. Consequently, each atom is disentangled from the cavity field both before and after the interaction, which implies that also the cavity field remains almost in a pure state after the interaction with each individual atom [since the unitary interaction (2.1) maps pure states of the atom-field system again onto pure states]. Furthermore, those intermediary field states are *also coherent states*, i.e., the cavity field climbs up on a ladder of coherent states. This is due to the property of the Jaynes-Cummings interaction described at the end of chapter 2.1. As we have seen there, with an appropriately chosen initial single-atom state, a coherent state can be transferred again to a coherent state with high fidelity and almost no entanglement with the atom. Note however, that, for a given ϕ , the remaining entanglement cannot be made arbitrarily small [compare Fig. 2.1(b), where for $\phi < 1$ the entanglement vanishes nearly, but

not completely.] Hence, even in the limit $N \rightarrow \infty$, a coherent state cannot be prepared *exactly* by a product of single-atom states. Only in the limit $\phi \rightarrow 0$ (of course to be taken *after* the limit $N \rightarrow \infty$), a fidelity of 100% can be achieved. This agrees with the findings of [83]: for small vacuum Rabi angles, the cavity field will approach a coherent state $|\alpha\rangle$ when pumped with a flux of atoms which are all prepared in the same state $a|u\rangle - ib|d\rangle$, with $a/b = \phi\alpha/2$. As discussed in chapter 3.3.1, the cavity field then converges to the cotangent state, Eq. (3.4), which reduces to the coherent state $|\alpha\rangle$, in the limit $\phi \rightarrow 0$.

While, having this in mind, it is not surprising that coherent states *can* be prepared by a product of single-atom states, it is not so obvious that, as our numerical results demonstrate, this is really very close to the *optimal* strategy (which yields the highest fidelity), where also entangled initial atomic states are allowed.

5.3 Mixed initial field states

So far in this chapter, we have always assumed the vacuum as the initial field state. However, we know from the property of asymptotic completeness that - in the limit $N \rightarrow \infty$ - the initial atomic state for the preparation of the desired target state $|\chi\rangle$ does not depend on the initial field state ('universal preparability', compare chapter 3.2). Therefore, the state preparation is also possible if we do not know the initial field state, or if we have only incomplete knowledge about its initial state as described by a mixed density matrix ρ_0 . [A mixed density matrix has a positive von-Neumann entropy $S(\rho_0) > 0$, compare Eq. (2.8), which quantifies our lack of knowledge about the state.] Since, finally, the field will be in the desired state $|\chi\rangle$, this means that the information about the initial state of the field (which cannot be lost during a unitary interaction) must be present in the final state of the atoms. Hence, our preparation scheme can be used not only to prepare arbitrary field states by the right choice of the initial atomic state (thereby transferring information from the atoms to the field), but also to transfer information from the field to the atoms.

In chapter 3.3, we have already described a possible strategy for the state preparation starting from an arbitrary initial state: first, we inject a sufficient number of ground state atoms in order to produce the cavity vacuum, then we proceed as described above. Since a sequence of ground state atoms (of, in principle, arbitrary length) can be easily generated experimentally, this method is also quite practical, although it is not necessarily the most efficient one (with respect to the total number of atoms needed for the preparation). However, if we are interested in the above mentioned aspect of information transfer, we would like to distribute the information about the initial field state on as few atoms as possible, in order to simplify a further processing of the information. Therefore, the question arises: what is the *optimal* strategy for the state preparation starting from mixed initial field states, which maximizes the fidelity for a given total number of atoms?

In principle, for a finite number of atoms, the optimal initial atomic state $|\psi_0^{(\text{opt})}\rangle$ is not independent from the initial field state ρ_0 , since the operator

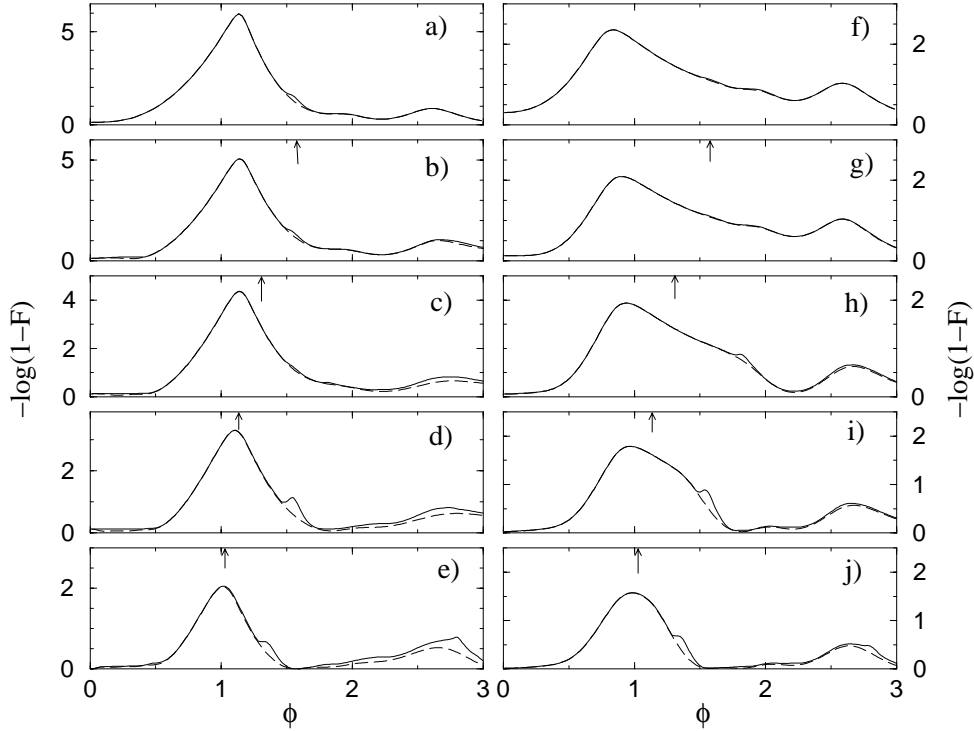


Figure 5.11: Maximum fidelity F_{\max} (solid line) and fidelity F achieved with $|\psi'_0\rangle$ (dashed), Eq. (4.7), for the preparation of the number states $|\chi\rangle = |n\rangle$, $n = 0, 1, 2, \dots, 4$ (top to bottom), with a sequence of $N = 10$ atoms injected into the resonator, as a function of the vacuum Rabi angle ϕ . The initial field states are $\rho_0 = \sum_{i=0}^3 |i\rangle\langle i|/4$ (left, a-e), and the thermal equilibrium state with mean photon number $n_b = 1$ (right, f-j). The arrows denote the optimal vacuum Rabi angle with the vacuum as initial field state [approximately given by Eq. (4.23), compare Fig. 5.1]. The state $|\psi'_0\rangle$, Eq. (4.7), (which is the optimal atomic state when starting from the vacuum, see chapter 5.1), almost perfectly reaches the maximum fidelity also in the case of mixed initial field states.

$M^{(\rho_0)}$, Eq. (4.3), which is needed for the calculation of $|\psi_0^{(\text{opt})}\rangle$, explicitly depends on ρ_0 . As argued in chapter 4.3, however, we may expect that, in fact, the optimal initial atomic state for the vacuum as initial field state gives a good approximation to the optimum result also when starting from different initial field states. In the following, we will test whether this expectation is justified.

An example is shown in Fig. 5.11. Here, we prepare the photon number states $|0\rangle, \dots, |4\rangle$ with $N = 10$ atoms. In contrast to Fig. 5.1, we consider also the vacuum as the target state. The initial field states are the maximally mixed state with up to 3 photons (left, a-e), and the thermal equilibrium state (right, f-j) with mean photon number $n_b = 1$ (which, in the microwave regime, corresponds to a temperature of about 1 K). The fidelity F achieved with the state $|\psi'_0\rangle$ (dashed line), Eq. (4.7), agrees very well with the maximum fidelity (solid line). Close to the maxima of F_{\max} and F , the agreement is exact in the two cases (a) and (f) of the vacuum as initial field state, whereas only

tiny deviations are observed in the other cases. This proves that, indeed, the state $|\psi'_0\rangle$ gives almost exactly the optimum result of the state preparation, also when starting from mixed initial field states. If the target field state is the vacuum, then $|\psi'_0\rangle = |d\dots d\rangle$, according to Eq. (4.7). It is not surprising that the state $|d\dots d\rangle$ is the optimal state to prepare the vacuum, since we have already verified this property in the case of number states as initial field states (using the time-reversal argument), and since both initial field states considered in Fig. 5.11 are mixtures of number states.

Furthermore, we marked in Fig. 5.11 the values of the vacuum Rabi angles which maximize the fidelity when starting with the vacuum as initial field state [approximately given by Eq. (4.23)]. Obviously, they do not always agree with the optimum values for mixed initial field states: with $\rho_0 = \sum_{i=0}^3 |i\rangle\langle i|/4$ (left, a-e), a good agreement is observed only for $n = 3$ and $n = 4$ (d and e), whereas for $n < 3$ the optimal ϕ approximately equals the one for $n = 3$. This agrees with our previous findings that the optimal vacuum Rabi angle depends on the relevant subspace of the photon field, such as to maximize the smallest one of the transition probabilities $|B_n|^2 = \sin^2(\phi\sqrt{n})$ in this subspace (compare chapter 4.2.2). Remember that the first atoms of the state $|\psi'_0\rangle$ enter the cavity almost in the ground state (compare Fig. 5.7). Therefore, the mean photon number of the cavity field at first decreases, before it increases again to reach the desired field state $|\chi\rangle$. Hence, the relevant subspace of the photon field is given by the maximum photon number either of the initial or of the target field state. In the example of Fig. 5.11, since the field initially contains up to 3 photons, the optimal ϕ is approximately constant for $n \leq 3$, whereas the 4-photon state comes into play in the case $n = 4$ (e). On the other hand, in the case of the thermal initial state, a close inspection of the right half of Fig. 5.11 (f-j) reveals that the optimal ϕ slightly increases with increasing n : for $n = 0$ (f), we have $\phi_{\text{opt}} = 0.84$. According to Eq. (4.23), this corresponds to a relevant field subspace of up to 7 photons (which, with $n_b = 1$, contains 99.6% of the thermal initial population), whereas $\phi_{\text{opt}} = 0.98$ for $n = 4$ (j), corresponding to up to 5 photons (thermal population: 98.4%). This behavior is again in accordance with the considerations in chapter 4.2.2: since the fidelity of the state preparation decreases with increasing n , the thermal initial population of higher photon numbers can be neglected for larger n , which leads to a smaller relevant field subspace.

Fig. 5.12 shows another example, for the preparation of coherent states. Here, we compare the maximum fidelity with the fidelities achieved by the optimal initial atomic state $|\psi_0^{(\text{vac})}\rangle$ when starting from the vacuum (dotted line) and by the state $|\psi'_0\rangle$ (dashed line). Since, unlike for the preparation of number states, the state $|\psi'_0\rangle$ does not yield the optimal fidelity when starting from the vacuum (see Fig. 5.4), it is not surprising that it neither does when starting from a mixed state, as proven by the fact that the dotted line is not identical to the solid one in Fig. 5.11. In most cases, $|\psi_0^{(\text{vac})}\rangle$ also gives a higher fidelity than $|\psi'_0\rangle$ for mixed states [apart from the exception in Fig. 5.12(b) around $\phi \simeq 1.2$, see below]. However, the maximum fidelity is not as well reproduced as in the case of targeted number states, see Fig. 5.11, where F_{max} can hardly be distinguished

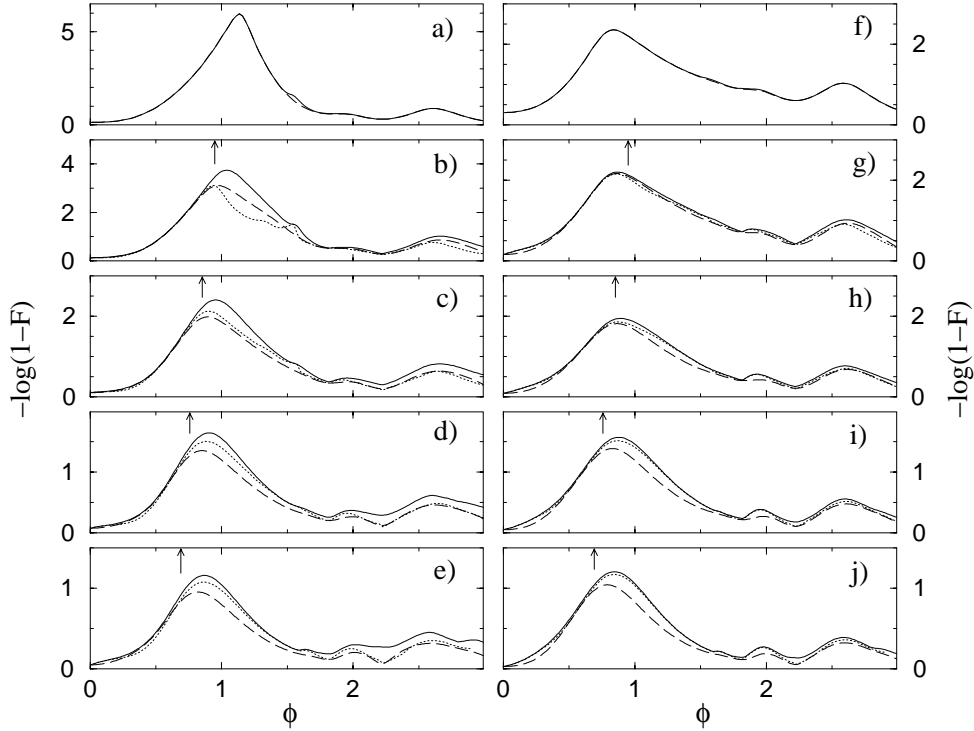


Figure 5.12: Same as Fig. 5.11, for the preparation of the coherent states $|\alpha\rangle$ with mean photon numbers $|\alpha|^2 = 0, 1, 2, \dots, 4$ (top to bottom). The dotted lines display the fidelity achieved by the optimal initial atomic state $|\psi_0^{(\text{vac})}\rangle$ in the case of the vacuum as initial field state, compare Fig. 5.9). Although the state $|\psi_0^{(\text{vac})}\rangle$ does not reproduce the maximum fidelity as well as in the case of number states (Fig. 5.11), it still gives a quite good approximation, especially for the thermal initial states (right).

from the fidelity achieved with $|\psi_0^{(\text{vac})}\rangle = |\psi'_0\rangle$. This can be understood if we consider the properties of the initial atomic states $|\psi_0^{(\text{vac})}\rangle$ examined in Figs. 5.7 and 5.9 (solid symbols): for the number states, the ground state population of the first few atoms is higher, which leads to a more efficient purification of the field (as discussed in chapter 4.3) than for the coherent states. Consequently, in the latter case, the ground state population of the first few atoms has to be slightly increased in order to reach the maximum fidelity F_{max} . The difference between F_{max} and the fidelity reached by $|\psi_0^{(\text{vac})}\rangle$ is most clearly pronounced in Fig. 5.11(b), for the coherent state with the smallest mean photon number $|\alpha|^2 = 1$, around $\phi \simeq 1.2$. The reason is the high maximum fidelity of the state preparation in this case, which almost reaches 99.99%. In order to achieve such a high fidelity, the purification of the initially mixed state has to be very efficient, and therefore the lower ground state population of the first few atoms of the state $|\psi_0^{(\text{vac})}\rangle$ has a larger impact.

Furthermore, Fig. 5.12 again displays the shift of the optimal vacuum Rabi angle induced by changing the initial field state from the vacuum to a mixed

state. In the case $\rho_0 = \sum_{i=0}^3 |i\rangle\langle i|/4$ (left, a-e), the optimal ϕ is always larger than for the vacuum. This is due to the fact that the purification of ρ into the vacuum is most efficient at a larger value of ϕ , see (a). With the thermal initial state (right), the optimal ϕ is shifted to a lower value in case (b), and reversely in the other cases. Here, we cannot give a simple interpretation of this behavior, since both, initial and final state, exhibit a nonvanishing population of higher photon numbers.

In summary, we have given numerical evidence that the optimal initial atomic state for the preparation of the field state $|\chi\rangle$ starting from the vacuum as initial field state gives nearly the optimal result also when starting from mixed initial field states. The optimal value of the vacuum Rabi angle ϕ , however, may significantly differ in both cases. As demonstrated in chapter 5.2, the optimal atomic state has the property that, for large N , the ground state population of the first few atoms is close to 1. Hence, the mean photon number in the cavity during the preparation process at first decreases almost to zero, and later increases again to reach the desired final state. This is similar to the simple picture outlined in chapter 3.3.3, according to which the preparation takes place in two steps: purification followed by preparation. However, the optimal strategy does not *strictly* follow this simple picture, as the first atoms do not enter the cavity precisely in the ground state. Furthermore, we have checked that the photon field does not exactly pass through the vacuum state during the preparation process, i.e., the population of the vacuum never reaches a value comparable to the final target state fidelity. As a typical example, in the situation of Fig. 5.11(e) (target state $|4\rangle$), for the optimal value of $\phi = 1.00$, the maximum vacuum population of 92.3%, reached after the fourth atom passing through the cavity, is much smaller (on the logarithmic scale) than the final fidelity of 99.1%. Note that, if we injected the first four atoms *precisely* in the ground state, the vacuum population after the fourth atom would be higher (i.e., 96.7%), but the final fidelity (when choosing the optimal initial state for the remaining 6 atoms) would be considerably lower, namely $F = 94.3\%$. Hence, although the general idea ‘first prepare the vacuum’ is roughly realized by the optimal strategy, we cannot give a really convincing argument why the optimal initial atomic state when starting from the vacuum as initial field state is so well adapted also to mixed initial field states, as our numerical calculations show.

5.4 Reaching the limit of asymptotic completeness

Up to now, we have used in all our numerical examples a constant number of atoms, $N = 10$. In this chapter, we will study the properties of our state preparation scheme as a function of N , in order to see how fast the limit $N \rightarrow \infty$ of asymptotic completeness will be reached.

5.4.1 Convergence of the fidelity

At first, let us examine the convergence of the maximum fidelity towards the ideal value 1, which is predicted by asymptotic completeness in the limit $N \rightarrow \infty$.

Initial field state: vacuum

Remember that, in the case of the vacuum as initial field state, we have derived explicit expressions for the lower bound F' , Eqs. (4.16,4.17), which exhibit an exponentially fast convergence of the fidelity with respect to target field states including at most a finite number n of photons. More precisely, for the optimal value (4.23) of the vacuum Rabi angle, the rate λ of the convergence (defined by $1 - F \propto 10^{-|\lambda|N}$) equals

$$\lambda = \log \left(\cos^2 \left(\frac{\pi}{1 + \sqrt{n}} \right) \right). \quad (5.4)$$

On the other hand, for field states with nonvanishing population also at infinitely large photon numbers, such as the coherent states, we do not expect an exponential convergence, since with increasing fidelity of the state preparation, the higher photon numbers of the target states must be taken into account. This introduces new transition probabilities $|B_n|^2$, thereby potentially decreasing the convergence rate (which is given by the smallest $|B_n|^2$.)

Does the same also apply to the maximum fidelity? [Since, in general, $F_{\max} \geq F'$, see Eq. (4.14), the convergence of F_{\max} cannot be slower.] The results of chapter 5.1 suggest a positive answer: as shown there, the lower bound F' is in most cases quite close to F_{\max} (especially in the here considered optimal regime of ϕ). However, since we examined only the case of $N = 10$ atoms in chapter 5.1, we still have to verify that the conjecture $F_{\max} \simeq F'$ remains valid also for other values of N .

For this purpose, we show in Fig. 5.13 the maximum fidelity for the preparation of the photon number state $|5\rangle$, of the phase state $|\chi_5\rangle$, truncated at $n = 5$, and of the coherent state $|\alpha\rangle$ with mean photon number $|\alpha|^2 = 4$, as a function of N . For comparison, we also plotted the lower bound F' (solid lines), the fidelity F achieved by the initial state $|\psi'_0\rangle$ (dashed lines), Eq. (4.7), and the convergence rate λ as predicted above (dotted lines, only the slope is relevant).

Firstly, the conclusions of chapter 5.1, for $N = 10$ and within the optimal regime of ϕ , are equally confirmed for other values of N : when preparing number states $F_{\max} = F = F'$, while in the case of phase states F_{\max} is almost equal to F , and slightly larger than F' . Furthermore, the difference between F_{\max} and F' in Fig. 5.13(a) (open circles and solid line) appears to be approximately constant (on the logarithmic scale) for $N \gtrsim 10$. For coherent states as target states, Fig. 5.13(b), larger deviations of F_{\max} , F , and F' are observed.

Secondly, the convergence of the fidelity with increasing N follows the behavior predicted above: it is exponentially fast in Fig. 5.13(a), where the photon number of the target field states does not exceed 5, and the corresponding convergence rate agrees with the rate λ , Eq. (5.4). In the case of the coherent state, Fig. 5.13(b), after attaining a maximum at $N \simeq 7$, the rate of convergence slightly decreases again with increasing N . Although for the higher values of N (i.e., $N \geq 12$), the convergence rate appears to be constant, we expect that it further decreases for $N > 15$. We have checked that this is the case for the lower bound F' , which - in contrast to F_{\max} - can be calculated also for very

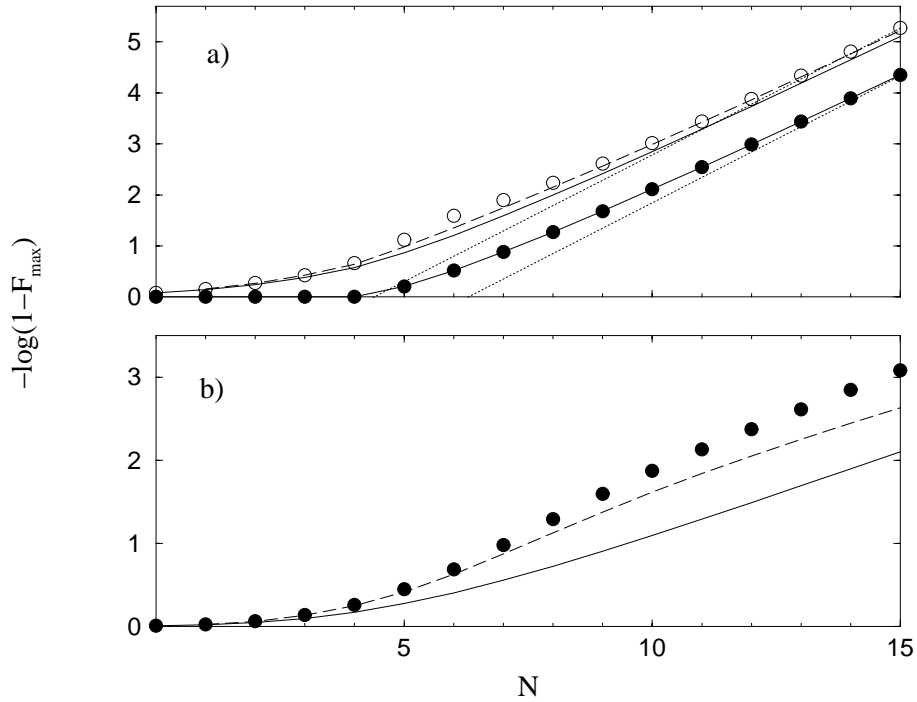


Figure 5.13: Convergence of the maximum fidelity F_{\max} for the preparation of (a) the 5-photon state $|\chi\rangle = |5\rangle$ (filled circles) and the truncated phase state $|\chi\rangle = \sum_{i=0}^5 |i\rangle/\sqrt{6}$ (open circles) of the cavity field, and of (b) the coherent state $|\alpha\rangle$ with mean photon number $|\alpha|^2 = 4$ (filled circles), as a function of the number N of atoms injected into the resonator. Vacuum Rabi angle: (a) $\phi_{\text{opt}}^{(5)} = 0.97$, according to the estimation (4.23), with $n = 5$ (for the number and phase state), and (b) $\phi = 0.69$ (optimal choice for the coherent state, see Fig. 5.4d). Initial field state: the vacuum $|0\rangle$. In the first two cases (a), F_{\max} approaches the ideal value 1 *exponentially* fast. For comparison, also the lower bound F' (solid lines) and the fidelity F achieved by the state $|\psi'_0\rangle$, Eq. (4.7) (dashed lines) are plotted, as well as the predicted convergence rate λ , Eq. (5.4) (dotted lines).

large N using Eq. (4.16). In order to test whether also F_{\max} follows this behavior, we can examine the preparation of a coherent state with a smaller mean photon number, where less atoms are required to reach the same fidelity. Such an example is shown in Fig. 5.14(b) (filled circles). Here, the decrease of the convergence rate is slightly more pronounced than for $|\alpha|^2 = 1$ in Fig. 5.13(b).

Mixed initial field states

Next, we want to see how the initial field state influences the convergence of the maximum fidelity. For this purpose, we examine mixed initial field states in Fig. 5.14. The target states are the 2-photon number state (a and c), and the coherent state $|\alpha\rangle$ with mean photon number $|\alpha|^2 = 1$ (b and d), whereas the initial field states are the maximally mixed states including up to n pho-

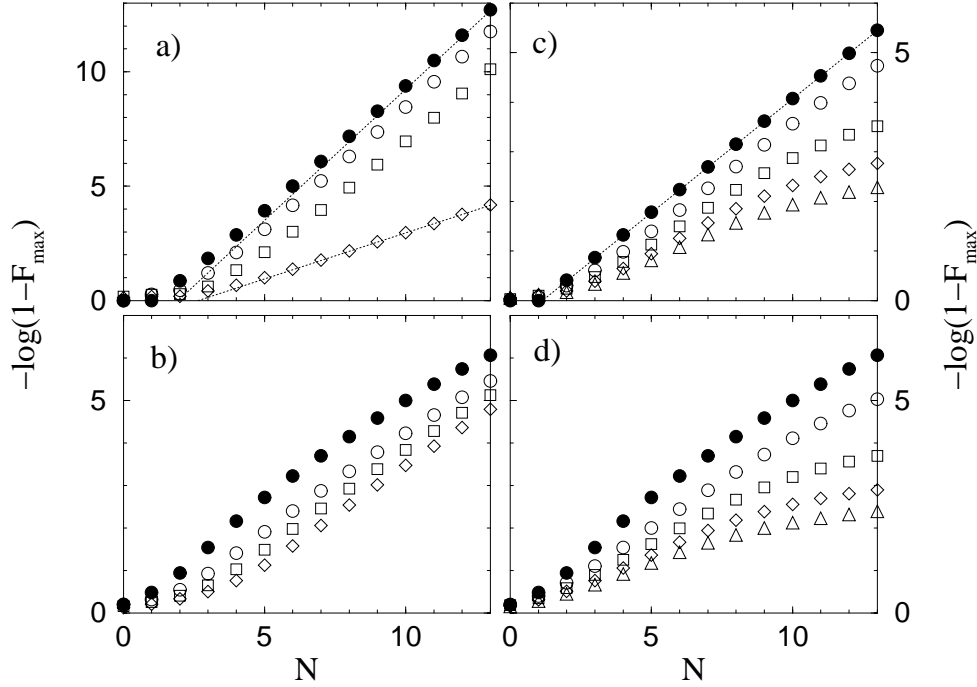


Figure 5.14: Maximum fidelity F_{\max} for the preparation of the 2-photon state $|\chi\rangle = |2\rangle$ (upper half, a and c), and of the coherent state $|\alpha\rangle$ with mean photon number $|\alpha|^2 = 1$ (lower half, b and d), as a function of the number N of atoms injected into the resonator, for different initial field states: the vacuum (filled circles), the maximally mixed states $\rho_0 = \sum_{i=0}^n |i\rangle\langle i|/(n+1)$, truncated at $n = 1, 2$ and 3 (open symbols in the left column, a and b), and thermal initial field states with mean photon numbers $n_b = 0.25, 0.5, 0.75$, and 1 (open symbols in the right column, c and d). The vacuum Rabi angle is (a): $\phi = 1.3$ [according to the estimation (4.23) with $n = 2$], (b) and (d): $\phi = 0.95$ (optimal for $N = 10$ and the vacuum as initial field state, see Fig. 5.4a), and (c): $\phi = 0.94$ (optimal for $N = 10$ and the thermal initial state with $n_b = 1$, see Fig. 5.11h). The dotted lines display an estimation of the convergence rate, given by the smallest transition probability in the relevant photon field subspace (compare chapter 4.2.2), namely $\lambda = \log(\cos^2(1.3))$ and $\log(\cos^2(1.3\sqrt{3}))$ in case (a), and $\lambda = \log(\cos^2(0.94))$ in case (c). The convergence to $F_{\max} = 1$ is exponentially fast if both, initial and final field state, possess a finite maximum photon number.

tons, i.e., $\rho_0 = \sum_{i=0}^n (|i\rangle\langle i|)/(n+1)$, with $n = 1, 2, 3$ (a and b), and thermal initial states with mean photon numbers $n_b = 0.25, 0.5, 0.75$, and 1 (b and d). For comparison, also the maximum fidelity with the vacuum as initial state is marked by the filled circles. In order to reach the asymptotic regime of very high fidelities also for mixed initial field states, we chose target field states with a lower mean photon number than in Fig. 5.13. (For comparison, the fidelity for target states with higher mean photon numbers, using $N = 10$ atoms, can be read from Figs. 5.11 and 5.12.)

In Fig. 5.14(a), exponential convergence is also observed for the mixed initial field states. This is due to the fact that both initial and final field states possess a finite maximum photon number. Furthermore, as discussed in chapter 4.2.2, the convergence rate is given by the smallest of the transition probabilities $|B_n|^2 = \sin^2(\phi\sqrt{n})$ in the relevant photon field subspace. Hence, we have $\lambda = \log(\cos^2(1.3)) = -1.15$, for maximum photon numbers of the initial field state below 3, while the convergence rate is smaller, i.e., $\lambda = \log(\cos^2(1.3\sqrt{3})) = -0.40$, for the maximally mixed state truncated at $n = 3$. This is not surprising, since the vacuum Rabi angle was chosen according to Eq. (4.23) with $n = 2$, and thereby optimized for initial and final field states including at most 2 photons. [If we optimized ϕ for maximum photon number $n = 3$, i.e., $\phi_{\text{opt}}^{(3)} = 1.15$, according to Eq. (4.23) with $n = 3$, we would obtain the same convergence rate in all the four cases of Fig. 5.14(a), namely $\lambda = \log(\cos^2(1.15)) = -0.78$.]

Fig. 5.14(c) shows the maximum fidelity for the preparation of the same target state $|2\rangle$, but starting from thermal initial states. Here, we chose a different vacuum Rabi angle than in (a), namely $\phi = 0.94$, which is better suited for thermal initial field states, see Fig. 5.11(h). Not surprisingly, the maximum fidelity when starting from the vacuum (filled circles) increases exponentially fast, with the convergence rate $\lambda = \log(\cos^2(0.94))$ [since $\sin^2(0.94)$ is the smallest relevant transition probability, see chapter 4.2.2], whereas in the case of thermal initial field states the convergence rate deviates from this prediction at high fidelities, where the initial state's population of the larger photon numbers becomes relevant.

Finally, Figs. 5.14(b) and (d) display the preparation of the coherent state $|\alpha\rangle$ with mean photon number $|\alpha|^2 = 1$. Here, we chose in both cases the vacuum Rabi angle $\phi = 0.95$, which is the optimal one for $N = 10$ atoms, starting from the vacuum (see Fig. 5.4a), and also nearly optimal for the mixed initial field states (see Fig. 5.11b and g). It is evident that, at larger numbers of atoms - and consequently higher fidelities - the preparation is more difficult with thermal states rather than truncated maximally mixed states as initial states. This is again due to the initial state's nonvanishing population of high photon numbers.

In summary, the convergence of the maximum fidelity with increasing number N of atoms is exponentially fast, if both initial and final field state possess a finite maximum photon number.

5.4.2 Convergence of the optimal initial atomic state

In chapter 5.4.1, we have examined the convergence of the fidelity towards 1 as a function of the N . Now, we want to see how the corresponding optimal initial atomic states change with N , and what happens when we approach the limit $N \rightarrow \infty$. Thereby, we will obtain a more detailed picture of the limit of asymptotic completeness than by only looking at the maximum fidelity.

As we have seen in chapter 5.2, in many cases the state $|\psi'_0\rangle$, Eq. (4.7), gives a good approximation for the optimal initial atomic state. Furthermore, we may use the explicit expression, Eq. (4.7), in order to study the behavior of $|\psi'_0\rangle$ as a function of N . In order to distinguish the states $|\psi'_0\rangle$ for different N 's, we write $|\psi_0'^{(N)}\rangle$. Then, we can try to establish a relation between $|\psi_0'^{(N)}\rangle$ and the state $|\psi_0'^{(N-1)}\rangle$ for $N - 1$ atoms.

Starting from the definition of $|\psi_0'^{(N)}\rangle$, Eq. (4.7), we have:

$$\begin{aligned} \sqrt{F'^{(N)}} |\psi_0'^{(N)}\rangle &= \langle 0|U_N^\dagger|\chi, d \dots d\rangle \\ &= \langle 0|U_1^\dagger U_{N-1}^\dagger|\chi, d \dots d\rangle, \end{aligned} \quad (5.5)$$

where U_1^\dagger operates on the first atom [but is applied *after* U_{N-1}^\dagger , since the dagger reverses the order of the N atoms in Eq. (2.4)], and U_{N-1}^\dagger on the remaining $N - 1$ atoms. The latter operation results in a final state of the field and the last $N - 1$ atoms which we write as follows:

$$U_{N-1}^\dagger|\chi, \underbrace{d \dots d}_{N-1}\rangle = \sum_{n=0}^{\infty} \sqrt{F_n'^{(N-1)}} |n, \psi_n'^{(N-1)}\rangle. \quad (5.6)$$

This equation defines the atomic state $|\psi_n'^{(N-1)}\rangle$ obtained when projecting the final state $U_{N-1}^\dagger|\chi, d \dots d\rangle$ onto the field state $|n\rangle$. For $n = 0$, this is the state $|\psi_0'^{(N-1)}\rangle$ given by Eq. (4.7). The coefficients $F_n'^{(N-1)}$ are required to normalize the states $|\psi_n'^{(N-1)}\rangle$, and give the fidelity of the state (5.6) with respect to the photon number state $|n\rangle$. Hence, they fulfill the normalization condition $\sum_n F_n'^{(N-1)} = 1$, and, for $n = 0$, the fidelity $F_0'^{(N-1)} = F'^{(N-1)}$ is identical to the lower bound F' as defined by Eq. (4.9).

Next, following Eq. (5.5), we calculate the operation of U_1^\dagger on the first atom, which is in state $|d\rangle$, and on the field, which is entangled with the last $N - 1$ atoms, as a consequence of Eq. (5.6). [Since the dagger transforms $-i$ in Eq. (2.1) into $+i$, the operation of U_1^\dagger is similar to Eq. (2.3), but with $+i$ instead of $-i$.] After projecting onto the field vacuum, we obtain:

$$\sqrt{F'^{(N)}} |\psi_0'^{(N)}\rangle = \sqrt{F'^{(N-1)}} |\psi_0'^{(N-1)}, d\rangle + i \sin(\phi) \sqrt{F_1'^{(N-1)}} |\psi_1'^{(N-1)}, u\rangle. \quad (5.7)$$

Since $F'^{(N-1)}$ is very close to 1 for large N , and consequently $F_1'^{(N-1)}$ almost zero, the main contribution to the state $|\psi_0'^{(N)}\rangle$ consists of the state $|\psi_0'^{(N-1)}\rangle$ for the last $N - 1$ atoms, which is supplemented by the first atom in the ground state. As a consequence, for large N , the first few atoms enter the cavity almost

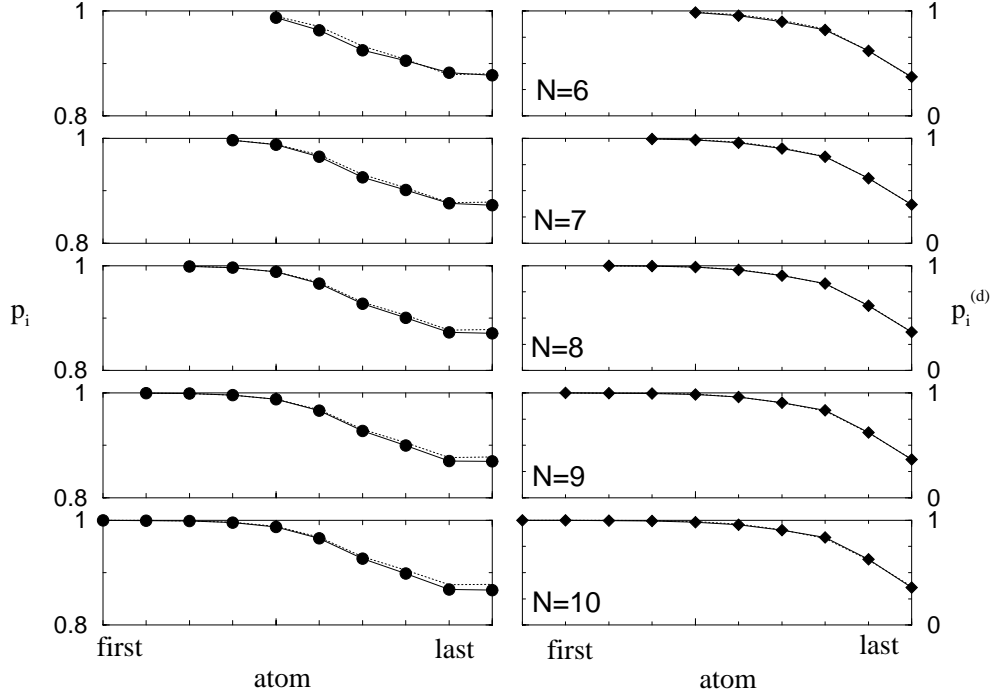


Figure 5.15: Optimal initial atomic state for the preparation of the (randomly chosen) state $|\chi\rangle = (0.34 - 0.36i)|0\rangle + (-0.14 - 0.31i)|1\rangle + (-0.02 + 0.28i)|2\rangle + (-0.16 + 0.004i)|3\rangle + 0.29|4\rangle$, with $N = 6, \dots, 10$ atoms (top to bottom), starting from the vacuum as initial field state. The symbols (connected by the solid lines) represent the optimal initial atomic state which is almost identical to the state $|\psi'_0\rangle$ (dotted lines), Eq. (4.7). As in Figs. 5.7-5.10, the ground state population of the i -th atom (right hand side) and its entanglement with the other ones (left hand side) are shown (remember: $p_i = 1/2$ indicates maximal and $p_i = 1$ no entanglement). Vacuum Rabi angle: $\phi_{\text{opt}}^{(4)} = 1.05$, according to the estimation (4.23), with $n = 4$. When increasing N , the first atoms enter the cavity *almost* exactly in the ground state, whereas the last atoms remain essentially unchanged. Note that the logarithmic fidelity increases from $f = 2.5$ at $N = 6$ to $f = 4.6$ at $N = 10$, whereas it would remain constant if the first atoms entered the cavity *precisely* in the ground state.

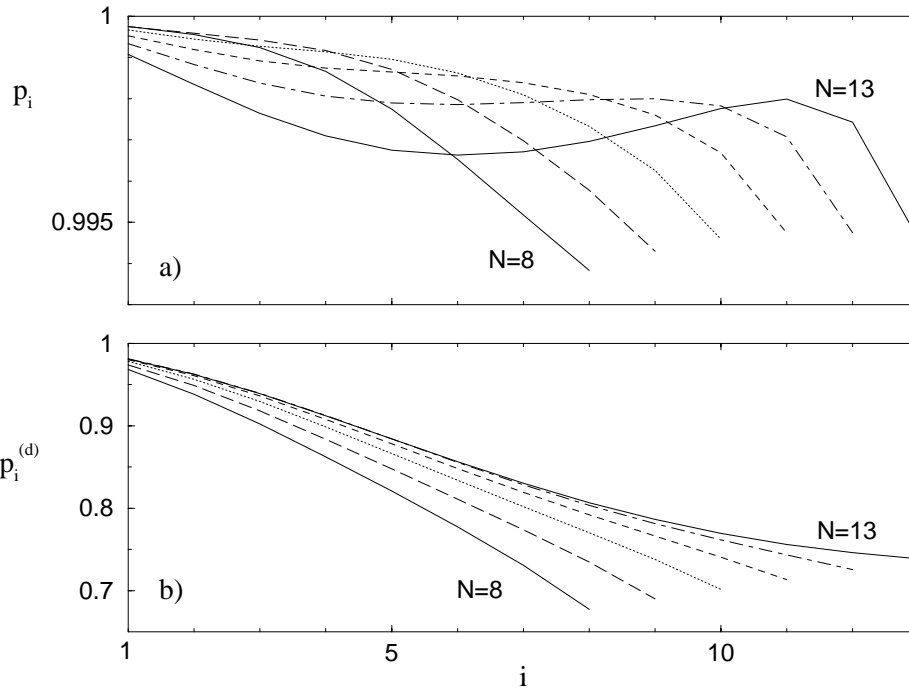


Figure 5.16: Optimal initial atomic state for the preparation of the coherent state $|\alpha\rangle$ with mean photon number $|\alpha|^2 = 1$, with $N = 8, 9, \dots, 13$ atoms, starting from the vacuum as initial field state. As in Figs. 5.7-5.15, the ground state population of the i -th atom (bottom) and its entanglement with the other ones (top) are shown for the optimal vacuum Rabi angle $\phi = 0.95$. The convergence behavior deviates from the one of $|\psi'_0\rangle$ depicted in Fig. 5.15: when increasing N , the ground state population of the last atom considerably changes, whereas the first atom approaches the ground state only very slowly.

exactly in the ground state, as we already argued in chapter 4.3. This is also confirmed by Fig. 5.7 for smaller photon numbers (where $N = 10$ is a ‘large’ number of atoms). This behavior holds for any value of ϕ (except for trapping state conditions). If ϕ is not close to its optimal value, however, we need a higher number N of atoms to reach a value of $F^{(N-1)}$ close to 1.

Note that if the first atom would enter the cavity *exactly* in the ground state, the maximum fidelity for N atoms would obviously be the same as for $N - 1$ atoms (since the first atom in the ground state does not have any effect on the field vacuum). Hence, it is the tiny part of the optimal atomic state (5.7) with the first atom in the upper state, which is responsible for the increase of the maximum fidelity.

Since the state $|\psi'_0\rangle$ is equal to the optimal initial atomic state $|\psi^{(\text{opt})}\rangle$ for the preparation of number states, and at least gives a good approximation in most other cases, we expect that the above conclusions are also valid for the optimal atomic state: at large N , the main contribution to $|\psi^{(\text{opt})}\rangle$ should be the first atom in the ground state and the optimal state for $N - 1$ atoms. Fig. 5.15 shows an example, which, indeed, confirms this prediction. In order to emphasize

that this rule not only holds for special field states such as number states or the truncated phase states, we have randomly chosen a target field state $|\chi\rangle$ including up to 4 photons according to Eq. (5.1), see caption of Fig. 5.15.[‡] Since, indeed, the optimal atomic state is almost identical to the state $|\psi'_0\rangle$ (solid and dotted lines in Fig. 5.15), its convergence for $N \rightarrow \infty$ follows the above predicted behavior.

Is this also the case if the optimal atomic state deviates more strongly from $|\psi'_0\rangle$, as, e.g., for the coherent states? Fig. 5.16 shows the answer. As already observed in Fig. 5.9 for $N = 10$, the ground state population of the first few atoms is not as high as for the state $|\psi'_0\rangle$. Although the ground state population $p_1^{(d)}$ of the first atom slightly increases with increasing N , see Fig. 5.16(b), it is unclear whether it will converge to 1 in the limit $N \rightarrow \infty$. Instead, it is rather the ground state population of the *last* atoms, which is influenced most strongly by the number N of atoms - in contrast to the behavior of the state $|\psi'_0\rangle$, where the state of the last atoms is almost unchanged when increasing N [see the above discussion of Eq. (5.7) and Fig. 5.15]. In all cases, the state remains quite close to a product state (note the scale of Fig. 5.16a). Furthermore, the smallest one of the eigenvalues p_i of the reduced density matrix [which gives an upper bound for the overlap with a product state, see Eq. (2.10)] is always the last one, $i = N$. Based on the range of $N = 8, \dots, 13$ covered in Fig. 5.16, we cannot draw precise conclusions about the limit $N \rightarrow \infty$ of the overlap with a product state: although, from $N = 8$ to $N = 11$, the smallest eigenvalue p_N increases, indicating an increasing overlap with a product state, this trend is not continued for larger values of N .

5.4.3 Other initial atomic states than the optimal one

So far, we have concentrated on the maximum fidelity of the state preparation. We have seen that the optimal initial atomic state, which prepares the desired field state $|\chi\rangle$ with the maximum fidelity when starting from the vacuum as initial field state, is also able to prepare $|\chi\rangle$ when starting from a mixed initial field state (and even achieves almost the maximum fidelity).

However, as discussed in chapter 3.2, the property of asymptotic completeness not only implies that there exists *one* atomic state which prepares the desired field state independently of the initial field state, but also that for *all other* initial atomic states the final field state will be independent of its initial state. In particular, as already argued on p. 26, we expect that among the other atomic states, there are some which also prepare the desired field state with high fidelity. How many such states are there? A simple answer to this question exists only in the limit $N \rightarrow \infty$, and if the photon field is of finite dimension n (i.e., in the case of a $|n - 1\rangle$ -trapping state). Then, the dimension of the atomic ‘high-fidelity subspace’ equals a fraction of $1/n$ of the dimension 2^N of the total atomic space [since the same ratio describes the degeneracies of the

[‡]In order to compare the state $|\chi\rangle$ with the other randomly chosen states in Fig. 5.5, we note that, using $N = 8$ atoms, the preparation of $|\chi\rangle$ succeeds with a maximum logarithmic fidelity of $f_{\max} = 3.6$, with a relative deviation $\Delta f_{\text{rel}} = 8.3\%$ from the lower bound f' , i.e. $|\chi\rangle$ lies almost exactly in the center of Fig. 5.5(b).

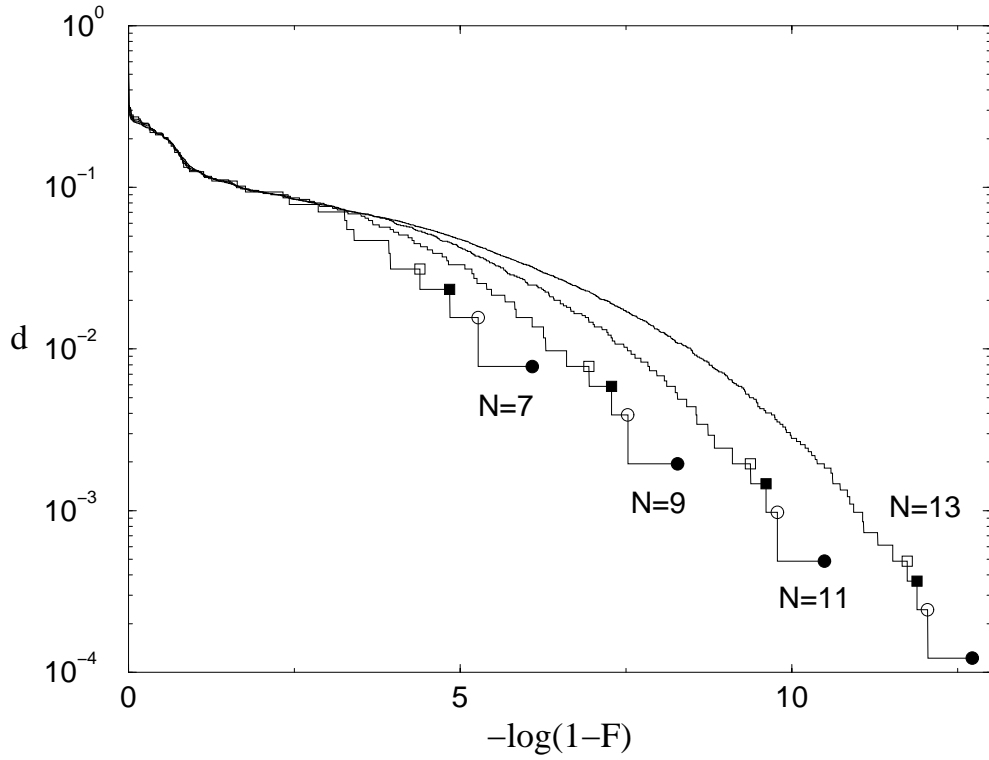


Figure 5.17: Fraction $d(F)$ of eigenvalues of $M^{|0\rangle\langle 0|}$ larger than F , for the preparation of the 2-photon number state, with $N = 7, 9, 11,$ and 13 atoms. Vacuum Rabi angle: $\phi_{\text{opt}}^{(2)} = 1.3$. For each N , the symbols mark the four largest eigenvalues. The first few eigenvalues approach $F = 1$ exponentially fast, whereas the main part of the spectrum [with $-\log(1 - F) \lesssim 3$, or $d(F) \gtrsim 10\%$] is approximately constant. In all four cases, the fraction of eigenvalues very close to zero is about 70%.

two eigenvalues 0 and 1 of the one-dimensional projection onto the desired field state, which are preserved under the unitary evolution of Eq. (3.2)]. However, even apart from the fact that the photon field is in general infinite-dimensional, we cannot make a similar prediction in the case of a finite number of N , since we do not know how fast the limit of asymptotic completeness is reached.

To examine this question, we show in Fig. 5.17 the distribution of the eigenvalues F of $M^{|0\rangle\langle 0|}$ for the preparation of the 2-photon number state, with different numbers of atoms, from $N = 7$ to $N = 13$. Remember that the fidelity achieved with an atomic initial state $|\psi_0\rangle$ is given by $F = \langle \psi_0 | M^{|0\rangle\langle 0|} | \psi_0 \rangle$, Eq. (4.2). Hence, the dimension $D(F)$ of the subspace of atomic states which achieve a fidelity larger than F equals the number of eigenvalues larger than F . To compare cases of different N , we divide this quantity by the total dimension: $d(F) = D(F)/2^N$. Furthermore, we choose a double logarithmic plot in order to emphasize the regime of very high fidelities, i.e., we plot $\log(d)$ as a function of $-\log(1 - F)$. In such a plot, the largest few eigenvalues can be clearly identified (see the symbols in Fig. 5.17), since the step size on the d -axis

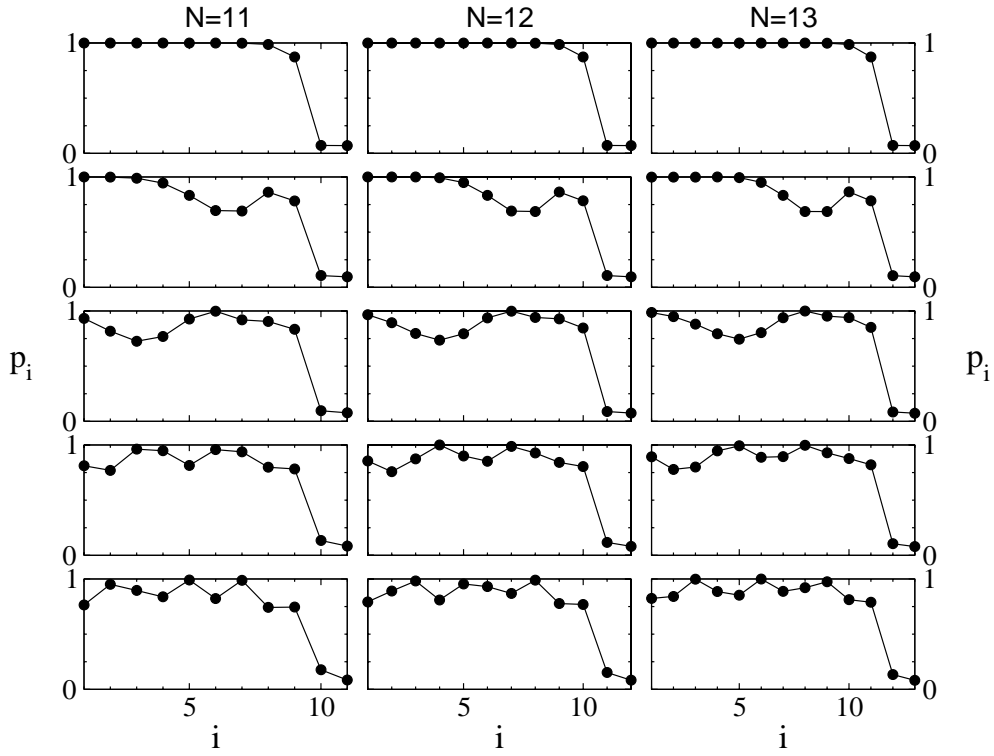


Figure 5.18: Eigenvectors of $M^{l^0 \langle 0|}$ (target state $|\chi\rangle = |2\rangle$), belonging to the five largest eigenvalues (top to bottom), for $N = 11, 12$, and 13 atoms injected into the cavity, and otherwise the same parameters as in Fig. 5.17. The ground state population of the i -th atom is shown (which also determines their amount of entanglement with the other atoms, since the target state $|\chi\rangle$ is a number state, see chapter 5.2). The correspondence between the eigenvectors for different N 's is clearly visible.

from the i -th eigenvalue (where $i = 1$ denotes the largest eigenvalue) to the next smallest one monotonically decreases with i . Moreover, for a fixed i , the logarithmic d -axis measures the number N of atoms on a linear scale (since the fraction of eigenvalues not smaller than the i -th largest one equals $d = i/2^N$). As evident from Fig. 5.17, not only the largest eigenvalue, but also the next few ones increase exponentially with N , with approximately the same rate as the largest one. Moreover, a one-to-one correspondence between those eigenvalues can be established in the sense that the eigenvectors evolve smoothly when increasing N . For the first five eigenvalues, this is displayed in Fig. 5.18, where the transition from $N = 11$ to $N = 13$ is shown. The second eigenvector shows a similar behavior as the largest one, with very high ground state population of the first few atoms. For smaller eigenvalues than the ones depicted in Fig. 5.18, however, the one-to-one correspondence between the eigenvectors belonging to different N 's will break down: it can certainly not hold for *all* eigenvalues, since the total number 2^N of eigenvalues depends on N .

Furthermore, it can be seen from Fig. 5.17 that in all the four illustrated

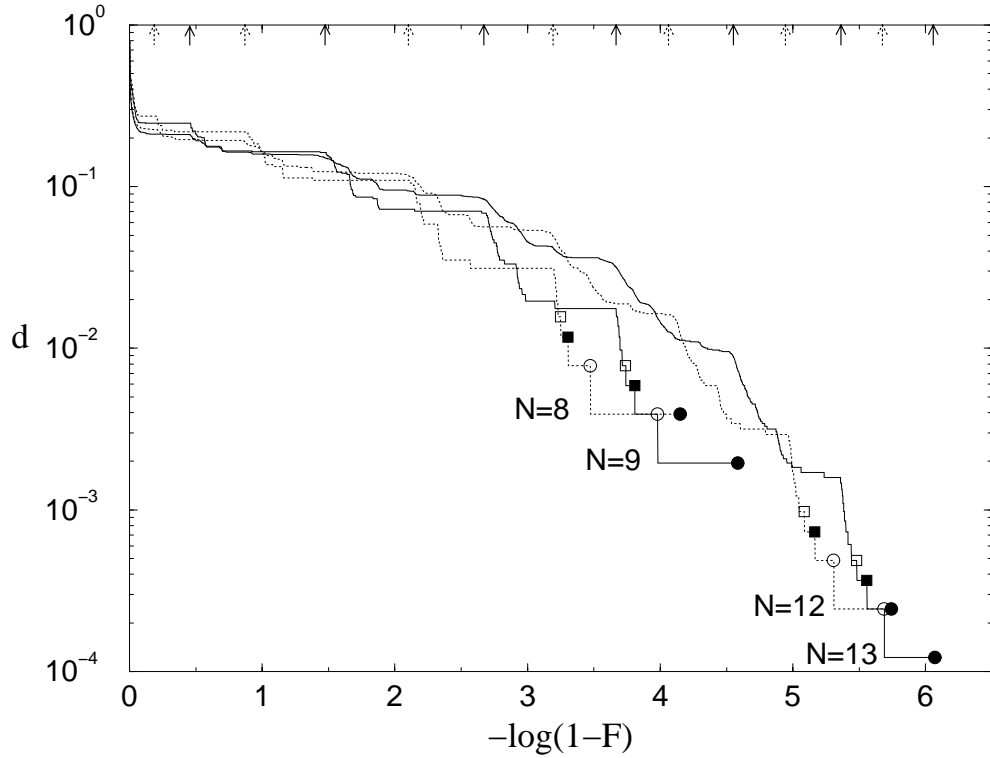


Figure 5.19: Fraction $d(F)$ of the eigenvalues of $M^{(0)}\langle 0|}$ larger than F , for the preparation of the coherent state $|\chi\rangle = |\alpha\rangle$ with mean photon number $|\alpha|^2 = 1$, for $N = 8, 9, 12$ and 13 atoms. Vacuum Rabi angle: $\phi = 0.95$. A plateau structure is observed (whose origin is not understood), indicating a clustering of eigenvalues at certain accumulation points, which are marked by the little arrows in the top (dotted for even, and solid for odd N). As in Fig. 5.17, the convergence of the spectrum of $M^{(0)}\langle 0|}$ to the limiting case, where almost all eigenvalues should be very close to either 0 or 1, cannot be inferred from the behavior for small values of $N \leq 13$.

cases the percentage of eigenvalues larger than 0.99 is about 10%, and about 70% of the eigenvalues are very close to zero (as indicated by the fact that the graphs seem to intersect the d -axis at about $0.3 = 1 - 0.7$). Also the intermediate distribution of the remaining 20% of the eigenvalues is almost independent of N . On the other hand, asymptotic completeness implies that in the limit $N \rightarrow \infty$, (almost) all eigenvalues have to be equal to either 0 or 1. Hence, we conclude that it takes many more than 13 atoms to reach this limit. For smaller N , the total distribution of eigenvalues hardly changes with N , and only in the logarithmic plot we see the convergence of the largest eigenvalues towards the ideal value 1.

To test whether such interpretation of Fig. 5.17 is generally valid, we show another example in Fig. 5.19, where the target field state is the coherent state $|\alpha\rangle$, with mean photon number $|\alpha|^2 = 1$. As in the previous example, the first four eigenvalues are marked by symbols, and they converge to 1 approxi-

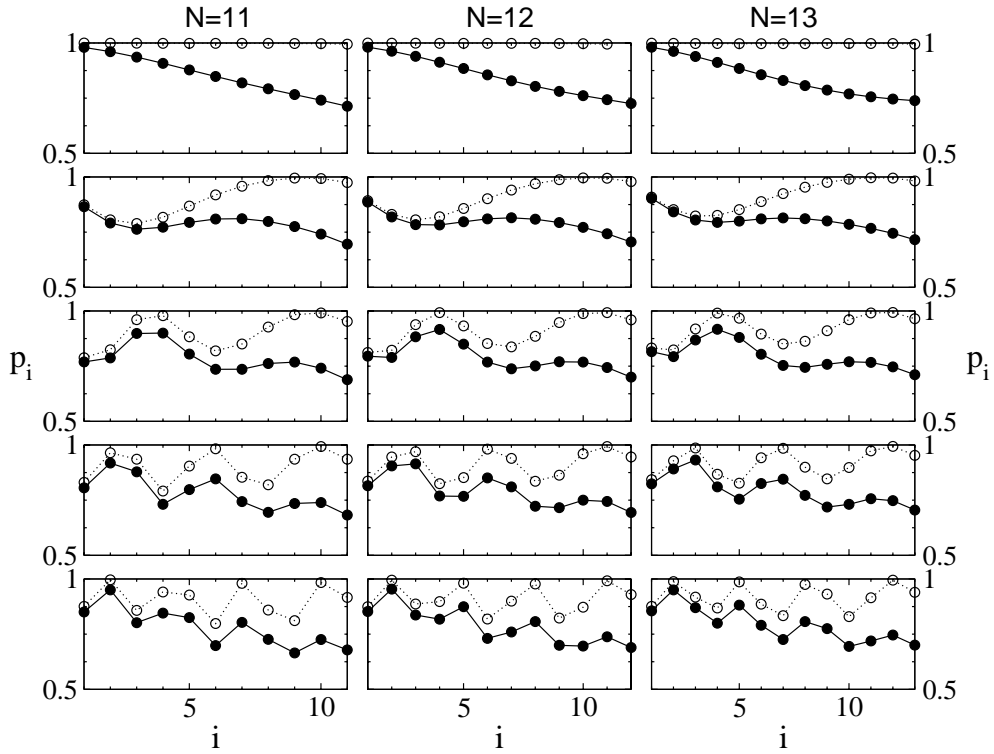


Figure 5.20: Eigenvectors of $M^{(0)\langle 0|}$ (target state: $|\alpha\rangle$, $\alpha = 1$), belonging to the five largest eigenvalues (top to bottom), for $N = 11, 12$, and 13 atoms injected into the cavity, and otherwise the same parameters as Fig. 5.19. The filled circles show the ground state population of the i -th atom, and the open diamonds the amount of entanglement with the other atoms (see chapter 5.2). The correspondence between the eigenvectors for different N 's is clearly visible.

mately as fast as the largest one. Again, the corresponding eigenvectors evolve smoothly when increasing N , see Fig. 5.20. Remarkably, the structure of the eigenvectors seems to get more complicated with decreasing magnitude of the eigenvalue. This tendency can also be observed in Fig. 5.18.

However, returning to the distribution of eigenvalues, Fig. 5.19, we observe a plateau structure which is not present in Fig. 5.17: at some points, the density of eigenvalues is very high, as indicated by a sudden decrease of the function d . Furthermore, the position of those accumulation points, which we have marked by small arrows in the top of Fig. 5.19, depends on whether N is even or odd (solid or dotted arrows). We have found empirically that at the i -th accumulation point F_i (counted from the right, i.e., $i = 0$ corresponds to the largest eigenvalue), the number of eigenvalues larger than F_i approximately equals $\binom{N}{i}$, $i = 0, \dots, N/2$ or $N/2 - 1$ (for even or odd N). With larger N , however, this structure appears to be smoothed out.

At present, we do not have an explanation for this behavior. The plateau structure seems to be of rather generic origin: e.g., for the preparation of the 2-photon state and a smaller vacuum Rabi angle $\phi = 0.8$ than in Fig. 5.17, we

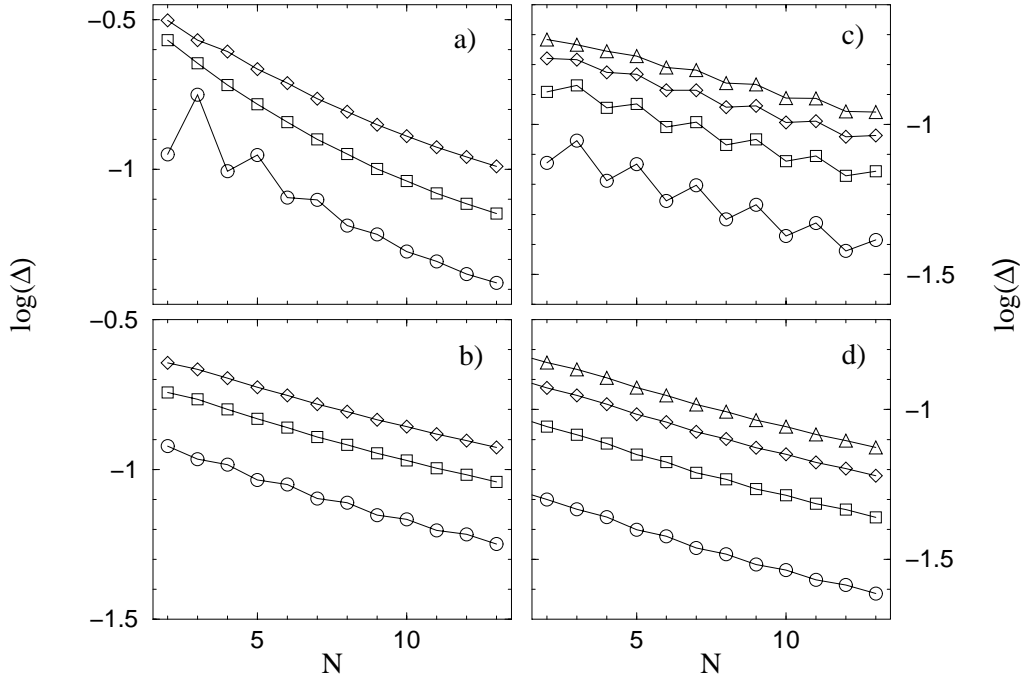


Figure 5.21: Deviation Δ (log. scale) of $M^{|0\rangle\langle 0|}$ from $M^{(\rho_0)}$, as defined by Eq. (5.8), for the same parameters as in Fig. 5.14 [preparation of $|\chi\rangle = |2\rangle$ (a,c) and $|\chi\rangle = |\alpha\rangle$, $\alpha = 1$ (b,d), starting from thermal (a,b) and truncated maximally mixed (c,d) initial field states]. The convergence towards $\Delta = 0$, which quantifies the independence of the final from the initial field state, as predicted by asymptotic completeness, Eq. (3.2), is much slower than the convergence of the maximum fidelities (Figs. 5.13 and 5.14), i.e., the largest eigenvalues of $M^{|0\rangle\langle 0|}$ and $M^{(\rho_0)}$. In (a) and (c), a non-monotonic behavior of unknown origin is observed.

observe a similar structure. The reason for its absence in Fig. 5.17 may be that the two relevant transition probabilities $|B_1|^2$ and $|B_2|^2$ are identical if $\phi = 1.3$.

Nevertheless, one of the above conclusions from Fig. 5.17 remains valid: the convergence of the total spectrum of $M^{|0\rangle\langle 0|}$ (i.e., also of those eigenvalues which are neither very close to 0 nor to 1) cannot be observed in Fig. 5.19. For example, in the regime around $F = 0.9$ [i.e., $-\log(1-F) = 1$], the distribution of the spectrum depends on whether N is even or odd, but otherwise does not drastically change with increasing N . Hence, it takes many more than 13 atoms to come close to the limit $N \rightarrow \infty$ of asymptotic completeness in Eq. (3.2).

5.4.4 Independence from the initial field state

Nevertheless, one might argue that, from a physical point of view, the limit $N \rightarrow \infty$ in Eq. (3.2) is not so important, as long as we are able to prepare the desired field state with high fidelity. As discussed in chapter 3.2, however, asymptotic completeness is more than the ability to prepare a given field state. It also implies independence of the final field state from the initial field state.

We have already examined this aspect in chapter 5.3. There, we always used the optimal initial atomic state and studied how the maximum fidelity of the state preparation starting from mixed initial field states converges to the ideal value 1. According to Eq. (3.2), the independence of the final from the initial field state should also hold for all other initial atomic states.

In order to verify this aspect of the asymptotic completeness numerically, we quantify the difference Δ between $M^{|\alpha\rangle\langle\alpha|}$ and $M^{(\rho_0)}$ by the Hilbert-Schmidt norm [85]:

$$\Delta^2 = \text{Tr} \left\{ \left(M^{(\rho_0)} - M^{|\alpha\rangle\langle\alpha|} \right)^2 \right\} / 2^N, \quad (5.8)$$

i.e., Δ^2 is the average over the square of all eigenvalues of $M^{(\rho_0)} - M^{|\alpha\rangle\langle\alpha|}$. In order to compensate for the increasing number of eigenvalues, the normalization factor 2^N is required. Asymptotic completeness is fulfilled if and only if $\Delta \rightarrow 0$ with $N \rightarrow \infty$, for all final and initial field states. Indeed, Fig. 5.21 confirms this prediction in all the four cases (for the two target states $|2\rangle$ and $|\alpha\rangle$, $\alpha = 1$, starting from thermal and truncated maximally mixed initial states). Furthermore, the convergence is again exponentially fast. Note, however, that the range of the $\log(\Delta)$ -axis corresponds to only one order of magnitude. Hence, the convergence is much slower than for the maximum fidelity (Figs. 5.13 and 5.14). Furthermore, the rate of convergence does not depend mainly on the target and initial field states, but rather on the vacuum Rabi angle, which is almost the same in the three cases (b), (c), and (d). For the preparation of number states (a and c), in some cases a zig-zag structure is observed, which indicates a dependence of Δ on whether N is even or odd. This feature is not yet understood.

In summary, although universal preparability is equivalent to asymptotic completeness in the limit $N \rightarrow \infty$, the first property is reached much faster than the second.

Chapter 6

The influence of noise

Whereas we have so far assumed idealized experimental conditions, in a real laboratory we have to deal with various noise sources: the initial atomic state cannot be prepared with perfect fidelity, the vacuum Rabi angle is not precisely the same for all atoms (e.g., due to a finite velocity spread of the atomic beam), and the photon field decays during the interaction with the cavity walls. In this chapter, we will examine the influence of those noise sources upon the fidelity of the state preparation.

6.1 Cavity dissipation

Since, under realistic experimental conditions, the cavity field is not perfectly isolated from its environment, the field decays due to the interaction with the cavity walls. This decay can be treated using standard techniques (see, e.g., chapter 15.1 in [59]): the environment is treated as a heat bath at temperature T , which has no memory (Markov approximation). Furthermore, the coupling between cavity field and heat bath is assumed to be weak, and mediated by the photon annihilation and creation operators a and a^\dagger . Under these general conditions, one arrives at the following master equation of the damped harmonic oscillator:

$$\dot{\rho} = \frac{\gamma}{2} (n_b + 1) (2a\rho a^\dagger - a^\dagger a \rho - \rho a^\dagger a) + \frac{\gamma}{2} n_b (2a^\dagger \rho a - a a^\dagger \rho - \rho a a^\dagger). \quad (6.1)$$

Here, γ is the decay rate of the cavity, and n_b the mean photon number at thermal equilibrium. The latter is connected to the temperature T of the heat bath via the familiar Boltzmann factor, i.e.,

$$n_b = \left(e^{\hbar\omega/kT} - 1 \right)^{-1}. \quad (6.2)$$

In the laboratory, temperatures of about $T \simeq 0.3 \text{ K}$ can be realized, corresponding to $n_b \simeq 0.03$ in the microwave regime ($\omega \simeq 20 \text{ GHz}$). Furthermore, with the high quality microwave cavities presently at use in the laboratory [93], average photon lifetimes as high as $\gamma^{-1} = 0.2 \text{ s}$ can be reached. On the other hand, the interaction times t_{int} of a single atom with the field are of the order of microseconds, and assuming a coupling constant of $\Omega \simeq 40 \text{ kHz}$ [93], a vacuum

Rabi angle of $\phi = \Omega t_{\text{int}} \simeq 1$ is realized with $t_{\text{int}} \simeq 25 \mu\text{s}$, which is about 4 orders of magnitudes smaller than the cavity decay rate γ^{-1} . Hence, it is a good approximation to neglect the decay during the atom-field interaction, which is therefore still described by Eq. (2.1). Only during the intervals between two successive atoms will we account for the decay via Eq. (6.1). For simplicity, we assume that those intervals are of constant length t_p . We do not expect that fluctuations of t_p significantly change the results presented below.*

In general, any interaction of the field with the environment will reduce the purity of the field state, and therefore also reduce the fidelity of the state preparation. The question is: can we do something against it by choosing a different initial atomic state? For example, this could be an atomic state with higher excitation number, compare Eq. (2.6), in order to compensate for the expected photon losses. Our numerical calculations (see below) give a negative answer: the optimal initial atomic state is nearly the same with or without dissipation. In order to explain this result, we will first examine how the decay alone affects the cavity field, without any atoms passing through the cavity.

6.1.1 Decay of the fidelity of a field state

If the cavity field is initially in the state $\rho = |\chi\rangle\langle\chi|$, the fidelity with respect to $|\chi\rangle$ will decrease as a consequence of Eq. (6.1). In order to find out how fast, we will restrict ourselves to short times, i.e., $t\gamma \ll 1$. As mentioned above, this may still be very much longer than the interaction time of a single atom with the cavity, and comparable to the total time $T = (N - 1)t_p$ of the preparation process. The fidelity at time t then reads $F(t) = 1 + \langle\chi|\dot{\rho}|\chi\rangle t$, at first order in γt . Insertion of Eq. (6.1) for $\dot{\rho}$ yields:

$$\begin{aligned} \Delta F = F(t) - 1 &= -\gamma t \left[(2n_b + 1) \left(\langle\chi|a^\dagger a|\chi\rangle - |\langle\chi|a|\chi\rangle|^2 \right) + n_b \right] \\ &= -\gamma t \left[(2n_b + 1) \underbrace{\left(\langle\chi|a^\dagger (\mathbb{1} - |\chi\rangle\langle\chi|) a|\chi\rangle \right)}_{0 \leq \dots \leq \langle\chi|a^\dagger a|\chi\rangle} + n_b \right]. \end{aligned} \quad (6.3)$$

Let us first discuss the case $n_b = 0$ of zero temperature. Then, Eq. (6.3) says that the decrease of the fidelity is given by γt multiplied with the norm of the projection of the state $a|\chi\rangle$ onto the subspace orthogonal to $|\chi\rangle$ (which, due to $0 \leq \mathbb{1} - |\chi\rangle\langle\chi| \leq \mathbb{1}$, is bounded between 0 and the mean photon number of $|\chi\rangle$). Therefore, $\Delta F = 0$ if and only if $|\chi\rangle$ is an eigenstate of a , i.e., a coherent state, since only then $a|\chi\rangle$ does not overlap any state orthogonal to $|\chi\rangle$. So, at zero temperature, coherent states do not decay at all, at first order in γt . In fact, it is not difficult to verify that, according to Eq. (6.1), a coherent state will always remain a coherent state, with an exponentially decaying amplitude

$$\alpha(t) = e^{-\frac{\gamma}{2}t} \alpha(0), \quad (n_b = 0). \quad (6.4)$$

*As we will see below, for small values of γt_p , the decrease ΔF of the fidelity will essentially be proportional to the total time $T \simeq N t_p$, for which the cavity field is exposed to the damping. Hence, if T fluctuates, the expectation value of ΔF is proportional to the mean value of T .

Only at the second order in γt does this lead to a finite decrease of the fidelity,

$$\Delta F = -\gamma^2 t^2 |\alpha|^2 / 4, \quad (n_b = 0). \quad (6.5)$$

On the other hand, for a number state $|\chi\rangle = |n\rangle$, the state $a|n\rangle = \sqrt{n}|n-1\rangle$ is orthogonal to $|n\rangle$, and the under-braced term in Eq. (6.3) assumes its maximum value, namely the mean photon number $\langle n \rangle = n$ of $|\chi\rangle$. Consequently, we obtain

$$\Delta F = -\gamma t n, \quad (n_b = 0). \quad (6.6)$$

Hence, number states are much more sensitive with respect to cavity decay than coherent states. Furthermore, it is clear that states with higher mean photon numbers decay faster, since then the absorption of a photon by the heat bath is more likely. [As can be derived from Eq. (6.1), if the cavity contains n photons, the probability of the heat bath absorbing one photon is proportional to n , see also the term proportional to γ in Eq. (C.9).]

In the case $n_b > 0$ of nonzero temperature, also a coherent state $|\alpha\rangle$ will turn into a mixed state (since then, the heat bath can also *emit* photons into the cavity via a^\dagger , and $a^\dagger|\alpha\rangle$ is not proportional to $|\alpha\rangle$). Consequently, also coherent states will then decay linearly in γt . From Eq. (6.3), we can derive the following generalization of the above expressions (6.5,6.6) for nonzero temperature:

$$\Delta F = -\gamma t n_b, \quad (6.7)$$

for the decay of a coherent state, independently of its mean photon number $|\alpha|^2$, and

$$\Delta F = -\gamma t [(2n_b + 1)n + n_b], \quad (6.8)$$

for a number state $|n\rangle$. As obvious from Eq. (6.3), the fact that the coherent states are most stable with respect to the cavity decay among all field states, remains valid also for $n_b > 0$ (since, as argued above, the under-braced term vanishes only for coherent states).

In order to achieve a higher fidelity of the field state with respect to $|\chi\rangle$ after the decay, one might have the idea to start with another initial field state $|\chi'\rangle$. Although the initial fidelity is then smaller than 1, i.e., $F'(0) = |\langle\chi|\chi'\rangle|^2$, it may be possible to reduce the decrease $\Delta F'$ of the fidelity induced by the decay, or maybe even reverse the sign of $\Delta F'$, such that in total $F'(t) = F'(0) + \Delta F'$ is larger than $F(t) = 1 + \Delta F$. For very small values of γt , however, this does not work, as we see with the following simple argument: similarly to Eq. (6.3), $\Delta F'$ is given by

$$\Delta F' = -\gamma t \left(\frac{1}{2} \left(\langle\chi|a^\dagger a|\chi'\rangle \langle\chi'|\chi\rangle + c.c. \right) - |\langle\chi|a|\chi'\rangle|^2 \right). \quad (6.9)$$

Although we assumed here $n_b = 0$, for simplicity, the following argument is also valid for $n_b > 0$. In fact, we need Eq. (6.9) only in order to verify that $\Delta F' / (\gamma t)$ is continuous in χ' , i.e., $\Delta F' / (\gamma t) \rightarrow \Delta F / (\gamma t)$ if $\chi' \rightarrow \chi$. (Obviously, this remains true for $n_b > 0$.) Now, for very small values of γt , we have to choose χ' very close to χ , i.e., $\chi' \rightarrow \chi$ if $\gamma t \rightarrow 0$ (otherwise, $F'(0) = |\langle\chi|\chi'\rangle|^2$

cannot be larger than $1 + \Delta F - \Delta F'$, since both $\Delta F'$ and ΔF are small, i.e., $\Delta F', \Delta F \rightarrow 0$ if $\gamma t \rightarrow 0$). Since $\Delta F'/(\gamma t)$ is continuous in χ' , according to Eq. (6.9), this implies that $\Delta F'/(\gamma t) \rightarrow \Delta F/(\gamma t)$ if $\gamma t \rightarrow 0$, or - in other words - that the difference between $\Delta F'$ and ΔF is of second order in γt . Hence, the decrease of the fidelity at first order in γt , as given by Eq. (6.3), cannot be reduced.

The above argumentation does not apply in the case of zero temperature and a coherent state $|\chi\rangle = |\alpha\rangle$, where $\Delta F = 0$ at first order in γt , and the second order is relevant, see Eq. (6.5). In this case, it follows from Eq. (6.4) that we can actually achieve $F'(t) = 1$ if we choose the initial state $|\chi'\rangle = |\alpha'\rangle$ with $\alpha' = \alpha e^{\frac{\gamma}{2}t}$. Note, however, that, $|\alpha'\rangle$ is only very slightly different from $|\alpha\rangle$, i.e., $|\langle\alpha'|\alpha\rangle|^2 = 1$ at first order in γt .

Hence, our conclusion is the following:

In order to maintain the highest possible fidelity with respect to a given state $|\chi\rangle$ after exposing the cavity field to the decay for a short time t , we have to choose the same $|\chi\rangle$ as initial field state.

In particular, it does not help anything to choose, for example, an initial state with a higher mean photon number (apart from a tiny improvement in the case of zero temperature and a coherent state $|\alpha\rangle$, as discussed above). Even if the mean photon number after the decay is the same as the one of the target state $|\chi\rangle$, this does not imply a large overlap with $|\chi\rangle$, since the decay results in general in a mixed field state.

6.1.2 Influence of the decay upon the state preparation

Naturally, the situation is much more complicated if we consider the influence of the decay on the *preparation* of field states. Here, also in the absence of dissipation, the state of the cavity is not constant in time, since it evolves from the initial state ρ_0 to the target state $|\chi\rangle$, due to the interaction with the atomic sequence. Furthermore, during the interaction the field is also entangled with the atoms. Due to these complications, the influence of the dissipation cannot be estimated as clearly as above. Nevertheless, the above considerations suggest the conclusion that the best way to achieve a high fidelity in the presence of dissipation is to do the same as in the absence of dissipation. In particular, it is apparently not a good strategy to choose the initial atomic state such that it would prepare a different field state $|\chi'\rangle$ without dissipation, and to hope that the latter brings $|\chi'\rangle$ closer to $|\chi\rangle$.

As we know from chapter 5.4.3, there exist more than one atomic states which prepare $|\chi\rangle$ with high fidelity. These may be affected differently by the dissipation. However, there are good reasons for the assumption that the optimal initial atomic state will remain optimal also in the presence of dissipation: we have seen in chapter 5.2 that the optimal state has (in most cases) the property that the first atoms enter the cavity almost in the ground state. If the field is initially in the vacuum state, it will therefore at first remain very close to the vacuum where it is insensitive to the cavity decay. On the other hand, if the

field is initially in a mixed state, the purpose of the first few atoms is to bring the field closer to the vacuum, and this is actually supported by the dissipation, at least at low temperatures, such that the vacuum population $(1+n_b)^{-1}$ of the thermal equilibrium state is not smaller than the maximum vacuum population of the field during the preparation process (compare chapter 5.3). Only for the preparation of coherent states starting from the vacuum, we have stated a somewhat different behavior of the optimal atomic state, see Fig. 5.16. As discussed in chapter 5.2, however, in this case the cavity field is always very close to a coherent state during the whole preparation process, i.e., it climbs up on a ladder of coherent states. Since these are quite insensitive to the cavity decay (see chapter 6.1.1), this preparation strategy should remain the optimal one also in the presence of dissipation.

Hence, we come to the remarkable conclusion that the optimal strategy to prepare a field state *in the absence of dissipation* is such that if we include dissipation its influence will be minimal. However, the above reasoning is based on rather qualitative arguments, and, in particular, we have not taken into account the possibility of an interplay between the dissipation and the interaction with the two-level atoms.

Calculation of the maximum fidelity

Therefore, we will resort to numerical calculations in order to determine the influence of the cavity decay on the state preparation more precisely. For this purpose, since the atomic operator $M^{(\rho_0)}$ needed for the calculation of the fidelity and of the atomic initial state (see chapter 4.1) is derived from the projector onto the desired field state propagated in the Heisenberg picture, we have to translate Eq. (6.1), which operates on the field states (i.e., in the Schrödinger picture), into the Heisenberg picture. The expectation value $\text{tr}(\rho A)$ is not affected by a change of the picture, and therefore the corresponding time evolution of a field operator A in the presence of dissipation can be easily derived from the condition $\text{tr}(\dot{\rho}A) = \text{tr}(\rho\dot{A})$. Using the cyclic permutation property of the trace, we obtain the dual equation:

$$\dot{A} = \frac{\gamma}{2} (n_b + 1) (2a^\dagger Aa - Aa^\dagger a - a^\dagger a A) + \frac{\gamma}{2} n_b (2a Aa^\dagger - Aaa^\dagger - aa^\dagger A). \quad (6.10)$$

For $t \rightarrow \infty$, $A(t)$ approaches a multiple $c\mathbb{1}$ of the identity operator, with c the expectation value of $A(0)$ in thermal equilibrium. For finite t , the solution of the linear equation (6.10) can be formally written as $A(t) = e^{\tilde{\mathcal{L}}t} A(0)$, with the linear ‘superoperator’ $\tilde{\mathcal{L}}$.[†] Hence, in order to account for the damping, we have to apply the superoperator $e^{\tilde{\mathcal{L}}t_p}$ between two successive atoms (remember that the damping is neglected during the atom-field interaction). In analogy to Eq. (A.9), the matrix elements of $M^{(\rho_0)}$ are then given by

$$\langle i_1 \dots i_N | M^{(\rho_0)} | j_1 \dots j_N \rangle = \text{tr} \left\{ \rho_0 T_{i_1 j_1} e^{\tilde{\mathcal{L}}t_p} T_{i_2 j_2} \dots e^{\tilde{\mathcal{L}}t_p} T_{i_N j_N} (|\chi\rangle\langle\chi|) \right\}. \quad (6.11)$$

As in chapter 4.1, the largest eigenvalue of $M^{(\rho_0)}$ gives the maximum fidelity of the state preparation, and the corresponding eigenvector is the optimal initial

[†]The solution can be found in analytical form in [94].

atomic state. However, our conclusion at the end of that chapter, based on the time-reversal symmetry of the Jaynes-Cummings interaction, is now invalid, since the dissipation destroys the time-reversal symmetry.

Results

Using this approach, we can calculate the maximum fidelity and the optimal initial atomic state in the presence of dissipation. As predicted above, we will find - in all cases - that the fidelity achieved with the optimal initial atomic state in the absence of dissipation is almost identical to the maximum fidelity which we can reach for nonvanishing coupling to the environment.

As an example, Fig. 6.1 shows the maximum fidelity for the preparation (a) of the number state $|5\rangle$, of the truncated phase state $|\chi_5\rangle$, and (b) of the coherent states $|\alpha\rangle$, with $|\alpha|^2 = 1$ and $|\alpha|^2 = 2$, as a function of the number N of atoms injected into the resonator, in the presence of dissipation. In order to analyze the influence of a finite temperature, we compared the experimentally realistic value $n_b = 0.03$ (i.e., $T = 0.3$ K) with the case of zero temperature $n_b = 0$ and a higher temperature $n_b = 0.2$ (i.e., $T = 0.6$ K). For the time interval between two successive atoms, we chose $t_p = 10^{-3}\gamma^{-1}$, which, as mentioned above, is still ten times longer than the interaction of a single atom with the cavity field.[‡] For comparison, also the maximum fidelity in the absence of dissipation is plotted (dashed line). Note that, in all cases, the fidelity achieved with the optimal initial atomic state for the dissipation free case (solid line) can hardly be distinguished from the maximum fidelity (symbols). This confirms our above conjecture that the dissipation does not influence the optimal initial atomic state. [An exception is the case $|\alpha|^2 = 1$ at zero temperature. Here, the fidelity can be slightly improved by choosing a different initial atomic state than in the dissipation free case. This can be understood by the fact that, at $n_b = 0$, coherent states decay again into coherent states, see Eq. (6.4).]

In Fig. 6.1(a), a saturation of the maximum fidelity is observed. This is not surprising: in these cases, the optimal atomic state is very close to the state $|\psi'_0\rangle$, Eq. (4.7). As shown in chapter 5.2, with increasing N , the first atoms enter the cavity almost in the ground state (and the cavity field remains in the almost dissipation-free vacuum state), while the state of the last atoms is basically unchanged. Hence, the effect of the dissipation is approximately the same for different N , and the maximum fidelity will be reduced by a constant amount ΔF . The saturation then sets in as soon as the deviation of the fidelity without dissipation from 1 is much smaller than the dissipation-induced decrease ΔF . Furthermore, we see that the decrease ΔF of the fidelity does not depend very strongly on the temperature (however, note the logarithmic scale!), in the regime $n_b \leq 0.2$: in the case of the number state $|\chi\rangle = |5\rangle$, we observe $\Delta F = 1.3\%$, 1.4% , and 1.9% for $n_b = 0$, 0.03 , and 0.2 , respectively, whereas in the case of the phase state $|\chi\rangle = |\chi_5\rangle$, $\Delta F = 0.15\%$, 0.17% , and 0.25% . In all cases, this

[‡]Therefore, the effect of the cavity dissipation could be further reduced if it were possible to control the arrival times of the individual atoms such that they pass through the cavity immediately one after the other. Recent progress [7, 8] in the experimental manipulation of single atoms suggests that such control is within reach.

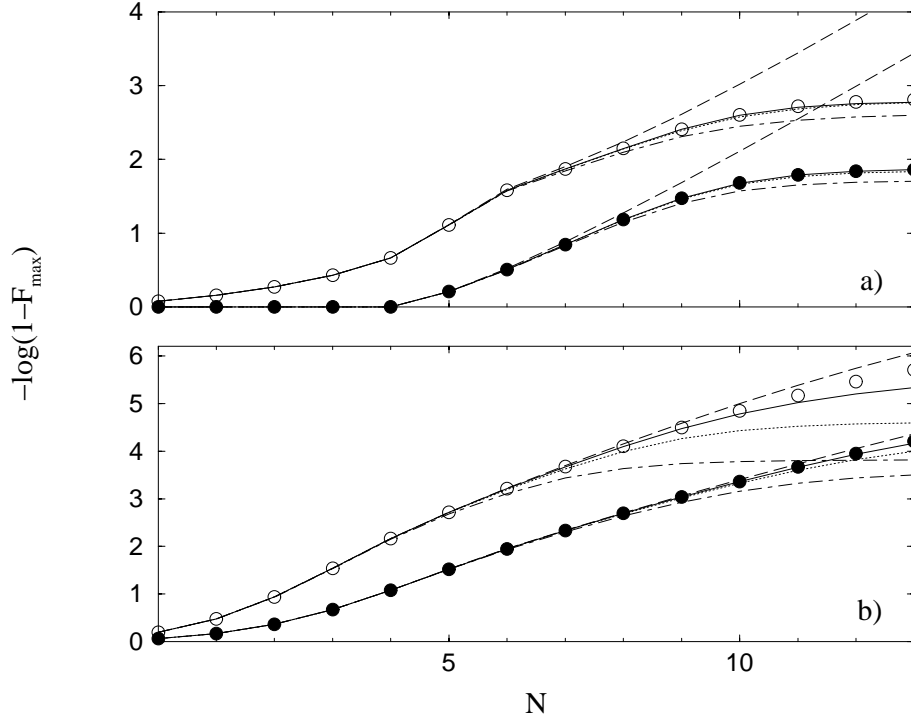


Figure 6.1: Maximum fidelity F_{\max} in the presence of dissipation ($\gamma t_p = 10^{-3}$) for the preparation (out of the vacuum) (a) of the 5-photon state $|\chi\rangle = |5\rangle$ (filled circles) and of the phase state $|\chi_5\rangle$, truncated at $n = 5$ (open circles), and (b) of the coherent states $|\alpha\rangle$, with $|\alpha|^2 = 1$ (open circles), and $|\alpha|^2 = 2$ (filled circles), as a function of the number N of atoms injected into the resonator. Three different values for the temperature of the heat bath are chosen: $n_b = 0$ (i.e., $T = 0$ K) (symbols), $n_b = 0.03$ (i.e., $T = 0.3$ K) (dotted lines), and $n_b = 0.2$ (i.e., $T = 0.6$ K) (dash-dotted lines). For each target state, the optimal vacuum Rabi angle was chosen, i.e., $\phi_{\text{opt}}^{(5)} = 0.97$ for the number and phase state (a), and $\phi = 0.95$ and 0.85 for the coherent states (b). For comparison, also the maximum fidelity without dissipation (dashed line) is shown. In the case $n_b = 0$, we plotted also the fidelity achieved with the optimal initial atomic state for the state preparation in the dissipation-free case (solid line), which can be distinguished from the maximum fidelity (symbols) only for $|\alpha|^2 = 1$ and $N \geq 9$ in (b), where the fidelity is extremely high. (In the cases $n_b = 0.03$ and $n_b = 0.2$, we would not see any difference at all.) This shows that the presence of dissipation has almost no influence on the optimal initial atomic state. In most cases - except for the preparation of coherent states (b) at zero temperature - we observe a saturation of the maximum fidelity induced by the dissipation.

corresponds to the decrease of the fidelity as predicted by Eq. (6.3), if the target state $|\chi\rangle$ is exposed to the decay for a time $t \simeq 2.7 t_p$. Not surprisingly, this is smaller than the total preparation time $T = (N - 1)t_p$: since the mean photon number in the cavity field increases from zero to $\langle n \rangle = \langle \chi | a^\dagger a | \chi \rangle$ during the preparation process, the cavity field decays, on average, slower than $|\chi\rangle$. Indeed, the ratio $t/T = 2.7/(N - 1)$ roughly equals the average photon number of the cavity field during the whole preparation process (for large enough N , i.e., in the saturated regime), in units of the target state's mean photon number. We have checked that for number states and phase states with other maximum photon numbers n , this ratio scales linearly with n , as expected from the fact that the number of atoms needed for the state preparation also scales linearly with n (see Fig. 4.2).

The impact of dissipation on the preparation of coherent states is much weaker, see Fig. 6.1(b), especially for zero temperature. Taking into account that, during the preparation of a coherent state, the cavity field always remains approximately in a coherent state (compare chapter 5.2), this agrees with Eq. (6.5), stating that, at $n_b = 0$, coherent states decay only at second order in γt . Consequently, for $n_b = 0$, dissipation becomes non-negligible only at fidelities for which the deviation from 1 is comparable to the second order $(\gamma N t_p)^2 \simeq 10^{-4}$ (for $N \simeq 10$), in agreement with Fig. 6.1(b).

On the other hand, for $n_b > 0$, also the coherent states decay linearly in γt . Consequently, also in these cases, we observe a saturation of the fidelity. For $n_b = 0.2$, the fidelity decrease ΔF is of comparable magnitude in both cases $|\alpha|^2 = 1$ and 2 (and the same is expected also for $n_b = 0.03$, where for $|\alpha|^2 = 2$ the saturation will occur at higher values of N). This is consistent with Eq. (6.7), where the decrease of the fidelity is also independent of $|\alpha|^2$. According to this equation, the observed values of $\Delta F = 2.5 \times 10^{-5}$ and 1.5×10^{-4} , for $n_b = 0.03$ and 0.2, respectively, correspond to the decrease of the fidelity when exposing a coherent state - irrespective of its mean photon number $|\alpha|^2$ - to the cavity decay for a time of $t \simeq 0.8 t_p$. Again, this is much smaller than the total preparation time $T = (N - 1)t_p$. In contrast to the above case (a), however, this difference cannot be explained by the evolution of the photon field state during the preparation process, since - as already mentioned - the dissipation-induced decrease of the fidelity with respect to a coherent state $|\alpha\rangle$ does not depend on $|\alpha|^2$, see Eq. (6.7). Hence, the only possible explanation is that the dissipation is suppressed by the interaction with the atoms.

In fact, this effect can already be demonstrated by the following simple example: we consider the preparation of the coherent state $\alpha' = 1$ starting from another coherent state $\alpha = \sqrt{0.85}$ as initial state, using a *single* atom, with vacuum Rabi angle $\phi = 0.95$. This corresponds to a typical single step on the ladder during the preparation of coherent states (compare chapter 5.2). Without dissipation, the maximum fidelity (using the optimal initial atomic state $|\psi\rangle = 0.82|u\rangle - i0.57|d\rangle$) would be $F_{\max}^{(n.d.)} = 99.25\%$. On the other hand, if the cavity field is exposed to the cavity decay, for a time $t_p = 10^{-3}\gamma^{-1}$ at temperature $n_b = 0.2$, before the atom arrives, the initial state is turned into a

mixed state ρ_0 , which, according to Eq. (6.1), is given by (for $\gamma t_p \ll 1$):

$$\begin{aligned} \rho_0 = & |\alpha\rangle\langle\alpha| + \gamma t_p \left\{ \left[(n_b + 1)|\alpha|^2 - n_b \right] |\alpha\rangle\langle\alpha| + n_b a^\dagger |\alpha\rangle\langle\alpha| a \right. \\ & \left. - (2n_b + 1) \left[\alpha a^\dagger |\alpha\rangle\langle\alpha| + \alpha^* |\alpha\rangle\langle\alpha| a \right] \right\}. \end{aligned} \quad (6.12)$$

Now, starting from ρ_0 as initial field state, the maximum fidelity for the preparation of $|\alpha'\rangle$ (using the same initial state as above) is $F_{\max} = 99.30\%$, which is *higher* than $F_{\max}^{(n.d.)} = 99.25\%$ in the dissipation-free case.

This example shows that, in order to estimate the effect of the cavity dissipation on the preparation of coherent states, we have to take into account the interplay between the dissipation and the interaction with the two-level atoms, which may actually diminish the influence of the dissipation. A similar effect, however, was not observed during the preparation of other field states (e.g., of number or phase states).

6.2 Imperfect initial atomic state

Next, let us consider the impact of an imperfect initial atomic state. For this purpose, we assume that the initial atomic state is given by a mixed state ρ_a , instead of the optimal initial atomic state. Then, the fidelity of the state preparation is given by $F = \text{tr}\{\rho_a M^{(\rho_0)}\}$, which is the obvious generalization of Eq. (4.2) to mixed atomic states. If the fidelity of ρ_a with respect to the optimal state $|\psi_0^{(\text{opt})}\rangle$ is

$$F_a = \langle\psi_0^{(\text{opt})}|\rho_a|\psi_0^{(\text{opt})}\rangle, \quad (6.13)$$

we obtain a lower bound for the fidelity of the state preparation as follows:

$$\begin{aligned} F &= \text{tr}\left\{\rho_a M^{(\rho_0)}\right\} = \\ &= \sum_{i=1}^{2^N} \langle\psi_i|\rho_a|\psi_i\rangle \langle\psi_i|M^{(\rho_0)}|\psi_i\rangle \geq \\ &\geq \langle\psi_0^{(\text{opt})}|\rho_a|\psi_0^{(\text{opt})}\rangle \langle\psi_0^{(\text{opt})}M^{(\rho_0)}|\psi_0^{(\text{opt})}\rangle = \\ &= F_a F_{\max}, \end{aligned} \quad (6.14)$$

where $\{|\psi_i\rangle\}$ is a basis of eigenstates of $M^{(\rho_0)}$ (including $|\psi_0^{(\text{opt})}\rangle$). Since this is only a lower bound, we might considerably underestimate the fidelity. As evident from the second line, this would be the case if the fidelity of ρ_a with respect to atomic states $|\psi_i\rangle$ orthogonal to $|\psi_0^{(\text{opt})}\rangle$, which also achieve a high fidelity $F_i = \langle\psi_i|M^{(\rho_0)}|\psi_i\rangle$, compare Eq. (4.2), was non-negligible. However, we know from chapter 5.4.3 that most eigenvalues of $M^{(\rho_0)}$ are much smaller than 1, and therefore the above lower bound can be expected to give a good approximation.

Hence, fluctuations of the initial atomic state do not have a very dramatic influence: the fidelity of the state preparation is at least as high as the maximum fidelity multiplied by the initial fidelity of the atomic state.

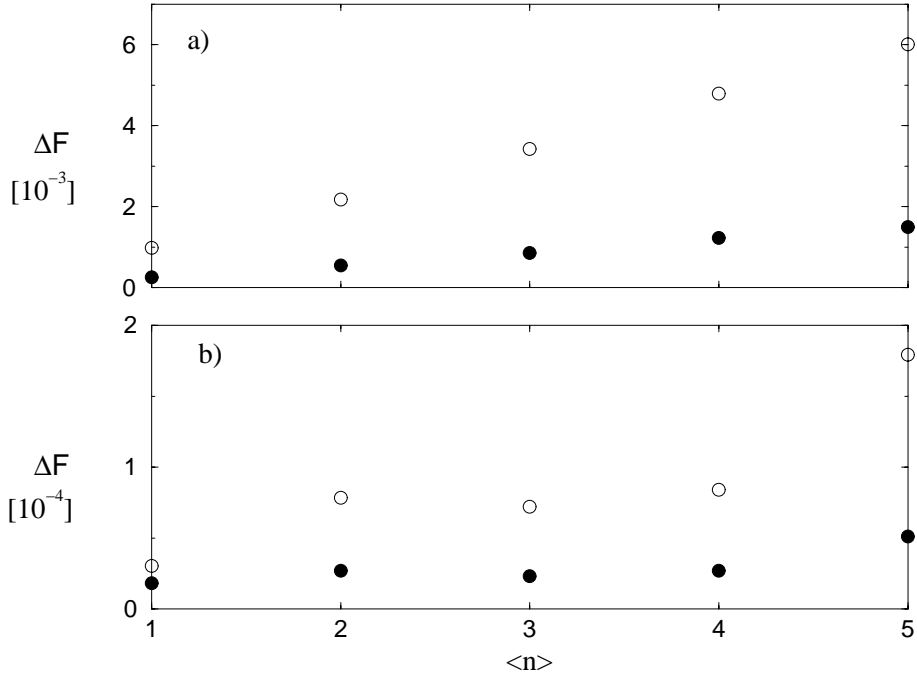


Figure 6.2: Decrease ΔF of the maximum fidelity, due to fluctuation $\Delta\phi/\langle\phi\rangle = 1\%$ (filled circles) and 2% (open circles) of the vacuum Rabi angle, preparing (a) number states $|n\rangle$ and (b) coherent states $|\alpha\rangle$, with mean photon number $\langle n \rangle$ ($= n$ or $|\alpha|^2$). The number of injected atoms is $N = 10$. Mean values of ϕ as in Figs. 5.7 and 5.9. For $\Delta\phi/\langle\phi\rangle = 1\%$, the decrease of the fidelity is reduced by a factor 4 as compared to $\Delta\phi/\langle\phi\rangle = 2\%$. The preparation of coherent states is more stable with respect to fluctuations of ϕ than the preparation of number states (note the different scales of the ΔF axis!).

6.3 Fluctuations of the vacuum Rabi angle

Besides the noise sources arising from the cavity dissipation and the initial atomic state, also the interaction between atom and field may be imperfect, e.g., due to a finite time-of-flight spreading of the incoming atomic beam, which leads to fluctuations $\Delta\phi$ of the vacuum Rabi angle ϕ . However, if the fluctuations are small enough, there will be no serious problems - at least if the mean value $\langle\phi\rangle$ of ϕ is known: the expected fidelity, using the optimal initial atomic state for $\langle\phi\rangle$, changes only at second order in $\Delta\phi$, since all terms linear in $\Delta\phi$ cancel when averaging over the fluctuations. [§]

This expectation is confirmed by our numerical calculations, see Fig. 6.2. Here, we assumed that ϕ fluctuates independently for each atom (according to a Gaussian distribution) with standard deviation $\Delta\phi$. Then, for the numerical evaluation of Eq. (A.9), we have to replace the operators T_{ij} by their average over ϕ . The target field states are, again, (a) number states, and (b) coherent

[§]Even if the change ΔF of the fidelity induced by a small deviation $\Delta\phi$ is proportional to $\Delta\phi$, the expected fidelity (averaging over $\Delta\phi$) does not change at first order in $\Delta\phi$, since the expectation value of $\Delta\phi$ is by definition zero.

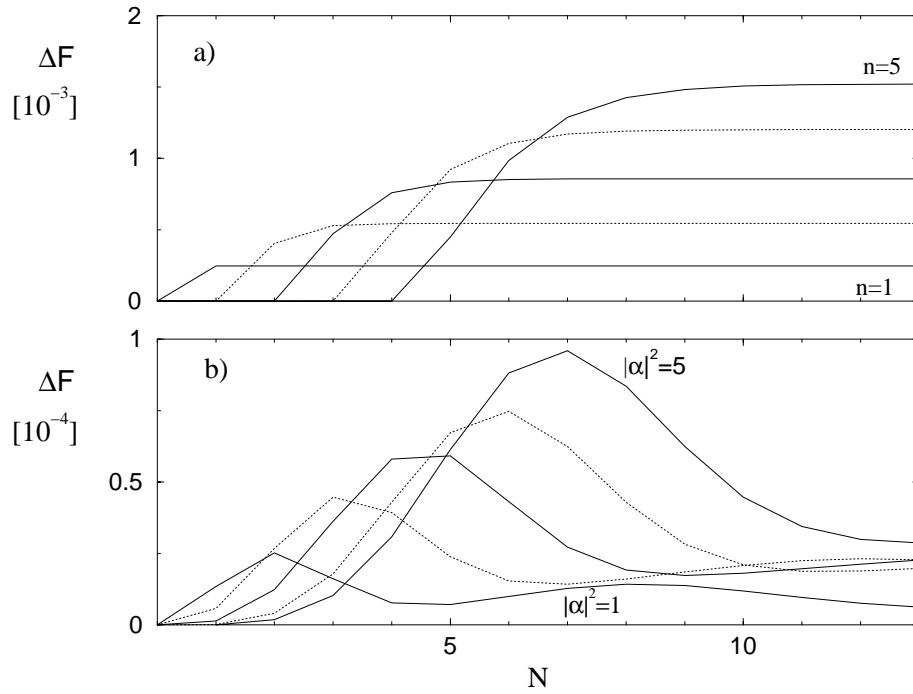


Figure 6.3: Decrease ΔF of the maximum fidelity due to fluctuations of the vacuum Rabi angle, $\Delta\phi/\langle\phi\rangle = 1\%$, as a function of the number N of atoms, when preparing (a) number states $|n\rangle$, $n = 1, \dots, 5$ and (b) coherent states $|\alpha\rangle$, $|\alpha|^2 = 1, \dots, 5$. Mean values of ϕ as in Fig. 6.2. While ΔF is constant for large N in the case of number states (a), the behavior is more complicated in the case of coherent states (b), where a maximum of ΔF as a function of N is observed.

states with mean photon numbers $\langle n \rangle = 1, \dots, 5$. For the strength of the fluctuations, we chose $\Delta\phi/\langle\phi\rangle = 1\%$ and 2% , which is experimentally realistic [93]. For the mean value $\langle\phi\rangle$, we chose in each case the optimal value of the vacuum Rabi angle (i.e., the same values as in Figs. 5.7 and 5.9).

The largest influence of $\Delta\phi$ is observed for the 5-photon number state, where the fidelity decreases by 0.0015 and 0.006, respectively. As predicted above, ΔF is quadratic in $\Delta\phi$: the decrease of the fidelity is always four times larger for $\Delta\phi/\langle\phi\rangle = 2\%$ than for $\Delta\phi/\langle\phi\rangle = 1\%$.

In general, the preparation of states with smaller photon numbers is less sensitive to fluctuations of ϕ . At first, one might try to explain this by the fact that the Rabi angle of the atom-field interaction increases with increasing photon number like $\phi\sqrt{n+1}$, see chapter 2.1, leading to a larger impact of a small change of ϕ if the photon number is larger. This effect, however, is counterbalanced by our choice $\langle\phi\rangle \simeq \pi/(1+\sqrt{n})$ of the mean value of ϕ in the optimal regime, see Eq. (4.23). Instead, the reason is as follows: as we have seen in chapter 5.2, the optimal initial atomic state is in most cases approximately (and in the case of number states exactly) given by the state $|\psi'_0\rangle$, Eq. (4.7). Now, as evident from Fig. 5.7 and 5.8, this state has the property that, for the preparation of states with smaller mean photon number, more of the first few

atoms enter the cavity almost in the ground state, and the field remains longer very close to the vacuum, independently of the exact value of ϕ . Furthermore, if we increase the number N of atoms, we will [for large enough N , i.e., $N \gtrsim 2n$, where the fidelity $F'(n)$ is close to 1, compare Fig. 4.2] essentially only add ground state atoms to the initial state, compare Fig. 5.16. Therefore, we expect that (again for large enough N), the fidelity decrease ΔF due to the fluctuations of ϕ should not depend on N . This expectation is confirmed by Fig. 6.3(a), where we plotted the fidelity decrease for number states as a function of N .

It is also evident from Figs. 6.3(a) and 6.2(a) that ΔF (in the saturated regime) depends linearly on the photon number n . This agrees with the fact that the number of atoms needed for the preparation of $|n\rangle$ also scales linearly with n , see Fig. 4.2. In total, we can extract from Fig. 6.3(a) or 6.2(a) that the decrease of the fidelity for the state preparation of number states $|n\rangle$ due to fluctuations of the vacuum Rabi angle (around the optimal mean value) is given by

$$\Delta F \simeq 3n (\Delta\phi/\langle\phi\rangle)^2. \quad (6.15)$$

The situation is different for the preparation of coherent states, where the optimal initial atomic state deviates from the state $|\psi'_0\rangle$, see Fig. 5.9. Here, we observe a non-monotonic behavior of ΔF as a function of the mean photon number $\langle n \rangle$. In order to explain this, let us look at the N -dependence of ΔF in Fig. 6.3(b). In contrast to the case of number states, Fig. 6.3(a), we observe a maximum of ΔF as a function of N . The reason of the decrease of ΔF for large N can be traced back to the property of coherent states as the eigenstates of the photon annihilation operator, which - as we will explain in more detail below - leads to a stabilization against the fluctuations of ϕ during the interaction with a single atom, if the cavity field is in a coherent state. Now, as we have discussed in chapter 5.2, during the preparation of coherent states, the cavity field climbs up on a ladder of coherent states, and is therefore relatively insensitive to fluctuations of ϕ . However, this is only true if the number of atoms is large enough, since for too small values of N , which are not sufficient to reach the final coherent state with high fidelity, the cavity field will not always remain in a coherent state. This leads to the maximum observed in Fig. 6.3(b). Obviously, the position of the maxima depends on the mean photon number: for smaller $|\alpha|^2$, less atoms are required in order to achieve a high fidelity. Note, that, in the case $|\alpha|^2 = 1$, we observe a second maximum at $N = 8$, whose origin we cannot explain. At larger values of N than shown in Fig. 6.3, the second maximum may be present also in the other cases $|\alpha|^2 > 1$. Anyway, it is obvious from Fig. 6.3 that - for a fixed value of N (and so for $N = 10$ in Fig. 6.2) - the decrease ΔF of the fidelity is in general not a monotonous function of $|\alpha|^2$.

Why coherent states are less sensitive to fluctuations of ϕ

Furthermore, we conclude from Figs. 6.2 and 6.3 that - as already mentioned above - the preparation of coherent states is significantly more robust with respect to fluctuations of ϕ as compared to the preparation of number states (note the different scales!). In order to understand this, we consider a single step

in the preparation of coherent states (compare chapter 5.2). Here, the cavity field is approximately transferred from a coherent state $|\alpha_1\rangle$ to another coherent state $|\alpha_2\rangle$, by the interaction with a single two-level atom, which initially was prepared in $|\psi_1\rangle$, and leaves the cavity in the state $|\psi_2\rangle$. Hence, we may write

$$U|\alpha_1\rangle \otimes |\psi_1\rangle \simeq |\alpha_2\rangle \otimes |\psi_2\rangle, \quad (6.16)$$

where U is the interaction with a single atom, Eq. (2.1). Now, if we consider a small deviation $\Delta\phi$ of the vacuum Rabi angle from its mean value, we have a slightly modified interaction operator U' , and Eq. (6.16) changes into

$$\begin{aligned} U'|\alpha_1\rangle \otimes |\psi_1\rangle &= \left(\mathbb{1} - i\Delta\phi(a^\dagger\sigma + a\sigma^\dagger) \right) U|\alpha_1\rangle \otimes |\psi_1\rangle \\ &\simeq \left(\mathbb{1} - i\Delta\phi(a^\dagger\sigma + a\sigma^\dagger) \right) |\alpha_2\rangle \otimes |\psi_2\rangle, \end{aligned} \quad (6.17)$$

where we have expanded U' at first order in $\Delta\phi$. Next, we note that the ground state population of the final state $|\psi_2\rangle$ is quite close to 1, since the conjecture ‘the optimal final atomic state is $|d\dots d\rangle$ ’ (compare chapter 4.2) is approximately also valid for the preparation of coherent states (see, e.g., the comparison between the optimal initial atomic state and $|\psi'_0\rangle$ in Fig. 5.9). Since $\sigma|d\rangle = 0$, we therefore neglect the term $a^\dagger\sigma$ in Eq. (6.17). On the other hand, the term $a\sigma^\dagger$ leaves the cavity field in the same state $|\alpha_2\rangle$ (which is an eigenstate of a). Thereby, we arrive at

$$U'|\alpha_1\rangle \otimes |\psi_1\rangle \simeq |\alpha_2\rangle \otimes (\mathbb{1} - i\alpha_2\Delta\phi\sigma^\dagger)|\psi_2\rangle. \quad (6.18)$$

Here, we see that $\Delta\phi$ mainly influences the final atomic state, but not the field state, what explains the robustness of the preparation of coherent states against fluctuations of the vacuum Rabi angle.

Summary

In summary, we investigated the impact of three different sources of noise on the state preparation. Under the influence of cavity dissipation and fluctuations of the vacuum Rabi angle, the preparation of coherent states is found to be more robust than the preparation of number states. Together with the fact that coherent states can be prepared by atomic product states (see chapter 5.2), this underlines their special role as the most ‘classical’ states.

Furthermore, we have seen that the effect of cavity dissipation cannot be reduced by a different choice of the initial atomic state. Nevertheless, quite high fidelities of the state preparation can be achieved also in the presence of dissipation, since the time-of-flight of the atoms through the cavity can be chosen very short compared to the cavity decay times which are nowadays achieved. This allows to complete the state preparation in a time span much shorter than the cavity decay time. Then, the quantitative influence of the dissipation can be estimated as follows: with increasing number of atoms N , the fidelity converges to a value $1 - \Delta F$ strictly smaller than 1. The corresponding fidelity decrease ΔF is roughly the same as if the target field state was exposed

to the cavity dissipation for a time of $t \simeq nt_p/2$, where t_p is the time interval between two subsequent atoms, and n the maximum photon number of the target state. Only for the preparation of coherent states, an interplay between dissipation and coherent atom-field interaction was observed, the latter *reducing* the effect of the former.

Also small fluctuations $\Delta\phi$ of the vacuum Rabi angle are not very critical, since the corresponding fidelity decrease ΔF is proportional to the *square* of the relative time-of-flight spread $\Delta\phi/\langle\phi\rangle$, compare Eq. (6.15). Experimentally, the latter can be kept as low as approximately 1%. From a theoretical point of view, also an imperfect atomic initial state does not have a very dramatic influence: the fidelity of the state preparation is at least as high as the fidelity achieved with the ideal atomic state multiplied by the fidelity of the imperfect atomic state. We have to keep in mind, however, that the generation of entangled atomic states with high fidelity is in itself a difficult experimental task.

Part II

Noise-Assisted Control of Quantum Jumps

Chapter 7

The coherently pumped micromaser

In the first part of this thesis, we have studied the preparation of field states via interaction with a sequence of two-level atoms. Since the field is prepared in a *pure* quantum state, this corresponds to a perfect control of the field state. As we have seen in the previous chapter, any kind of noise in general reduces the fidelity of the state preparation. Hence, the influence of the noise should be kept as low as possible. In particular, we have to choose an entangled initial atomic state, in order to avoid finally any entanglement of the exiting atoms with the cavity field. The latter would result in a mixed instead of the desired pure state of the cavity field.

However, the generation of the required entangled initial atomic state is a very difficult task. Experimentally, it is much more practical to consider a steady flux of atoms, originating, e.g., from a thermal source, which arrive at the cavity at random times, and are all prepared in the same initial single-atom state. The realization of this experimental setup is known as the micromaser [69, 95, 96]. In contrast to the deterministic state preparation outlined in the first part, a random influence on the photon field is now inevitable: firstly, the entanglement between atom and field leads to measurement noise acting on the photon field when detecting the final state of the exiting atoms. Secondly, we have to take into account cavity dissipation (see chapter 6.1), which can be neglected only for a small number of atoms interacting with the cavity field. Finally, also the random arrival times of the atoms constitute a source of noise.

It is obvious that the presence of noise now prevents a perfect quantum control of the cavity field. Nevertheless, the noise may also play a *constructive* role in controlling the photon field in a statistical sense, as we will see in the present second part of this thesis.

In the following two chapters, we examine the maser dynamics resulting from the interplay of the above noise sources and the coherent atom-field interaction. Under certain experimental conditions, we will observe a bistable behavior, where the photon field exhibits quantum jumps between two metastable states, which can be monitored by measurement of the exiting atoms. The positive influence of the noise then will be demonstrated in chapter 9: in the presence

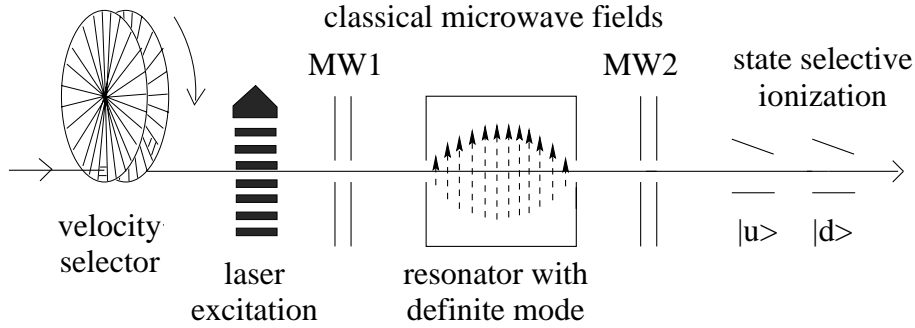


Figure 7.1: Schematic experimental setup of the micromaser

of a small external periodic signal, we can achieve the best synchronization of the quantum jumps with the periodic signal at an *optimal, nonvanishing temperature* of the environment. Our especial interest will be devoted to the influence of an injected or measured atomic coherence on this synchronization effect.

7.1 Experimental setup

Fig. 7.1 schematically shows a typical experimental setup [97] which realizes the coherently pumped micromaser. The atoms are emitted by a thermal source (i.e., with thermal velocity distribution) at random, uncorrelated times.

Then, each atom having passed the velocity filter is prepared by a pump laser and a subsequent classical microwave pulse (MW1) in an initial state which is, in general, a superposition of the two energy eigenstates $|u\rangle$ and $|d\rangle$, see chapter 7.2.1. Inside the cavity, the atom resonantly interacts with the cavity field mode according to the Jaynes-Cummings Hamiltonian. As discussed in chapter 2.1, field and atom perform Rabi oscillations and may exchange a single photon. Finally, the atom is detected in either of the states $|u\rangle$ or $|d\rangle$ via field ionization. By applying a second classical microwave pulse (MW2) on each atom just before detection, we can vary the basis in which the atom is detected and thereby read out either the population of the levels $|u\rangle$ and $|d\rangle$ or the coherence between them, see chapter 7.2.2.

In addition to the interaction with the atoms, the radiation field is also coupled to its environment, which is supposed to be in thermal equilibrium, at very low temperatures $T \lesssim 1$ K. This corresponds to an average thermal photon number of less than 1 (in the microwave regime, $\omega \simeq 20$ GHz), see Eq. (6.2). Furthermore, the cavity decay rate γ is much smaller than the atomic flux r (defined as the average number of atoms crossing the maser cavity per time unit), so that, before the field has time to relax into thermal equilibrium, the next atom arrives in the cavity. Under these circumstances, the photon field will finally reach a stationary state $\rho^{(ss)}$ far from thermal equilibrium. However, before we turn to the quantitative description of the photon field dynamics in chapter 7.3, let us first describe in more detail the role of the two classical microwave fields MW1 and MW2, which control the preparation and detection

of the atoms.

7.2 Preparation and detection of the atoms

The frequency of these classical fields equals the one of the quantized cavity mode, i.e., they are in resonance with the atomic transition between the two levels $|u\rangle$ and $|d\rangle$. By varying the amplitude and phase of such a pulse, any unitary transformation in the two dimensional atomic Hilbert space can be performed (see, e.g., chapter 15.3 in [24]).

7.2.1 Coherent and incoherent pumping

In this way, we can use the first microwave field MW1 to prepare each atom in a coherent superposition

$$|\psi\rangle = a|u\rangle - ib|d\rangle, \quad (7.1)$$

where $a, b \in \mathbb{R}$, and $|a|^2 + |b|^2 = 1$. The reason for this particular choice of the phases (which, anyway, implies no loss of generality) will become clear later: as we will see in chapter 7.3, due to the phase coherence between the photon field and the incoming atoms, the density operator ρ of the field will then have only real matrix elements (in the photon number representation). If amplitude and phase of the microwave pulse remain constant, such that all atoms enter the cavity in the same state $|\psi\rangle$ given by Eq. (7.1), with constant coefficients a and b , we speak of ‘*coherent pumping*’. The corresponding initial atomic density matrix reads:

$$\tau = |\psi\rangle\langle\psi| = \begin{pmatrix} |a|^2 & ic \\ -ic & |b|^2 \end{pmatrix}, \quad (7.2)$$

with the initial atomic coherence $c = ab \in \mathbb{R}$. In order to ensure a positive energy transfer to the cavity (which may counterbalance the photon losses due to damping), we choose $|a|^2 > |b|^2$.

On the other hand, if the phase of the microwave pulse fluctuates randomly between subsequent atoms, the atoms enter the cavity in an *incoherent* superposition of $|u\rangle$ and $|d\rangle$ (*incoherent pumping*). In this case, the initial atomic state τ is described by a diagonal density matrix, with vanishing coherence $c = 0$ in Eq. (7.2). Since in the following we will be especially interested in the role of the initial atomic coherence c , we will often compare the corresponding cases of coherent and incoherent pumping.

7.2.2 Final state detection

The final state detection is controlled by the second microwave pulse MW2, which is considered as a part of the measurement device. We require the phases of MW2 and MW1 to be the same, as would be the case, e.g., if the two pulses originate from the same source. This is necessary in order to preserve the phase coherence between the incoming atoms and the field, see chapter 7.3.

In the following, we will express the final state of the exiting atoms in terms of the Bloch vector $\langle\vec{\sigma}\rangle$, i.e., the expectation values of the Pauli matrices $\sigma_x, \sigma_y,$

and σ_z . The basis is chosen such that $\sigma_z|u\rangle = |u\rangle$ and $\sigma_z|d\rangle = -|d\rangle$. Consequently, a measurement of σ_z or σ_y with result ‘+1’ or ‘-1’ would correspond to a detection in the following final state:

	+1	-1
σ_z	$ u\rangle$	$ d\rangle$
σ_y	$(u\rangle + i d\rangle)/\sqrt{2}$	$(u\rangle - i d\rangle)/\sqrt{2}$

Whereas the measurement of σ_z depends on the *population* of the two levels $|u\rangle$ and $|d\rangle$, the *y* component σ_y measures the *coherence* between them. A measurement of σ_x is excluded by our requirement that the phases of MW1 and MW2 should be the same. [The phase of MW1 is chosen such that $\langle\psi|\sigma_x|\psi\rangle = 0$, as a consequence of Eq. (7.1), with $a, b \in \mathbb{R}$, and if the phase of MW2 is the same, also the detected final state has a vanishing *x* component.]

Since we cannot perform direct measurements on the photon field, the atomic detections are used to gain information about it. By measuring different components of the atomic Bloch vector, we will probe different properties of the photon field. In fact, the atomic Bloch vector $\langle\vec{\sigma}\rangle$ on exit from the cavity depends on the photon field through:

$$\langle\vec{\sigma}\rangle = \text{Tr} \left\{ (\mathbb{1} \otimes \vec{\sigma}) U(\rho \otimes \tau) U^\dagger \right\}, \quad (7.3)$$

with ρ the state of the photon field just before the atom arrives, τ the initial state of the atom according to Eq. (7.2), and U the atom-field interaction, Eqs. (2.2,2.3). Provided that $c \in \mathbb{R}$ and the matrix elements $\rho_{n,m}$ are all real (which, as discussed above, is guaranteed if we do not measure σ_x), the various components of $\langle\vec{\sigma}\rangle$ are given by:

$$\langle\sigma_x\rangle = 0, \quad (7.4)$$

$$\begin{aligned} \langle\sigma_y\rangle = & \sum_{n=0}^{\infty} -2c A_n A_{n+1} \rho_{n,n} \\ & + 2(|b|^2 A_n B_{n+1} - |a|^2 A_{n+2} B_{n+1}) \rho_{n+1,n} \\ & + 2c B_{n+2} B_{n+1} \rho_{n+2,n}, \end{aligned} \quad (7.5)$$

$$\begin{aligned} \langle\sigma_z\rangle = & \sum_{n=0}^{\infty} (2|a|^2 A_{n+1}^2 + 2|b|^2 B_n^2 - 1) \rho_{n,n} \\ & - 4c A_{n+1} B_{n+1} \rho_{n+1,n}, \end{aligned} \quad (7.6)$$

with the coefficients

$$A_n = \cos(\phi\sqrt{n}), \quad B_n = \sin(\phi\sqrt{n}), \quad (7.7)$$

which reflect the Rabi dynamics of the atom-field interaction. In the case of incoherent pumping ($c = 0$), it is obvious from Eqs. (7.5,7.6) that $\langle\sigma_z\rangle$ only depends on the main diagonal $\rho_{n,n}$ of the photon field, whereas $\langle\sigma_y\rangle$ is completely determined by the first off-diagonal $\rho_{n,n+1}$. In the case of coherent

pumping, however, $\langle\sigma_z\rangle$ and $\langle\sigma_y\rangle$ depend both on the main and the first off-diagonal, and $\langle\sigma_y\rangle$ additionally on the second off-diagonal.

Each measurement of an atom is accompanied by the usual quantum mechanical state reduction. Importantly, as a consequence of the entanglement between atom and field (compare chapter 2.1), also the photon field is affected by the state reduction. For example, if the density matrix of the field is given by ρ before the atom arrives, the new photon field ρ' reads, according to Eqs. (2.2,2.3):

$$\begin{aligned} \frac{1 + \langle\sigma_z\rangle}{2} \rho'_{n,m} &= |a|^2 A_{n+1}A_{m+1} \rho_{n,m} - c B_{n+1}A_{m+1} \rho_{n+1,m} \\ &\quad - c A_{n+1}B_{m+1} \rho_{n,m+1} + |b|^2 B_{n+1}B_{m+1} \rho_{n+1,m+1}, \end{aligned} \quad (7.8)$$

after detection of the atom in $|u\rangle$ (i.e., $\sigma_z = +1$), and

$$\begin{aligned} \frac{1 - \langle\sigma_z\rangle}{2} \rho'_{n,m} &= |b|^2 A_nA_m \rho_{n,m} + c B_nA_m \rho_{n-1,m} \\ &\quad + c A_nB_m \rho_{n,m-1} + |a|^2 B_nB_m \rho_{n-1,m-1}, \end{aligned} \quad (7.9)$$

after a detection $|d\rangle$ (i.e., $\sigma_z = -1$). The expressions for the measurement of σ_y are more complicated, since both, initial and final atomic state, are superpositions of $|u\rangle$ and $|d\rangle$:

$$\begin{aligned} \frac{1 \pm \langle\sigma_y\rangle}{2} \rho'_{n,m} &= \frac{1}{2} \times \\ &\times \left[(|a|^2 A_{n+1}A_{m+1} + |b|^2 A_nA_m \pm c A_{n+1}A_m \mp c A_nA_{m+1}) \rho_{n,m} \right. \\ &\quad + |b|^2 B_{n+1}B_{m+1} \rho_{n+1,m+1} + |a|^2 B_nB_m \rho_{n-1,m-1} \\ &\quad + (-c B_{n+1}A_{m+1} \pm |b|^2 B_{n+1}A_m) \rho_{n+1,m} \\ &\quad + (-c A_{n+1}B_{m+1} \pm |b|^2 A_nB_{m+1}) \rho_{n,m+1} \\ &\quad + (c B_nA_m \mp |a|^2 B_nA_{m+1}) \rho_{n-1,m} + (c A_nB_m \mp |a|^2 A_{n+1}B_m) \rho_{n,m-1} \\ &\quad \left. \pm c B_{n+1}B_m \rho_{n+1,m-1} \pm c B_nB_{m+1} \rho_{n-1,m+1} \right], \end{aligned} \quad (7.10)$$

after a detection in $(|u\rangle \pm i|d\rangle)/\sqrt{2}$ (i.e., $\sigma_y = +1$ or $\sigma_y = -1$, respectively). Here, the prefactors $(1 \pm \langle\sigma_{z,y}\rangle)/2$ are the probabilities of the corresponding measurement results, which are needed to normalize the state, and are given by Eqs. (7.5, 7.6). Obviously, if all matrix elements $\rho_{n,m}$ are real, this is also the case after a measurement of σ_z or σ_y , as claimed above. Furthermore, it is evident from the above equations that the final state detection of the atoms does not only yield information about the photon field, but also plays an active role in its dynamics, mediated by the atom-field entanglement. This will be relevant in the following chapter, where the dynamics of the photon field conditioned on a measured sequence of atomic detection results will be studied.

7.3 Dynamics of the photon field

At first, however, we want to examine the *average* behavior of the photon field. Here, we are interested in the photon field alone, without looking at the heat

bath or the atoms exiting the cavity, i.e., we trace over all atoms that have crossed the cavity, and over the heat bath.

7.3.1 Master equation

Under these conditions, the time evolution of the photon field density matrix is described by a master equation of the general form

$$\dot{\rho} = \dot{\rho}|_{\text{at}} + \dot{\rho}|_{\text{env}}, \quad (7.11)$$

where $\dot{\rho}|_{\text{at}}$ and $\dot{\rho}|_{\text{env}}$ distinguish the influence of the atomic beam and the environment, respectively.

As for the atomic part $\dot{\rho}|_{\text{at}}$, let us first examine the influence of a single atom onto the cavity field. If the photon field is given by a density matrix ρ just before an atom in the initial state τ , see Eq. (7.2), arrives, the resulting photon field ρ' after the atom has left the cavity is obtained by applying the atoms-field interaction U , Eq. (2.1), and then tracing over the atom:

$$\rho' = \text{tr}_a\{U\rho \otimes \tau U^\dagger\}. \quad (7.12)$$

In the following, we assume that the duration t_{int} of the atom-field interaction is much shorter than all other relevant time scales, i.e., the passage of a single atom is treated as an instantaneous kick on the photon field. Consequently, the master equation (7.11) is valid only on time scales much longer than t_{int} .

Suppose now that the photon field at time t is described by a density matrix $\rho(t)$. Since the atoms arrive at random, uncorrelated times with average rate r , the probability that one atom arrives during the time interval $[t, t + \Delta t]$ equals $r\Delta t$, whereas with probability $1 - r\Delta t$ nothing happens.* Then, according to Eq. (7.12), the photon field at time $t + \Delta t$ reads:

$$\rho(t + \Delta t) = r\Delta t \rho' + (1 - r\Delta t) \rho. \quad (7.13)$$

With $\Delta t \rightarrow 0$, and inserting the interaction U , Eq. (2.1), into ρ' , Eq. (7.12), we arrive at the following expression for the atomic part of the master equation (in the photon number representation):

$$\begin{aligned} \dot{\rho}_{n,m}|_{\text{at}} = & r [|a|^2 A_{n+1} A_{m+1} + |b|^2 A_n A_m - 1] \rho_{n,m} \\ & + r |a|^2 B_n B_m \rho_{n-1,m-1} + r |b|^2 B_{n+1} B_{m+1} \rho_{n+1,m+1} \\ & + i r c A_{n+1} B_{m+1} \rho_{n,m+1} - i r c^* B_{n+1} A_{m+1} \rho_{n+1,m} \\ & - i r c B_n A_m \rho_{n-1,m} + i r c^* A_n B_m \rho_{n,m-1}, \end{aligned} \quad (7.14)$$

with the coefficients A_n and B_n given by Eq. (7.7).

For the damping part, we assume the standard master equation for the damped harmonic oscillator, see Eq. (6.1) (translated into the photon number representation):

$$\begin{aligned} \dot{\rho}_{n,m}|_{\text{env}} = & -\frac{\gamma}{2} [n_b(n+m+2) + (n_b+1)(n+m)] \rho_{n,m} \\ & + \gamma n_b \sqrt{n} \sqrt{m} \rho_{n-1,m-1} \\ & + \gamma (n_b+1) \sqrt{n+1} \sqrt{m+1} \rho_{n+1,m+1}, \end{aligned} \quad (7.15)$$

*Two-atom events can be neglected in the limit $\Delta t \rightarrow 0$.

where, as in Eq. (6.1), γ denotes the cavity decay rate, and n_b the mean number of photons in thermal equilibrium.

Evidently, the damping equation (7.15) does not couple different diagonals of the density matrix (i.e., elements $\rho_{n,n+k}$ and $\rho_{m,m+l}$ with $k \neq l$). Only the last four terms in the atomic equation (7.14) couple neighboring diagonals of ρ , via terms proportional to the initial atomic coherence c . They describe the transfer of atomic coherence to the cavity field [98]: due to these terms, non-diagonal elements $\rho_{n,m}$, $n \neq m$, of the photon field will appear, even if the photon field initially exhibits no such coherences (e.g., in thermal equilibrium). Note that, according to Eq. (7.14), all elements $\rho_{n,n+k}$ on the same diagonal k will acquire the same phase factor. Furthermore, the phase difference between neighboring diagonals is given by the phase of the atomic coherence ic (which, in turn, depends on the phase of the first microwave field MW1). With our choice $ic \in \mathbb{R}$, see Eqs. (7.1,7.2), all matrix elements $\rho_{n,m}$ will stay real under the temporal evolution (7.11). This fact expresses the phase coherence between atoms and field.

On the other hand, in the case of incoherent pumping ($c = 0$), the non-diagonal elements of the photon field density matrix will not be populated, or will be damped away, if coherences are present in the initial field state.

7.3.2 Stationary state

For $t \rightarrow \infty$, each solution of (7.11) will approach a stationary state $\rho^{(\text{ss})}$, characterized by a dynamical equilibrium, where photon losses due to the damping of the field are counterbalanced by photon gains due to the pumping by the atoms. The stationary state is uniquely determined, i.e., independent of the initial field state (in the absence of trapping states). This behavior reminds us of asymptotic completeness (chapter 3.2), where the cavity field finally also loses the memory of its initial state. Due to the presence of the heat bath, however, which leads to a non-unitary evolution of the atoms-field system, we now cannot draw the conclusion that we are able to prepare the cavity field in arbitrary states, as we could in chapter 3.2 (compare also chapter 6.1, where the influence of the heat bath on the state preparation is discussed).

Instead, as shown in [70], for $|a|^2 = 1$ (i.e., if the atoms enter the cavity in the upper state $|u\rangle$) the steady state is essentially determined (for a fixed temperature T of the heat bath) by a single experimental parameter, namely the so-called ‘pump parameter’ $\theta = \phi\sqrt{N_{\text{ex}}}$, where $N_{\text{ex}} = r\gamma^{-1}$ is the atomic flux in units of the cavity decay rate γ . More precisely, if the vacuum Rabi angle ϕ and the atomic flux r are varied such that θ remains constant, the photon number populations $\langle n|\rho^{(\text{ss})}|n\rangle$ (i.e., the diagonal elements of $\rho^{(\text{ss})}$) are almost unaffected, apart from the fact that the photon number n has to be scaled according to $\nu = n/N_{\text{ex}}$ (i.e., increasing the atomic flux increases the mean photon number of the steady state). If the atoms enter the cavity partly in the lower state $|d\rangle$, i.e., $|a|^2 < 1$ (but mainly in the upper state, i.e., $|a|^2 > 1/2$, in order to ensure a positive energy transfer to the cavity), we have found numerically (both for coherent and incoherent pumping) that the photon statistics

still roughly depends on a single parameter, the generalized pump parameter

$$\theta = \phi \sqrt{N_{\text{ex}}}, \quad \text{with } N_{\text{ex}} = (2|a|^2 - 1) r \gamma^{-1}, \quad (7.16)$$

and the corresponding scaling behavior $\nu = n/N_{\text{ex}}$ of the photon number n is the same as above. Hence, increasing the lower state population of the incoming atoms has approximately the same effect as decreasing the atomic flux r . Furthermore, the steady state photon statistics are quite similar for coherent and incoherent pumping. Only for coherent pumping, however, the steady state will exhibit coherences between different photon numbers, i.e., non-diagonal elements in the photon number representation, see below.

Now, for certain values of the experimental parameters, namely if θ is roughly an integer multiple of 2π [70, 34] (and the temperature T is not too high [99]), the stationary photon number distribution $p_n^{(\text{ss})} = \rho_{n,n}^{(\text{ss})}$ displays two maxima as a function of n , corresponding to the *bistable operation mode* of the micromaser. The origin of the bistability can be traced back to the Rabi dynamics during the atom-field interaction: since the frequency of the Rabi oscillations depends on the photon number n , see Eqs. (2.2,2.3), the probability that an atom leaves the cavity in its lower state (and therefore emits a photon into the cavity) shows an oscillatory behavior as a function of n . Hence, there may exist several equilibrium points, where the photon gain rate due to the pumping with the atom equals the photon loss rate due to the coupling to the cavity walls (which depends linearly on n , for low temperatures $n_b \ll n$).

An example of such a double-peaked stationary state is shown in Fig. 7.2, obtained by numerical diagonalization of the master equation (7.11).[†] We chose $\omega = 21.5$ GHz, $\gamma^{-1} = 0.06$ s, $r = 40\gamma$, $t_{\text{int}} = 2.9 \times 10^{-5}$ s and $\phi = 1.1$, typical values in state of the art experiments [34]. (These values are used in all numerical examples given in Part II.) The two peaks in Fig. 7.2, which we denote $\rho^{(1)}$ and $\rho^{(2)}$, located around $n_1 = 4$ and $n_2 = 21$, represent the two metastable states of the photon field. They are defined by the two (normalized) subdomains of $\rho_{n,m}^{(\text{ss})}$ with $n, m < n_3$ or $n, m > n_3$, respectively, where the cut is performed at the local minimum $n_3 = 10$ of $p_n^{(\text{ss})}$ between its two maxima. Note that there exist coherences between different photon numbers n and m , if both are associated with either $\rho^{(1)}$ or $\rho^{(2)}$, but practically none between photon numbers of the macroscopically distinct metastable states. This is not surprising, as a single atom can only couple neighboring photon states (through emission or absorption of a photon), and the damping of the coherences $\rho_{n,m}$ between macroscopically distinct photon numbers n and m is too strong (i.e., much faster than the time needed for at least $|n - m|$ atoms to build up such a coherence). The lack of coherence between $\rho^{(1)}$ and $\rho^{(2)}$ is already a hint that, on long time scales, the dynamics of the photon field may be described in terms of transition rates between the two metastable states $\rho^{(1)}$ and $\rho^{(2)}$, see chapter 8.

The inset of Fig. 7.2 compares the case of coherent and incoherent pumping (on a logarithmic scale). The bistability is present in both cases, but for inco-

[†]An analytical expression of the stationary state exists for incoherent pumping, see Eq. (8.1).

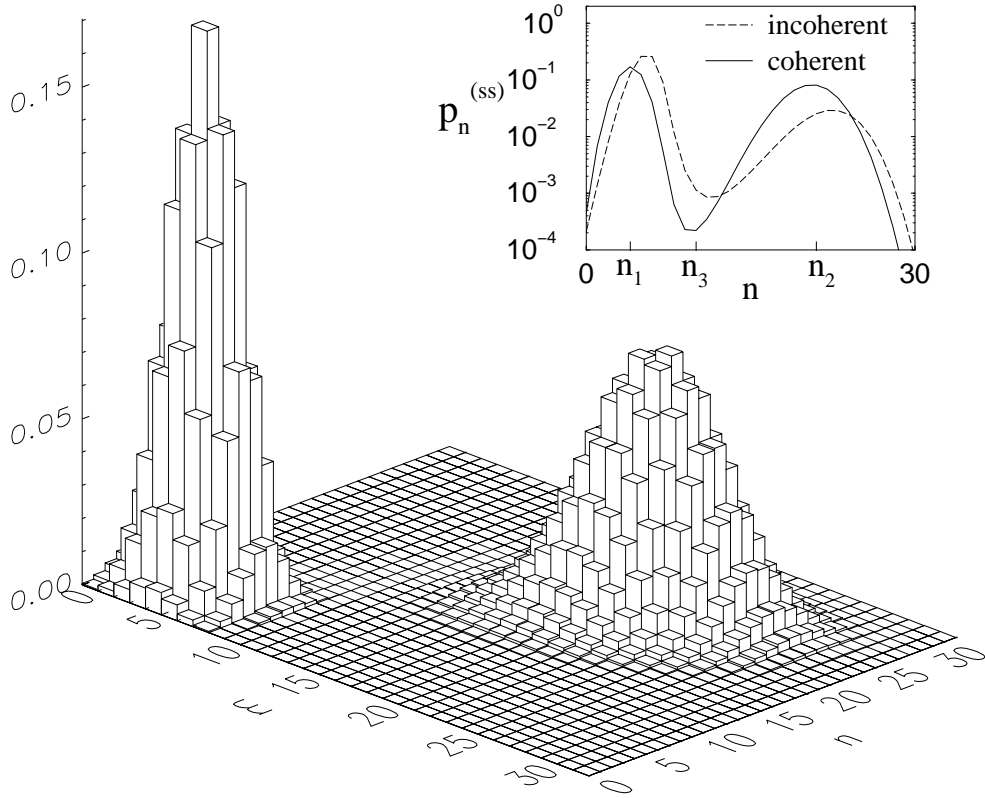


Figure 7.2: Stationary state of the photon field density matrix $\rho_{n,m}^{(ss)}$, with two metastable states $\rho^{(1)}$ (left peak) and $\rho^{(2)}$ (right peak). Nonvanishing coherences between different photon numbers n and m only exist if both, n and m , belong to either $\rho^{(1)}$ or $\rho^{(2)}$. Initial atomic superposition, Eq. (7.1): $a = \sqrt{0.9}$, $b = \sqrt{0.1}$ (coherent pumping), temperature $T = 0.5$ K. The inset shows the photon number distribution $p_n = \rho_{n,n}$, and compares it to the case of incoherent pumping ($|a|^2 = 0.9$, $c = 0$). Field frequency $\omega = 21.5$ GHz, decay rate $\gamma^{-1} = 0.06$ s, atomic flux $r = 40\gamma$, and vacuum Rabi angle $\phi = 1.1$.

herent pumping the minimum between the two maxima is less pronounced. As we will see in chapter 8.2, this leads to enhanced transition rates between the two metastable states, for incoherent pumping.

Chapter 8

Bistability of the maser dynamics

In the previous section, we have seen that - under certain conditions - the stationary state of the photon field exhibits two well separated maxima. However, the stationary solution of the master equation implies an average over all possible atomic detection results, whereas in an experiment we are confronted with a single sequence of detections. What can we say about the corresponding dynamics of the photon field, conditioned on such an observed sequence of measurement results?

A double-peaked stationary state as in Fig. 7.2 suggests the conclusion that in a single realization the maser dynamics is bistable. Then, the photon field would at each time be localized around either one of the two maxima ρ_1 or ρ_2 , and perform transitions between these two metastable states at random times. This would also be consistent with the observed lack of coherence between ρ_1 and ρ_2 in the stationary state. However, such a conclusion is not stringent: a priori, there is no reason why the photon field could not be double-peaked also in a single realization. Furthermore, as already mentioned at the end of chapter 7.2.2, the dynamics of the photon field in a single realization also depends on the applied measurement scheme.

8.1 Quantum jumps of the maser field

In order to answer these questions, we will resort to numerical simulations of single realizations of the maser dynamics. Obviously, the stochastic influences arising from the random arrival times of the atoms and the atomic detections have to be simulated by producing random numbers on the computer. For our numerical studies, we used an efficient quantum trajectory method [100, 101, 102, 103], which is described in detail in appendix C.

Examples of thereby obtained single realizations of the maser dynamics are shown in Fig. 8.1. Here, the cases of coherent and incoherent pumping are compared for two different measurement schemes of the exiting atoms (in z and y direction) with the same parameters as in Fig. 7.2. Figs. 8.1(a-c) clearly display a bistable behavior: the measured component $\langle \sigma_{z,y} \rangle$ of the atomic Bloch

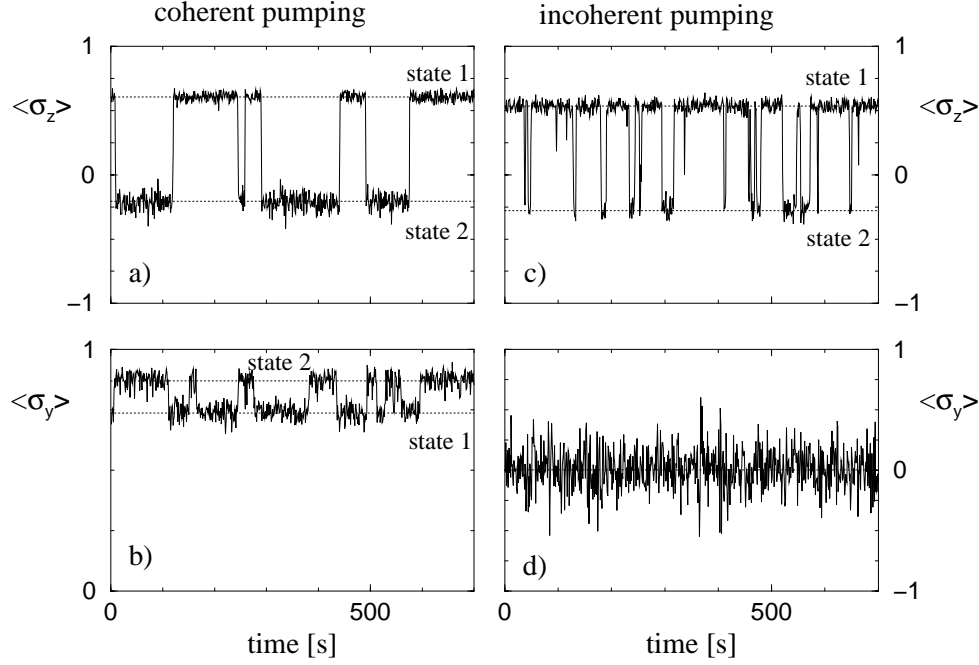


Figure 8.1: Single realizations of the maser dynamics, for the same parameters as in Fig. 7.2. Left column (a and b): coherent pumping. Right column (c and d): incoherent pumping. Upper half (a and c): measurement of the z component σ_z of the atomic Bloch vector $\langle \vec{\sigma} \rangle$, i.e., detection of the exiting atoms in $|u\rangle$ or $|d\rangle$. Lower half (b and d): measurement of σ_y , i.e., detection in $(|u\rangle - i|d\rangle)/\sqrt{2}$ or $(|u\rangle + i|d\rangle)/\sqrt{2}$. In all four cases, $\langle \sigma_{z,y} \rangle$ is obtained by averaging the atomic detection events over time intervals of length $\Delta t = 1$ s (ca. 700 detection events, for $r = 40\gamma^{-1} = 667 \text{ s}^{-1}$). With coherent pumping, the bistability of the maser dynamics can be monitored both in the z and the y component of $\langle \vec{\sigma} \rangle$. The transition rates between the metastable states are faster for incoherent than for coherent pumping, see also the inset of Fig. 7.2.

vector jumps between two metastable states $\langle \sigma_{z,y} \rangle^{(1)}$ and $\langle \sigma_{z,y} \rangle^{(2)}$. In the case of coherent pumping, Figs. 8.1(a,b), the bistability is observed both in the atomic population $\langle \sigma_z \rangle$ and in the coherence $\langle \sigma_y \rangle$, whereas for incoherent pumping, the quantum jumps can be seen in the population, Fig. 8.1(c), but not in the atomic coherence, Fig. 8.1(d).

Since the probability of detecting an atom in a definite final state depends on the photon field the atom encounters in the cavity, see Eqs. (7.4-7.6), these jumps are a signature of underlying jumps of the photon field. The observed values of $\langle \sigma_i \rangle^{(1,2)}$ confirm our above conjecture that the corresponding metastable states of the photon field are given by the two peaks $\rho^{(1)}$ and $\rho^{(2)}$ of the stationary state. Indeed, with the parameters of Fig. 8.1, inserting $\rho^{(1,2)}$ into Eqs. (7.4-7.6) yields $\langle \sigma_z \rangle^{(1)} = 0.61$, $\langle \sigma_z \rangle^{(2)} = -0.21$, $\langle \sigma_y \rangle^{(1)} = 0.74$ and $\langle \sigma_y \rangle^{(2)} = 0.87$, for coherent pumping, and $\langle \sigma_z \rangle^{(1)} = 0.54$, $\langle \sigma_z \rangle^{(2)} = -0.28$ for incoherent pumping. These values are marked by the dotted lines in Figs. 8.1(a-c), and agree with

the numerical simulation.

The separation of time scales is obvious: The average residence times in the two metastable states 1 and 2 (several seconds) are much longer than all other time scales in the micromaser, in particular the intrastate fluctuations, and the time needed for transitions between 1 and 2. Indeed, the latter do not occur instantaneously, but consist of several ‘microscopic’ quantum jumps caused both by atomic detection events and exchange of photons with the heat bath (see also appendix C). Typically, such a transition needs a time comparable to the cavity decay time $\gamma^{-1} = 0.06$ s. In the following, we will focus on long time scales, where, with good approximation, the dynamics of the photon field can be described in terms of a two-state model: At (almost) any time, the photon field is concentrated around either one of the two maxima $\rho^{(1,2)}$ of the steady state distribution, see Fig. 7.2. Between these two metastable states, transitions occur with rates W_1 (from 1 to 2) and W_2 (from 2 to 1), see chapter 8.2.

Clearly, such a simple two-state model can only be approximately valid: in exceptional cases, e.g., during the transitions between the metastable states, a perfect distinction between state 1 and 2 is not always possible. Indeed, we have observed that, when measuring in y direction, situations where the photon field shows nonvanishing population at both maxima n_1 and n_2 are slightly more frequent than when measuring in z direction. The reason for this is the smaller separation between the two metastable states of $\langle\sigma_y\rangle$ as compared to those of $\langle\sigma_z\rangle$, see Figs. 8.1a,b. Hence, a measurement of σ_y does not as clearly distinguish between states 1 and 2 as a measurement of σ_z . In other words, a measurement of σ_z and the resulting state reduction of the photon field, Eqs. (7.8,7.9), leads to a clearer preference of either state 1 or 2.

In the case of incoherent pumping, the bistability cannot be observed in the expectation value $\langle\sigma_y\rangle$ of the atomic coherence of the exiting atoms (Fig. 8.1d). Nevertheless, we have checked that also in this case (i.e., measuring $\langle\sigma_y\rangle$) the evolution of the photon field conditioned on the observed atomic detection sequence shows the above described bistable behavior. Hence, the information whether the photon field is in state 1 or 2 must be present in the atomic detection sequence. Since the expectation value of $\langle\sigma_y\rangle$ does obviously not distinguish between state 1 and 2, the information must be contained in statistical quantities which include correlations between different atomic detection events. As a simple example, we can look at the mean number $\langle N_S \rangle$ of successive detector clicks of the same kind ($\sigma_y = +1$ or $\sigma_y = -1$) [104]. For the parameters of Fig. 8.1(d), the exact formula given in [105] yields $\langle N_S \rangle^{(1)} = 2.42$ if the photon field is in state 1, and $\langle N_S \rangle^{(2)} = 2.67$ in state 2.*

8.2 Transition rates

In the last section we have seen that the maser dynamics can be approximated by a two-state model [56, 99]. At each time, the maser field is either in state 1 or 2, and transitions between them occur at random times. Thereby, the maser

*Of course, a direct calculation of the photon field conditioned on the atomic measurement result discriminates the two states much more efficiently than $\langle N_S \rangle$.

dynamics is on long time scales completely described by the two transition rates W_1 (from 1 to 2) and W_2 (vice versa).

8.2.1 Incoherent pumping

First, we consider the case of incoherent pumping, where each atom enters the cavity either in the state $|u\rangle$ (with probability $|a|^2$) or $|d\rangle$ (with probability $|b|^2$), without any coherence between them. Furthermore, we assume that also the final state detection measures the atom in one of those two states (i.e., measurement of σ_z). In this case, the dynamics of the photon field can be described as a jump process between neighboring photon numbers, see appendix C, with the ‘microscopic’ transition probabilities t_n^\pm from n to $n+1$ or $n-1$ photons, respectively, given by Eqs. (C.8,C.9). The average of one single realization of this jump process over a sufficiently long time approaches the following distribution (chapter 7.1 in [106]):

$$p_n^{(\text{ss})} = p_0^{(\text{ss})} \prod_{k=1}^n \frac{t_{k-1}^+}{t_k^-}, \quad (8.1)$$

where $p_0^{(\text{ss})}$ is determined by normalization. This distribution is identical to the stationary state of the ensemble average (chapter 7.3.2), i.e., ergodicity is fulfilled. A double-peaked stationary distribution, with two maxima at n_1 and n_2 (see inset of Fig. 7.2), occurs if t_n^+ and t_n^- as a function of n intersect (at least) three times: at n_1 and n_2 (stable equilibrium), and at the minimum n_3 (unstable equilibrium). In this case, the photon number will be found almost always near one of the two maxima at n_1 or n_2 , and transitions between these metastable states occur. The transition rates of these ‘macroscopic’ jumps of the photon field can be expressed in terms of the rates for the microscopic jumps (chapter 7.4 in [106]):

$$W_1^{-1} = \sum_{n=n_1}^{n_2-1} [p_n^{(\text{ss})} t_n^+]^{-1} \sum_{m=0}^n p_m^{(\text{ss})}, \quad (8.2)$$

$$W_2^{-1} = \sum_{n=n_1+1}^{n_2} [p_n^{(\text{ss})} t_n^+]^{-1} \sum_{m=n}^{\infty} p_m^{(\text{ss})}, \quad (8.3)$$

where $p_n^{(\text{ss})}$ is given by Eq. (8.1).

8.2.2 Coherent pumping

In the case of coherent pumping, the quantum trajectory of the photon field is much more complicated, and simple expressions for the transition rates do not exist. In order to calculate the transition rates in this case, let us first look at the dynamics of the two-state model. On average, the probabilities p_1 and $p_2 = 1 - p_1$ of state 1 and 2, respectively, fulfill the following rate equation:

$$\begin{pmatrix} \dot{p}_1 \\ \dot{p}_2 \end{pmatrix} = \begin{pmatrix} -W_1 & W_2 \\ W_1 & -W_2 \end{pmatrix} \begin{pmatrix} p_1 \\ p_2 \end{pmatrix}. \quad (8.4)$$

The solution is easily obtained by diagonalizing the above 2×2 -matrix, which has two real eigenvalues $\lambda_0 = 0$ and $\lambda_1 = -W_1 - W_2$. The eigenvector corresponding to $\lambda_0 = 0$ gives the stationary state

$$p_1^{(\text{ss})} = \frac{W_2}{W_1 + W_2}, \quad p_2^{(\text{ss})} = \frac{W_1}{W_1 + W_2}, \quad (8.5)$$

and $|\lambda_1| = W_1 + W_2$ defines the relaxation rate towards the stationary state.

The above equation (8.4) describes the ensemble-averaged dynamics of the two-state model (i.e., averaged over all possible jump sequences), in the same way as the master equation (7.11) describes the ensemble-averaged dynamics of the whole photon field. In general, the master equation does not describe all properties of a single realization of the dynamics. Nevertheless, under the assumption that the two-state approximation is valid on long time scales (as we have verified in the previous section), it should be possible to extract the transition rates W_1 and W_2 between the two metastable states from the master equation in a similar way as from the solution of Eq. (8.4). For this purpose, we write Eq. (7.11) in the form

$$\dot{\rho} = \mathcal{M}\rho, \quad (8.6)$$

where the ‘superoperator’ \mathcal{M} (i.e., an operator which acts in the space of density operators ρ) is given by Eqs. (7.14,7.15). Next, we solve the eigenvalue problem

$$\mathcal{M}\rho^{(i)} = \lambda_i\rho^{(i)}. \quad (8.7)$$

One eigenvalue is $\lambda_0 = 0$, and the corresponding eigenvector $\rho^{(0)}$ is the stationary state $\rho^{(0)} = \rho^{(\text{ss})}$. In the bistable regime, $\rho^{(\text{ss})}$ exhibits two peaks, and in analogy to Eq. (8.5) the ratio of their weights $S_{1,2}$ gives the inverse ratio of the two transition rates:

$$\frac{W_1}{W_2} = \frac{S_2}{S_1}, \quad (8.8)$$

with the weights defined as

$$S_1 = \sum_{n=0}^{n_3-1} \rho_{n,n}^{(\text{ss})}, \quad \text{and} \quad S_2 = \sum_{n=n_3+1}^{\infty} \rho_{n,n}^{(\text{ss})}. \quad (8.9)$$

Here, n_3 denotes the local minimum of the steady state distribution $p_n^{(\text{ss})}$, see the inset of Fig. 7.2. The remaining (in general complex) eigenvalues λ_i determine the various time scales of the maser dynamics. Assuming that on long time scales the dynamics follows a two-state model, we expect that one of the remaining eigenvalues, e.g., λ_1 , has a much smaller absolute value than all others, which then defines the sum of the two transition rates:

$$|\lambda_1| = W_1 + W_2, \quad (8.10)$$

Thereby, the transition rates W_1 and W_2 are given in terms of the stationary state $\rho^{(\text{ss})}$ and the smallest nonvanishing eigenvalue λ_1 of the master equation, according to Eqs. (8.8) and (8.10).

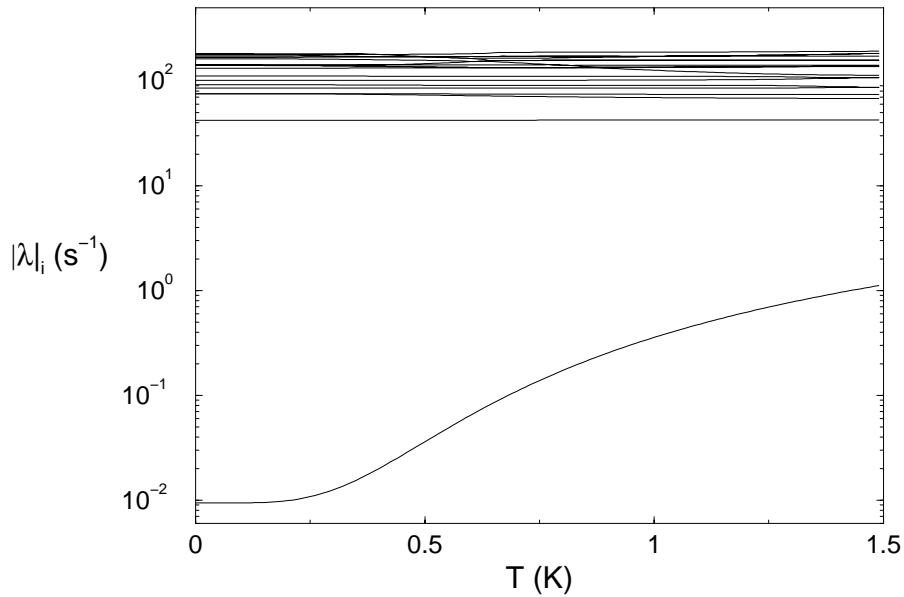


Figure 8.2: Absolute values $|\lambda_i|$ of the 20 smallest (nonzero) eigenvalues of the master equation (7.11), as a function of temperature T , for the same parameters as Figs. 7.2 and 8.1 (coherent pumping). The separation of time scales is clearly visible. The smallest nonvanishing eigenvalue $|\lambda_1|$ gives the sum of the transition rates $W_1 + W_2$.

With the same parameters as employed for Figs. 7.2 and 8.1 (coherent pumping), Fig. 8.2 shows the 20 smallest nonzero eigenvalues of Eq. (8.7), as a function of the temperature T . Indeed, the above considerations are confirmed: one of the eigenvalues is much smaller than the others. Not surprisingly, $|\lambda_1|$ increases with increasing temperature T : the higher the temperature, the more frequent are the transitions between the two states. The other eigenvalues - that set the time scale for the intrastate dynamics - are less sensitive with respect to changes of the temperature.

The validity of Eq. (8.10) is confirmed by Fig. 8.3, which shows the average residence times $W_{1,2}^{-1}$, as calculated from Eqs. (8.8) and (8.10). They agree very well with the residence times as directly determined from single realizations of the maser dynamics (such as in Fig. 8.1). For this purpose, we evaluate the jumps of the photon field by following the time evolution of the mean photon number $\langle n \rangle$: whenever $\langle n \rangle$ is smaller (or larger) than the equilibrium value $\langle n \rangle^{(1,2)} = \text{tr}\{a^\dagger a \rho^{(1,2)}\}$ corresponding to state 1 (or 2), the photon field is defined to be in state 1 (or 2). If $\langle n \rangle$ is between these values, the state of the photon field is unchanged.

A close inspection of Fig. 8.3 reveals a small difference of the transition rates when changing the measurement scheme: the transitions are slightly faster (about 1%) when measuring in y direction. This is consistent with the observation that in a single realization a double-peaked photon field occurs more often when measuring in y direction. Hence, the two-state approximation (i.e., the photon field is at each time either in state 1 or in state 2) is not as precisely

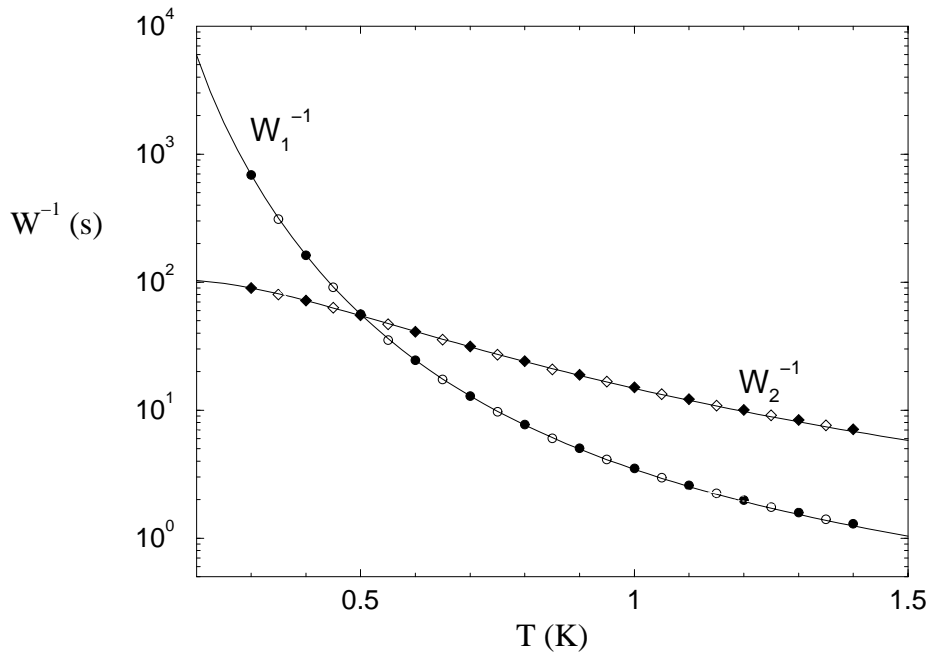


Figure 8.3: Average residence times $W_{1,2}^{-1}$ in the two metastable states of the photon field, as a function of the temperature T , for coherent pumping. W_1^{-1} is the graph that depends more strongly on T . Parameters as in Fig. 8.2. The solid lines show $\langle W_{1,2} \rangle$ as determined from the master equation, with Eqs. (8.8, 8.10), whereas the symbols are obtained from single realizations, with measurement of σ_z (filled) and σ_y (open). At $T = 0.5$ K, the residence times in state 1 and 2 are equal, $W_1^{-1} = W_2^{-1} = 54$ s.

fulfilled as when measuring in z direction, which explains the small difference.

As obvious from Fig. 8.3, the temperature dependences of the two transition rates $W_{1,2}$ are distinct: the rate W_1 from state 1 (with the smaller mean photon number) to state 2 (with the larger mean photon number) is more sensitive to changes in T . This is so because the probability of absorbing a thermal photon (and thereby enhancing transitions from 2 to 1) is proportional to $n_b + 1$, see Eq. (C.9), whereas the probability of emitting a thermal photon (enhancing transitions from 1 to 2) is proportional to n_b (and thereby approaches zero at $T \rightarrow 0$), see Eq. (C.8). As a consequence, the two rates intersect at $T \simeq 0.5$ K.

Fig. 8.4 shows the average residence times for incoherent pumping. The results from the master equation, Eqs. (8.8,8.10), agree quite well with the mean passage times, Eqs. (8.2,8.3). The small deviations show the limitations of the two-state model, which cannot be valid exactly. As already obvious from Fig. 8.1(c), the transition rates for incoherent pumping are faster than for coherent pumping. This fact also reflects itself in the stationary state (inset of Fig. 7.2), where the population at the minimum between the two maxima is higher for incoherent pumping. Intuitively, the increase of the transition rates can be understood as a consequence of the additional noise source, i.e., the fluctuations of the phase of the initial atomic state. Comparing the transition rates

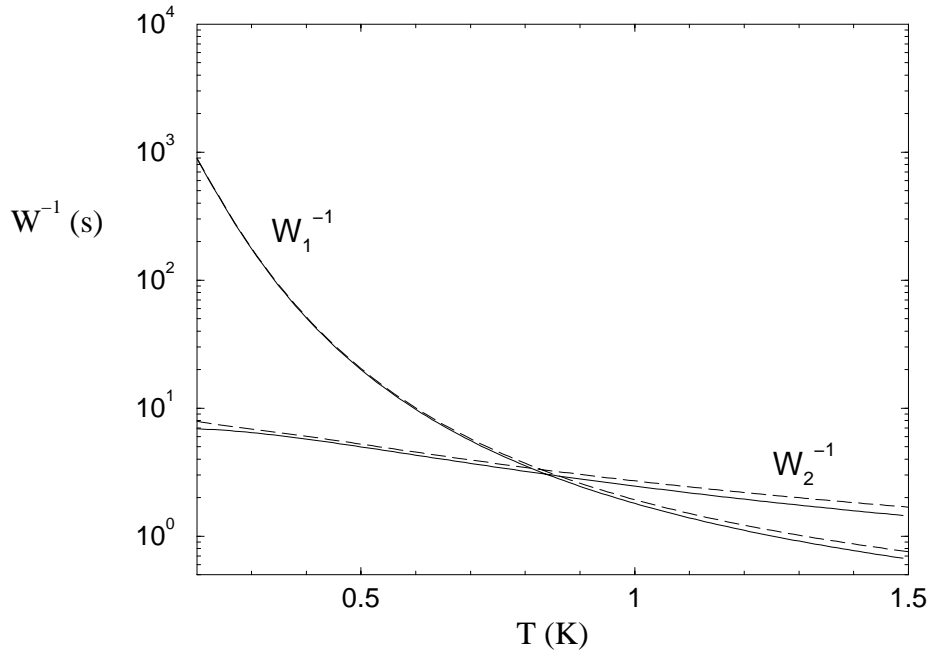


Figure 8.4: Average residence times $W_{1,2}^{-1}$ in the two metastable states of the photon field, as a function of the temperature T , for incoherent pumping ($|a|^2 = 0.9$) and otherwise the same parameters as in Figs. 7.2-8.3. W_1^{-1} is the graph that depends more strongly on T . The solid lines show the results of Eqs. (8.8, 8.10), whereas the dashed lines show the mean passage times between n_1 and n_2 , Eqs. (8.2,8.3). For incoherent pumping, the transition rates (especially W_2) are faster than in the corresponding case of coherent pumping (Fig. 8.3).

in the case of coherent (Fig. 8.3) and incoherent pumping (Fig. 8.4), we observe that the rate W_2 , from state 2 to 1, is more strongly affected by the atomic phase fluctuations than W_1 (compare Figs. 8.3 and 8.4). Consequently, for incoherent pumping, the intersection $W_2 = W_1$ occurs at a higher temperature $T \simeq 0.85$ K.

The strong sensitivity of W_2 with respect to fluctuations of the initial atomic phase is consistent with the following property of the rates t_n^\pm of the microscopic jumps $n \rightarrow n \pm 1$ of the photon field in the case of incoherent pumping, see Eqs. (C.8,C.9): The term $\sin^2(\phi\sqrt{n})$ (responsible for the measurement noise, i.e., the random influence on the photon field induced by the interaction with the atoms and their subsequent detection) is small (close to 0) in the regime between n_1 and n_3 (important for transitions $1 \rightarrow 2$), while it is large (close to 1) between n_3 and n_2 (important for transitions $2 \rightarrow 1$).[†] In other words, if the photon number is between n_1 and n_3 , the atom is probably detected in the same state as its initial state (either $|u\rangle$ or $|d\rangle$ in the case of incoherent pumping), corresponding to a full cycle of the Rabi dynamics, whereas in the regime between n_3 and n_2 , an emission or absorption of a cavity photon by

[†]This behavior of the term $\sin^2(\phi\sqrt{n})$ follows from the fact that t_n^+ and t_n^- intersect at n_1 , n_2 , and n_3 .

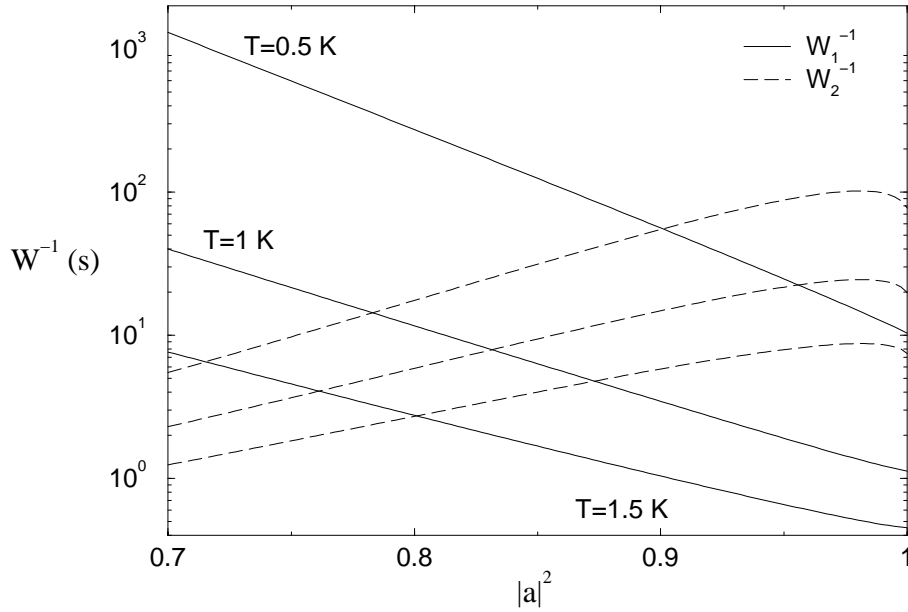


Figure 8.5: Average residence times W_1^{-1} (solid lines) and W_2^{-1} (dashed lines) in the two metastable states of the photon field, as a function of the initial atomic state, Eq. (7.1), for three different temperatures $T = 0.5$ K, $T = 1$ K, and $T = 1.5$ K (from top to bottom). Parameters as in Figs. 7.2-8.3 (coherent pumping). The two transition rates $W_{1,2}$ evolve differently with the initial atomic state (W_1^{-1} decreases and W_2^{-1} increases with increasing $|a|^2$), except for the vicinity of $|a|^2 = 1$ (where the limit of incoherent pumping is approached).

the atom is very likely. Hence, the measurement noise depends more strongly on whether the atom actually enters the cavity in the upper state ($|a|^2 = 1$, $|b|^2 = 0$) or in the lower state ($|a|^2 = 0$, $|b|^2 = 1$) if the photon field is in the regime corresponding to a transition from 2 to 1.

Finally, Fig. 8.5 shows the average residence times $W_{1,2}^{-1}$ as a function of the initial atomic state, Eq. (7.1). As can be seen, the residence times depend roughly exponentially on $|a|^2$. While the residence times in state 1 decrease with increasing $|a|^2$, the residence times in state 2 show the opposite behavior. Only for $|a|^2$ very close to 1 the residence times in state 2 slightly decrease. We have not yet found a convincing explanation of this small decrease. [It may have to do with the fact that the atomic coherence $|c| = \sqrt{|a|^2(1 - |a|^2)}$, which tends to stabilize the metastable states, goes to zero for $|a|^2 \rightarrow 1$.]

Let us stress here that the noise sources, which activate the quantum jumps of the maser field, and thereby determine the transition rates $W_{1,2}$, are of genuine quantum origin: they arise mainly from the entanglement of the photon field with the strongly coupled two-level atoms crossing the cavity, and with the heat bath. Hence, the measurement of the exiting atoms and the corresponding quantum mechanical state reduction ('measurement noise') directly influences the photon field, and plays a crucial role for the transitions between the two metastable states. Also the thermal fluctuations are partly of quantum origin,

due to the entanglement with the heat bath. This leads to nonvanishing thermal fluctuations also at vanishing temperature: at $T = 0$ K, the photon field can still spontaneously emit photons into the heat bath at *random times*, due to the term $n_b + 1$ in the master equation (7.11). On the other hand, the random atomic arrival times and the incomplete knowledge of the heat bath (as characterized by the temperature T) are rather classical noise sources.

Chapter 9

Stochastic resonance

In the previous section, we have investigated the maser dynamics in the bistable regime. On long time scales, the dynamics is completely described in terms of transition rates between the two metastable states $\rho^{(1,2)}$. As described in chapter 7.3.2, these states arise from the interplay between the coherent pumping by the atoms and the dissipation arising from the thermal cavity walls. Obviously, in contrast to part I, where we chose entangled initial atomic states and neglected the cavity dissipation, we cannot perfectly control the quantum state of the photon field. Instead, the states $\rho^{(1,2)}$ are determined by only a few experimental parameters, namely essentially by the pump parameter θ , Eq. (7.16), (which should be chosen close to 2π in order to stay in the bistable regime), and the initial atomic coherence c , compare Eq. (7.2), which controls the magnitude of the coherences between different photon numbers within the metastable state $\rho^{(1)}$ or $\rho^{(2)}$, see Fig. 7.2. In particular, due to the presence of noise, these states are mixed rather than pure quantum states, corresponding to an average over the intrastate fluctuations on short time scales.

However, what can we say about the time when the next transition to the other metastable state occurs? Although the *average* time scale of these jumps can be controlled by varying the temperature of the heat bath (see Fig. 8.3) and the initial atomic state (see Fig. 8.5), the *individual* jumps occur at unpredictable times (see Fig. 8.1). The situation changes if we feed a periodic signal into the maser, e.g., a small modulation of the initial atomic state (‘small’ in the sense that it preserves the bistability of the maser dynamics and does not deterministically enforce transitions between the two states). Then, due to the ensuing modulation of the transition rates, the jumps are more likely at certain times than at others. In order to achieve a synchronization of the quantum jumps with the external signal, we exploit in this chapter the general mechanism of *stochastic resonance* [36, 39, 40], which predicts a cooperative effect between noise and a small periodic signal in bistable systems at some optimal, *nonvanishing* level of the noise strength. Thereby, adding noise to the system allows us an efficient control of the quantum jumps of the maser field.

On the other hand, the noise arising from the coupling of a quantum system to an environment also induces decoherence: any generic quantum state will rapidly decohere into a mixture of certain preferred states (the so-called ‘pointer

states') which are most stable with respect to environment-induced decoherence [107]. The most fundamental example is the spin-boson system [108], i.e., a two-state system coupled to a bath of harmonic oscillators. For most parameters (except low temperatures and weak coupling), incoherent tunneling between the 'left' and 'right' state (which are defined by the coupling to the bath) prevails over the coherent dynamics. Correspondingly, in the driven spin-boson system, no signatures of quantum stochastic resonance can be observed in the coherence between those states [53, 54]. In our case, this apparent dilemma is circumvented by inducing the metastability of the two-level atoms not via direct coupling to an environment, but rather by its coherent interaction with the bistable maser field, which - in turn - is coupled to a thermal bath. As shown in the previous chapter, the jumps of the maser field can then be monitored by measuring different components of the atomic Bloch vector. Consequently, we expect that the stochastic resonance effect can be read out not only in the populations but also the coherences of the exiting two-level atoms.*

9.1 Modulation of the initial atomic state

We want to synchronize the quantum jumps with a weak periodic signal, which we inscribe into the maser dynamics by modulation of the amplitudes of the initial coherent superposition of the atoms injected into the cavity:

$$a(t) = [0.9 + 0.05 \sin(\omega_s t)]^{1/2}, \quad (9.1)$$

$$b(t) = [0.1 - 0.05 \sin(\omega_s t)]^{1/2}. \quad (9.2)$$

For the modulation period, we choose $t_s = 2\pi/\omega_s = 100$ s. (Then, the most favorable scenario for stochastic resonance will be realized by the same experimental parameters as in the numerical examples from the previous chapters.) According to Eq. (7.1), each atom enters the cavity in the state $|\psi\rangle(t) = a(t)|u\rangle - ib(t)|d\rangle$, depending on its arrival time t . As described in chapter 7.2.1, Eqs. (9.1,9.2) can be realized by intensity modulation of the classical microwave field MW1 (see Fig. 7.1). The above modulation of the initial atomic state leads to a modulation of the two transition rates $W_{1,2}$ with opposite phase, see Fig. 8.5: Increasing $|a|$ enhances transitions from state 1 to 2, whereas transitions from 2 to 1 are suppressed. On the other hand, the *average* transition rates can be varied by changing the temperature T of the heat bath, compare Fig. 8.3, thereby changing the strength of the noise in the maser. We expect a cooperative effect between signal and noise if the sum of the average residence times in the two metastable states roughly equals the modulation period [37]. Furthermore, it is intuitively clear (and discussed in more detail in [99]), that both average residence times should approximately be equal (i.e., half a

*Also with respect to any other basis than the energy eigenstates $|u\rangle$ and $|d\rangle$, the coherences (i.e., the nondiagonal elements of the density matrix) of the exiting atoms do not vanish. This follows from the fact that the two Bloch vectors $\langle\vec{\sigma}\rangle^{1,2}$ of the exiting atoms corresponding to state 1 and state 2 are not parallel (since $\langle\sigma_z\rangle^1$ and $\langle\sigma_z\rangle^2$ are of opposite sign, whereas $\langle\sigma_y\rangle^{1,2}$ are both positive, see Fig. 8.1).

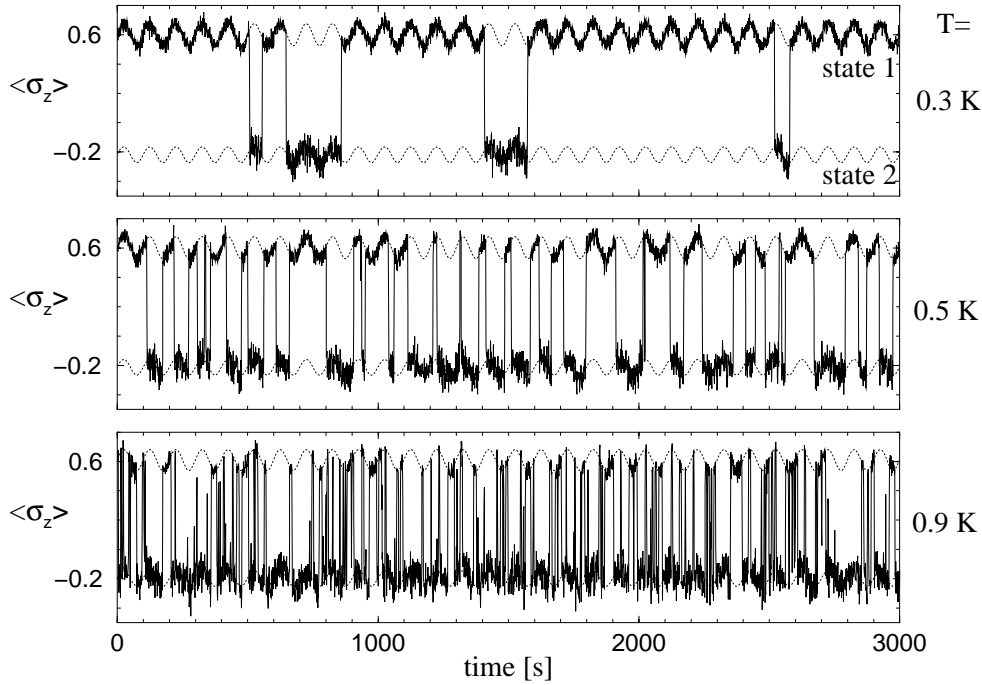


Figure 9.1: Single realizations of the maser dynamics: Time evolution of $\langle \sigma_z \rangle$, for three different temperatures $T = 0.3$ K, 0.5 K, and 0.9 K (from top to bottom). The initial coherent atomic superposition is modulated according to Eqs. (9.1,9.2), with modulation period $t_s = 100$ s. Remaining parameters as in Figs. 7.2-8.5. Stochastic resonance is observed in $\langle \sigma_z \rangle$: The noise-induced synchronization of the quantum jumps is poor for the lowest temperature (rare quantum jumps), optimal for the intermediate temperature (almost regular quantum jumps), and again poor for the highest temperature (too frequent quantum jumps).

modulation period), in order to achieve a good synchronization. With the parameters of Figs. 7.2-8.3, and the modulation period $t_s = 100$ s, this is the case for $T \simeq 0.5$ K.[†]

9.2 Optimal synchronization of the quantum jumps

Numerical simulations of the maser dynamics are illustrated in Fig. 9.1, for three different temperatures, by the detection signal of the exiting atoms in the state $|u\rangle$ or $|d\rangle$. The presence of the periodic signal given by Eqs. (9.1,9.2) is clearly visible in Fig. 9.1, since the modulation of the initial atomic state influences not only the transition rates, but also the two metastable states themselves. Here, the states $\rho^{(1,2)}(t)$ at time t can be obtained from the corresponding time-independent stationary state (adiabatic approximation): since the intrastate

[†]The modulation of a and b , Eqs. (9.1,9.2), leads to average residence times only slightly different from the unmodulated case of Fig. 8.3.

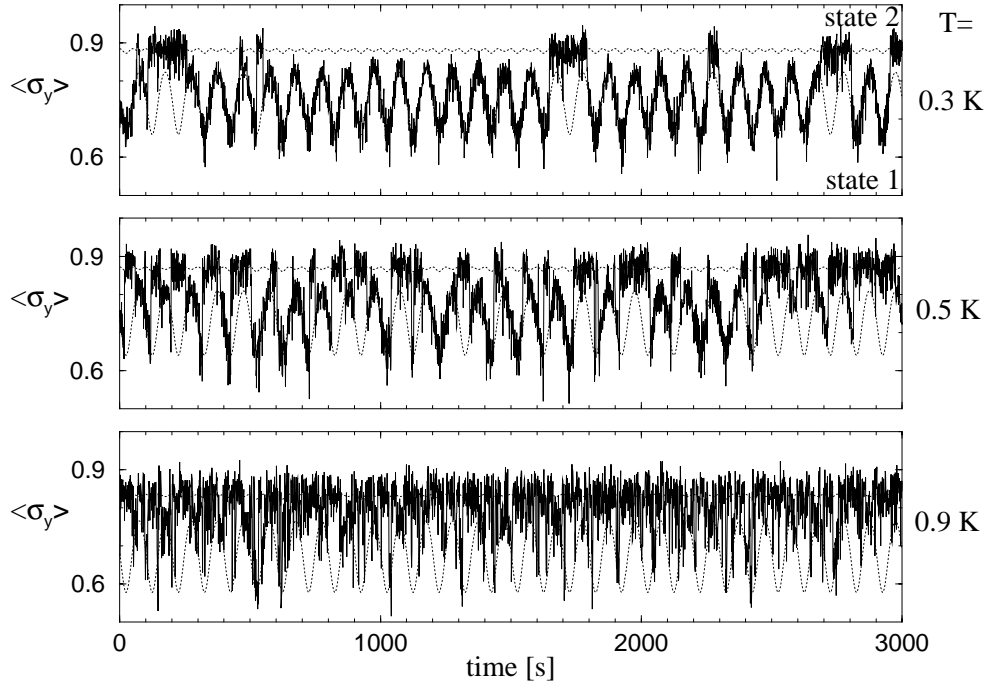


Figure 9.2: Same as Fig. 9.1, but for measurement of $\langle \sigma_y \rangle$ of the exiting atoms. The optimal synchronization of the quantum jumps at an optimal, nonvanishing temperature is also observed in the atomic coherence $\langle \sigma_y \rangle$, at $T = 0.5\text{ K}$, though strongly masked by the intrastate modulation (dotted lines) in state 1.

relaxation time (of the order of $\gamma^{-1} = 0.06\text{ s}$) is much smaller than the modulation period ($t_s = 100\text{ s}$), the two states $\rho^{(1,2)}(t)$ follow the modulation almost instantaneously. The ensuing modulations of the metastable equilibrium values $\langle \sigma_z \rangle^{(1,2)}(t)$, as defined by Eq. (7.6), are plotted as dotted lines in Fig. 9.1, and are well reproduced by the numerical simulation.

Indeed, Fig. 9.1 clearly demonstrates the stochastic resonance. The best synchronization of the quantum jumps of the maser field with the periodic signal is observed for the intermediate temperature $T = 0.5\text{ K}$. In most cases, the maser field jumps from one state to the other and back again once during a modulation period. In contrast, for the lower temperature, $T = 0.3\text{ K}$, the quantum jumps are too rare compared to the signal period t_s . Especially the average residence time in state 1 (with the smaller mean photon number) is much longer than $t_s = 100\text{ s}$ (compare also Fig. 8.3), and it is not possible to predict after how many signal periods the next jump will occur. On the other hand, if the temperature is too high, $T = 0.9\text{ K}$, the quantum jumps are too frequent, so that signal and noise lose the cooperativity observed for $T = 0.5\text{ K}$. Hence, the best control over the quantum jumps is achieved at a finite, *nonvanishing* temperature of the environment.

From Fig. (8.1), we know that (in the case of coherent pumping) the Bloch vector of the exiting atoms is not oriented solely along the z axis, but has a nonvanishing y component, too, which also distinguishes between the two

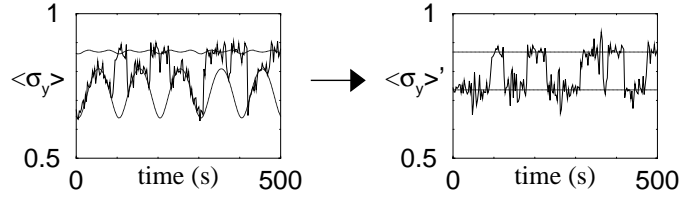


Figure 9.3: Illustration of Eq. (9.3): filtering out the intrastate modulation.

metastable states 1 and 2. [Remember that the x component vanishes due to our choice of the phase of the initial state (7.1).] Furthermore, as shown in Fig. 8.3, the transition rates between the two metastable states of the maser field are almost unaffected by a change of the measurement scheme. Therefore, we expect that the stochastic resonance effect can also be observed when detecting the atomic coherence $\langle \sigma_y \rangle$ instead of the population $\langle \sigma_z \rangle$. This is confirmed by Fig. 9.2, where the optimal synchronization of the quantum jumps occurs at the same temperature $T \simeq 0.5$ K as in Fig. 9.1. As already discussed in chapter 8, the amplitude of the jumps of $\langle \sigma_y \rangle$ is smaller than that of $\langle \sigma_z \rangle$. In fact, it is not very much larger than the intrastate modulation of $\langle \sigma_y \rangle$ in state 1, but large enough to discriminate the two states during the entire modulation period.

Thereby, we have demonstrated stochastic resonance by a visual inspection of a sequence of quantum jumps in Figs. 9.1 and 9.2. Of course, we also would like to describe the effect in a quantitative way.

9.3 Quantitative analysis of the synchronization effect

For this purpose, for example the Fourier transform of the graphs shown in Figs. 9.1 and 9.2 could be appropriate. In the thereby obtained power spectrum, we would expect a strong peak at the signal frequency in the case of nearly periodic quantum jumps. However, also the intrastate modulation (dotted lines) contributes to the power spectrum of $\langle \sigma_z \rangle$, and especially of $\langle \sigma_y \rangle$, obscuring the contribution of the jumps between the metastable states.

We therefore subject $\langle \sigma_{z,y} \rangle$ to an affine transformation in order to filter out the intrastate modulation, see Fig. 9.3:

$$\langle \sigma_{z,y} \rangle' = m(t) \langle \sigma_{z,y} \rangle + c(t). \quad (9.3)$$

In (9.3), $m(t)$ and $c(t)$ are chosen such that $\langle \sigma_{z,y} \rangle'^{(1,2)}$ do not depend on time, and equal the average of $\langle \sigma_{z,y} \rangle^{(1,2)}(t)$ over one modulation period. Again, $\langle \sigma_{z,y} \rangle^{(1,2)}(t)$ are defined by inserting the time-dependent metastable state $\rho^{(1,2)}$ of the photon field into Eqs. (7.4-7.6), respectively (dotted lines in Figs. 9.1 and 9.2). Now, the power spectrum of our output variable $x(t) = \langle \sigma_{z,y} \rangle'(t)$ is obtained by Fourier transformation:

$$P(\omega) = \left| \int_0^{t_{\max}} dt x(t) e^{i\omega t} \right|^2 / t_{\max}. \quad (9.4)$$

Generally, $P(\omega)$ is a sum of two parts, $P(\omega) = P_N(\omega) + P_S(\omega)$, where the noise background $P_N(\omega)$ has an approximately Lorentzian shape [42], whereas the signal part $P_S(\omega)$ consists of sharp peaks at the signal frequency ω_s , and integer multiples thereof. The main signal peak at ω_s quantifies the response of the system to the small periodic modulation. In the case of stochastic resonance, the response is maximized at a definite nonvanishing noise level [36].[‡] In other words, the strength of the signal peak exhibits a maximum as a function of the temperature of the environment.

9.3.1 First harmonic - the stochastic resonance peak

The strength of the signal peak is given by the output signal power S [37], which is defined as the area under the signal peak at $\omega = \omega_s$:

$$S = \int_{\omega_s - \Delta\omega/2}^{\omega_s + \Delta\omega/2} d\omega P_S(\omega). \quad (9.5)$$

$\Delta\omega$ must be larger than the width of the peak, which gets smaller for higher integration time t_{\max} , whereas its area S is independent of t_{\max} .

An equivalent definition of S makes use of the asymptotic periodic response $\langle x(t) \rangle_{\text{as}}$. The subscript ‘as’ stands for the asymptotic limit $t \rightarrow \infty$ [where $x(t)$ is independent of the initial condition $x(0)$, but still depends on time, due to the driving], and the brackets denote an average over all noise realizations. The strength S of the output signal is defined as the amplitude (or first harmonic) of $\langle x(t) \rangle_{\text{as}}$:

$$S = \frac{2\pi}{t_s^2} \left| \int_0^{t_s} dt \langle x(t) \rangle_{\text{as}} e^{i\omega_s t} \right|^2. \quad (9.6)$$

In the case of a simple two-state model, where the dynamics of $x(t)$ can be described in terms of transition rates $W_{1,2}$ between two different values x_1 and x_2 , the output signal power only depends on the separation between the two states (i.e., S is proportional to $|x_1 - x_2|^2$) and the time-dependent transition rates $W_{1,2}(t)$, see [51]. According to chapter 8, we expect such a two-state model to be a good approximation for the bistable micromaser, provided the average residence times $W_{1,2}^{-1}$ and the modulation period t_s are sufficiently long.

From $\langle \sigma_z \rangle'$ and $\langle \sigma_y \rangle'$ we now extract the output signal power S , as a function of the temperature T of the environment. The results are shown in Fig. 9.4. The diamonds are obtained, according to Eq. (9.5), from single realizations of $\langle \sigma_{z,y} \rangle'(t)$ (integration time $t_{\max} = 37500$ s, corresponding to 25 million atomic detection events), whereas the solid lines show the result of Eq. (9.6), obtained numerically from the asymptotic solution $\rho_{\text{as}}(t)$ of the master equation (7.11), together with Eqs. (7.4-7.6), and (9.3). Clearly, in both cases S assumes a

[‡]Often, the signal-to-noise ratio, i.e., the strength S of the signal peak divided by the noise background at the signal frequency, is used instead of the signal S alone as a quantitative measure of stochastic resonance [37, 42]. Furthermore, stochastic resonance can also be analyzed via the residence time distributions in the two metastable states [37, 42, 56]. (Note that these measures need not always give the same answer concerning the occurrence of stochastic resonance [37].)

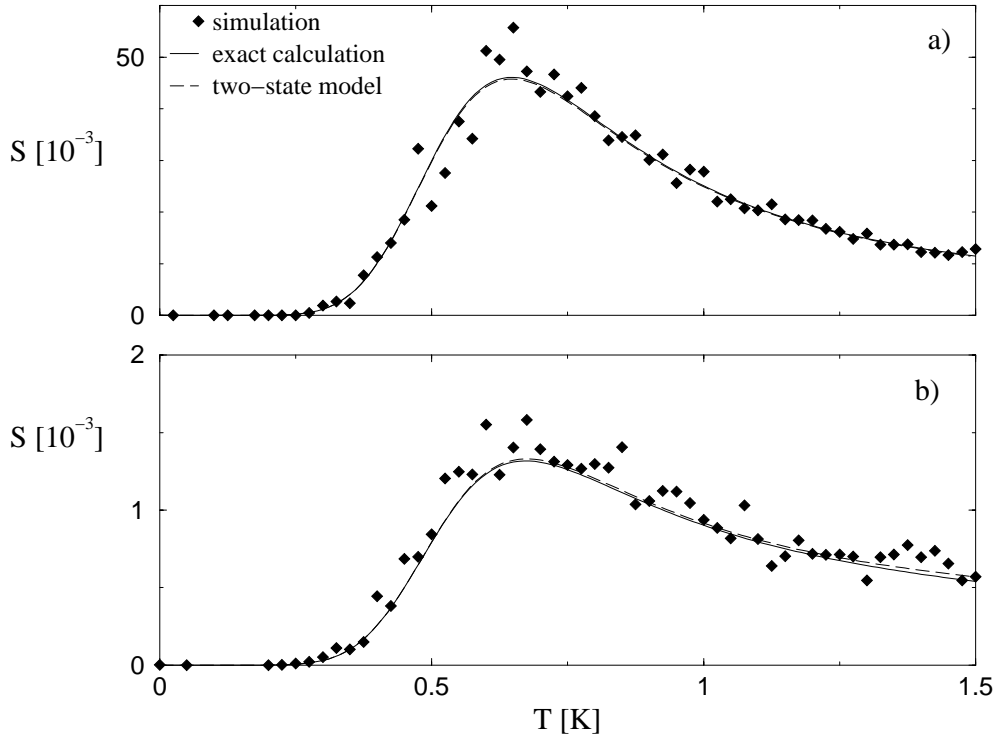


Figure 9.4: Output signal power S of (a) the z -, and of (b) the y -component $\langle \sigma_{z,y} \rangle'$ of the modified atomic Bloch vector, Eq. (9.3), vs. temperature T , in response to a weak periodic modulation of the coherent atomic superposition, Eqs. (9.1, 9.2), at period $t_s = 100$ s. Remaining parameters as in Figs. 9.1 and 9.2. Both when measuring the atomic population σ_z and the coherence σ_y , stochastic resonance is observed: at an optimal temperature of $T \simeq 0.6$ K, the output signal power exhibits a maximum.

maximum at about $T = 0.6$ K, and noise-induced signal enhancement is observed. The cause of the similar temperature dependence of $S(T)$ in both cases is the weak dependence of the transition rates between the metastable states on the applied measurement scheme. Closer inspection of Fig. 9.4 reveals, however, some differences: when measuring σ_z , the signal power is about 30 times stronger than in the other two cases, and the decrease of S with increasing temperature is faster as compared to the measurement of σ_y . Since in a two-state system, the power spectrum is proportional to the square of the amplitude of the jumps, these features are simply explained by the dependence of $|\langle \sigma_{z,y} \rangle'^{(2)} - \langle \sigma_{z,y} \rangle'^{(1)}|$ on T , which either slightly increases with T (σ_y), or is approximately constant (σ_z) [as can be confirmed by a careful inspection of the intrastate modulation of $\langle \sigma_{z,y} \rangle'^{(1,2)}$ in Figs. 9.1 and 9.2 (dotted lines), whose mean value defines $\langle \sigma_{z,y} \rangle'^{(1,2)}$]. Finally, the dashed lines in Fig. 9.4 (hardly discernible) show the results for the two-state model [51], with the transition rates from chapter 8.2, Eqs. (8.8,8.10). The very good agreement with the exact solution (solid lines) stresses the validity of the two-state model.

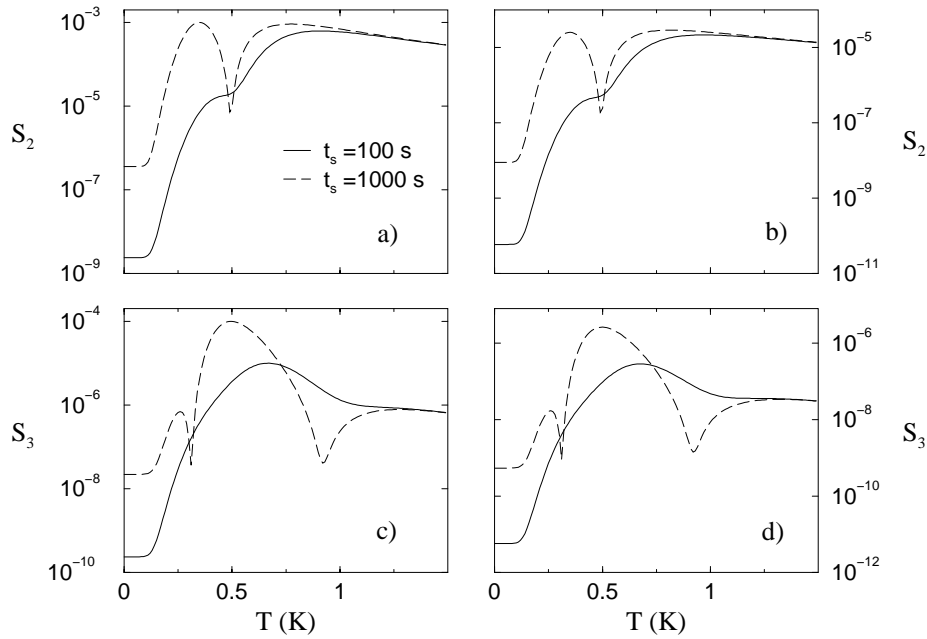


Figure 9.5: Second and third harmonic S_2 (a,b) and S_3 (c,d) of the output signal of $\langle \sigma_z \rangle'$ (a,c) and $\langle \sigma_y \rangle'$ (b,d), for two different signal periods $t_s = 100$ s (solid lines) and $t_s = 1000$ s (dashed lines). Otherwise, the same parameters as in Fig. 9.4 have been chosen. For the long modulation period $t_s = 1000$ s, a noise-induced suppression of S_2 by approximately two orders of magnitude is observed at $T = 0.49$ K, and of S_3 at $T = 0.32$ K and $T = 0.85$ K. This agrees with the general theory of [109], which predicts a suppression of the second harmonic if the two unmodulated transition rates $W_{1,2}$ (see Fig. 8.3) are equal, and of the third harmonic if their ratio equals $(\sqrt{3} + 1)/(\sqrt{3} - 1) \simeq 3.7$ or $(\sqrt{3} - 1)/(\sqrt{3} + 1) \simeq 0.27$.

Let us note that the signal-to-noise ratio of $\langle \sigma_{z,y} \rangle'$ (which is often used for a quantitative analysis of stochastic resonance instead of the signal S alone, see the footnote on p. 118) does not show a maximum as a function of T , but rather monotonically increases. This can be traced back to an untypical behavior of the modulated transition rates $W_{1,2}(t)$, the modulation amplitudes of which increase with increasing temperature T (instead of being approximately constant, as in standard examples of stochastic resonance) [56]. On the other hand, the analysis of the residence-time distributions does exhibit signatures of stochastic resonance, and the optimal temperature approximately coincides with the position of the maximum in the signal S [56].

9.3.2 Suppression of higher harmonics

Besides the main signal peak, the power spectra of $\langle \sigma_{z,y} \rangle(t)$ also exhibit higher harmonics, i.e., peaks at integer multiples of the signal frequency. The generation of higher harmonics of the input signal is a general property of periodically driven, nonlinear systems [110]. In the language of signal processing, it

amounts to a distortion of the transmitted signal (in addition to the presence of a noise background in the output). In this section, we want to see whether also the higher harmonics can be controlled by varying the noise level, as we have demonstrated it for the first harmonic, employing the stochastic resonance.

Alike the first harmonic S of the output signal, Eq. (9.5), the strength S_j of the higher harmonics is defined as the area under the j -th signal peak of the power spectrum $P(\omega)$, i.e., by Eq. (9.5) [or, equivalently, Eq. (9.6)] with ω_s replaced by $j \times \omega_s$. According to the general theory in [109], we expect the appearance of so called *noise-induced resonances* [47], which manifest themselves in a strong suppression of higher harmonics at certain values of the noise level and large signal periods t_s . More precisely, suppressions of the j -th harmonic should occur at zeros of the $(j + 1)$ -th cumulant[§] of the undriven process. In a two-state system, this is the case for $j = 2$ if the two (unmodulated) transition rates $W_{1,2}$ are equal, and for $j = 3$ if their ratio is given by $(\sqrt{3} + 1)/(\sqrt{3} - 1) \simeq 3.7$ (or its inverse) [109]. The case $j = 2$ can be understood by a symmetry argument due to which all even harmonics ($j = 2n$, $n \in \mathbb{N}$) are completely suppressed if the two transition rates are modulated symmetrically, i.e., $W_1(t) = W_2(t + t_s/2)$ [37]. (No such simple argument exists - to our knowledge - for $j = 3$.)

The above expectations are confirmed by Fig. 9.5: for the large modulation period $t_s = 1000$ s, the second and third harmonic of $\langle \sigma_z \rangle'$ and $\langle \sigma_y \rangle'$ (obtained from the asymptotic solution of the master equation) show noise-induced suppressions at those temperatures where the transition rates (see Fig. 8.3) fulfill the above conditions. Again, the effect is present both in the atomic population $\langle \sigma_z \rangle'$ (left column) and coherence $\langle \sigma_y \rangle'$ (right column), and the temperature dependence is in both cases very similar, as predicted by the two-state model.

Incoherent pumping

Finally, Fig. 9.6 shows the output signal power S and its harmonics S_2 and S_3 for incoherent pumping, with $|a|^2$ modulated according to Eq. (9.1). Only the z component of $\langle \vec{\sigma} \rangle'$ is plotted, since, in the case of incoherent pumping, no signal can be observed in the atomic coherences $\langle \sigma_{x,y} \rangle$ (see Fig. 8.1d). Because of the higher transition rates for incoherent pumping (compare chapter 8.2), the maximum of S is attained at a higher temperature ($T = 0.7$ K) than for coherent pumping ($T = 0.6$ K). Again, for large modulation periods, noise-induced suppressions of S_2 and S_3 occur at temperatures where the above-mentioned conditions for the transition rates are fulfilled (compare with Fig. 8.4). Due to the shift of the intersection between the two rates (compare Figs. 8.3 and 8.4), a suppression of S_3 occurs at only one temperature $T = 0.5$ K, where $W_2/W_1 \simeq 3.7$, for incoherent pumping (and the experimental parameters from Fig. 9.6), whereas two such resonances are observed for coherent pumping (Fig. 9.5), at $T = 0.32$ K, where $W_2/W_1 \simeq 3.7$, and at $T = 0.85$ K, where $W_2/W_1 \simeq 0.27$.

[§]The cumulants of a random process $x(t)$ are given in terms of the momenta $\langle x^n \rangle$ (where the bracket denotes an average over long times). Explicitly, the first four cumulants K_1, \dots, K_4 read as follows: $K_1 = \langle x \rangle$, $K_2 = \langle x^2 \rangle - \langle x \rangle^2$, $K_3 = \langle x^3 \rangle - 3\langle x^2 \rangle \langle x \rangle + 2\langle x \rangle^3$, and $K_4 = \langle x^4 \rangle - 4\langle x^3 \rangle \langle x \rangle - 3\langle x^2 \rangle^2 + 12\langle x^2 \rangle \langle x \rangle^2 - 6\langle x \rangle^4$.

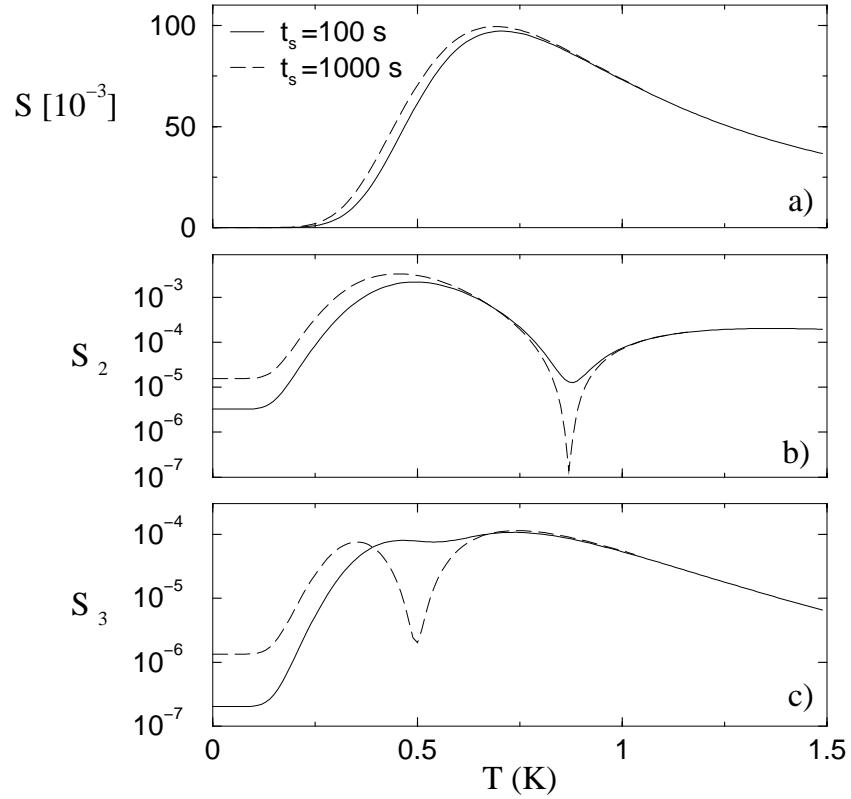


Figure 9.6: (a) Output signal power S of $\langle \sigma_z \rangle'$, (b) its second and (c) third harmonic, S_2 and S_3 , in response to a weak periodic modulation of $|a|^2$ (incoherent pumping) according to Eq. (9.1), with two different modulation periods $t_s = 100$ s (solid lines) and $t_s = 1000$ s (dashed lines). S exhibits a stochastic resonance maximum at $T = 0.7$ K. Noise-induced suppressions of the harmonics S_2 and S_3 are observed at $T = 0.87$ K and $T = 0.5$ K, respectively, in accordance with the general theory of [109]. Remaining parameters as in Figs. 9.4,9.5.

Part III

Entanglement of mixed two-qubit states

In both schemes of quantum state control discussed in the previous two parts of this thesis, entanglement between atoms and a single mode quantized electromagnetic field fundamentally affected - and even controlled - the time evolution of the atoms-field system. This is only one example of the important role entanglement plays in the dynamics of interacting quantum systems. Nevertheless, a satisfactory theoretical description of this phenomenon has not yet been achieved. To give an example, although several proposals for quantitative measures of entanglement are on the market, they do not always provide the same answer to the question which among two given states exhibits ‘more’ entanglement.

Therefore, in the last part of this thesis, we focus on entanglement, and present a new result on quantifying entanglement in the simplest possible case of two interacting two-level systems, commonly known as qubits, living on a four-dimensional Hilbert space. Whereas this result has no immediate connection to the results of part I and II, it conveys an idea of the intrinsic algebraic structures generating the dynamics of multipartite quantum systems, which we have already encountered.

To be specific, an interesting description of entanglement was recently achieved by defining the best separable approximation of a given mixed state. In the simplest case of a 2×2 dimensional quantum system, it consists of a decomposition of the state into a sum of a pure, entangled, and a mixed, separable one, with maximal weight of the latter. Here, we will formulate and prove necessary and sufficient conditions fulfilled by this optimal decomposition, which, in particular, allow its construction for an arbitrary given entangled state of full rank, in a purely algebraic way.

Before presenting our own results, however, let us warm up by briefly introducing some important concepts used for the characterization of mixed state entanglement.

10.1 Entanglement measures

Given a *pure* state of a bipartite quantum system living on a Hilbert space $\mathcal{H} = \mathcal{H}_A \otimes \mathcal{H}_B$, its entanglement $E(\Psi)$ can be uniquely quantified by the von-Neumann entropy of the reduced density matrix, as described in chapter 2.2.1. In particular, a pure state $|\Psi\rangle$ is not entangled if and only if it can be written as a product of two states of the subsystems A and B , respectively, i.e., $|\Psi\rangle = |\psi\rangle_A \otimes |\psi\rangle_B$.

Now, one might think that it should be easy to generalize this entanglement measure also to mixed states, making use of the fact that any mixed state ρ can be decomposed in terms of pure states:

$$\rho = \sum_i p_i |\Psi_i\rangle\langle\Psi_i|, \quad p_i \geq 0, \quad \sum_i p_i = 1. \quad (10.7)$$

According to Eq. (10.7), the state ρ can be interpreted as a mixture, where $|\Psi_i\rangle$ occurs with probability p_i . Hence, the entanglement of ρ should be the

corresponding average

$$E(\rho) = \sum_i p_i E(\Psi_i) \quad (10.8)$$

over the pure states. The problem is that the decomposition (10.7) of a given mixed state ρ is not unique. As an example, the state $\rho = \frac{1}{2}|00\rangle\langle 00| + \frac{1}{2}|11\rangle\langle 11|$, which is a mixture of the two *product* states $|00\rangle$ and $|11\rangle$, and therefore $E(\rho) = 0$, can also be written as $\rho = \frac{1}{2}|00 + 11\rangle\langle 00 + 11| + \frac{1}{2}|00 - 11\rangle\langle 00 - 11|$, i.e., as a mixture of two *maximally entangled* states $|00 + 11\rangle$ and $|00 - 11\rangle^*$, which yields $E(\rho) = 1$. [In this simple example, both decompositions consist of eigenvectors of ρ . Also for a non-degenerate ρ , however, the decomposition (10.7) is not unique, since the $|\Psi_i\rangle$'s need in general not be eigenvectors of ρ , i.e., they need not be orthogonal.] In order to obtain a well-defined measure of entanglement, we can look for the *optimal* decomposition of ρ , which yields the smallest average entanglement (10.8). The latter is known as *entanglement of formation* E_F [111]. Apart from this rather abstract definition, E_F can also be interpreted in a more intuitive way: it is closely connected to the maximal number N of qubit pairs in the given state ρ , which can be produced by *local* operations (possibly with classical communication between the two parties[†]), if the two parties A and B initially share a given number M of maximally entangled qubit pairs (and the remaining $N - M$ qubit pairs are initially in a product state).[‡] Furthermore, it has been shown that E_F is a ‘good’ measure of entanglement, i.e., it is invariant under unitary local operations $U \otimes V$, and non-increasing under arbitrary local operations,[†] which are obvious requirements that any measure of entanglement should fulfill [112]. In particular, $E_F(\rho) = 0$ if and only if ρ can be expressed as a mixture of product states:

$$\rho = \sum_i p_i \rho_i^A \otimes \rho_i^B, \quad p_i \geq 0, \quad \sum_i p_i = 1, \quad (10.9)$$

where ρ_i^A, ρ_i^B are legitimate (i.e., hermitian and positive definite) density matrices of the subsystems. Such states ρ are called *separable* [114]. They exhibit only classical correlations between A and B , since, starting from a product state $|\psi\rangle_A \otimes |\psi\rangle_B$ (which does not contain any correlation), they can be generated

*Here, the states $|00 \pm 11\rangle$ are defined to be correctly normalized, i.e. $|00 \pm 11\rangle := (|00\rangle \pm |11\rangle)/\sqrt{2}$.

[†] By ‘local operation’, we mean a quantum operation acting on the two parties A and B separately, but possibly exhibiting classical correlations. Any such operation may be written as follows [112]:

$$\rho \rightarrow \sum_i A_i \otimes B_i \rho A_i^\dagger \otimes B_i^\dagger,$$

where $\sum_i A_i^\dagger A_i \otimes B_i^\dagger B_i = \mathbb{1}$.

[‡]More precisely, the asymptotic ratio M/N (in the limit $M, N \rightarrow \infty$) is given by [113]

$$E'_F := \lim_{n \rightarrow \infty} \frac{1}{n} E_F(\underbrace{\rho \otimes \dots \otimes \rho}_{n \text{ copies}}).$$

(It is commonly believed, but not yet proved, that $E'_F = E_F$, i.e., E_F fulfills the property of additivity).

by a local operation, which transforms $|\psi\rangle_A$ into ρ_i^A and $|\psi\rangle_B$ into ρ_i^B with probability p_i . (Here, both parties A and B have to use the *same* randomly chosen i . This obviously requires communication between the two parties, what in general leads to correlations.)

Note that, in the general case of a $M_1 \times M_2$ dimensional quantum system, there is no general prescription how to find out whether a given ρ is separable or not. As observed in [115], however, a simple *necessary condition* for the separability of ρ is that its *partial transpose*, defined as

$$\rho^{\tau_B} := \sum_i p_i \rho_i^A \otimes (\rho_i^B)^\tau, \quad (10.10)$$

is positive definite, i.e., is also a legitimate density matrix for the composite system. [Here, we define the operation of partial transposition by Eq. (10.10) also in the case of an arbitrary, not necessarily separable state, when ρ_i^A and ρ_i^B do not need to be positive or/and the p_i are not all positive - such a decomposition obviously exists for an arbitrary ρ]. Therefore, any state ρ with negative partial transpose has to be entangled. Note, however, that there exist also entangled states with positive partial transpose [116].

Only for low dimensional (2×2 and 2×3) systems, the above condition is also sufficient [116]. Therefore, we can easily check whether a two-qubit state ρ is separable or not, by simply calculating the smallest eigenvalue of its partial transpose. In fact, for two qubits, also the degree of entanglement, as quantified by the entanglement of formation, can be determined analytically. For this purpose, the *concurrence* $c(\rho)$ was introduced in [117], defined as

$$c(\rho) = \max\{0, c_1 - c_2 - c_3 - c_4\}, \quad (10.11)$$

where $c_1 \geq c_2 \geq c_3 \geq c_4$ are the square roots of the (real and positive) eigenvalues of the matrix

$$X := \Sigma \rho^* \Sigma \rho, \quad \Sigma = \sigma_2 \otimes \sigma_2, \quad \sigma_2 := \begin{bmatrix} 0 & -i \\ i & 0 \end{bmatrix}, \quad (10.12)$$

and ρ^* denotes the complex conjugation of ρ . The entanglement of formation of ρ is then given by [117]

$$E_F(\rho) = h\left(\frac{1 + \sqrt{1 - c^2(\rho)}}{2}\right); \quad (10.13)$$

$$h(x) = -x \log_2 x - (1 - x) \log_2 (1 - x). \quad (10.14)$$

Note that E_F is a strictly monotonous function of $c(\rho)$ (compare footnote § on p. 16), which maps the interval $[0, 1]$ onto $[0, 1]$. Hence, the concurrence $c(\rho)$ is also a good measure of entanglement.

Now, is the problem of quantifying two-qubit entanglement solved by Eqs. (10.11-10.14)? This is not the case: there exist also other good measures of entanglement, which are - unlike the concurrence - not equivalent to the entanglement of formation, in the sense that they give a different ordering of mixed

states with respect to their amount of entanglement. A simple example is the *negativity* of $E_N(\rho)$ [118],

$$E_N(\rho) = 2 |\min\{0, \lambda_1^{\tau B}, \lambda_2^{\tau B}, \lambda_3^{\tau B}, \lambda_4^{\tau B}\}|, \quad (10.15)$$

where $\lambda_i^{\tau B}$ are the eigenvalues of the partial transpose $\rho^{\tau B}$. The non-equivalence of E_F and E_N was demonstrated in [119, 120]. This shows that - even in the simplest case of two qubits - the properties of entanglement are not yet completely understood.[§]

10.2 Optimal Lewenstein-Sanpera decomposition

A better insight into the properties of an entangled state ρ may possibly be obtained by studying particular decompositions of ρ . For example, as described above, the entanglement of formation is given by a decomposition into pure states, which minimizes the average entanglement over the pure states, see Eq. (10.8). Another way of decomposing a mixed quantum state ρ in a way which is determined by its entanglement properties was recently introduced in [122]. Here, the authors considered decompositions of ρ into a sum of an entangled and a separable state, i.e., $\rho = (1-\lambda)\rho_e + \lambda\rho_s$. The decomposition with the largest weight λ of the separable part is the *optimal Lewenstein-Sanpera decomposition*, which they proved to be uniquely determined. According to its definition, all the non-separability properties of ρ are concentrated in the entangled part ρ_e , whose weight is as small as possible. The separable part of this decomposition is called the *best separable approximation* (BSA) of ρ ,[¶] and its weight λ the *separability*. Furthermore, in the case of a two-qubit state, which we will restrict to in the following, it can be shown [122] that the entangled part ρ_e of the optimal Lewenstein-Sanpera decomposition is always a pure state,^{||} i.e.,

$$\rho = (1-\lambda)|\psi\rangle\langle\psi| + \lambda\rho_s. \quad (10.16)$$

We will call any such decomposition of ρ as a sum of a *pure* entangled and a mixed separable state, a Lewenstein-Sanpera decomposition (LSD). For a given ρ , there exists in general a continuum of different LSD's [123], one of them (with the largest λ) the optimal LSD.

Now, how can we find the optimal LSD for a given ρ ? At first sight, this might not appear to be a very difficult task, since the decomposition is already

[§]For higher-dimensional quantum systems, additional difficulties arise, which have to do with the existence of entangled states with positive partial transpose, and with the phenomenon of 'bound entanglement'[121], i.e., non-separable states which can not be transformed by local operations into a maximally entangled state.

[¶]Note, however, that ρ_s does in general *not* minimize the distance of ρ to the set of separable states, as quantified, e.g., by the Hilbert-Schmidt metric, or other measures, compare the footnote * on p. 26.

^{||}This is due to the fact that any two-dimensional subspace of a 2×2 system, and hence also the range of a non-pure state ρ_e , contains a product vector $|e, f\rangle$. Then, a small amount $\epsilon|e, f\rangle\langle e, f|$ of this vector can be subtracted from ρ_e (with ϵ small enough, such that ρ_e remains positive) and added to ρ_s (which remains separable, since $|e, f\rangle$ is a product state), thereby obtaining a new decomposition with larger weight of the separable part.

determined by a single state vector $|\psi\rangle$, and one real parameter λ . Nevertheless, only a numerical method for constructing the optimal LSD in 2×2 systems was proposed in the original paper [122], and some analytical results for special cases were found in [123]. Here, we show how to find the optimal LSD of an arbitrary 2×2 state ρ in a purely algebraic way, without employing any maximization or optimization procedure. As a byproduct, we prove that, in the case that the BSA ρ_s of ρ is of rank 4, the weight $1 - \lambda$ of the pure state in the optimal LSD equals the concurrence of ρ , see Eq. (10.11). Furthermore, the pure part is maximally entangled in this case (the last fact was proven by other means in [124]).

The situation is more complicated if the BSA ρ_s is not of full rank. As we will see, for $\text{rank}(\rho) = 4$ but $\text{rank}(\rho_s) < 4$, the components of the BSA are determined by a set of two nonlinear equations which can be solved numerically. In this case, there is no simple relation between the concurrence of the state and the weight of the entangled part, as we were able to prove for $\text{rank}(\rho_s) = 4$.

We will now formulate the main results of this chapter, which are summarized by the following two Theorems.

Theorem 1.

Let ρ be an entangled state with $\text{rank}(\rho) = 4$. Then, $\rho = (1 - \lambda)|\psi\rangle\langle\psi| + \lambda\rho_s$ is the optimal Lewenstein-Sanpera decomposition if and only if:

$\text{rank}(\rho_s^{\tau_B}) = 3$, i.e., $\exists_{|\phi\rangle} \rho_s^{\tau_B}|\phi\rangle = 0$, and either

(i) $\text{rank}(\rho_s) = 4$, and $\exists_{\alpha>0} |\phi\rangle\langle\phi|^{\tau_B}|\psi\rangle = -\alpha|\psi\rangle$, or

(ii) $\text{rank}(\rho_s) = 3$, i.e., $\exists_{|\tilde{\phi}\rangle} \rho_s|\tilde{\phi}\rangle = 0$, and

$$\exists_{\alpha,\nu\geq 0} [\nu|\tilde{\phi}\rangle\langle\tilde{\phi}| + |\phi\rangle\langle\phi|^{\tau_B}]|\psi\rangle = -\alpha|\psi\rangle.$$

According to Lemma 2 of appendix D, $|\psi\rangle$ is maximally entangled in case (i).**

The first condition, which demands that the partial transpose of the BSA ρ_s be of rank 3, simply states that ρ_s lies on the boundary between the set of separable and the set of entangled states (which have a negative partial transpose, see chapter 10.1), i.e., ρ_s is a ‘barely separable state’ [125]. The two conditions (i) and (ii) describe the relation between the entangled and the separable part of the optimal decomposition. Remarkably, the only relevant properties of ρ_s are the vectors $|\phi\rangle$, and possibly $|\tilde{\phi}\rangle$, in the kernels of $\rho_s^{\tau_B}$ and ρ_s .

Theorem 1 allows us to check immediately whether a given decomposition of ρ is the optimal one. Reversely, it also simplifies the construction of the BSA for a given ρ . Indeed, case (i), i.e., any BSA with rank 4, can be solved explicitly, according to the following

**We believe that also in case (ii), the pure state $|\psi\rangle$ may be maximally entangled, but have not yet found an explicit example.

Theorem 2.

If the BSA ρ_s of ρ has full rank [i.e., in the case (i) of Theorem 1], the vector $|\phi\rangle$ in the (one-dimensional, see Theorem 1) kernel of $\rho_s^{\tau B}$ is an eigenvector of

$$Y = \Sigma \rho^{\tau A} \Sigma \rho^{\tau B}, \quad (10.17)$$

belonging to the smallest eigenvalue γ of Y . The weight $1 - \lambda$ of the entangled part in the optimal decomposition is given by $1 - \lambda = 2\sqrt{\gamma} = c(\rho)$, where $c(\rho)$ is the concurrence of ρ .

The above Theorem 2 allows us to check whether a given ρ has a BSA ρ_s of full rank, i.e., whether it fulfills the first case (i) of Theorem 1. In this case, the optimal LSD is given analytically through Theorem 2 and Theorem 1(i) (see the ‘recipe for constructing the optimal LSD’ below). As a general rule of thumb, we have found that the BSA ρ_s is of rank 4, if ρ is close to a separable state (i.e., if its separability λ is large), whereas $\text{rank}(\rho_s) < 4$ if ρ is close to a non-maximally entangled pure state.

Recipe for constructing the optimal Lewenstein-Sanpera decomposition

Before we present the proofs of Theorem 1 and 2 in chapters 10.4 and 10.5, we want to demonstrate how to use the above results in order to construct the BSA for a given entangled ρ of rank 4:

- First, calculate the smallest eigenvalue γ and the corresponding eigenvector $|\phi\rangle$ of the 4×4 matrix Y , given by Eq. (10.17). (The eigenvalue γ is not degenerate, see Lemma 7 in appendix D.)
- Then, calculate $\rho_s = \rho/\lambda - (1 - \lambda)|\psi\rangle\langle\psi|/\lambda$, according to Eq. (10.16), where $\lambda = 1 - 2\sqrt{\gamma}$ is obtained from Theorem 2, and $|\psi\rangle$ from Theorem 1(i), as the eigenvector of $|\phi\rangle\langle\phi|^{\tau B}$ with negative eigenvalue.
 - If ρ_s is positive and separable, it is the BSA, according to Theorem 1(i). (It is not necessary to check $\rho_s^{\tau B}|\phi\rangle = 0$, since this follows from the construction of $|\phi\rangle$, see Lemma 7 and Lemmata 3-5, appendix D)
 - If not, this proves that the first case (i) of Theorem 1 is not fulfilled. Consequently, the BSA has rank 3, and we obtain the following set of equations from Theorem 1(ii):

$$\left[\rho|\tilde{\phi}\rangle\langle\tilde{\phi}|\rho \right]^{\tau B} |\phi\rangle = \langle\tilde{\phi}|\rho|\tilde{\phi}\rangle \rho^{\tau B} |\phi\rangle, \quad (10.18)$$

$$\nu'|\tilde{\phi}\rangle + |\phi\rangle\langle\phi|^{\tau B}\rho|\tilde{\phi}\rangle = -\alpha \rho|\tilde{\phi}\rangle. \quad (10.19)$$

Here, we used $|\psi\rangle = \rho|\tilde{\phi}\rangle$, and $(1 - \lambda)^{-1} = \langle\tilde{\phi}|\rho|\tilde{\phi}\rangle$, see Eqs. (10.38) and (10.39) below, and defined $\nu' = \nu\langle\tilde{\phi}|\rho|\tilde{\phi}\rangle$. These equations have to be solved numerically for $|\tilde{\phi}\rangle$, $|\phi\rangle$, α , and ν' . Possibly, there exist several solutions, but only one (due to the uniqueness of the optimal

LSD) with $\alpha, \nu' \geq 0$ and yielding a positive and separable state ρ_s via Eq. (10.16). This solution gives the optimal LSD, according to Theorem 1(ii).

Thereby, we have found the optimal Lewenstein-Sanpera decomposition of ρ in a purely algebraic way, without employing any maximization or optimization procedure.

However, we have only decomposed states of full rank, so far. Can we also use the above method to find the optimal LSD for states of lower rank? [Here, $\text{rank}(\rho) = 3$ is of particular interest, since $\text{rank}(\rho) = 2$ has already been solved analytically [123].] First, we note that any state ρ of lower rank can be obtained as a limit from the full-rank case. To demonstrate this explicitly, we define $\rho_\epsilon := (1 - \epsilon)\rho + \epsilon\mathbb{1}/4$ (where $\mathbb{1}$ is the 4×4 identity operator). Obviously, $\text{rank}(\rho_\epsilon) = 4$, for $\epsilon > 0$, and $\rho = \lim_{\epsilon \rightarrow 0} \rho_\epsilon$. Since the optimal decomposition of ρ_ϵ varies continuously with ϵ (this follows from the uniqueness of the optimal LSD), we obtain the optimal LSD of ρ in the limit $\epsilon \rightarrow 0$. Hence, it should be possible to generalize Theorem 1 to the case of lower rank. If we consider the second condition (ii) of Theorem 1, however, we cannot exclude the possibility that the parameter ν goes to infinity in the limit $\epsilon \rightarrow 0$. (This might even be the generic behavior in this case.) Then, the condition (ii) would reduce to $\langle \tilde{\phi} | \psi \rangle = 0$ (implying that $|\tilde{\phi}\rangle$ is in the kernel of ρ), what does not help us to find the optimal LSD of ρ directly, without using the limiting procedure described above. Therefore, although the lower-rank case may be treated numerically as a limit of the full-rank case, an analytic solution would still be desirable, also in order to understand the behavior of the optimal LSD for states of rank 4 which are close to states of lower rank (in particular, to answer the question if ν remains bounded or not).

10.3 Does the optimal LSD yield a measure of entanglement?

Furthermore, Theorem 2 provides a connection between the BSA and the concurrence of ρ , which was originally [126] introduced as an auxiliary quantity in order to calculate the entanglement of formation E_F [111]. Apart from the explicit formula (10.11), the concurrence of a mixed state is defined (similarly to E_F) as the minimum of the average concurrence $\langle c \rangle = \sum_i p_i c(\psi_i)$ over all decompositions $\rho = \sum_i p_i |\psi_i\rangle\langle\psi_i|$ of ρ into pure states. After decomposing ρ_s into product states, also the optimal LSD, Eq. (10.16), defines a particular decomposition, and it follows that

$$c(\rho) \leq (1 - \lambda) c(\psi). \quad (10.20)$$

Since $c(\psi) \leq 1$, this inequality implies $c(\rho) + \lambda \leq 1$, which has already been conjectured in [125]. According to Theorem 2, equality in Eq. (10.20) holds if the BSA of ρ has full rank [in this case, $c(\rho) = 1 - \lambda$ and $c(\psi) = 1$]. In other words: the decomposition (10.16) is also optimal in the sense that it minimizes the average concurrence.

One might assume that this is true in general, i.e., also in the second case (ii) of Theorem 1, where the BSA ρ_s is not of full rank. Indeed, there exist examples where the inequality (10.20) is saturated also in this case, e.g., the generalized Werner states $\rho = x|\phi\rangle\langle\phi| + (1-x)\mathbb{1}/4$, with $|\phi\rangle$ not maximally entangled. (The optimal decomposition of these states is given in [123].) In general, however, we have found that the equality in (10.20) does *not* always hold. Nevertheless, we believe that the right-hand side of (10.20), i.e.,

$$E_{LS}(\rho) := (1-\lambda)c(\psi) \quad (10.21)$$

is also a good measure of entanglement.

In order to establish the quantity E_{LS} , Eq. (10.21), which is obtained from the optimal LSD, as a good measure of entanglement, we have to show the following [112]:

- (i) it vanishes if and only if ρ is separable,
- (ii) it is invariant under local unitary operations, and
- (iii) its expectation value is non-increasing under general local operations.

The first two conditions are obviously fulfilled. In order to verify the third one, let us consider an arbitrary local operation, see footnote [†] on p. 126, which transforms $\rho = (1-\lambda)|\psi\rangle\langle\psi| + \lambda\rho_s$ (optimal LSD) into $\rho_i = A_i \otimes B_i \rho A_i^\dagger \otimes B_i^\dagger / p_i$, with probability p_i . Then, we have the following LSD

$$\rho_i = (1-\lambda)|\psi_i\rangle\langle\psi_i|/p_i + \lambda\rho_{s_i}/p_i, \quad (10.22)$$

of ρ_i , with $|\psi_i\rangle = A_i \otimes B_i |\psi\rangle$, and $\rho_{s_i} = A_i \otimes B_i \rho_s A_i^\dagger \otimes B_i^\dagger$.

- First, let us assume that (10.22) is the optimal LSD of ρ_i . Then, according to Eq. (10.21), $E_{LS}(\rho_i) = (1-\lambda)|\psi_i|c(\psi_i)/p_i$ (where $|\psi_i| = \langle\psi_i|\psi_i\rangle$ is the norm of $|\psi_i\rangle$), and the expectation value of E_{LS} equals

$$\langle E_{LS} \rangle = \sum_i p_i E_{LS}(\rho_i) = (1-\lambda) \sum_i c(\psi_i)|\psi_i|, \quad (10.23)$$

which is not larger than $E_{LS}(\rho) = (1-\lambda)c(\psi)$, since the concurrence is a good entanglement measure [and hence its expectation value $\sum_i c(\psi_i)|\psi_i|$ is not larger than $c(\psi)$].

- However, what happens if (10.22) is not the optimal LSD? Then, we have to show that $(1-\lambda)|\psi_i|c(\psi_i)/p_i \geq E_{LS}(\rho_i)$. Note that, if the BSA of ρ_i is of rank 4, i.e., Theorem 1(i), then $E_{LS}(\rho_i) = c(\rho_i)$, and $(1-\lambda)|\psi_i|c(\psi_i)/p_i \geq E_{LS}(\rho_i)$ follows by the same argument as Eq. (10.20). It remains to be shown that the same is also true in the case $\text{rank}(\rho_i) = 3$. For this purpose, it would be sufficient to prove that, among all possible LSD's of ρ , not only the quantity $1-\lambda$ is minimal in the optimal LSD (according to its definition), but also $(1-\lambda)c(\psi)$. So far, we have not yet completed the proof of this conjecture.

Therefore, we cannot say with certainty that E_{LS} is non-increasing under local transformation, as it is required by a good measure of entanglement. Note that, if this were the case, then $c(\rho)$ and E_{LS} provide two non-equivalent measures of entanglement, i.e., there exists a pair of states such that the two measures would give contradictory results concerning the question which state exhibits more entanglement.^{††} Presently, we do not have a simple explanation or interpretation of this fact, which deserves further investigations.

10.4 Proof of Theorem 1

Let Eq. (10.16) be the optimal LSD of the entangled state ρ . The idea of the following proof is to examine an infinitesimal neighborhood of the optimal decomposition. For this purpose, we note that the maximality condition for λ and the uniqueness of the BSA [122] imply [123]:

- (a) the state $\rho_s + \epsilon|\psi\rangle\langle\psi|$ is non-separable for $\epsilon > 0$, and
- (b) the state $\rho - (1 - \lambda)|\psi'\rangle\langle\psi'|$ is either non-separable or non-positive for each $|\psi'\rangle \neq |\psi\rangle$.

In order to simplify the notation, we define $\mu = 1 - \lambda$.

According to the Peres-Horodecki criterion of separability [115, 116] (that the separable states are those with non-negative partial transpose, see chapter 10.1), condition (a) implies:

$$\forall \epsilon > 0 \exists |\phi_\epsilon\rangle \langle\phi_\epsilon| \rho_s^{\tau B} + \epsilon|\psi\rangle\langle\psi|^{\tau B} |\phi_\epsilon\rangle < 0. \quad (10.24)$$

On the other hand, since ρ_s is separable, the same criterion establishes the positivity of $\rho_s^{\tau B}$. Thus, from (10.24) and the continuity argument, there is such ϕ that

$$\rho_s^{\tau B} |\phi\rangle = 0. \quad (10.25)$$

Since we assumed $\text{rank}(\rho) = 4$ and the rank of a projection is one, the rank of ρ_s must be at least three. Then $\text{rank}(\rho_s^{\tau B}) = 3$, as a consequence of Lemma 1, appendix D. Thereby, we have shown that the BSA ρ_s is barely separable (which has already been found in [125]).

Now we exploit condition (b). Let us consider a different decomposition of ρ , where the pure part slightly differs from the one of the optimal LSD, Eq. (10.16):

$$\rho = \mu |\psi'\rangle\langle\psi'| + \lambda \rho'_s, \quad (10.26)$$

with

$$|\psi'\rangle = \frac{|\psi\rangle + \epsilon |\Delta\psi\rangle}{\sqrt{1 + \epsilon^2}}, \quad (10.27)$$

^{††}This follows from the fact that, for each value of the concurrence c , we can find a state ρ where the equality in Eq. (10.20) is fulfilled [namely any state ρ with BSA of rank 4, and $1 - \lambda = c$; the construction of such a state is possible according to Theorem 1(i)], whereas, as stated above, there are also some cases where the equality is not fulfilled.

where $\langle \Delta\psi | \Delta\psi \rangle = 1$ and $\langle \psi | \Delta\psi \rangle = 0$. (Obviously, any pure state can be written in this form.) Since the optimal LSD is unique, the state ρ'_s defined by Eq. (10.26) cannot be positive *and* separable (for $\epsilon \neq 0$).

In the following, we will consider $|\psi'\rangle$ to be infinitesimally close to $|\psi\rangle$, and therefore expand ρ'_s to the first two orders in ϵ :

$$\lambda\rho'_s = \lambda\rho_s - \mu (\epsilon |\psi\rangle \langle \Delta\psi| + \epsilon |\Delta\psi\rangle \langle \psi| + \epsilon^2 |\Delta\psi\rangle \langle \Delta\psi| - \epsilon^2 |\psi\rangle \langle \psi|). \quad (10.28)$$

In fact, at first we will only need the first order in ϵ . (The second order terms will be relevant later, when proving the second case and the reverse direction of Theorem 1.)

Next, we consider separately two cases of different ranks of ρ_s , which will lead us to the two cases (i) and (ii) of Theorem 1.

(i) First case: $\text{rank}(\rho_s) = 4$

Then, for ϵ sufficiently small, ρ'_s is positive definite for each $|\Delta\psi\rangle$. According to the optimality condition (b) above, ρ'_s must be non-separable, i.e., there exists $|\phi'\rangle$ such that $\langle \phi' | \rho_s'^{TB} | \phi' \rangle < 0$.

Since $\rho_s'^{TB}$ has rank 3, $|\phi'\rangle$ has to be close to $|\phi\rangle$, i.e.,

$$|\phi'\rangle = |\phi\rangle + |\Delta\phi\rangle, \quad (10.29)$$

with $|\Delta\phi\rangle \rightarrow 0$ if $\epsilon \rightarrow 0$. Now from (10.25) we obtain, at first order in ϵ :

$$\langle \Delta\phi | \lambda\rho_s'^{TB} | \Delta\phi \rangle - \mu\epsilon \langle \phi | [|\psi\rangle \langle \Delta\psi| + |\Delta\psi\rangle \langle \psi|]^{TB} | \phi \rangle \leq 0. \quad (10.30)$$

But ρ_s is, by assumption, separable - consequently $\rho_s'^{TB}$ is positive definite

$$\langle \Delta\phi | \lambda\rho_s'^{TB} | \Delta\phi \rangle \geq 0, \quad (10.31)$$

and (10.30) implies

$$\langle \phi | [|\psi\rangle \langle \Delta\psi| + |\Delta\psi\rangle \langle \psi|]^{TB} | \phi \rangle \geq 0, \quad (10.32)$$

which can be equivalently written as

$$\text{Tr} \left\{ \left[|\psi\rangle \langle \Delta\psi| + |\Delta\psi\rangle \langle \psi| \right]^{TB} | \phi \rangle \langle \phi| \right\} \geq 0. \quad (10.33)$$

For arbitrary operators A and B , we have $\text{Tr} A^{TB} B = \text{Tr} A B^{TB}$, thus, from (10.33), we obtain

$$\text{Tr} \left\{ \left[|\psi\rangle \langle \Delta\psi| + |\Delta\psi\rangle \langle \psi| \right] | \phi \rangle \langle \phi|^{TB} \right\} \geq 0. \quad (10.34)$$

This, however, is equivalent to

$$\langle \Delta\psi | | \phi \rangle \langle \phi|^{TB} | \psi \rangle + \langle \psi | | \phi \rangle \langle \phi|^{TB} | \Delta\psi \rangle \geq 0. \quad (10.35)$$

Since (10.35) is linear in $|\Delta\psi\rangle$, changing $|\Delta\psi\rangle$ into $-|\Delta\psi\rangle$ reverses the inequality, hence in fact it must be that

$$\langle \Delta\psi | | \phi \rangle \langle \phi|^{TB} | \psi \rangle = 0. \quad (10.36)$$

The above equality must be fulfilled by all $|\Delta\psi\rangle \perp |\psi\rangle$. This is possible only if $|\psi\rangle$ is an eigenvector of $A = |\phi\rangle\langle\phi|^{\tau_B}$.^{*} To arrive at the first case (i) of Theorem 1, it remains to be shown that the sign of the corresponding eigenvalue α is negative. This, however, follows from the limit $\epsilon \rightarrow 0$ of Eq. (10.24),

$$\langle\phi| |\psi\rangle\langle\psi|^{\tau_B} |\phi\rangle \leq 0, \quad (10.37)$$

after using again the identity $\text{Tr}A^{\tau_B}B = \text{Tr}AB^{\tau_B}$. Furthermore, α cannot be zero - otherwise (according to Lemma 2, appendix D), $|\phi\rangle$ would be a separable, i.e., a product state: $|\phi\rangle = |e, f\rangle$, and since $\rho_s^{\tau_B}|e, f\rangle = 0$, see (10.25), we have $\rho_s|e, f^*\rangle = 0$, cf. Eq. (D.3), which contradicts the assumption $\text{rank}(\rho_s) = 4$. From Lemma 2, appendix D, we infer that $|\psi\rangle$ is maximally entangled. This provides an alternative proof of the fact (proved in [124]) that, if ρ and ρ_s are of maximal rank, then $|\psi\rangle$ in (10.16) is maximally entangled.

(ii) Second case: $\text{rank}(\rho_s) < 4$

We assumed that ρ has rank 4, so $\text{rank}(\rho_s) = 3$ (since ρ_s is obtained from ρ by subtracting a state of rank 1). From Lemma 1 in [122], we know that, if we subtract $(1 - \lambda)|\psi\rangle\langle\psi|$ from ρ [which gives ρ_s , see Eq. (10.16)], we obtain a non-negative operator of rank 3 if and only if

$$1 - \lambda = \frac{1}{\langle\psi|\rho^{-1}|\psi\rangle}. \quad (10.38)$$

Furthermore, it is easy to check that the kernel of ρ_s is given by

$$|\tilde{\phi}\rangle = \rho^{-1}|\psi\rangle, \quad (10.39)$$

i.e., $\rho_s|\tilde{\phi}\rangle = 0$. Since $\text{rank}(\rho_s) = 3$, the separable part ρ'_s , Eq. (10.28), of the infinitesimally changed decomposition (10.26) is positive definite if

$$\langle\tilde{\phi}| (\epsilon|\psi\rangle\langle\Delta\psi| + \epsilon|\Delta\psi\rangle\langle\psi| + \epsilon^2|\Delta\psi\rangle\langle\Delta\psi| - \epsilon^2|\psi\rangle\langle\psi|) |\tilde{\phi}\rangle < 0. \quad (10.40)$$

– Obviously, this condition is fulfilled if $|\Delta\psi\rangle \perp |\tilde{\phi}\rangle$. [$\langle\psi|\tilde{\phi}\rangle \neq 0$ follows from Eq. (10.38).] Hence, as in case (i), all such $|\Delta\psi\rangle$ must fulfill Eq. (10.36). This is equivalent to

$$(1 - |\psi\rangle\langle\psi| - |\tilde{\psi}\rangle\langle\tilde{\psi}|) |\phi\rangle\langle\phi|^{\tau_B} |\psi\rangle = 0, \quad (10.41)$$

where $|\tilde{\psi}\rangle$ is defined such that $|\tilde{\psi}\rangle \perp |\psi\rangle$, and $|\tilde{\psi}\rangle$ and $|\psi\rangle$ span the same two-dimensional subspace as $|\tilde{\phi}\rangle$ and $|\psi\rangle$. (We assume that $\psi \neq \tilde{\phi}$; otherwise, ρ'_s is positive for *all* $|\Delta\psi\rangle$, and we get the same result as in the first case, which, below, will turn out to be a special case of the result in the second case.)

^{*}Note that, although τ_B and $|\phi\rangle$ depend on the local basis of \mathcal{H}_B , the operator A is basis-independent, i.e., transforms in the usual way, Eq. (D.1), under local unitary transformations.

- But what happens if $|\Delta\psi\rangle = |\tilde{\psi}\rangle$? Then, it is always possible to multiply $|\Delta\psi\rangle$ by a phase factor such that ρ'_s is positive, see Eq. (10.40), at first order in ϵ . This leads us, as in case (i), to Eq. (10.35). It follows that

$$-\nu \langle \tilde{\psi} | \tilde{\phi} \rangle \langle \tilde{\phi} | \psi \rangle = \langle \tilde{\psi} | |\phi\rangle \langle \phi|^{\tau_B} | \psi \rangle, \quad (10.42)$$

with a non-negative, real parameter ν . Otherwise, $|\Delta\psi\rangle$ could be multiplied by a phase factor such that Eq. (10.40) is fulfilled and Eq. (10.35) not. [Note that $\langle \tilde{\psi} | \tilde{\phi} \rangle \langle \tilde{\phi} | \psi \rangle \neq 0$, since $\langle \psi | \tilde{\phi} \rangle \neq 0$ follows from Eq. (10.38), and $\langle \tilde{\psi} | \tilde{\phi} \rangle \neq 0$ from the construction of $\tilde{\psi}$.]

The two conditions Eqs. (10.42,10.41) are equivalent to the following condition: $|\psi\rangle$ is an eigenvector of the operator

$$A = \nu |\tilde{\phi}\rangle \langle \tilde{\phi}| + |\phi\rangle \langle \phi|^{\tau_B}. \quad (10.43)$$

To complete the first part of the proof of Theorem 1, we will now show that the corresponding eigenvalue α cannot be positive.

As a consequence of Lemma 2, appendix D, A has at least three non-negative eigenvalues. However, there is also at least one non-positive eigenvalue. This follows from the existence of a product vector $|e, f\rangle$ in the range of ρ_s such that $|e, f^*\rangle$ is in the range of $\rho_s^{\tau_B}$, as shown in [124], which implies $\langle e, f | A | e, f \rangle = 0$, cf. Eq. (D.3). Furthermore, A cannot have more than one zero eigenvalue: otherwise, $|\phi\rangle$ would have to be a product vector (see Lemma 2, appendix D), and $|\tilde{\phi}\rangle$ would be the corresponding partially transposed product vector. Hence, $|\tilde{\phi}\rangle \langle \tilde{\phi}|$ and $|\phi\rangle \langle \phi|^{\tau_B}$ would be identical and proportional to A , and $|\psi\rangle$, as an *entangled* eigenvector of A , would have to be perpendicular to $|\tilde{\phi}\rangle$, i.e., $\text{rank}(\rho) = 3$, which contradicts the assumption $\text{rank}(\rho) = 4$.

The above considerations about the spectrum of A are useful for the following reason: let us assume that there exists an entangled state ρ' with $\alpha' < 0$, which has the property that $\rho(x) = x\rho + (1-x)\rho'$ is entangled for all $x \in [0, 1]$. (ρ' may be a state with BSA of rank 4, for which we have already shown above that $\alpha' < 0$.) Now, the optimal decomposition (10.16) - in particular the eigenvalue $\alpha(x)$ - changes smoothly when varying x from 0 to 1 (this follows from the uniqueness of the optimal decomposition). Since, as shown above, A (having one non-positive and three non-negative eigenvalues) cannot have two zero eigenvalues, a crossing of eigenvalues at zero is not possible, and $\alpha = \alpha(1) \leq 0$ follows from $\alpha' = \alpha(0) < 0$.

It remains to be shown that a state ρ' with the above properties exists. For this purpose, we consider the Werner states $\rho' = y|\psi'\rangle \langle \psi'| + \frac{1-y}{4}\mathbb{1}$, with maximally entangled $|\psi'\rangle$. For these states, it has been shown in [123] that the pure state in the optimal decomposition equals $|\psi'\rangle$ and $\lambda' = 3(1-y)/2$. It follows that $\text{rank}(\rho'_s) = 4$, and $\alpha' < 0$, as shown above (first case). Now, we choose $|\psi'\rangle$ as the eigenvector of $|\chi\rangle \langle \chi|^{\tau_B}$ with negative eigenvalue (such an eigenvalue exists according to Lemma 2, appendix D),

where $|\chi\rangle$ is an entangled pure state with $\langle\chi|\rho^{\tau_B}|\chi\rangle < 0$ (exists, since ρ is entangled). Using $\langle\psi'|\chi\rangle\langle\chi|^{\tau_B}|\psi'\rangle = \langle\chi|\psi'\rangle\langle\psi'|^{\tau_B}|\chi\rangle$, it follows that $\langle\chi|(\rho')^{\tau_B}|\chi\rangle < 0$ for large enough y , hence also $\langle\chi|\rho(x)^{\tau_B}|\chi\rangle < 0$ for $x \in [0, 1]$, i.e. $\rho(x)$ is entangled for all $x \in [0, 1]$.

Finally, we will prove the reverse direction of Theorem 1, i.e., that both cases (i) and (ii) are also *sufficient* for the optimality of the decomposition (10.16). For this purpose, let us assume that there exists another decomposition with larger λ . Then, because of the convexity of the set of separable states, such a decomposition with larger λ also exists in the infinitesimal neighborhood of $\{\lambda, |\psi\rangle\}$. Hence, for each (infinitesimally small) $\epsilon > 0$, there exists $\lambda' = \lambda + \Delta\lambda$ (with $\Delta\lambda > 0$, and $\Delta\lambda \rightarrow 0$ if $\epsilon \rightarrow 0$) and $|\Delta\psi\rangle \perp |\psi\rangle$ such that

$$\begin{aligned} \lambda' \rho'_s &= \lambda \rho_s + \Delta\lambda |\psi\rangle\langle\psi| - (1 - \lambda') \left[\epsilon |\psi\rangle\langle\Delta\psi| + \epsilon |\Delta\psi\rangle\langle\psi| \right. \\ &\quad \left. + \epsilon^2 |\Delta\psi\rangle\langle\Delta\psi| - \epsilon^2 |\psi\rangle\langle\psi| \right] \end{aligned} \quad (10.44)$$

is separable. Now, let us assume that there exists $|\phi\rangle$ with $\rho_s^{\tau_B}|\phi\rangle = 0$, and either condition (i) or (ii) from Theorem (i) is fulfilled. In the following, we will show that both (i) or (ii) lead to a contradiction, since they imply that ρ_s is either non-positive or non-separable.

(i) implies

$$\begin{aligned} \langle\Delta\psi|\phi\rangle\langle\phi|^{\tau_B}|\psi\rangle &= 0, \\ \langle\psi|\phi\rangle\langle\phi|^{\tau_B}|\psi\rangle &< 0, \text{ and} \\ \langle\Delta\psi|\phi\rangle\langle\phi|^{\tau_B}|\Delta\psi\rangle &> 0. \end{aligned} \quad (10.45)$$

The third inequality follows from the spectrum of $|\phi\rangle\langle\phi|^{\tau_B}$, see Lemma 2, appendix D. Insertion into Eq. (10.44) immediately yields

$$\langle\phi|\rho_s'^{\tau_B}|\phi\rangle < 0, \quad (10.46)$$

i.e., ρ_s is non-separable.

(ii) implies

$$\begin{aligned} \langle\psi|\phi\rangle\langle\phi|^{\tau_B}|\psi\rangle &= \alpha - \nu\langle\psi|\tilde{\phi}\rangle\langle\tilde{\phi}|\psi\rangle, \text{ and} \\ \langle\Delta\psi|\phi\rangle\langle\phi|^{\tau_B}|\psi\rangle &= -\nu\langle\Delta\psi|\tilde{\phi}\rangle\langle\tilde{\phi}|\psi\rangle. \end{aligned} \quad (10.47)$$

Insertion into Eq. (10.44) yields:

$$\langle\phi|\rho_s'^{\tau_B}|\phi\rangle = \Delta\lambda \alpha + (1 - \lambda')\epsilon^2(\alpha - \beta) - \nu\langle\tilde{\phi}|\rho_s'|\tilde{\phi}\rangle, \quad (10.48)$$

where $\beta = \langle\Delta\psi|A|\Delta\psi\rangle$. Since $\alpha \leq 0$ and $\alpha < \beta$ (remember that $A = \nu|\tilde{\phi}\rangle\langle\tilde{\phi}| + |\phi\rangle\langle\phi|^{\tau_B}$ has three non-negative eigenvalues, and at most one zero eigenvalue, which, due to $\alpha \leq 0$, implies that α is strictly the smallest eigenvalue of A), it follows that ρ_s' is either non-positive or non-separable. \square

10.5 Proof of Theorem 2

Let us assume that Eq. (10.16) is the optimal LSD of the entangled state ρ , with ρ_s of rank 4. According to Theorem 1 (and Lemma 2, appendix D), we know that $|\psi\rangle$ is maximally entangled, i.e., $c(\psi) = 1$, see Eq. (D.5). Hence, we can use Lemma 3, appendix D, to write

$$\lambda \rho_s^{\tau B} = \rho^{\tau B} - \mu |\psi\rangle\langle\psi|^{\tau B} = \rho^{\tau B} - \mu \left(\frac{1}{2} \mathbb{1} - |\tilde{\psi}\rangle\langle\tilde{\psi}| \right), \quad (10.49)$$

where $|\tilde{\psi}\rangle$ is defined by

$$|\psi\rangle\langle\psi|^{\tau B} |\tilde{\psi}\rangle = -\frac{1}{2} |\tilde{\psi}\rangle. \quad (10.50)$$

Consequently, for an arbitrary $|\phi'\rangle$,

$$0 \leq \lambda \langle\phi'|\rho_s^{\tau B}|\phi'\rangle = \langle\phi'|\rho^{\tau B}|\phi'\rangle + \mu |\langle\phi'|\tilde{\psi}\rangle|^2 - \frac{\mu}{2}. \quad (10.51)$$

For $|\phi'\rangle = |\phi\rangle$, the above equation, due to (10.25), reads

$$0 = \langle\phi|\rho^{\tau B}|\phi\rangle + \mu |\langle\phi|\tilde{\psi}\rangle|^2 - \frac{\mu}{2}. \quad (10.52)$$

Observe now that because of Theorem 1(i) and (10.50), we can apply Lemma 5, appendix D, concluding that $|\phi\rangle$ and $|\tilde{\psi}\rangle$ have a common Schmidt basis, hence, according to Lemma 4, appendix D, we can rewrite (10.52) as

$$0 = \langle\phi|\rho^{\tau B}|\phi\rangle + \frac{\mu}{2} c(\phi). \quad (10.53)$$

Using the results of the same Lemma, we can estimate the last two terms on the right-hand side of (10.51) by $\mu c(\phi')/2$:

$$0 \leq \langle\phi'|\rho^{\tau B}|\phi'\rangle + \frac{\mu}{2} c(\phi'). \quad (10.54)$$

In order to simplify the equations below, let us make the following observation. Both, equation (10.53) and inequality (10.54), are bilinear in $|\phi\rangle$, if only we calculate the concurrence according to (D.5), regardless of the normalization of $|\psi\rangle$. Obviously, such a quantity is not bounded from above, but this will not play any role in the following. The final formula will involve only normalized vectors.

Substituting $|\phi'\rangle = |\phi\rangle + \varepsilon|\Delta\phi\rangle$ (with arbitrary ε and $|\Delta\phi\rangle$) into (10.54) and using (10.53), we obtain, at the lowest order in ε ,

$$0 \leq \varepsilon \left(\langle\Delta\phi|\rho^{\tau B}|\phi\rangle + \langle\phi|\rho^{\tau B}|\Delta\phi\rangle + \frac{\mu}{2} \left. \frac{dc(\phi + \varepsilon\Delta\phi)}{d\varepsilon} \right|_{\varepsilon=0} \right). \quad (10.55)$$

From the definition of concurrence, Eq. (D.5), we obtain, at first order in ε ,

$$c(\phi + \varepsilon\Delta\phi) = c(\phi) + \varepsilon \langle\Delta\phi|\Sigma|\phi^*\rangle + \varepsilon \langle\phi^*|\Sigma|\Delta\phi\rangle, \quad (10.56)$$

after adjusting the phase of $|\phi\rangle$ to make $\langle\phi|\Sigma|\phi^*\rangle$ real and positive and using $\langle\Delta\phi|\Sigma|\phi^*\rangle = \langle\phi|\Sigma|\Delta\phi^*\rangle = \langle\Delta\phi^*|\Sigma|\phi\rangle^* = \langle\phi^*|\Sigma|\Delta\phi\rangle^*$, which is a consequence of $\Sigma = \Sigma^\dagger = \Sigma^*$. Thus, we can rewrite (10.55) as

$$\langle\Delta\phi|\rho^{\tau_B}|\phi\rangle + \langle\phi|\rho^{\tau_B}|\Delta\phi\rangle + \frac{\mu}{2}\left(\langle\Delta\phi|\Sigma|\phi^*\rangle + \langle\phi^*|\Sigma|\Delta\phi\rangle\right) \geq 0, \quad (10.57)$$

which is valid for an arbitrary $|\Delta\phi\rangle$. Again, considering (10.57) for $|\Delta\phi\rangle$ and $-|\Delta\phi\rangle$, we conclude that, in fact, (10.57) is an equality

$$\langle\Delta\phi|\Psi\rangle + \langle\Psi|\Delta\phi\rangle = 0, \quad (10.58)$$

where

$$|\Psi\rangle = \rho^{\tau_B}|\phi\rangle + \frac{\mu}{2}\Sigma|\phi^*\rangle. \quad (10.59)$$

Since $|\Delta\phi\rangle$ is arbitrary, we have $|\Psi\rangle = 0$, and, consequently,

$$\rho^{\tau_B}|\phi\rangle = -\frac{\mu}{2}\Sigma|\phi^*\rangle. \quad (10.60)$$

Short manipulations, using $\Sigma^2 = 1$, allow to rewrite (10.60) as an eigenvalue equation

$$\Sigma(\rho^{\tau_B})^*\Sigma\rho^{\tau_B}|\phi\rangle = \frac{\mu^2}{4}|\phi\rangle. \quad (10.61)$$

In Lemma 6, appendix D, we show that the smallest eigenvalue γ of $Y = \Sigma(\rho^{\tau_B})^*\Sigma\rho^{\tau_B}$ is given by $\gamma = c^2(\rho)/4$, where $c(\rho)$ is the concurrence of ρ . Furthermore, it follows from Lemma 7, appendix D, that $\mu^2/4$ is the smallest eigenvalue of Y , since $\langle\phi|\rho^{\tau_B}|\phi\rangle < 0$ according to Eq. (10.60). \square

Chapter 11

Conclusion

In the first part of this thesis, we have shown that arbitrary quantum states of the electromagnetic field in a single mode cavity can be prepared by interaction with a sequence of two-level atoms. In contrast to other preparation schemes, we do not require a final state measurement of the atoms, which would lead to a finite success probability of the state preparation. Furthermore, we use a simple time-independent atom-field interaction (according to the Jaynes-Cummings model), and need not be able to control the interaction Hamiltonian. Instead, the state preparation is achieved solely by choosing an appropriate initial atomic state, which may (and in general must) also exhibit entanglement between the atoms. Fortunately, it turns out that our preparation scheme exhibits a rapid (and often exponential) convergence into the target state, as a function of the number N of atoms injected in the cavity. This convergence property is of crucial importance for any experimental realization, since it not only relaxes the burden to entangle an arbitrary number of two-level-atoms injected into the cavity, but also allows to establish a viable compromise between optimizing the target state fidelity and minimizing the influence of uncontrollable noise sources.

In general, the highest fidelities with respect to the desired final field state, for a given number of atoms, are reached if we start from the vacuum as initial field state. Then, an appropriate initial atomic state can be obtained (analytically) from a time-reversal argument, using the fact that, starting from the desired field state as initial state, the cavity vacuum can be prepared by injecting all atoms in their ground state. In fact, for the preparation of photon number states, this argument yields the optimal initial atomic state, which - under the Jaynes-Cummings interaction - generates the target field state with maximal fidelity, whereas the same argument still leads to high fidelities close to the optimal in most other cases. The largest deviations from optimality were observed when the time reversal argument is employed for the preparation of coherent states of the cavity field. Here, the optimal initial atomic state is found to be almost a product state of the individual atoms.

As already alluded to, the preparation of pure field states requires a good isolation from the environment, in order to keep the influence of noise as low as possible. In contrast, the second part of this thesis demonstrated a constructive

effect of noise on the control of a fundamental *open* (i.e., *noisy*) quantum system, the cavity field of the coherently pumped micromaser. Here, the noise arises from the coupling of the field to a thermal environment (even at zero temperature) and from the atom-field entanglement, which entails a random influence on the photon field if the final state of the exiting atom is measured ('measurement noise'). Due to the influence of these quantum mechanical sources of noise, the cavity field exhibits quantum jumps between two metastable mixed equilibrium states. We demonstrated how to determine the corresponding transition rates, and have seen that an injected atomic coherence reduces the rates of the jumps, whereas a change of the measurement scheme hardly affects the transition rates.

Furthermore, we showed that the quantum jumps of the maser field can be synchronized with an externally applied weak periodic signal (i.e., a modulation of the initial atomic state), at an optimal *nonvanishing* temperature of the environment. This effect can be read out in an arbitrary component of the Bloch vector of the two-level atoms which pump the maser cavity, particularly in the atomic coherence. It is a clear signature of stochastic resonance in an open, driven quantum system, and well-predicted by the two-state model of the maser dynamics. The latter point agrees with the findings in the driven spin-boson system [51, 53, 54], where quantum stochastic resonance is found in parameter regions where incoherent tunneling prevails over the coherent dynamics. Hence, it seems that - also in the quantum case - the basic mechanism (though not always the exact quantitative behavior, see [53, 54]) of stochastic resonance can always be understood in terms of a simple two-state model (with quantum noise-activated transition rates), in accordance with the intuitive classical picture of stochastic resonance.

In the above, rather complementary approaches to quantum state control, entanglement plays an important role: for the deterministic preparation of pure fields states, an appropriately entangled atomic initial state has to be chosen, in order to avoid any final entanglement between the atoms and the field (and, hence, to avoid measurement noise), and for the control scheme exploiting stochastic resonance, the atom-field entanglement is at the origin of one of the noise sources activating the quantum jumps of the maser field.

However, a complete, general characterization of entanglement, in particular a unique, quantitative measure, has not been formulated yet, even not in the simplest case of a system composed of two qubits. As a particular way of describing the entanglement properties of a two-qubit state, we examined the best separable approximation of an entangled bipartite quantum state, which is obtained by the optimal decomposition of the state into a sum of an entangled and a separable state, with maximal weight of the latter one. We proved sufficient and necessary conditions for the optimality of the decomposition. In particular, these results allow an efficient construction of the best separable approximation, for any given entangled two-qubit state of full rank. Furthermore, we conjectured that the optimal decomposition yields a quantitative measure of entanglement.

Perspectives

In the present thesis, the interaction of a single-mode quantized radiation field with a sequence of *entangled* two-level atoms was examined for the first time. The reason why a possible entanglement of the initial atomic state has so far been neglected in the literature is probably the difficulty of generating such states experimentally. Whilst recent experimental progress in the laboratory suggests that such a perspective becomes nonetheless more and more realistic, the scenario developed in this thesis can also be turned upside-down: some of our ideas may in fact also be useful in order to *produce* many-particle entanglement. Given the ability to prepare certain classes field states (by a method which does not require many-particle entanglement), we can produce a variety of entangled atomic states, for example by injecting a sequence of ground state atoms into the cavity.* This calls for a systematic examination of the N -atoms entangled states thereby obtainable from atomic states which are easier to prepare (e.g., product states).

Throughout the thesis, we have concentrated mainly on the *optimal* initial atomic state which prepares the desired field state with the maximum fidelity for a given number of atoms. However, there exist also other atomic states which achieve a high fidelity (see chapter 5.4.3). Among them may also be states which do not require entanglement between all N atoms, but may be written as a product of M -atom states, with a small $M < N$. Since the difficulty of generating such a state experimentally is mainly determined by the number M of atoms which have to be entangled (and not by the total number of atoms N), we would like to know how the set of field states which can be prepared with high fidelity by using M -atom entanglement (but admitting large values of N) grows when increasing M . Among these field states, we expect to find some ‘ M -invariant’ states, i.e., states that remain unchanged when interacting with an appropriately chosen M -atom state $|\psi_0\rangle$. Due to the property of asymptotic completeness, the field will - independently of its initial state - approach the invariant state when pumped by a steady flux $|\psi_0\rangle \otimes |\psi_0\rangle \otimes \dots$ of those M -atom states. As an example, any photon number state $|n\rangle$ can be obtained by using only two-particle entanglement [127]. Apart from this example, however, the M -invariant field states are so far completely unexplored (except for $M = 1$, see chapter 3.3.1).

Furthermore, as we have demonstrated, our state preparation scheme is also applicable when starting from mixed initial field states. In this case, since the information about the initial field state cannot be lost during the unitary atoms-field interaction, it has to be transferred to the final atomic state. At the same time, the final field state is completely determined by the initial atomic state. Hence, quantum state preparation implies some sort of quantum information transfer, which can and should be studied from an information theoretical point of view.

As for stochastic resonance, we can easily predict that this robust phenom-

*These states would be of the form $T_N|\psi'_0\rangle$, with $|\psi'_0\rangle$ given by Eq. (4.7). Some of their properties were examined in chapter 5.2. (Note that the time-reversal operator T_N , Eq. (3.5), reverses the order of the N atoms.)

enon has a wide range of potential applications in various quantum optical systems which exhibit bistability and/or quantum jumps, in the presence of noise. Given recent progress in the manipulation of single atoms or ions confined to traps or periodic potentials, quantum jumps between electronic sublevels of the trapped atom/ion, or between different lattice sites may be controlled by stochastic resonance.

Appendix A

Some properties of $M^{(\rho_0)}$

In this appendix, we show how to calculate the atomic operator $M^{(\rho_0)}$, Eq. (4.3), which is needed to compute the maximum fidelity and the corresponding optimal initial atomic state, see chapter 4.1.

We start with the simplest case $N = 1$, where the field interacts with a single atom. With respect to the atomic basis $|1\rangle = |u\rangle$ and $|2\rangle = |d\rangle$, the interaction operator U reads as follows:

$$U = \begin{pmatrix} U_{11} & U_{12} \\ U_{21} & U_{22} \end{pmatrix}. \quad (\text{A.1})$$

According to the Jaynes-Cummings model, Eq. (2.1), the field operators U_{ij} are given by

$$U_{11} = \cos(\phi\sqrt{aa^\dagger}), \quad U_{12} = -ia \frac{\sin(\phi\sqrt{a^\dagger a})}{\sqrt{a^\dagger a}}, \quad (\text{A.2})$$

$$U_{21} = -ia^\dagger \frac{\sin(\phi\sqrt{aa^\dagger})}{\sqrt{aa^\dagger}}, \quad U_{22} = \cos(\phi\sqrt{a^\dagger a}). \quad (\text{A.3})$$

Now, the field operator $A \otimes \mathbb{1}$ after the atom-field interaction (in the Heisenberg picture) reads:

$$U^\dagger(A \otimes \mathbb{1})U = \begin{pmatrix} T_{11}(A) & T_{12}(A) \\ T_{21}(A) & T_{22}(A) \end{pmatrix}, \quad (\text{A.4})$$

where the field superoperators T_{ij} are defined by

$$T_{11}(A) = U_{11}^\dagger A U_{11} + U_{21}^\dagger A U_{21} \quad (\text{A.5})$$

$$T_{12}(A) = U_{11}^\dagger A U_{12} + U_{21}^\dagger A U_{22} \quad (\text{A.6})$$

$$T_{21}(A) = U_{12}^\dagger A U_{11} + U_{22}^\dagger A U_{21} \quad (\text{A.7})$$

$$T_{22}(A) = U_{12}^\dagger A U_{12} + U_{22}^\dagger A U_{22}. \quad (\text{A.8})$$

The generalization to $N > 1$ is straightforward, and from Eq. (4.3) we obtain the following matrix elements:

$$\langle i_1 \dots i_N | M^{(\rho_0)} | j_1 \dots j_N \rangle = \text{tr}\{\rho_0 T_{i_1 j_1} \dots T_{i_N j_N}(|\chi\rangle\langle\chi|)\}. \quad (\text{A.9})$$

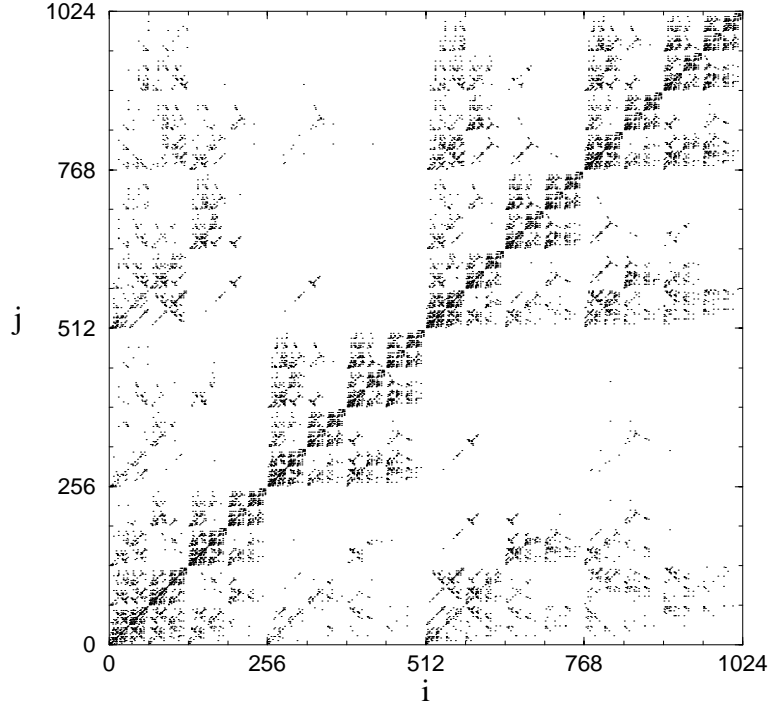


Figure A.1: Self-similar structure of the operator $M^{(\rho_0)}$ for the preparation of the 2-photon state $|\chi\rangle = |2\rangle$, starting from the vacuum $\rho_0 = |0\rangle\langle 0|$ as initial state, choosing the optimal vacuum Rabi angle $\phi = 1.3$, with $N = 10$ atoms. All matrix elements $\langle i | M^{(\rho_0)} | j \rangle > 10^{-3}$ are marked by a dot. Here, the atomic basis state $|i\rangle$ represents the state $|i_1 \dots i_{10}\rangle$ according to $i = \sum_k 2^{10-k} i_k$ (binary representation), i.e., the finest scales correspond to the last atoms.

Here, the indices i_k, j_k refer to the k -th atom that crosses the cavity. According to Eq. (A.9), for each set of indices $i_1 j_1, \dots, i_n j_n$, the corresponding photon field state $T_{i_1 j_1} \dots T_{i_n j_n} (|\chi\rangle\langle\chi|)$ has to be calculated. Asymptotic completeness is fulfilled if all those states approach a multiple of the identity operator (since only then the trace in Eq. (A.9) is independent of ρ_0). Note that $T_{11}\mathbb{1} = T_{22}\mathbb{1} = \mathbb{1}$, whereas $T_{12}\mathbb{1} = T_{21}\mathbb{1} = 0$. Hence, if asymptotic completeness was precisely realized already with N atoms, then the matrix M_{N+1} for $N + 1$ atoms would be $M_{N+1} = \begin{pmatrix} M_N & 0 \\ 0 & M_N \end{pmatrix}$. In other words: the state of the first atom would not matter at all, since the photon field would already be completely determined by the last N atoms. In our case of the Jaynes-Cummings interaction, however, the asymptotic completeness is never precisely realized with a finite number of atoms (even if we restrict ourselves to a finite dimensional photon field space by setting an appropriate trapping state). Then, the operation of T_{12} or T_{21} (onto a photon field state then not precisely a multiple of $\mathbb{1}$) typically leads to smaller matrix elements than the operation of T_{11} or T_{22} . This entails a self-similar structure of the operator $M^{(\rho_0)}$ as depicted in Fig. A.1.

As for the calculation on a computer, the most efficient way to determine

$M^{(\rho_0)}$ is to use a recursive procedure, where the photon field states for N atoms are directly calculated from the ones for $N - 1$ atoms, starting with the state $|\chi\rangle\langle\chi|$ for $N = 0$.

In some cases, the calculation is simplified by the following property of $M^{(\rho_0)}$: if the target field state is a photon number state, $|\chi\rangle = |n\rangle$, and the initial field state is diagonal in the photon number representation, $\rho_0 = \sum_m p_m |m\rangle\langle m|$, then all matrix elements $\langle\psi_1|M^{(\rho_0)}|\psi_2\rangle$ between two atomic energy eigenstates $|\psi_1\rangle$ and $|\psi_2\rangle$ with different energy vanish identically, i.e., all eigenvectors of $M^{(\rho_0)}$ must have a well defined energy (or, in other units, a well defined excitation number, i.e., number of atoms in the upper state). This property can be deduced from Eq. (4.3), making use of the energy conservation, Eq. (2.6).

Nevertheless, for a large number of atoms (e.g., $N \geq 10$), the calculation and diagonalization of $M^{(\rho_0)}$ is computationally quite expensive, due to the high dimension of $2^N \times 2^N$. Then, it may be more efficient to use the following iterative procedure in order to find the largest eigenvalue, especially if the initial field state ρ_0 is a pure state: starting with an arbitrary initial guess $|\psi_0\rangle$ (e.g., the state $|\psi'_0\rangle$ from chapter 4.2), we calculate iteratively

$$|\psi_{i+1}\rangle \propto M^{(\rho_0)}|\psi_i\rangle = \sum_n p_n \langle\chi_n|U_N^\dagger(|\chi\rangle\langle\chi| \otimes \mathbb{1})U_N|\chi_n, \psi_i\rangle, \quad (\text{A.10})$$

where $\sum_n p_n |\chi_n\rangle\langle\chi_n| = \rho_0$ is a decomposition of the initial field state into pure states. (The sign \propto instead of $=$ means that the state $|\psi_{i+1}\rangle$ has to be normalized, since $M^{(\rho_0)}$ is not unitary.) With $i \rightarrow \infty$, the state $|\psi_i\rangle$ converges to the desired eigenvector $|\psi_0^{(\text{opt})}\rangle$, unless $|\psi_0\rangle$ was chosen orthogonal to $|\psi_0^{(\text{opt})}\rangle$. The reason for the potentially better efficiency of the iterative procedure is that we are dealing with vectors of dimension $M \times 2^N$, with M the cutoff dimension of the photon field, instead of a matrix of dimension $2^N \times 2^N$. Furthermore, the operation of U_N onto a pure state is a product of single-atom operations, see Eq. (2.4), and therefore easy to compute. If the fidelity is very close to 1, however, those advantages of the iterative method may be compensated by the fact that in this case the convergence can be very slow (since then also the next largest eigenvalues are very close to 1, i.e., almost identical to the largest one).

Note that if $\rho_0 = |\chi_0\rangle\langle\chi_0|$ is a pure state, Eq. (A.10) can be read as follows: we take an arbitrary atomic state, calculate the atoms-field interaction, project onto the final field state, calculate the reverse interaction and project again onto the initial field state. According to Eq. (A.10), we thereby obtain an atomic state which prepares the final field state with higher fidelity, unless the initial atomic state is an eigenvector of $M^{|\chi_0\rangle\langle\chi_0|}$, when the above operation does not change anything. The latter point can be extended to the following

Lemma (Time reversal property of $M^{|\chi_0\rangle\langle\chi_0|}$).

The spectrum of $M^{|\chi_0\rangle\langle\chi_0|}$ for the preparation of the field state $|\chi\rangle$, starting from the initial state $|\chi_0\rangle$, is the same as the spectrum of $M_0^{|\chi\rangle\langle\chi|}$ for the preparation of $|\chi_0\rangle$, starting from $|\chi\rangle$. The corresponding eigenvectors are connected as follows: if $|\psi_0\rangle$ is an eigenvector of $M^{|\chi_0\rangle\langle\chi_0|}$ with eigenvalue F , then the time-reversed final atomic state $|\tilde{\psi}\rangle = T_N\langle\chi|U_N|\chi_0, \psi_0\rangle/\sqrt{F}$, compare Eq. (4.5), is an eigenvector of $M_0^{|\chi\rangle\langle\chi|}$ with the same eigenvalue.

Proof. Since $|\psi_0\rangle$ is an eigenvector of $M^{|\chi_0\rangle\langle\chi_0|}$, we may write:

$$\langle\chi_0|U_N^\dagger(|\chi\rangle\langle\chi|\otimes\mathbb{1})U_N|\chi_0,\psi_0\rangle = F|\psi_0\rangle. \quad (\text{A.11})$$

Inserting the definition of $|\tilde{\psi}\rangle$ yields:

$$\langle\chi_0|U_N^\dagger T_N|\chi,\tilde{\psi}\rangle = \sqrt{F}|\psi_0\rangle. \quad (\text{A.12})$$

Surely, this equation remains valid if we add the field state $|\chi_0\rangle$ to both sides, and apply the operation $T_N U_N$:

$$T_N U_N(|\chi_0\rangle\langle\chi_0|\otimes\mathbb{1})U_N^\dagger T_N|\chi,\tilde{\psi}\rangle = \sqrt{F} T_N U_N|\chi_0,\psi_0\rangle. \quad (\text{A.13})$$

Finally, by projection onto the field state $|\chi\rangle$, and taking into account the time reversal symmetry (3.5), we obtain the operator $M_0^{|\chi\rangle\langle\chi|}$ on the left-hand side, and the state $|\tilde{\psi}\rangle$ on the right-hand side:

$$M_0^{|\chi\rangle\langle\chi|}|\tilde{\psi}\rangle = F|\tilde{\psi}\rangle. \quad \square \quad (\text{A.14})$$

Hence, the eigenstates of $M^{|\chi_0\rangle\langle\chi_0|}$ fulfill the time-reversal property in the following sense: the preparation of $|\chi\rangle$ out of $|\chi_0\rangle$ by the initial atomic state $|\psi_0\rangle$ yields the same fidelity as the preparation of $|\chi_0\rangle$ out of $|\chi\rangle$ by the corresponding time-reversed atomic final state. On the other hand, if $|\psi_0\rangle$ is not an eigenstate of $M^{|\chi_0\rangle\langle\chi_0|}$, the latter fidelity is strictly larger than the first one. An example is the relation between the fidelity F achieved by the state $|\psi'_0\rangle$, Eq. (4.7), and the lower bound F' , see chapter 4.2: in general, $F \geq F'$, and the equality holds only if $|d\dots d\rangle$ is an eigenstate of $M_0^{|\chi\rangle\langle\chi|}$ (and then, also $|\psi'_0\rangle$ is an eigenstate of $M^{|0\rangle\langle 0|}$, according to the above lemma).

One photon trapping state

As discussed in chapter 2, if the vacuum Rabi angle fulfills the 1 photon trapping condition, i.e., $\phi = k\pi/\sqrt{2}$, $k \in \mathbb{Z}$, no photon number population can be transferred from 1 to 2, or vice versa. Hence, if the field is initially, e.g., in the vacuum state, it will always remain in the two dimensional subspace spanned by $|0\rangle$ and $|1\rangle$. We have found (compare chapter 5.1) that - in the case of an *odd* trapping state, i.e., $\phi = (2k+1)\pi/\sqrt{2}$, $k \in \mathbb{Z}$ - for any final and initial field states $|\chi\rangle$ and ρ_0 , and any number N of atoms, the operator $M^{(\rho_0)}$ is highly degenerate, with only two eigenvalues, both of them 2^{N-1} fold degenerate.

Most probably, the degeneracy $M^{(\rho_0)}$ can be traced back to the following symmetry of the Jaynes-Cummings interaction U_2 , Eq. (2.4), with *two* atoms. We have found that, in the case of an odd 1 photon trapping state, the interaction operator U_2 is unchanged if we apply transformations A and B on the initial and final *atomic* states, respectively:

$$B U_2 A = U_2. \quad (\text{A.15})$$

Here, the atomic operators A and B are most conveniently defined in the following two bases:

$$\begin{aligned} |\psi_1\rangle &= |\text{uu}\rangle, & |\psi_2\rangle &= \frac{|\text{ud}\rangle + \cos(\phi) |\text{du}\rangle}{\sqrt{1 + \cos^2(\phi)}}, \\ |\psi_3\rangle &= \frac{-\cos(\phi) |\text{ud}\rangle + |\text{du}\rangle}{\sqrt{1 + \cos^2(\phi)}}, & |\psi_4\rangle &= |\text{dd}\rangle, \end{aligned} \quad (\text{A.16})$$

for the initial atomic states, and

$$\begin{aligned} |\tilde{\psi}_1\rangle &= |\text{uu}\rangle, & |\tilde{\psi}_2\rangle &= \frac{\cos(\phi) |\text{ud}\rangle + |\text{du}\rangle}{\sqrt{1 + \cos^2(\phi)}}, \\ |\tilde{\psi}_3\rangle &= \frac{-|\text{ud}\rangle + \cos(\phi) |\text{du}\rangle}{\sqrt{1 + \cos^2(\phi)}}, & |\tilde{\psi}_4\rangle &= |\text{dd}\rangle, \end{aligned} \quad (\text{A.17})$$

for the final states, respectively. Then, the operator A is defined by

$$\begin{aligned} A |\psi_1\rangle &= |\psi_1\rangle, & A |\psi_2\rangle &= -|\psi_2\rangle, \\ A |\psi_3\rangle &= |\psi_3\rangle, & A |\psi_4\rangle &= -|\psi_4\rangle, \end{aligned} \quad (\text{A.18})$$

and likewise

$$\begin{aligned} B |\tilde{\psi}_1\rangle &= |\tilde{\psi}_1\rangle, & B |\tilde{\psi}_2\rangle &= -|\tilde{\psi}_2\rangle, \\ B |\tilde{\psi}_3\rangle &= |\tilde{\psi}_3\rangle, & B |\tilde{\psi}_4\rangle &= -|\tilde{\psi}_4\rangle. \end{aligned} \quad (\text{A.19})$$

Then, Eq. (A.15) can be easily verified by an explicit calculation. Now, from Eq. (A.15) and the definition of $M^{(\rho_0)}$, Eq. (4.3), it follows that A commutes with $M^{(\rho_0)}$:

$$A^{-1} M^{(\rho_0)} A = M^{(\rho_0)}. \quad (\text{A.20})$$

Let us now consider the case of N atoms. We denote the operator which acts as A on the i -th and $(i+1)$ -th atom, and as the identity on the other atoms, by A_i . Then, due to the product structure of U_N , Eq. (2.4), the operator $M^{(\rho_0)}$ commutes with all the operators A_i , $i = 1, \dots, N-1$. Hence, if $|\psi\rangle$ is an eigenvector of $M^{(\rho_0)}$ with eigenvalue F , also $A_i |\psi\rangle$ is an eigenvector of $M^{(\rho_0)}$ with the same eigenvalue. What remains to be shown in order to prove that the eigenvalues of $M^{(\rho_0)}$ are (at least) 2^{N-1} fold degenerate, is that the smallest atomic subspace which is invariant under all the transformations A_i , $i = 1, \dots, N-1$, is of dimension 2^{N-1} . (We have not yet completed this part of the proof.)

Appendix B

A small combinatorial lemma

Lemma: Given $N, n \in \mathbb{N}$, and n mutually different nonzero complex numbers A_1, A_2, \dots, A_n , we have the following formula:

$$\sum_{\substack{k_1, \dots, k_n \geq 0 \\ k_1 + \dots + k_n = N}} \prod_{i=1}^n (A_i)^{k_i} = \sum_{k=1}^n (A_k)^{N+n-1} \prod_{\substack{i=1 \\ i \neq k}}^n \frac{1}{A_k - A_i}. \quad (\text{B.1})$$

Proof: In order to get rid of the constraint $\sum_i k_i = N$ in the sum over k_1, \dots, k_n , we introduce an auxiliary variable x , and using

$$\frac{1}{N!} \frac{d^N}{dx^N} x^m \Big|_{x=0} = \delta_{N;m}, \quad (\text{B.2})$$

we obtain

$$\begin{aligned} \sum_{\substack{k_1, \dots, k_n \geq 0 \\ k_1 + \dots + k_n = N}} \prod_{i=1}^n (A_i)^{k_i} &= \frac{1}{N!} \frac{d^N}{dx^N} \sum_{k_1, \dots, k_n=0}^{\infty} \prod_{i=1}^n (xA_i)^{k_i} \Big|_{x=0} \\ &= \frac{1}{N!} \frac{d^N}{dx^N} \prod_{i=1}^n \frac{1}{1 - xA_i} \Big|_{x=0}. \end{aligned} \quad (\text{B.3})$$

In the second line, we have applied the formula for the geometric series. For the evaluation of the N -fold derivative, we use Cauchy's formula:

$$\frac{1}{N!} \frac{d^N}{dx^N} \prod_{i=1}^n \frac{1}{1 - xA_i} \Big|_{x=0} = \frac{1}{2\pi i} \oint_{\gamma_1} dz \frac{1}{z^{N+1}} \prod_{i=1}^n \frac{1}{1 - zA_i}. \quad (\text{B.4})$$

Here, γ_1 is a closed contour around $z = 0$. Since the integrand approaches zero faster than $1/|z|$ with $|z| \rightarrow \infty$, we may add the contour γ_2 to γ_1 (see Fig. B.1). Then, the area enclosed by γ_2 and γ_1 contains n simple poles at $z_k = 1/A_k$, $k = 1, \dots, n$, and the residual theorem yields:

$$\frac{1}{2\pi i} \oint_{\gamma_1, \gamma_2} dz \frac{1}{z^{N+1}} \prod_{i=1}^n \frac{1}{1 - zA_i} = - \sum_{k=1}^n (A_k)^{N+1} \frac{1}{-A_k} \prod_{i \neq k} \frac{1}{1 - \frac{A_i}{A_k}}. \quad (\text{B.5})$$

The minus sign in front of the sum originates from the orientation of γ_2 . Dividing each factor of the product over i by A_k leads us to Eq. (B.1) \square

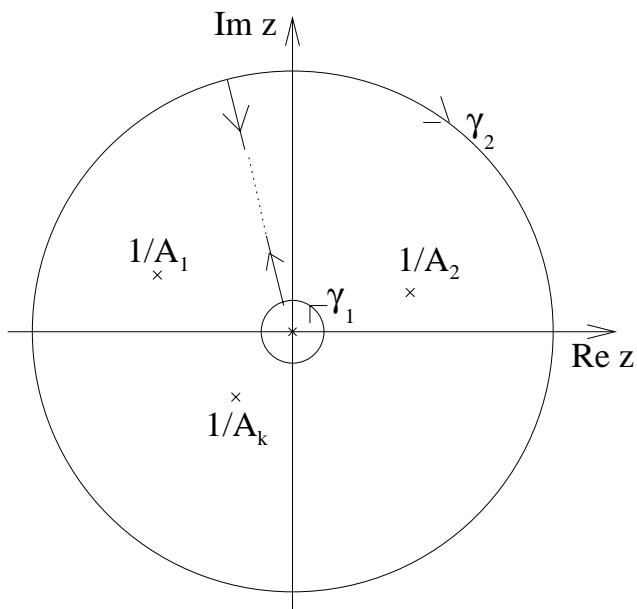


Figure B.1: Adding the contour γ_2 transforms the $(N + 1)$ -fold pole at $z = 0$ into n simple poles at $z_k = 1/A_k$, $k = 1, \dots, n$.

Appendix C

Quantum trajectories

In this appendix, we describe a numerical procedure to obtain a single realization of the micromaser dynamics. We employ a quantum trajectory method [100, 101, 102, 103], where not only arrival times and detection results for subsequent atoms are determined by drawing random numbers, but also the cavity damping is treated as a stochastic process. In this way, the dynamics of the photon field can be efficiently described as a stochastic evolution of a *pure* field state.

We proceed as follows:

- (i) The initial state of the field, at time $t_0 = 0$, is the vacuum $|\chi(0)\rangle = |0\rangle$.
- (ii) Determine the arrival time t_1 of the next atom by drawing a random number $\alpha \in [0, 1]$ (uniformly distributed): $t_1 = -\ln(\alpha)/r + t_0$. In the case of incoherent pumping, the initial atomic state $|\psi\rangle = |u\rangle$ (with probability $|a|^2$) or $|\psi\rangle = |d\rangle$ (with probability $1 - |a|^2$) is determined by an additional random number.
- (iii) Determine the state $|\chi(t_1)\rangle$ of the photon field, after damping of the field during the time interval $[t_0, t_1]$ (see below).
- (iv) Calculate the probability of detecting the atom in the final state $\sigma_z = +1$ (or $\sigma_y = +1$, depending on the chosen measurement scheme, see chapter 7.2.2), after interaction with the cavity field $|\chi(t_1)\rangle$, according to Eqs. (2.2,2.3). Whether the atom is detected in $\sigma_{z,y} = +1$ or $\sigma_{z,y} = -1$ is determined by another random number.
- (v) Perform the corresponding quantum mechanical state reduction, which yields the new field state $|\chi(t_1)'\rangle$ after the detection.

Steps (ii)-(v) are repeated until all atoms have crossed the cavity. Note that the chosen measurement scheme explicitly enters in the last two steps, (iv) and (v), whereas it plays no role in the ensemble average over all quantum trajectories, as given by the master equation (7.11).

We still have to explain the damping step (iii). To obtain a single realization of the damping process, we use the following model for the heat bath: it consists of an additional ‘thermal’ atomic beam, which interacts with the photon field

in the same way as the strongly coupled atomic beam, but with very small vacuum Rabi angle ϕ_{th} [97]. The atoms of this thermal beam enter the cavity either in the upper or lower state $|u\rangle$ or $|d\rangle$, with the ratio of the corresponding rates r_u and r_d given by the thermal Boltzmann factor $r_u/r_d = n_b/(n_b + 1)$, and are measured in either $|u\rangle$ or $|d\rangle$ after interaction with the cavity field. The weak coupling approximation is obtained by taking the limit $\phi_{\text{th}} \rightarrow 0$. Since, in this limit, the probability that a thermal atom emits or absorbs a photon from the cavity vanishes like $\sin^2(\phi_{\text{th}}\sqrt{n+1}) \propto \phi_{\text{th}}^2$, we must at the same time increase the thermal atomic flux r_{th} , such that $r_{\text{th}}\phi_{\text{th}}^2$ remains finite. Then, the above model yields the standard master equation (7.15) for the damped harmonic oscillator, with the decay rate $\gamma = r_{\text{th}}\phi_{\text{th}}^2/(2n_b + 1)$.

In principle, we could simulate the weakly interacting atoms, which model the heat bath, in the same way as the strongly coupled atoms, following the above steps (ii), (iv), and (v). However, this would be very inefficient, since in the weak-coupling limit ($\phi_{\text{th}} \rightarrow 0$, $r_{\text{th}} \rightarrow \infty$, $r_{\text{th}}\phi_{\text{th}}^2 = \text{const.}$) the flux r_{th} of the thermal atoms becomes infinitely large. Instead, we will use a more elegant method, where the limit $\phi_{\text{th}} \rightarrow 0$ can be performed exactly. Only one random number is needed to determine the time of the next absorption or emission of a thermal photon, and the photon field evolves smoothly (though non-unitarily) during time intervals without emission or absorption [102, 128].

Suppose the field at time t_0 is given by the coefficients $d_n(t_0)$ (normalized, i.e., $\sum_n |d_n(t_0)|^2 = 1$). Obviously, in the weak coupling limit $\phi_{\text{th}} \rightarrow 0$, almost all of the thermal atoms are detected in the same state as they enter the cavity, i.e., an absorption or emission of a thermal photon is very unlikely. According to Eqs. (2.2,2.3), if during the time interval $[t_0, t]$ no absorption or emission takes place, the field at time t reads:

$$d_n(t) = d_n(t_0) \cos^{N_u}(\phi_{\text{th}}\sqrt{n+1}) \cos^{N_d}(\phi_{\text{th}}\sqrt{n}), \quad (\text{C.1})$$

where $N_u = \gamma n_b(t - t_0)/\phi_{\text{th}}^2$ is the number of atoms that enter the cavity in the upper state $|u\rangle$ during $[t_0, t]$, and likewise $N_d = \gamma(n_b + 1)(t - t_0)/\phi_{\text{th}}^2$ the number of atoms in $|d\rangle$.^{*} The norm $N(t) = \sum_n |d_n(t)|^2$ gives the probability that no absorption or emission takes place.

The limit $\phi_{\text{th}} \rightarrow 0$ of Eq. (C.1) is given by:

$$d_n(t) = d_n(t_0) e^{-\frac{\gamma}{2}[n_b(n+1)+(n_b+1)n](t-t_0)}, \quad (\text{C.2})$$

and, consequently:

$$N(t) = \sum_{n=0}^{\infty} |d_n(t_0)|^2 e^{-\gamma[n_b(n+1)+(n_b+1)n](t-t_0)}. \quad (\text{C.3})$$

With help of Eq. (C.3), the time t^* of the next absorption or emission of a thermal photon is obtained by drawing a (uniformly distributed) random number $\alpha \in [0, 1]$, and solving $\alpha = N(t^*)$ for t^* . If t^* is larger than the arrival time t_1 of the next strongly coupled atom, as determined in step (ii),

^{*}The fluctuations of $N_{u,d}$ due to the random arrival times of the atoms (Poisson distribution) can be neglected in the weak coupling limit $\phi_{\text{th}} \rightarrow 0$ ($N_{u,d} \rightarrow \infty$).

no absorption or emission takes place during step (iii), and the field state at time t_1 is given by $|\chi(t_1)\rangle = \sum_n d_n(t_1)|n\rangle/\sqrt{N(t)}$, according to Eqs. (C.2,C.3). If $t^* < t_1$, an emission or absorption takes place during step (iii). Whether emission or absorption is determined in the following way: the probability of emission at time t^* is the product of the probability that a $|u\rangle$ -atom arrives at time t^* , which is proportional to r_u , and the probability that the $|u\rangle$ -atom is detected in $|d\rangle$. The probability of absorption is obtained in a similar way. Consequently, the probability ratio of emission over absorption is:

$$\begin{aligned} \frac{P_{\text{em}}}{P_{\text{abs}}} &= \lim_{\phi_{\text{th}} \rightarrow 0} \frac{r_u \sum_n |d_{n-1}(t^*)|^2 \sin^2(\phi_{\text{th}}\sqrt{n})}{r_d \sum_n |d_{n+1}(t^*)|^2 \sin^2(\phi_{\text{th}}\sqrt{n+1})} \\ &= \frac{\sum_n |d_n(t^*)|^2 n_b(n+1)}{\sum_n |d_n(t^*)|^2 (n_b+1)n}. \end{aligned} \quad (\text{C.4})$$

Now, we draw another random number $\alpha \in [0, 1]$. If $\alpha/(1-\alpha) < P_{\text{em}}/P_{\text{abs}}$, an emission takes place, and otherwise an absorption. Finally, according to Eqs. (2.2,2.3) with $\phi_{\text{th}} \rightarrow 0$, the new photon field at time t^* is given by

$$d_n'(t^*) = -i\sqrt{n} d_{n-1}(t^*) \quad (\text{emission}), \quad (\text{C.5})$$

$$d_n'(t^*) = -i\sqrt{n+1} d_{n+1}(t^*) \quad (\text{absorption}). \quad (\text{C.6})$$

After normalization of the d_n' , the above steps are repeated: The time t^* of the next emission or absorption is determined via Eq. (C.3), etc., until $t^* > t_1$, what completes step (iii).

The ensemble of quantum trajectories [100, 101, 102, 103] obtained in this way depends on our specific model for the heat bath, and there exist many other ways of ‘unraveling’ the damping master equation (e.g., choosing another measurement scheme on the heat bath). In this sense, the physical meaning of such trajectories is somewhat unclear. At least, however, they can be regarded as a useful tool for an efficient simulation of a single sequence of atomic detection events. The statistics of the latter are not affected by how we simulate single realizations of the thermal damping process, as long as their ensemble average is given by the same master equation.

Incoherent pumping

In the case of incoherent pumping, the above described ensemble of quantum trajectories reduces to a jump process between neighboring photon number states. Here, each atom enters the cavity either in the state $|u\rangle$ (with probability $|\alpha|^2$) or $|d\rangle$ (with probability $|\beta|^2$). Furthermore, we assume that also the final state detection measures the atom in one of those two states (i.e., measurement of σ_z). Hence, if the cavity field is in a photon number state $|n\rangle$ just before an atom arrives, it will still have a definite photon number after detection of the atom: obviously, the photon number is unchanged if the atom is detected in the same state as its initial state, and otherwise it changes by $+1$ (initial atomic state: $|u\rangle$, detected final state: $|d\rangle$) or -1 (initial state: $|d\rangle$, final state: $|u\rangle$). The same holds for the damping process, too (modeled as incoherent pumping with a weakly interacting thermal atomic beam, see above): neither

Eq. (C.2) nor Eqs. (C.5,C.6) create any coherences between different photon number states. Therefore (since also the initial field state $|0\rangle$ has a definite photon number), the quantum trajectory of the photon field is described simply by a jump process between neighboring photon number states. If the transition probabilities from n to $n + 1$ or $n - 1$ photons are denoted by t_n^+ and t_n^- , respectively, such a jump process leads to the following time evolution for the occupation probability $p_n = \langle n|\rho|n\rangle$ of the n -photon state:

$$\dot{p}_n = -(t_n^+ + t_n^-) p_n + t_{n-1}^+ p_{n-1} + t_{n+1}^- p_{n+1}. \quad (\text{C.7})$$

By comparison with the master equation (7.11) (for incoherent pumping, $c = 0$), we obtain:

$$t_n^+ = r |a|^2 \sin^2(\phi\sqrt{n+1}) + \gamma n_b(n+1), \quad (\text{C.8})$$

$$t_n^- = r |b|^2 \sin^2(\phi\sqrt{n}) + \gamma (n_b + 1)n. \quad (\text{C.9})$$

In the bistable regime of the maser dynamics (see chapter 8), the ‘macroscopic’ transition rates between the metastable states 1 and 2 can be expressed in terms of the above ‘microscopic’ rates, see Eqs. (8.2,8.3). In the general case of coherent pumping, however, the quantum trajectory of the photon field is much more complicated, and simple expressions for the transition rates do not exist.

Appendix D

Two-qubit lemmata

In this appendix we formulate and prove several Lemmata used in part III for the proofs of the main results on the optimal Lewenstein-Sanpera decomposition, Theorems 1 and 2. Lemmata 1-5 show some more general properties of mixed states of 2×2 systems, whereas Lemmata 5 and 6 are mainly devoted to a technical lemma, concerning the calculation of the concurrence, Eq. (10.11).

Partial transposition

We start by examining the transformation behavior of the partial transpose of ρ under local unitary transformations [which differs from the behavior of ρ , since the result of partial transposition, Eq. (10.10), depends on the basis in subspace \mathcal{H}_B .] If we change the bases of \mathcal{H}_A and \mathcal{H}_B by a local transformation $U \otimes V$, i.e., by unitary rotations U and V in the spaces \mathcal{H}_A and \mathcal{H}_B , respectively, the matrix ρ will be transformed according to

$$\rho' = U \otimes V \rho (U \otimes V)^\dagger = \sum_i^k p_i U \rho_i^A U^\dagger \otimes V \rho_i^B V^\dagger. \quad (\text{D.1})$$

On the other hand, the partial transposition, Eq. (10.10), gives

$$\rho'^{\tau B} = \sum_i^k p_i U \rho_i^A U^\dagger \otimes (V \rho_i^B V^\dagger)^\tau = U \otimes V^* \rho^{\tau B} (U \otimes V^*)^\dagger, \quad (\text{D.2})$$

where the star denotes the complex conjugation. From (D.2), it follows that the spectrum of $\rho^{\tau B}$ is independent of the basis in which the partial transposition is performed.

Observe also the following form of the definition of partial transposition

$$\langle e, f | \rho | e, f \rangle = \langle e, f^* | \rho^{\tau B} | e, f^* \rangle, \quad (\text{D.3})$$

where $|e, f\rangle$ denotes the product vector $|e\rangle \otimes |f\rangle$.

Concurrence of a pure state

By a straightforward calculation, it is easy to verify that the concurrence, Eq. (10.11), of a pure state,

$$|\psi\rangle = a_1|00\rangle + a_2|01\rangle + a_3|10\rangle + a_4|11\rangle = [a_1, a_2, a_3, a_4]^\tau, \quad (\text{D.4})$$

equals

$$c(\psi) = 2|a_1a_4 - a_2a_3| = |\langle \psi | \Sigma | \psi^* \rangle|, \quad (\text{D.5})$$

with Σ given by Eq. (10.12). Due to the normalization condition $1 = \langle \psi | \psi \rangle = |a_1|^2 + |a_2|^2 + |a_3|^2 + |a_4|^2$, we have $0 \leq c(\psi) \leq 1$. The maximum $c(\psi) = 1$ is attained for the states called maximally entangled. The degree of entanglement (i.e., the concurrence) is invariant under local unitary transformations (i.e., transformations of the form $U \otimes V$).

By local transformation, a pure state can be brought to its Schmidt form $|\psi\rangle = \lambda_1|e_1\rangle \otimes |f_1\rangle + \lambda_2|e_2\rangle \otimes |f_2\rangle$, where $\{|e_1\rangle, |e_2\rangle\}$ and $\{|f_1\rangle, |f_2\rangle\}$ are appropriately chosen orthonormal bases in \mathcal{H}_A and \mathcal{H}_B . In these bases thus $\psi = [\lambda_1, 0, 0, \lambda_2]^T$, and it is easy to show that the most general form of a maximally entangled state in the original bases reads

$$|\psi\rangle = a_1|00\rangle + a_2|01\rangle \mp (a_2^*|10\rangle - a_1^*|11\rangle) = \begin{bmatrix} a_1 \\ a_2 \\ \mp a_2^* \\ \pm a_1^* \end{bmatrix}, \quad |a_1|^2 + |a_2|^2 = \frac{1}{2}. \quad (\text{D.6})$$

Lemma 1.

Let ρ_s be a two qubit density matrix.

If $\text{rank}(\rho_s^{\tau B}) \leq 2$, then $\text{rank}(\rho_s) = \text{rank}(\rho_s^{\tau B})$.

Proof: Since every two-dimensional subspace contains a product vector [122], also the kernel of $\rho_s^{\tau B}$ must do so, i.e. $\rho_s^{\tau B}|e, f\rangle = 0$. It follows that $\rho_s|e, f^*\rangle = 0$. Indeed, from (D.3) we have $\langle e, f^* | \rho | e, f^* \rangle = \langle e, f | \rho^{\tau B} | e, f \rangle = 0$, and since ρ_s as a density matrix is positive definite, $\rho|e, f^*\rangle = 0$. By local unitary transformations in both subspaces we can choose $|e, f^*\rangle = |0, 0\rangle = |e, f\rangle$. The equations $\rho|0, 0\rangle = 0$ and $\rho^{\tau B}|0, 0\rangle = 0$, together with hermiticity of both matrices, leave only six nonvanishing elements in each of them, and by inspection one checks that their characteristic polynomials (hence also the spectra) are identical.

Lemma 2.

For an arbitrary $|\phi\rangle$, the matrix $|\phi\rangle\langle\phi|^{\tau B}$ has eigenvalues

$$-\frac{c}{2}, \frac{c}{2}, \frac{1 - \sqrt{1 - c^2}}{2}, \frac{1 + \sqrt{1 - c^2}}{2}, \quad (\text{D.7})$$

where $c = c(\phi)$ is the concurrence of $|\phi\rangle$, Eq. (D.5). If $c > 0$, the eigenvector belonging to the negative eigenvalue is maximally entangled.

Proof: The first part of the Lemma is proven by an explicit calculation. In order to prove the second statement, let $L = U \otimes V$ be a local transformation, and $|\phi'\rangle = L|\phi\rangle$. Then, according to Eq. (D.2),

$$|\phi'\rangle\langle\phi'|^{\tau B} = L' |\phi\rangle\langle\phi|^{\tau B} L'^{\dagger}, \quad (\text{D.8})$$

where $L' = U \otimes V^*$. Observe that L' is a local transformation, hence it does

not influence the concurrence of vectors. Now,

$$|\phi\rangle\langle\phi|^{\tau_B}|\psi\rangle = -\frac{c(\phi)}{2}|\psi\rangle \Leftrightarrow |\phi'\rangle\langle\phi'|^{\tau_B}|\psi'\rangle = -\frac{c(\phi)}{2}|\psi'\rangle, \quad (\text{D.9})$$

where $|\psi'\rangle = L'|\psi\rangle$. Let us now choose L such that it brings $|\phi\rangle$ to its Schmidt basis:

$$|\phi'\rangle = L|\phi\rangle = \begin{bmatrix} \lambda_1 \\ 0 \\ 0 \\ \lambda_2 \end{bmatrix}. \quad (\text{D.10})$$

It is now straightforward to show that $|\psi'\rangle$ in (D.10) has the form

$$|\psi'\rangle = \frac{1}{\sqrt{2}} e^{i\delta} \begin{bmatrix} 0 \\ 1 \\ -1 \\ 0 \end{bmatrix}, \quad (\text{D.11})$$

hence $|\psi'\rangle$ is maximally entangled and the same is true about $|\psi\rangle$, which is obtained from $|\psi'\rangle$ by a local transformation L' .

(Similar versions of Lemma 1 and Lemma 2 can also be found in [129].)

Lemma 3.

If $|\psi\rangle$ is maximally entangled, then

$$|\psi\rangle\langle\psi|^{\tau_B} = \frac{1}{2} \mathbb{1} - |\tilde{\psi}\rangle\langle\tilde{\psi}|, \quad (\text{D.12})$$

where $\mathbb{1}$ is the 4×4 identity operator, and $|\tilde{\psi}\rangle$ is the eigenvector of $|\psi\rangle\langle\psi|^{\tau_B}$ with the negative eigenvalue, i.e.,

$$|\psi\rangle\langle\psi|^{\tau_B}|\tilde{\psi}\rangle = -\frac{1}{2}|\tilde{\psi}\rangle. \quad (\text{D.13})$$

According to Lemma 2, $|\tilde{\psi}\rangle$ is maximally entangled.

Proof: Since $|\psi\rangle\langle\psi|^{\tau_B}$ is Hermitian, it has, in addition to $|\psi_4\rangle := |\tilde{\psi}\rangle$, three other orthogonal eigenvectors $|\psi_i\rangle$, $i = 1, 2, 3$, fulfilling, according to Lemma 2

$$|\psi\rangle\langle\psi|^{\tau_B}|\psi_i\rangle = \frac{1}{2}|\psi_i\rangle, \quad i = 1, 2, 3. \quad (\text{D.14})$$

Using (D.14) and (D.13), together with the orthonormality of the eigenvectors, $\langle\psi_i|\psi_j\rangle = \delta_{ij}$, $i = 1, 2, 3, 4$, one sees that the actions of both sides of (D.12) give the same results on the complete orthonormal set $|\psi_i\rangle$, $i = 1, 2, 3, 4$, which establishes (D.12) as a matrix equation.

Lemma 4.

For arbitrary $|\phi\rangle$,

$$\max_{m.e.} |\langle\phi|\psi\rangle|^2 = \frac{1}{2} + \frac{1}{2} c(\phi), \quad (\text{D.15})$$

where the maximum is taken over all maximally entangled $|\psi\rangle$. The maximum is attained only if $|\psi\rangle$ and $|\phi\rangle$ have a common Schmidt basis.

Proof: By a local unitary transformation (which does not change neither $|\langle\phi|\psi\rangle|^2$ nor the entanglements of $|\phi\rangle$ and $|\psi\rangle$), we can bring $|\phi\rangle$ to its Schmidt basis:

$$|\phi\rangle = \begin{bmatrix} \lambda_1 \\ 0 \\ 0 \\ \lambda_2 \end{bmatrix}, \quad \lambda_i \geq 0, \quad \lambda_1^2 + \lambda_2^2 = 1. \quad (\text{D.16})$$

Using the general form (D.6) of a maximally entangled state, we conclude that, in the new basis,

$$\begin{aligned} |\langle\phi|\psi\rangle|^2 &= |a_1\lambda_1 \pm a_1\lambda_2|^2 & (\text{D.17}) \\ &\leq |a_1|^2 (\lambda_1 + \lambda_2)^2 = |a_1|^2 (1 + 2\lambda_1\lambda_2) = |a_1|^2 [1 + c(\phi)], \end{aligned}$$

and the maximum is attained only if $|a_1|^2$ is maximal, i.e., $|a_1|^2 = 1/2$ and $a_2 = 0$, which completes the proof.

Lemma 5.

Let $|\phi\rangle$ be an entangled state, and $|\psi\rangle$ the eigenvector of $|\phi\rangle\langle\phi|^{\tau_B}$ with the negative eigenvalue, i.e.,

$$|\phi\rangle\langle\phi|^{\tau_B}|\psi\rangle = -\frac{c(\phi)}{2}|\psi\rangle. \quad (\text{D.18})$$

Then, $|\phi\rangle$ and $|\tilde{\psi}\rangle$ have a common Schmidt basis, where $|\tilde{\psi}\rangle$ is the eigenvector of $|\psi\rangle\langle\psi|^{\tau_B}$ with the negative eigenvalue, i.e.

$$|\psi\rangle\langle\psi|^{\tau_B}|\tilde{\psi}\rangle = -\frac{1}{2}|\tilde{\psi}\rangle. \quad (\text{D.19})$$

Proof: From (D.18), we have

$$-\frac{c(\phi)}{2} = \langle\psi| |\phi\rangle\langle\phi|^{\tau_B} |\psi\rangle = \text{Tr}(|\phi\rangle\langle\phi|^{\tau_B}|\psi\rangle\langle\psi|) \quad (\text{D.20})$$

$$= \text{Tr}(|\phi\rangle\langle\phi| |\psi\rangle\langle\psi|^{\tau_B}) = \langle\phi| |\psi\rangle\langle\psi|^{\tau_B} |\phi\rangle. \quad (\text{D.21})$$

From Lemma 2, we know that $|\psi\rangle$ is maximally entangled. Thus, according to Lemma 3, in the last term we can substitute $|\psi\rangle\langle\psi|^{\tau_B}$ by $\frac{1}{2}\mathbb{1} - |\tilde{\psi}\rangle\langle\tilde{\psi}|$, consequently:

$$\langle\phi|\tilde{\psi}\rangle\langle\tilde{\psi}|\phi\rangle = \frac{1}{2} + \frac{c(\phi)}{2}. \quad (\text{D.22})$$

Hence, due to Lemma 4, $|\phi\rangle$ and the maximally entangled $|\tilde{\psi}\rangle$ have a common Schmidt basis.

Lemma 6.

If ρ is an entangled state, i.e., its concurrence $c(\rho)$ is positive, then $c^2(\rho)/4$ equals the smallest eigenvalue of $Y = \Sigma (\rho^{\tau_B})^ \Sigma \rho^{\tau_B}$.*

Proof: If $d_1^2/4, \dots, d_4^2/4$ are the eigenvalues of $Y = \Sigma (\rho^{\tau_B})^* \Sigma \rho^{\tau_B}$, and $c_1^2 \geq \dots \geq c_4^2$ the (real and positive, see [117]) eigenvalues of $X = \Sigma \rho^* \Sigma \rho$, see Eq. (10.12), the following relation holds:

$$d_1^2 = (c_1 + c_2 + c_3 - c_4)^2, \quad (\text{D.23})$$

$$d_2^2 = (c_1 + c_2 - c_3 + c_4)^2, \quad (\text{D.24})$$

$$d_3^2 = (c_1 - c_2 + c_3 + c_4)^2, \quad (\text{D.25})$$

$$d_4^2 = (-c_1 + c_2 + c_3 + c_4)^2. \quad (\text{D.26})$$

Indeed, invoking the anticommutation relations for Pauli matrices, we check that, for an arbitrary local transformation $L = U \otimes V$, $U, V \in SU(2)$,

$$L^* = \Sigma L \Sigma. \quad (\text{D.27})$$

We can thus use local transformations to bring ρ in $X = \Sigma \rho^* \Sigma \rho$ and $Y = \Sigma (\rho^{\tau_B})^* \Sigma \rho^{\tau_B}$ to a relatively simple form. An arbitrary hermitian ρ can be decomposed as

$$\rho = \frac{1}{4} \mathbb{1} + \sum_k (a'_k \sigma_k \otimes \mathbb{1}_2 + b'_k \mathbb{1}_2 \otimes \sigma_k) + \sum_{nm} C_{nm} \sigma_m \otimes \sigma_n, \quad (\text{D.28})$$

with real a'_k, b'_k , and C_{mn} . By local transformations, we can bring the 3×3 matrix C to diagonal form with non-negative diagonal elements μ_1, μ_2 , and μ_3 [130, 131]. The desired transformation changes a'_k and b'_k to some other real a_k and b_k , hence finally

$$\rho = \frac{\mathbb{1}}{4} + \begin{bmatrix} a_3 + b_3 + \mu_3 & b_1 - ib_2 & a_1 - ia_2 & \mu_1 - \mu_2 \\ b_1 + ib_2 & a_3 - b_3 - \mu_3 & \mu_1 + \mu_2 & a_1 - ia_2 \\ a_1 + ia_2 & \mu_1 + \mu_2 & -a_3 + b_3 - \mu_3 & b_1 - ib_2 \\ \mu_1 - \mu_2 & a_1 + ia_2 & b_1 + ib_2 & -a_3 - b_3 + \mu_3 \end{bmatrix}. \quad (\text{D.29})$$

Somewhat tedious, but straightforward calculations show that

$$\text{Tr} Y = \text{Tr} X \quad (\text{D.30})$$

$$\text{Tr} Y^2 = \text{Tr} X^2 - \delta_2 \quad (\text{D.31})$$

$$\text{Tr} Y^3 = \text{Tr} X^3 - \delta_3 \quad (\text{D.32})$$

$$\text{Tr} Y^4 = \text{Tr} X^4 - \delta_4 \quad (\text{D.33})$$

where

$$\delta_2 = 6d + \frac{3}{2} \text{Tr} X^2 - \frac{3}{4} (\text{Tr} X)^2, \quad (\text{D.34})$$

$$\delta_3 = \frac{5}{4} \delta_2 \operatorname{Tr} X, \quad (\text{D.35})$$

$$\delta_4 = \frac{7}{12} \delta_2 (2\operatorname{Tr} X^2 + (\operatorname{Tr} X)^2 - \delta_2), \quad (\text{D.36})$$

$$d^2 = \det X. \quad (\text{D.37})$$

On the other hand, as (this time rather short) calculations show, the same relations hold for two diagonal matrices

$$X' = \operatorname{diag}(c_1^2, c_2^2, c_3^2, c_4^2), \quad Y' = \operatorname{diag}(d_1^2, d_2^2, d_3^2, d_4^2)/4, \quad (\text{D.38})$$

where

$$d_1^2 = (c_1 + c_2 + c_3 - c_4)^2, \quad (\text{D.39})$$

$$d_2^2 = (c_1 + c_2 - c_3 + c_4)^2, \quad (\text{D.40})$$

$$d_3^2 = (c_1 - c_2 + c_3 + c_4)^2, \quad (\text{D.41})$$

$$d_4^2 = (-c_1 + c_2 + c_3 + c_4)^2, \quad (\text{D.42})$$

if we choose $d = +(\det X)^{1/2}$, or

$$d_1^2 = (-c_1 + c_2 + c_3 - c_4)^2, \quad (\text{D.43})$$

$$d_2^2 = (-c_1 + c_2 - c_3 + c_4)^2, \quad (\text{D.44})$$

$$d_3^2 = (-c_1 - c_2 + c_3 + c_4)^2, \quad (\text{D.45})$$

$$d_4^2 = (c_1 + c_2 + c_3 + c_4)^2, \quad (\text{D.46})$$

if $d = -(\det X)^{1/2}$. Since there is a one-to-one correspondence between the set of eigenvalues of a n -dimensional matrix and the traces of its first n powers, the relation between the eigenvalues c_i^2 of X and the eigenvalues $d_i^2/4$ of Y must be given by (D.39-D.42) or (D.43-D.46). The second case, $d < 0$, is excluded, due to the positivity of ρ . Indeed, one checks that:

$$d = \frac{1}{6} \delta_2 - \frac{1}{4} \operatorname{Tr} X^2 + \frac{1}{8} (\operatorname{Tr} X)^2 = \det(\rho) \geq 0. \quad (\text{D.47})$$

The first equality in (D.47) follows from (D.34), whereas the second is established by an explicit calculation, using (D.29) and the definition of X in terms of ρ .

Thus, the eigenvalues d_1^2, \dots, d_4^2 , Eqs. (D.39-D.42), of $4Y$ are real and positive, and the smallest eigenvalue d_4^2 equals $c(\rho)^2$, see Eq. (10.11).

Lemma 7.

If $\operatorname{rank}(\rho) \geq 3$, where ρ is an entangled state, the smallest eigenvalue of $Y = \Sigma (\rho^{\tau B})^ \Sigma \rho^{\tau B}$ is non-degenerate. If $|\phi_4\rangle$ denotes the corresponding eigenvector, and $|\phi_i\rangle$, $i = 1, 2, 3$, the other three eigenvectors, the following holds:*

$$\langle \phi_4 | \rho^{\tau B} | \phi_4 \rangle = -\frac{1}{2} c(\rho) c(\phi_4), \quad (\text{D.48})$$

$$\langle \phi_i | \rho^{\tau B} | \phi_i \rangle \geq 0, \quad i = 1, 2, 3. \quad (\text{D.49})$$

Proof: Let $d_1^2/4 \geq \dots \geq d_4^2/4$ denote the (real and positive, see Lemma 6) eigenvalues of Y , and $c_1^2 \geq \dots \geq c_4^2$ the eigenvalues of $X = \Sigma \rho^* \Sigma \rho$. According to Lemma 6, the relation between d_i and c_i is given by Eqs. (D.39-D.42), in particular $d_4 = c(\rho)$. From $c(\rho) > 0$ and the definition of concurrence, Eq. (10.11), it follows that $c_1 > c_2$. Now, if $\text{rank}(\rho) \geq 3$, it is easy to show that $c_2 > 0$ [since $\text{rank}(\Sigma) = 4$ and therefore $\text{rank}(X) \geq 2$], and then Eqs. (D.41,D.42) imply $d_4 < d_3$. Hence, $d_4^2/4$ is a non-degenerate eigenvalue.

By splitting the eigenvalue equation $Y|\phi_i\rangle = \frac{1}{4}d_i^2|\phi_i\rangle$ (with real d_i) into its real and imaginary part, one can derive that $|\phi_i\rangle$ fulfills

$$\Sigma \rho^{\tau B} |\phi_i\rangle = \frac{1}{2} e^{i\chi_i} d_i |\phi_i^*\rangle, \quad (\text{D.50})$$

where $e^{i\chi_i}$ is a phase factor. Using $\Sigma^2 = 1$, Eq. (D.5), and the hermiticity of $\rho^{\tau B}$, we conclude that

$$\langle \phi_i | \rho^{\tau B} | \phi_i \rangle = \pm \frac{1}{2} d_i c(\phi_i). \quad (\text{D.51})$$

In order to complete the proof of Lemma 7, it remains to be shown that the sign on the right hand side must be negative for $i = 4$ and non-negative for $i = 1, 2, 3$. Due to continuity, it is sufficient to consider the case $\text{rank}(\rho) = 4$. Then, $|\phi_i\rangle$ cannot be a product vector [since inserting $|\phi_i\rangle = |e, f\rangle$ into Eq. (D.51) would imply $\langle e, f^* | \rho | e, f^* \rangle = 0$, compare Eq. (D.3)], i.e., the right hand side of Eq. (D.51) cannot be zero. [$d_i > 0$ follows from $d_4 = c(\rho) > 0$.] Now, if ρ is infinitesimally close to an entangled pure state, $\rho \rightarrow |\psi\rangle\langle\psi|$, it is easy to check that, indeed, Eq. (D.51) is valid with the minus sign for $i = 4$, and the plus sign for $i = 1, 2, 3$. (For $|\psi\rangle = [\lambda_1, 0, 0, \lambda_2]^\tau$, one finds that $|\phi_{1,2}\rangle = [\lambda_2, 0, 0, \pm\lambda_1]^\tau$, $|\phi_3\rangle = [0, 1, 1, 0]^\tau/\sqrt{2}$, and $|\phi_4\rangle = [0, 1, -1, 0]^\tau/\sqrt{2}$.) Next, we consider the one-parameter family $\rho(\lambda') = \mu'|\psi\rangle\langle\psi| + \lambda'\rho_s$, with $\mu' = 1 - \lambda'$ and $\lambda' \in [0, \lambda]$, where ρ_s is the BSA of $\rho = \rho(\lambda)$. Since $\rho_s^{\tau B}$ is positive, $\langle \chi | \rho^{\tau B} | \chi \rangle < 0$ implies $\langle \chi | \rho(\lambda')^{\tau B} | \chi \rangle < 0$, hence $c(\rho(\lambda')) > 0$ for all $\lambda' \in [0, \lambda]$. Finally, continuity implies that the sign of the right hand side of Eq. (D.51) does not change when increasing λ' from 0 to λ .

Bibliography

- [1] W. Neuhauser, M. Hohenstatt, P. Toschek, and H. Dehmelt, *Localized Visible Ba⁺ Mono-Ion Oscillator*, Phys. Rev. A **22**, 1137 (1980).
- [2] D. Wineland and W. Itano, *Spectroscopy of a Single Mg⁺ Ion*, Phys. Lett. A **82**, 75 (1981).
- [3] W. Nagourney, J. Sandberg, and H. Dehmelt, *Shelved Optical Electron Amplifier: Observation of Quantum Jumps*, Phys. Rev. Lett. **56**, 2797 (1986).
- [4] J. Bergquist, R. Hulet, W. Itano, and D. Wineland, *Observation of Quantum Jumps in a Single Atom*, Phys. Rev. Lett. **57**, 1699 (1986).
- [5] T. Sauter, R. Blatt, W. Neuhauser, and P. Toschek, *'Quantum Jumps' Observed in the Fluorescence of a Single Atom*, Opt. Comm. **60**, 287 (1986).
- [6] F. Diedrich and H. Walther, *Nonclassical Radiation of a Single Stored Ion*, Phys. Rev. Lett. **58**, 203 (1987).
- [7] S. Kuhr, W. Alt, D. Schrader, M. Müller, V. Gomer, and D. Meschede, *Deterministic Delivery of a Single Atom*, Science **293**, 278 (2001).
- [8] G. Guthörlein, M. Keller, K. Hayasaka, W. Lange, and H. Walther, *A Single Ion as a Nanoscopic Probe of an Optical Field*, Nature **414**, 49 (2001).
- [9] S. Rice and D. Tannor, *Coherent Pulse Sequence Control of Product Formation in Chemical Reactions*, Adv. Chem. Phys. **70**, 441 (1988).
- [10] P. Brumer and M. Shapiro, *Laser Control of Molecular Processes*, Ann. Rev. Phys. Chem. **43**, 257 (1992).
- [11] W. Warren, H. Rabitz, and M. Dahleh, *Coherent Control of Quantum Dynamics: The Dream Is Alive*, Science **259**, 1581 (1993).
- [12] R. Gordon and S. Rice, *Active Control of the Dynamics of Atoms and Molecules*, Ann. Rev. Phys. Chem. **48**, 601 (1997).
- [13] D. Tannor and A. Bartana, *On the Interplay of Control Fields and Spontaneous Emission in Laser Cooling*, J. Phys. Chem. A **103**, 10359 (1999).

- [14] G. Huang, T. Tarn, and J. Clark, *On the Controllability of Quantum-Mechanical Systems*, J. Math. Phys. **24**, 2608 (1983).
- [15] V. Ramakrishna, M. Salapaka, M. Dahleh, H. Rabitz, and A. Peirce, *Controllability of Molecular Systems*, Phys. Rev. A **51**, 960 (1995).
- [16] U. Gaubatz, P. Rudecki, S. Schieman, and K. Bergmann, *Population Transfer Between Molecular Vibrational Levels by Stimulated Raman-Scattering with Partially Overlapping Laser Fields - a New Concept and Experimental Results*, J. Chem. Phys. **92**, 5363 (1990).
- [17] J. Martin, B. Shore, and K. Bergmann, *Coherent Population Transfer in Multilevel Systems with Magnetic Sublevels .3. Experimental Results*, Phys. Rev. A **54**, 1556 (1996).
- [18] A. ten Wolde, L. Noordam, A. Lagendijk, and H. van Linden van den Heuvell, *Observation of Radially Localized Atomic Electron Wave Packets*, Phys. Rev. Lett. **61**, 2099 (1988).
- [19] G. Lankhuijzen and L. Noordam, *Streak-Camera Probing of Rubidium Rydberg Wave Packet Decay in an Electric Field*, Phys. Rev. Lett. **76**, 1784 (1996).
- [20] T. Weinacht, J. Ahn, and P. Bucksbaum, *Controlling the Shape of a Quantum Wavefunction*, Nature **397**, 233 (1999).
- [21] A. Assion, T. Baumert, M. Bergt, T. Brixner, B. Kiefer, V. Seyfried, M. Strehle, and G. Gerber, *Control of Chemical Reactions by Feedback-Optimized Phase-Shaped Femtosecond Laser Pulses*, Science **282**, 919 (1998).
- [22] D. Deutsch, *Quantum-Theory, the Church-Turing Principle and the Universal Quantum Computer*, Proc. R. Soc. London, Ser. A **400**, 97 (1985).
- [23] A. Steane, *Quantum Computing*, Rep. Prog. Phys. **61**, 117 (1998).
- [24] L. Mandel and E. Wolf, *Optical Coherence and Quantum Optics* (Cambridge University Press, Cambridge, 1995).
- [25] K. Vogel, V. Akulin, and W. Schleich, *Quantum State Engineering of the Radiation Field*, Phys. Rev. Lett. **71**, 1816 (1993).
- [26] G. Harel and G. Kurizki, *Fock-State Preparation from Thermal Cavity Fields by Measurement on Resonant Atoms*, Phys. Rev. A **54**, 5410 (1996).
- [27] G. Harel, G. Kurizki, J. McIver, and E. Coutsias, *Optimized Preparation of Quantum States by Conditional Measurement*, Phys. Rev. A **53**, 4534 (1996).
- [28] A. Parkins, P. Marte, P. Zoller, and H. Kimble, *Synthesis of Arbitrary Quantum States via Adiabatic Transfer of Zeeman Coherence*, Phys. Rev. Lett. **71**, 3095 (1993).

- [29] A. Parkins, P. Marte, P. Zoller, O. Carnal, and H. Kimble, *Quantum State Mapping between Multilevel Atoms and Cavity Light Fields*, Phys. Rev. A **51**, 1578 (1995).
- [30] C. Law and J. Eberly, *Arbitrary Control of a Quantum Electromagnetic Field*, Phys. Rev. Lett. **76**, 1055 (1996).
- [31] C. Law, J. Eberly, and B. Kneer, *Preparation of an Arbitrary Density Matrix of a Harmonic Oscillator*, J. Mod. Opt. **44**, 2149 (1997).
- [32] B. Kümmerer and H. Maassen, *A Scattering Theory for Markov Chains*, Infin. Dimens. Anal. Quantum Probab. Relat. Top. **3**, 161 (2000).
- [33] D. Janzig, F. Armknecht, R. Zeier, and T. Beth, *Quantum Control without Access to the Controlling Interaction*, Phys. Rev. A **65**, 022104 (2002).
- [34] O. Benson, G. Raithel, and H. Walther, *Quantum Jumps of the Micro-maser Field: Dynamic Behavior Close to Phase Transition Points*, Phys. Rev. Lett. **72**, 3506 (1994).
- [35] N. Bohr, *On the Constitution of Atoms and Molecules*, Philosophical Magazine **26**, 1 (1913).
- [36] R. Benzi, A. Sutera, and A. Vulpiani, *The Mechanism of Stochastic Resonance*, J. Phys. A **14**, L453 (1981).
- [37] L. Gammaitoni, P. Hänggi, P. Jung, and F. Marchesoni, *Stochastic Resonance*, Rev. Mod. Phys. **70**, 223 (1998).
- [38] R. Benzi, G. Parisi, A. Sutera, and A. Vulpiani, *A Theory of Stochastic Resonance in Climatic Change*, SIAM J. Appl. Math. **43**, 565 (1983).
- [39] J.-P. Eckmann and L. Thomas, *Remarks on Stochastic Resonance*, J. Phys. A **15**, L261 (1982).
- [40] S. Fauve and F. Heslot, *Stochastic Resonance in a Bistable System*, Phys. Lett. A **97**, 5 (1983).
- [41] G. Vemuri and R. Roy, *Stochastic Resonance in a Bistable Ring Laser*, Phys. Rev. A **39**, 4668 (1988).
- [42] B. McNamara and K. Wiesenfeld, *Theory of Stochastic Resonance*, Phys. Rev. A **39**, 4854 (1989).
- [43] L. Gammaitoni, F. Marchesoni, M. Martinelli, L. Pardi, and S. Santucci, *Stochastic Resonance in Bistable Systems*, Phys. Rev. Lett. **62**, 349 (1989).
- [44] R. Fox and Y. Lu, *Analytic and Numerical Study of Stochastic Resonance*, Phys Rev. E **48**, 3390 (1993).
- [45] R. N. Mantegna and B. Spagnolo, *Stochastic Resonance in a Tunnel Diode*, Phys. Rev. E **49**, R1792 (1993).

- [46] J. Douglass, L. Wilkens, E. Pantazelou, and F. Moss, *Noise Enhancement of Information Transfer in Crayfish Mechanoreceptors by Stochastic Resonance*, *Nature* **365**, 337 (1993).
- [47] R. Bartussek and P. Hänggi, *Stochastic Resonance in Optical Bistable Systems*, *Phys. Rev. E* **49**, 3930 (1994).
- [48] K. Wiesenfeld and F. Moss, *Stochastic Resonance and the Benefits of Noise: From Ice Ages to Crayfish and SQUIDS*, *Nature* **373**, 33 (1995).
- [49] A. Bulsara and L. Gammaitoni, *Tuning in to Noise*, *Physics Today* **49**, 39 (March 1996).
- [50] P. Jung and K. Wiesenfeld, *Too Quiet to Hear a Whisper*, *Nature* **385**, 291 (1997).
- [51] R. Löfstedt and S. Coppersmith, *Stochastic Resonance: Nonperturbative Calculation of Power Spectra and Residence Time Distributions*, *Phys. Rev. E* **49**, 4821 (1994).
- [52] R. Löfstedt and S. N. Coppersmith, *Quantum Stochastic Resonance*, *Phys. Rev. Lett.* **72**, 1947 (1994).
- [53] M. Grifoni and P. Hänggi, *Coherent and Incoherent Quantum Stochastic Resonance*, *Phys. Rev. Lett.* **76**, 1611 (1996).
- [54] M. Grifoni and P. Hänggi, *Nonlinear Quantum Stochastic Resonance*, *Phys. Rev. E* **54**, 1390 (1996).
- [55] A. Buchleitner and R. Mantegna, *Quantum Stochastic Resonance in a Micromaser*, *Phys. Rev. Lett.* **80**, 3932 (1998).
- [56] T. Wellens and A. Buchleitner, *Stochastic Resonance in a Fundamental Quantum System*, *J. Phys. A* **32**, 2895 (1999).
- [57] E. Jaynes and F. Cummings, *Comparison of Quantum and Semiclassical Radiation Theories with Application to the Beam Maser*, *Proc. IEEE* **51**, 89 (1963).
- [58] F. Cummings, *Stimulated Emission of Radiation in a Single Mode*, *Phys. Rev.* **140**, A1051 (1965).
- [59] P. Meystre and M. Sargent III, *Elements of Quantum Optics* (Springer, Berlin, 1990).
- [60] P. Meystre, E. Geneux, and A. Quattropani, *Long-Time Behavior of a Two-Level System in Interaction with an Electromagnetic Field*, *Nuovo Cimento B* **25**, 521 (1975).
- [61] T. von Förster, *A Comparison of Quantum and Semi-Classical Theories of the Interaction between a Two-Level Atom and the Radiation Field*, *J. Phys. A* **8**, 95 (1975).

- [62] J. Eberly, N. Narozhny, and J. Sanchez-Mondragon, *Periodic Spontaneous Collapse and Revival in a Simple Quantum Model*, Phys. Rev. Lett. **44**, 1323 (1980).
- [63] P. Filipowicz, J. Javanainen, and P. Meystre, *Quantum and Semiclassical Steady States of a Kicked Cavity Mode*, J. Opt. Soc. Am. B **3**, 906 (1986).
- [64] P. Meystre, G. Rempe, and H. Walther, *Very-Low-Temperature Behavior of a Micromaser*, Opt. Lett. **13**, 1078 (1988).
- [65] M. Hillery and J. Škvarček, *Disentanglement-Preserving States in Micromaser*, Acta Physica Slovaca **48**, 239 (1998).
- [66] C. Bennett, H. Bernstein, S. Popescu, and B. Schumacher, *Concentrating Partial Entanglement by Local Operations*, Phys. Rev. A **53**, 2046 (1996).
- [67] R. Glauber, *Coherent and Incoherent States of the Radiation Field*, Phys. Rev. **131**, 2766 (1963).
- [68] J. Gea-Banacloche, *Atom- and Field-State Evolution in the Jaynes-Cummings Model For Large Initial Fields*, Phys. Rev. A **44**, 5913 (1991).
- [69] D. Meschede, H. Walther, and G. Müller, *One-Atom Maser*, Phys. Rev. Lett. **54**, 551 (1985).
- [70] P. Filipowicz, J. Javanainen, and P. Meystre, *Theory of a Microscopic Maser*, Phys. Rev. A **34**, 3077 (1986).
- [71] S. Popescu and D. Rohrlich, *Thermodynamics and the Measure of Entanglement*, Phys. Rev. A **56**, R3319 (1997).
- [72] G. Vidal, *Entanglement Monotones*, J. Mod. Opt. **47**, 355 (2000).
- [73] V. Vedral, M. Plenio, K. Jacobs, and P. Knight, *Statistical Inference, Distinguishability of Quantum States and Quantum Entanglement*, Phys. Rev. A **56**, 4452 (1997).
- [74] N. Linden, S. Popescu, B. Schumacher, and M. Westmoreland, *Reversibility of Local Transformations of Multi-Particle Entanglement*, quant-ph/9912039 (1999).
- [75] M. Murao, D. Jonathan, M. Plenio, and V. Vedral, *Quantum telecloning and Multiparticle Entanglement*, Phys. Rev. A **59**, 156 (1999).
- [76] C. Bennett, S. Popescu, D. Rohrlich, J. Smolin, and A. Thapliyal, *Exact and Asymptotic Measures of Multipartite Pure-State Entanglement*, Phys. Rev. A **63**, 012307 (2000).
- [77] H. Barnum and N. Linden, *Monotones and Invariants for Multi-Particle Quantum States*, J. Phys. A **34**, 6787 (2001).
- [78] N. Linden and S. Popescu, *On Multiparticle Entanglement*, Fortschr. Phys. **46**, 567 (1998).

- [79] M. Reed and B. Simon, *Methods of Modern Mathematical Physics, III: Scattering Theory* (Academic Press, San Diego, 1979).
- [80] B. Kümmerer, in *Quantum Probability and Applications III*, edited by L. Accardi and W. von Waldenfels (Springer, Heidelberg, 1988), pp. 228–244.
- [81] B. Kümmerer, private communication.
- [82] B. Kümmerer *et. al.*, in preparation.
- [83] J. Slosser, P. Meystre, and S. Braunstein, *Harmonic Oscillator Driven by a Quantum Current*, Phys. Rev. Lett. **63**, 934 (1989).
- [84] J. Slosser and P. Meystre, *Tangent and Cotangent States of the Electromagnetic Field*, Phys. Rev. A **41**, 3867 (1990).
- [85] M. Reed and B. Simon, *Methods of Modern Mathematical Physics, I: Functional Analysis* (Academic Press, Boston, 1980).
- [86] M. Hübner, *Explicit Calculation of the Bures Distance for Density Matrices*, Phys. Lett. A **163**, 239 (1992).
- [87] G. Lindblad, *Expectations and Entropy Inequalities for Finite Quantum Systems*, Comm. Math. Phys. **39**, 111 (1974).
- [88] D. Pegg and S. Barnett, *Phase Properties of the Quantized Single-Mode Electromagnetic Field*, Phys. Rev. A **39**, 1665 (1989).
- [89] A. Hurwitz, *Über die Erzeugung der Invarianten durch Integration*, Gött. Nachrichten 71 (1897).
- [90] K. Życzkowski and H.-J. Sommers, *Induced Measures in the Space of Mixed Quantum States*, J. Phys. A **34**, 7111 (2001).
- [91] C. Sackett, D. Kielpinski, B. King, C. Langer, V. Meyer, C. Myatt, M. Rowe, Q. Turchette, W. Itano, D. Wineland, and I. Monroe, *Experimental Entanglement of Four Particles*, Nature **404**, 256 (2000).
- [92] A. Rauschenbeutel, G. Nogues, S. Osnaghi, P. Bertet, M. Brune, J. Raimond, and S. Haroche, *Step-by-Step Engineered Multiparticle Entanglement*, Science **288**, 2024 (2000).
- [93] M. Weidinger, B. Varcoe, R. Heerlein, and H. Walther, *Trapping States in the Micromaser*, Phys. Rev. Lett. **82**, 3795 (1999).
- [94] H.-J. Briegel and B.-G. Englert, *Quantum Optical Master Equations: The Use of Damping Bases*, Phys. Rev. A **47**, 3311 (1993).
- [95] H.-J. Briegel, B.-G. Englert, N. Sterpi, and H. Walther, *One-Atom Maser: Statistics of Detector Clicks*, Phys. Rev. A **49**, 2962 (1994).

- [96] G. Raithel, C. Wagner, H. Walther, L. Narducci, and M. Scully, in *Cavity Quantum Electrodynamics*, edited by P. Berman (Academic Press, Boston, 1994).
- [97] B.-G. Englert, *Elements of Micromaser Physics*, quant-ph/0203052 (1994).
- [98] J. Krause, M. O. Scully, and H. Walther, *Quantum Theory of the Micromaser: Symmetry Breaking via Off-Diagonal Atomic Injection*, Phys. Rev. A **34**, 2032 (1986).
- [99] T. Wellens, *Stochastische Resonanz im Mikromaser*, diploma thesis (LMU Munich, 1998).
- [100] P. Meystre and E. Wright, *Measurement-Induced Dynamics of a Micromaser*, Phys. Rev. A **37**, 2524 (1988).
- [101] J. Dalibard, Y. Castin, and K. Mølmer, *Wave-Function Approach to Dissipative Dynamics in Quantum Optics*, Phys. Rev. Lett. **68**, 580 (1992).
- [102] R. Dum, P. Zoller, and H. Ritsch, *Monte-Carlo Simulation of the Atomic Master Equation for Spontaneous Emission*, Phys. Rev. A **46**, 4382 (1992).
- [103] H. Carmichael, *An Open Systems Approach to Quantum Optics* (Springer, Berlin, 1993).
- [104] C. Wagner, R. Brecha, A. Schenzle, and H. Walther, *Phase Diffusion, Entangled States, and Quantum Measurements in the Micromaser*, Phys. Rev. A **47**, 5068 (1993).
- [105] B.-G. Englert, T. Gantsog, A. Schenzle, C. Wagner, and H. Walther, *One-Atom Maser: Phase-Sensitive Measurements*, Phys. Rev. A **53**, 4386 (1996).
- [106] C. Gardiner, *Handbook of Stochastic Methods*, 2nd ed. (Springer Verlag, Berlin, 1983).
- [107] J. P. Paz, S. Habib, and W. H. Zurek, *Reduction of the Wave Packet: Preferred Observable and Decoherence Time Scale*, Phys. Rev. D **47**, 488 (1993).
- [108] A. Leggett, S. Chakravarty, A. Dorsey, M. Fisher, A. Garg, and W. Zwerger, *Dynamics of the Dissipative Two-State System*, Rev. Mod. Phys. **59**, 1 (1987).
- [109] P. Jung and P. Talkner, *Suppression of Higher Harmonics at Noise-Induced Resonances*, Phys. Rev. E **51**, 2640 (1995).
- [110] M. Grifoni and P. Hänggi, *Driven Quantum Tunneling*, Phys. Rep. **304**, 229 (1997).

- [111] C. H. Bennet, D. P. DiVincenzo, J. Smolin, and W. K. Wootters, *Mixed-State Entanglement and Quantum Error Correction*, Phys. Rev. A **54**, 3824 (1996).
- [112] V. Vedral and M. B. Plenio, *Entanglement Measures and Purification Procedures*, Phys. Rev. A **57**, 1619 (1998).
- [113] P. Hayden, M. Horodecki, and B. Terhal, *The Asymptotic Entanglement Cost of Preparing a Quantum State*, J. Phys. A **34**, 6891 (2001).
- [114] R. Werner, *Quantum States with Einstein-Podolsky-Rosen Correlations Admitting a Hidden-Variable Model*, Phys. Rev. A **40**, 4277 (1989).
- [115] A. Peres, *Separability Criterion for Density Matrices*, Phys. Rev. Lett. **77**, 1413 (1996).
- [116] M. Horodecki, P. Horodecki, and R. Horodecki, *Separability of Mixed States: Necessary and Sufficient Conditions*, Phys. Lett. A **223**, 1 (1996).
- [117] W. Wootters, *Entanglement of Formation of an Arbitrary State of Two Qubits*, Phys. Rev. Lett. **80**, 2245 (1998).
- [118] G. Vidal and R. Werner, *A Computable Measure of Entanglement*, Phys. Rev. A **65**, 032314 (2002).
- [119] J. Eisert and M. Plenio, *A Comparison of Entanglement Measures*, J. Mod. Opt. **46**, 145 (1999).
- [120] F. Verstraete, K. Audenaert, J. Dehaene, and B. de Moor, *A Comparison of the Entanglement Measures Negativity and Concurrence*, J. Phys. A **34**, 10327 (2001).
- [121] M. Horodecki, P. Horodecki, and R. Horodecki, *Mixed-State Entanglement and Distillation: Is There a 'Bound' Entanglement in Nature?*, Phys. Rev. Lett. **80**, 5239 (1998).
- [122] M. Lewenstein, , and A. Sanpera, *Separability and Entanglement of Composite Quantum Systems*, Phys. Rev. Lett. **80**, 2261 (1998).
- [123] B.-G. Englert and N. Metwally, *Separability of Entangled Q-bit Pairs*, J. Mod. Opt. **47**, 2221 (2000).
- [124] S. Karnas and M. Lewenstein, *Separable Approximations of Density Matrices of Composite Quantum Systems*, J. Phys. A **34**, 6919 (2001).
- [125] B.-G. Englert and N. Metwally, *Remarks on 2-Q-Bit States*, Appl. Phys. B - Lasers O **72**, 35 (2001).
- [126] S. Hill and W. Wootters, *Entanglement of a Pair of Quantum Bits*, Phys. Rev. Lett. **78**, 5022 (1997).

- [127] T. Wellens, A. Buchleitner, B. Kümmerer, and H. Maassen, *Quantum State Preparation via Asymptotic Completeness*, Phys. Rev. Lett. **85**, 3361 (2000).
- [128] J. Cresser and S. Pickles, *A Quantum Trajectory Analysis of the One-Atom Micromaser*, Quantum Semiclass. Opt. **8**, 73 (1996).
- [129] A. Sanpera, R. Tarrach, and G. Vidal, *Local Description of Quantum Inseparability*, Phys. Rev. A **58**, 826 (1998).
- [130] R. Horodecki and M. Horodecki, *Information-Theoretic Aspects of Inseparability of Mixed States*, Phys. Rev. A **54**, 1838 (1996).
- [131] M. Kuś and K. Życzkowski, *Geometry of Entangled States*, Phys. Rev. A **63**, 032307 (2001).

Publications

Parts of this thesis have been published in the following articles:

- T. Wellens and A. Buchleitner, *Stochastic Resonance in the Coherence of a Quantum System*, Phys. Rev. Lett. **84**, 5118 (2000).
- T. Wellens and A. Buchleitner, *Bistability and Stochastic Resonance in an Open Quantum System*, Chem. Phys. **268**, 131 (2001).
- T. Wellens, A. Buchleitner, B. Kümmerer and H. Maassen, *Quantum State Preparation via Asymptotic Completeness*, Phys. Rev. Lett. **85**, 3361 (2000).
- T. Wellens and M. Kuś, *Separable Approximation for Mixed States of Composite Quantum Systems*, Phys. Rev. A **64**, 052302 (2001).

Name Thomas Wellens
Geburtsdatum 17. Juni 1974
Geburtsort Solothurn (CH)
Familienstand ledig

Schulbildung

1980 - 1982 Görresschule Neuss
1982 - 1984 Grundschule Königswiesen Regensburg
1984 - 1993 Albertus-Magnus-Gymnasium Regensburg
9. Juli 1993 **Abitur**
Leistungskurse Mathematik und Englisch
Grundkurse Geschichte und Physik

Studium der Physik

1993 - 1995 Universität Regensburg
15. September 1995 **Physik Vordiplom**
1995 - 1998 Ludwig-Maximilians-Universität München
27. November 1998 **Physik Diplom**
Betreuer Dr. A. Buchleitner und Prof. A. Schenzle
'Stochastische Resonanz im Mikromaser'
angefertigt am Max-Planck-Institut für Quantenoptik
freier Mitarbeiter am MPI für Quantenoptik
Dez. 1998 - Feb. 1999

Promotion in Physik

März 1999 - Mai 2002 MPI für Physik komplexer Systeme, Dresden
Betreuer Priv. Doz. A. Buchleitner
Nov. 2000 - März 2001 Zentrum für theoretische Physik der polnischen
Akademie der Wissenschaften, Warschau
3. Mai 2002 **Promotion**
an der Fakultät für Physik der LMU München

Stipendien

Nov. 1993 - Nov. 1998 Stipendium nach dem Bayerischen
Begabtenförderungsgesetz
Nov. 2000 - März 2001 Deutscher Akademischer Austauschdienst
(Kurzstipendium für Doktoranden)